Stony Brook University

Defining Polymer Structure Requirements for Activation of Mouse Sperm Acrosomal Exocytosis

A Dissertation Presented

by

He Huang

to

The Graduate School

in Partial Fulfillment of the

Requirements

for the Degree of

Doctor of Philosophy

in

Chemistry

Stony Brook University

December 2016

Stony Brook University

The Graduate School

He Huang

We, the dissertation committee for the above candidate for the

Doctor of Philosophy degree, hereby recommend

acceptance of this dissertation.

Nicole S. Sampson – Dissertation Advisor
Professor of Chemistry

Robert B. Grubbs - Chairperson of Defense
Professor of Chemistry

Surita R. Bhatia - Third Member of Defense
Professor of Chemistry

Yizhi Meng - Outside Member of Defense
Assistant Professor of Materials Science and Engineering

This dissertation is accepted by the Graduate School

Charles Taber

Dean of the Graduate School

Abstract of the Dissertation

Defining Polymer Structure Requirements for Activation of Mouse Sperm Acrosomal Exocytosis

by

He Huang

Doctor of Philosophy

in

Chemistry

Stony Brook University

2016

Acrosomal exocytosis (AE) in spermatozoa is a prerequisite for successful mammalian fertilization. However, the molecular mechanism of AE activation is still poorly understood. Mouse egg zona pellucida (ZP) terminal carbohydrate motifs are one of the primary inducers of AE. Previous studies in Sampson's group have employed ring-opening metathesis polymerization (ROMP) to synthesize polynorbornyl backbone homopolymers displaying sugar moieties to mimic the ZP terminal sugars. Polymers displaying mannose, fucose and GlcNAc are three effective inducers and each carbohydrate is proposed to have a distinct binding site on the sperm cell surface. In order to better reflect the complexity of the heterogeneous display of the ZP carbohydrates, different polymeric architectures have been designed with variations in polymer backbone flexibility, inter-ligand spacing, ligand density, and formation of "multidomain" structures. Glycopolymers with the more flexible cyclooctene backbone were synthesized via ROMP in order to define polymer backbone requirements for activation of mouse sperm AE. To confirm the

different flexibilities of norbornene (NB) and cyclooctene (COE) backbones, the conformations of glycopolymers in their aqueous solution state were characterized by small angle X-ray scattering (SAXS). Poly(NB)s form rigid or flexible cylinders. However, poly(COE)s demonstrate much more flexbility than poly(NB)s and form random coils or collapsed strucutres. Furthermore, the efficacy of polymers to activate AE were determined through a triple-stain flow cytometry method. The results revealed that poly(COE)s displaying fucose and GlcNAc were less effective inducers of AE in comparison to their norbornene backbone counterparts. Whereas, poly(COE)s with mannose polymers were the most effective AE inducers. Copolymerization of effective ligands with biologically inert ligand were utilized to tune the ligand density. The potencies of AE induction suggest that the ability of these random copolymers to induce AE does not decrease as the effective concentration decreases. Additionally, block copolymers were used to build hetero-structure combinations of two effective ligand motifs. But there was no synergic induction of AE. In summary, the induction of mouse sperm in AE by polymers with different architectures further support each sugar has their independent ligand-receptor interaction.

Table of Contents

List of Figures

List of Tables

List of Schemes

List of Abbreviations

AC	adenylate clyclase
Ac	acetyl
ADAM	a disintegrin and metalloprotease
AE	acrosomal exocytosis
AMP	adenosine monophosphate
ATRP	atom transfer radical polymerization
BSA	bovine serum albumin
cAMP	cyclic adenosine monophosphate
CatSper	sperm-specific Ca^{2+} channel
COE	cyclooctene
DBU	1, 8-diazabicyclo[5.4.0]undec-7-ene
ddI H_2O	distilled and deionized water
DIC	differential interference contrast
DIEA	N,N-diisopropylethylamine
DMAP	4-dimethylaminopyridine
DMSO	dimethyl sulfoxide
Et_2O	diethyl ether
EtOAc	ethyl
Fuc	fucose
Glc	glucose

GlcNAc	D-N-acetylglucosamine
GPC	gel permeation chromatography
h	hour
IP_3	1,4,5- inositol triphosphate
Man	mannose
Mn	number-average molecular weight
Mw	weight-average molecular weight
N_2	nitrogen gas
NB	norbornene
NMR	Nuclear magnetic resonance
PBS	Phosphate-buffered saline
PI	propidium iodide
PKA	protein kinase A
PLCβ1	phospholipase C β1
PLCγ	phospholipase C γ
PMA	phosphmolybdic acid
ppm	parts per million
ROMP	ring opening metathesis polymerizaiton
rt	room temperature
Ru	ruthenium
SANS	small angle neutron scattering
SAXS	small angle X-ray scattering
SBTI	soybean trypsin inhibitor

Sp56	sperm protein-56
THF	tetrahydrofuran
TLC	thin layer chromatography
UV	ultraviolet
ZP	zona pellucida

Chapter 1 Introduction

1.1 Overview of Male Infertility

Infertility remains a highly prevalent global condition. 15% of couples in the world are affected by infertility, amounting to 48.5 million couples.[1] 50% of cases overall are male-related.[2] With a steadily increasing world population, infertility problems have distressed a significant proportion of humanity.

Conventional methods for the prediction of male fertility are based on sperm features such as sperm morphology, motility and counts.[3,4] However, conventional semen analysis cannot precisely diagnose fertility or infertility or determine or molecular defects in spermatozoa because it does not assess sperm function.[5] There are still a significant portion of patients with normal and abnormal semen analyses showing unexplained infertility.

The development of new approaches to optimize fertility prediction in human and domestic animal species beyond conventional tools is extraordinarily important. The ability of spermatozoa to fertilize any oocyte needs to be investigated at the molecular level to answer the global concern of male infertility. The acrosomal exocytosis (AE) testing based on sperm physiology, involving capacitation and acrosomal exocytosis, has been shown to be a stable parameter of sperm function.[6] In a recent report, calcium ionophore-induced acrosomal exocytosis results have been shown to be a reliable indicator of fertility potential in addition to routine semen analysis for selection of patients for conventional IVF treatment cycles.[7] However, the mechanism of the arosomal exocytosis induced by ionophores differs from the physiological acrosomal exocytosis induced by the zona pellucida. The development of universal molecular probes to understand the acrosomal exocytosis mechanism at the molecular level is urgently needed. Furthermore, the probes could be a very useful tool for examination of sperm fertility.[8]

1.2 Mammalian Fertilization and Sperm Acrosomal Exocytosis

1.2.1 Overview of mammalian fertilization

Mammalian fertilization is the fusion of the male and female gamete through a sequence of coordinated molecular events, shown in **Figure 1-1**.[9] The maturation of the oocyte is required to achieve successful fertilization. The oocyte or the egg complex is arrested at metaphase of meiosis II and the size reaches about 20 μm in diameter. It is surrounded by two cell layers. The first layer is extracellular matrix-- the zona pellucida (ZP). The mouse ZPs consist of three glycoproteins, ZP1, ZP2 and ZP3. The glycoproteins are synthesized and secreted by the oocyte. The outer layer is the cumulus cells, which is granulosa cells enriched with hyaluronic acid.[10-11]

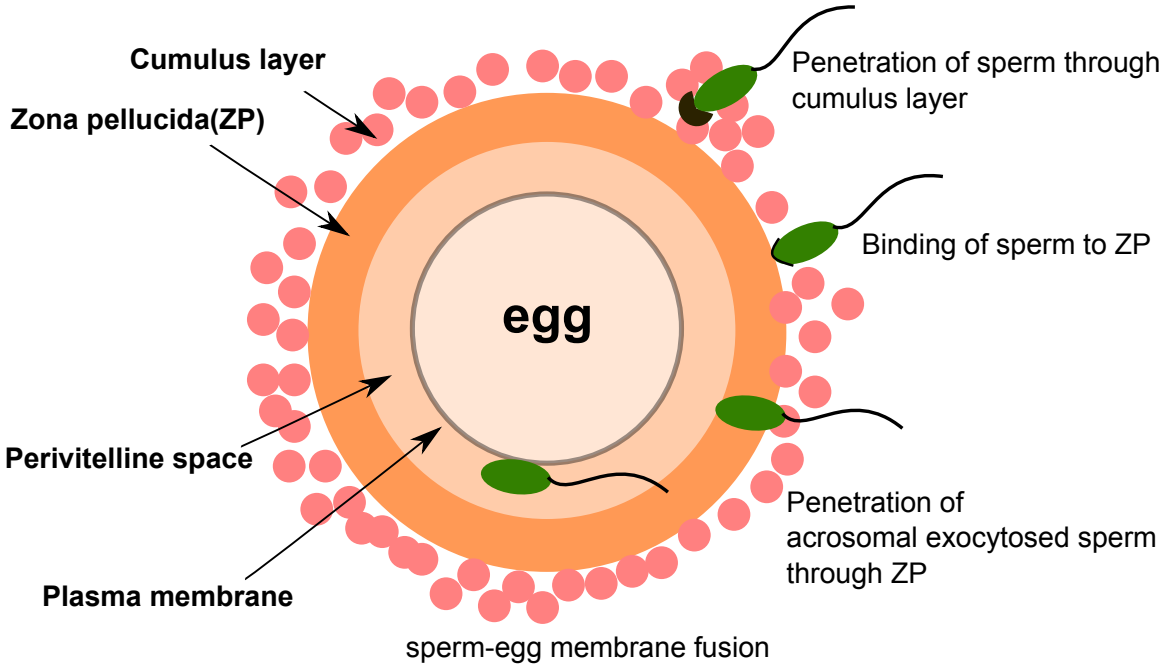

Figure 1-1. Mammalian Fertilization

There are four stages of fertilization. First, the sperm get capacitated and penetrate through the ZP layer. Second, the sperm reach the perivitelline space of the egg. Third, the merging of the sperm with the egg, cell adhesion and membrane fusion between sperm and the egg take place

followed by cortical reaction. Finally, the pronuclei and the intermingling of the maternal and paternal chromosoes are fused to form an zygote.[12]

1.2.2 Sperm preparation: capacitation and acrosomal exocytosis

1.2.2.1 Sperm structure

Sperm is the male gamete and consists of two major parts, a head, and a tail. The head of normal sperm has an oval shape and the three dimension sizes are 3-5μm long, 2-3μm wide and 1.5μm thick. The head contains the nucleus and the acrosome (**Figure 1-2**).[13] The sperm head is covered by four types of membrane: the plasma membrane, the outer acrosomal membrane (OAM), the inner acrosomal membrane (IAM) and the nuclear envelope.

The sperm acrosome is located at the anterior half of the sperm head and enclosed by the OAM and IAM. It is subdivided into the anterior acrosome (AA) and posterior acrosome (PA) or the equatorial segment (ES), which is the gamete fusion site. During acrosomal exocytosis, the hydrolytic enzymes contained in the acrosome are released. The compacted DNA stored in the nucleus, is covered by the nuclear membrane and the metascosome sheath. The tail consists of a total of ten pairs of fibrils and is responsible for the typical sperm motility. The head and the tail are connected by the mid-piece, where the cellular elements, centroles, microtubules and mitochondria are stored.[9]

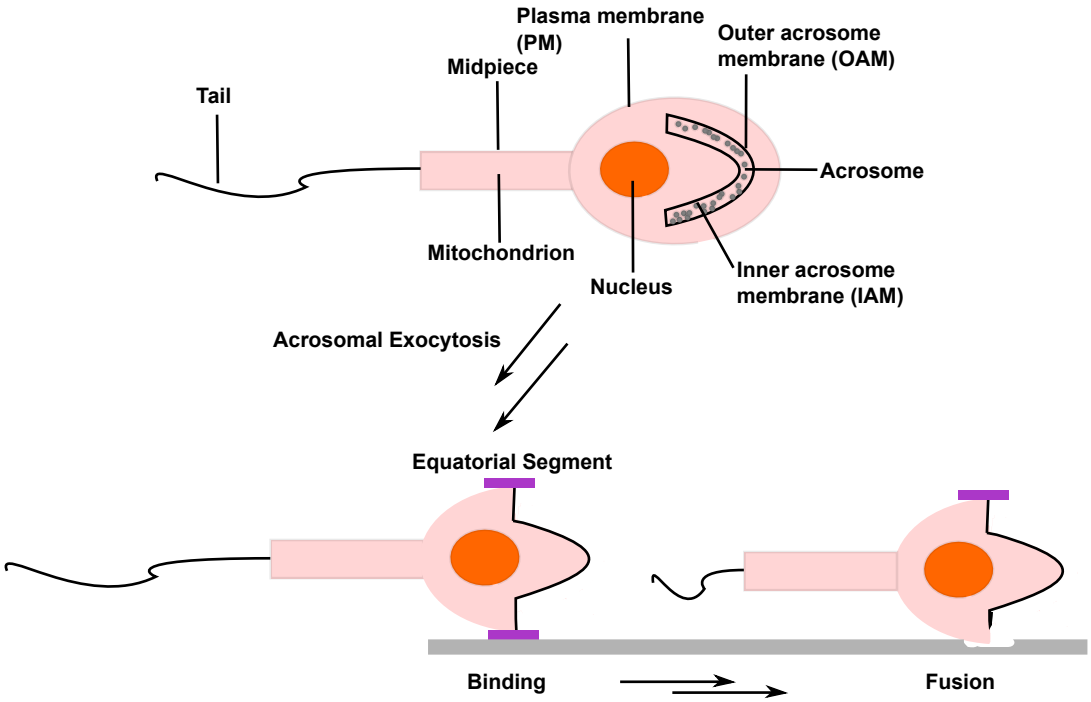

Figure 1-2. Sperm Structure

1.2.2.2 Sperm capacitation

Freshly ejaculated spermatozoa that are motile are still unable to fertilize the oocyte. Upon ejaculation, the environment in the female reproductive tract can alter the spermatozoa state physiologically, a process called capacitation. Capacitation encompasses a number of processes, such as plasma membrane reorganization, ion permeability regulation, cholesterol loss and changes in the phosphorylation state of many proteins.[14] The sterol-binding proteins present in the oviduct can accelerate cholesterol efflux from sperm, resulting in an increase in membrane fluidity.[15-16] Also, the bicarbonate concentration in the seminal plasma/female reproductive tract is higher than that in epididymal environment. In addition, CO_2 is converted to HCO_3^- by sperm extracellular glycosyl phosphatidylinositol-anchored carbonic anhydrase IV in the female oviduct. The high HCO_3^- concentration activatives the sperm soluble adenyl cyclase (sAC) in a pH-independent manner and promotes HCO_3^- transporters to deliver HCO_3^- into sperm cells.[17-18]

Subsequently, both the intracellular cAMP and HCO_3^- levels are elevated due to the HCO_3^- activation. Increase of cAMP then induces phosphorylation of protein kinase A (PKA)[19] to increase flagellar beating and sperm motility. Moreover, the level of intracellular Ca^{2+} and pH[17] are elevated during capacitation.[19-20] Inhibitory factors, including glycoproteins, seminal plasma proteins and membrane cholesterol, are removed. Subsequently, the sperm are hyperactivated and have swimming capacity.[21,13] Upon completion of capacitation, spermatozoa are ready to undergo acromomal exocytosis.

1.2.2.3 Sperm acrosomal exocytosis

Capacitated spermatozoa are competent to migrate through the layer of cumulus cells and then bind to ZP layer to activate the acrosome reaction. Since the acrosome is a single and huge vesicle, the fusion of the outer acrosomal and sperm plasma membrane occurs at multiple sites (**Figure 1-3**). The exocytosis follows conserved principles of calcium-regulated exocytosis in neurons or other neurosecretory cells, including the initial vesicle docking/ priming steps and calcium triggered SNARE-mediated membrane fusion.[22] However, the topology and kinetics are distinct from those exocytotic process in neuroendocrine cells.[23]

Initially, the secretory stimulus triggers a calcium increase through a fast process. But the acrosomal swelling is the rate determining step in the kinetics of acrosomal exocytosis. After the swelling is completed, the fusion pores open and the hybrid vesicles release in seconds.[23] Different inducers initiate membrane fusion in different patterns. The binding of sperm to ZP results in an ordered fusion pore formation. The fusion starts at the posterior acrosomal region and consistently proceeds in an anterograde direction. The progression is zipper-like. Whereas, the fusion simultaneously starts at random different locations if the sperm are treated with calcium

ionophore.[24] A number of proteases are released during membrane fusion. Acrosin is the major released serine protease, and digests a path for the sperm through the ZP for decades.[25] Recent advances in understanding acrosin demonstrated that the acrosin is located on the IAM and converts into active form as a result of acrosomal exocytosis (AE).[26] The role of the acrosin is still under investigation. As a final point, the oocyte-recognition protein Izumo on the sperm surface becomes exposed upon AE, and allows the sperm-egg membranes to fuse.[27]

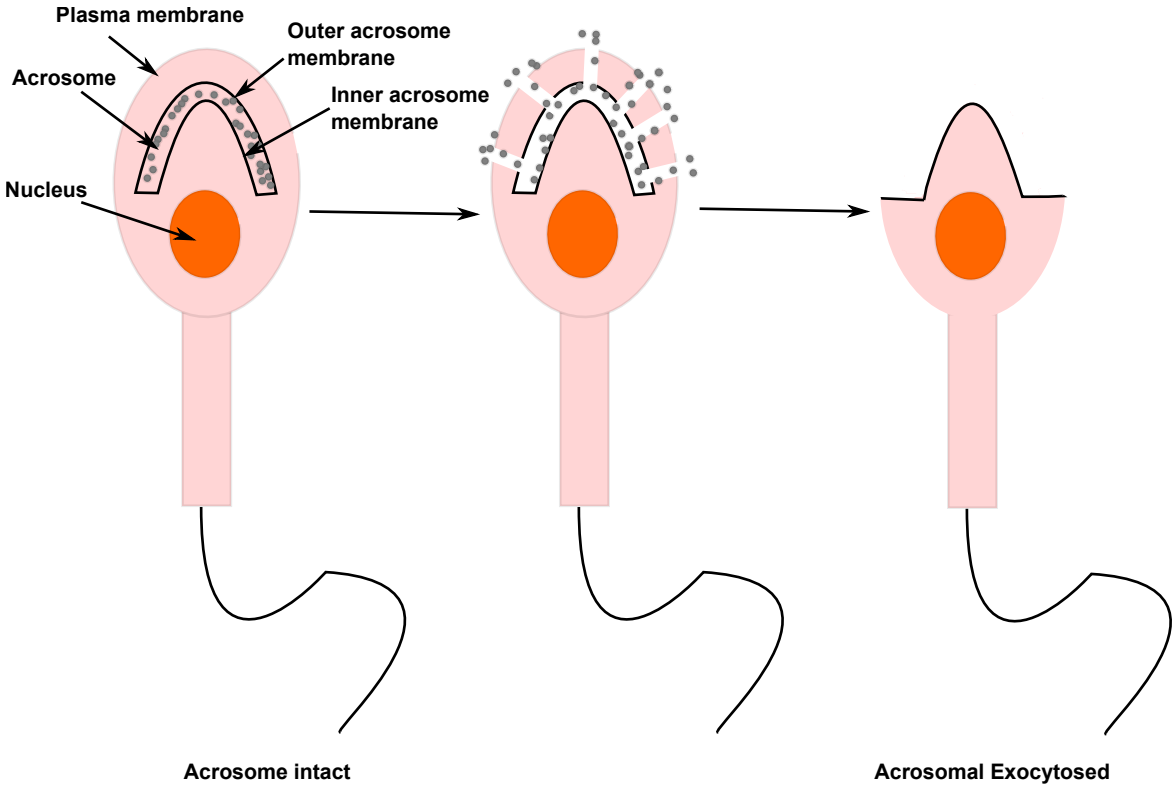

Figure 1-3. Sperm Acrosomal Exocytosis

1.2.3 Sperm- egg binding and cortical reaction

After sperm are acrosome reacted, fusion with the plasma membrane of the oocyte takes place in the microvilli-rich region around the egg.[28-29] After the inner acrosomal membrane of sperm is

exposed upon acrosomal exocytosis, the posterior head of the sperm attaches and fuses to the oocyte.[30] Fertilin α,β and cyritestin, known as ADAM1, ADAM2 and ADAM3, are the key molecules involved in the gamete binding.[30] This family consists of a signal sequence domain, a metalloprotease domain, a disintergrin-like domain, a cysteine-rich domain and an epidermal growth factor-like repeat. ADAMs are not essential for binding but enhance adhesion.[31]

The receptors for sperm ADAMs on the egg surface include α6β1[32] and CD46. An integrin-associated protein, CD9 is essential for sperm-egg interactions and CD-9 deficient mice show reduced fertility.[33] Another sperm-specific protein, IZUMO is essential for sperm-egg membrane binding and fusion.[34] As regards oocytes, JUNO is a member of the folate receptor family and recognizes the sperm IZUMO, facilitating fertilization.[27]

Once the sperm fuses with the oocyte, the sperm stop moving immediately and the oocyte release the contents of cortical granules to block polyspermy.[12] The fusion of sperm and the oocyte membrane appear to cause the polymerization of actin and microvilli extension. The sperm instead is drawn into the oocyte by elongation and fusion of the microvilli of the egg. As a result, the sperm nucleus and other organelles are incorporated into the oocyte cytoplasm. The actin filaments are essential for the attraction of the sperm into the oocyte. The cytoplasm swells and forms egg colliculus (~ 7 microns in length and 2 microns wide) resembling a so-called fertilization cone.[35]

1.3 Sperm Acrosomal Exocytosis Activation

1.3.1 Acrosomal exoctyosis inducers

The Zona Pellucida (ZP) has been considered as an “inducer” or “stimulator” of acrosomal exocytosis for a long time, attributable to the presence of receptors for sperm in ZP. These

receptors, to a large extent, restrict binding of sperm from heterologous species and can be detected by *in vitro* fertilization assays using solubilized egg ZP.[36] The ZP of mammalian eggs is composed mainly of three glycoproteins, two of them, ZP2 and ZP3, assemble into long filaments, while the other, ZP1, cross-links the filaments into a three-dimensional network.[37]

Traditionally, it was thought sperm-ZP binding is a simple ligand-receptor binding, like one ZP protein binds one sperm ligand. This concept seems to be oversimplified. Pioneering work by Wassarman *et al* indicated that a ZP glycoprotein in mice--mZP3 was the receptor to which acrosome-intact sperm bind.[38] However, later research suggested that ZP3 receptor/sp 56 present on sperm was not essential for fertilization in mice.[39]

Studies on ZP3 have demonstrated that it is the sugar terminus on oligosaccharide that induces acrosome reaction not polypeptides of ZP3 protein.[40] Galactose at the nonreducing terminus of O-linked oligosaccharides of mouse egg zona pellucida glycoprotein ZP3 is essential for glycoprotein's sperm receptor activity.[41] Mannose, N-acetylglucosamine, N-acetylgalactosamine, when attached to a protein backbone, can mimic mouse ZP3 glycoprotein and induce acrosome reaction, while glucose or galactose do not.[42] Lewis X-containing neoglycoproteins mimic the intrinsic ability of ZP3 to induce the acrosome reaction in capacitated mouse sperm.[43] Ultrasensitive mass spectrometric analyses revealed that the sialyl-Lewis X sequence is the most abundant terminal sequence on the N- and O-glycans of human ZP.[44] However, sialyl-Lewis X binding did not induce AE. Additionally, the sugar ligand-fucosyl residue is required for a high affinity sperm-binding ligand, which may also be involve in activation of acrosomal exocytosis.[45]

In addition to the ZP, non-physiological inducers, including calcium ionophore and lectins, can activate AE in spermatozoa *in vtro*. For *in vitro* studies, the physiological inducers, including

progesterone, prostaglandins, sterol sulfate, and glycosaminoglycan have been employed as AE inducers.[21]

1.3.2 Signaling pathway to induce acrosomal exocytosis

There are many different inducers the acrosomal exocytosis. However, the mechanism behind this exocytosis remains elusive.[46] ZP matrix is a generally accepted natural agonist, which initiates the acrosome reaction upon the binding of the sperm. Thus, the ZP-induced AE signaling pathway have been proposed by Gupta et al[47] (**Figure 1-4**). There are several different receptor-mediated signaling pathways in the sperm plasma membrane responsible for ZP-induced AE. G_i protein-coupled receptor pathway are involved in the induction of AE.[48] Subtypes G_{i1} and G_{i2} are selectively responsible for the signaling pathway.[49] However, the receptors which activate sperm G protein are still undefined.

The coupling of G-protein with the corresponding receptors are intracellular second messenger system as well as calcium ionic conductance. One possible signaling pathway of G-protein-coupling is activation of the phospholipase $C_{\beta1}$($PLC_{\beta1}$). One downstream signaling pathway involves the activation of adenylate cyclase that increases cyclic adenosine monophosphate (cAMP) levels.[50] Subsequently, the tyrosine phosphorylation is followed by phosphorylation of protein kinase A.[51] The other downstream signaling pathway involves increasing levels of 1, 2-diacylglycerol (DAG) and inositol 1, 4, 5- triphosphate (IP_3). The increase of DAG may be followed by phosphorylation of protein kinase C(PKC). The binding of IP_3 to its receptor results in release of intracellular calcium stores.[52]

ZP-induced AE is also dependent on a sustained release of calcium, involving an elevation in [Ca^{2+}] mediated primarily by T-type voltage-operated calcium channels (VOCC).[53] The depolarization of the sperm membrane from -60 mV to -30 mV opens the T-type VOCCs and leads to calcium influx into the sperm cell. The participation of L-type VOCC has also been proposed.[54-55] The activation of sodium/proton (Na^+/H^+) exchange pump is another possible cascade to lead to alkalinisation and acrosomal exocytosis.[56] As a final point, the plasma membrane and outer acrosome membrane undergo fusion.

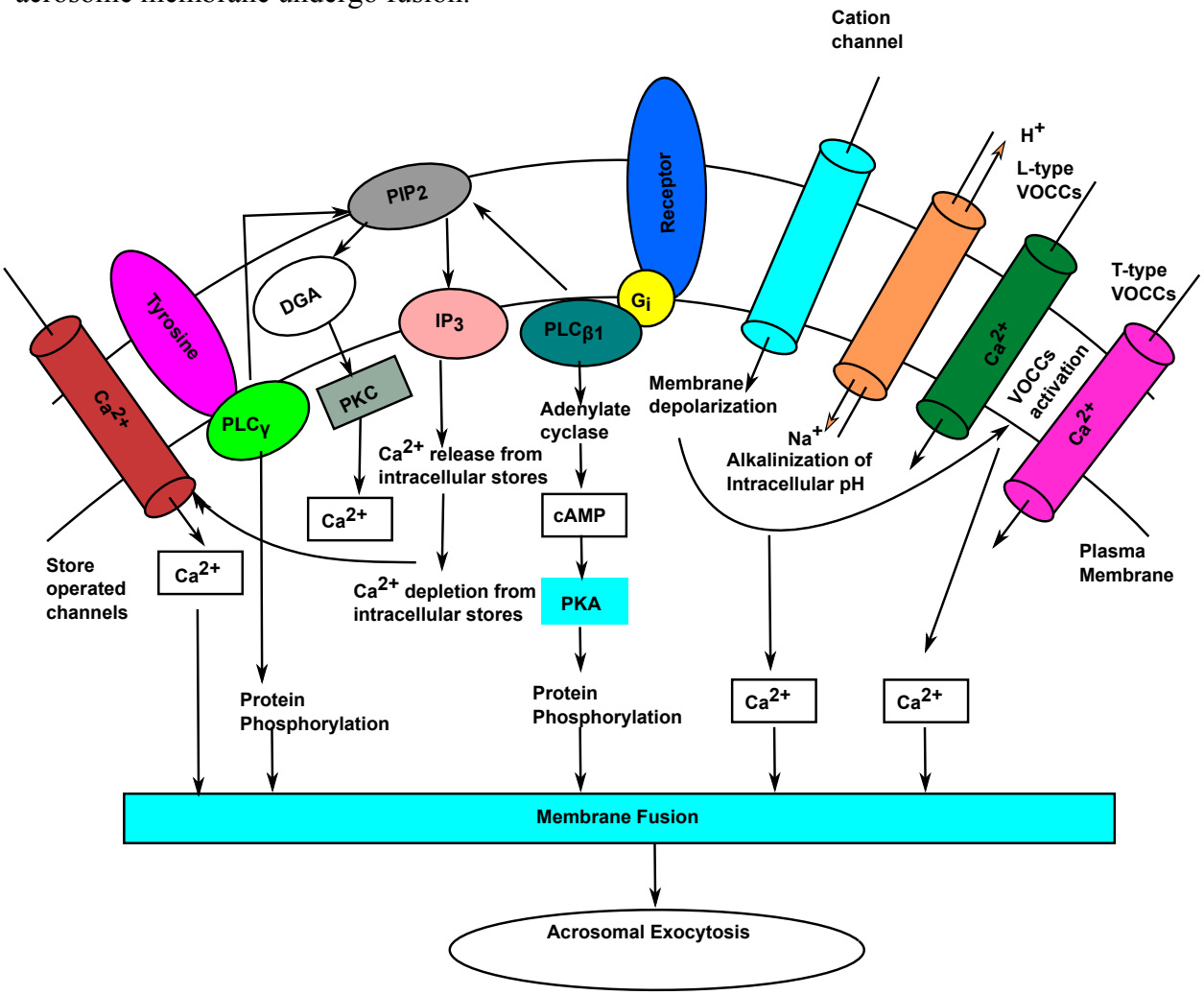

Phospholipase $C_{\beta1}$: $PLC_{\beta1}$, cyclic adenosine monophosphate: cAMP,
1, 2- diacylglyceroal: DAG, inositol 1, 4, 5- triphosphate: IP_3, voltage-operated calcium channel: VOCC

Figure 1-4. ZP-induced Signaling Pathway of AE

1.3.3 Unresolved problems in sperm acrosomal exocytosis activation

Although intense efforts have been made to study sperm acrosomal exocytosis, there are still many underlying molecular mechanisms largely unknown.[46] One of the most critical questions about induction of AE is where and when does the AE occur under physiologically normal circumstances if ZP is not the inducer? Does acrosomal exocytosis take place in response to ligand binding of a receptor and what is the signal to trigger exocytosis? [46] In Sampson's group, the elegant ring-opening metathesis polymerization (ROMP) polymer chemistry has been utilized to synthesize glycopolymers[57] with alterations in ligand valency, density and architecture, so that complexity of the ligands can be mimicked. The strategy provides an easy method to study the ligand-receptor events[58] in initiation of AE and the signaling pathway related to initiation.

1.4 Multivalent Interactions and glyconanomaterials

1.4.1 Multivalent interactions

The individual carbohydrate ligands binding to their lectins or receptors are very weak and the interactions are enhanced by multivalency of ligands. The phenomenon was first observed referred to as the "cluster" or "multivalent" glycoside effect.[59] It has found a wide range of application in biology and medicine. Synthetic glycoconjugate (glycopolymers) with presentation to multivalent ensembles has been an attractive strategy to mimic natural carbohydrate in enhance the binding affinities,[60] selectivity of glycan interactions,[61] as well as set thresholds for triggering signaling responses.[62]

However, the model of multivalent interactions is still poorly understood. Thermodynamically, the binding conditions are more complicated. The model was studied by Mammen *et al*[63] and

derived from the monovalent binding of a ligand to the receptor. In monovalent system, there are only two states: bound and unbound. The thermodynamics are determined by the free binding enthalpy (ΔG_{mono}). The entire entropy changes are the sum of the changes in the solvation, rotation, and translation entropy ($\Delta S_{mono} = \Delta S_{trans} + \Delta S_{rot} + \Delta S_{sol}$).[64] In the multivalent binding system, the binding conditions should be determined before the calculation of the free binding enthalpy $\Delta G_{LR}^{(n)}$. The conditions are far more complicated than bound and unbound states. In this situation, the first ligand-receptor binding is entropically more difficult due to the interconnection between ligands. Therefore, some translation (ΔS_{trans}) and rotation entropy (ΔS_{rot}) are already reduced at the first step. Furthermore, there are some loss of the conformational entropy (ΔS_{conf}) for spacer.[63] Therefore, the change in the entropy of the *n*-fold binding has the same contributions as the monovalent binding of a single ligand except conformational entropy. Furthermore, the enthalpy of monovalent binding (ΔH_{mono}) increase was considered in a multivalent binding regardless of the spacer ($\Delta S_{multi} = n\Delta H_{mono}$). So that the difference in the free binding enthalpies is represented in **Equation 1**.

$$\Delta\Delta G = \Delta G_{LR}^{(n)} - n\Delta G_{mono} = T(n-1)\,\Delta S_{mono} - t\Delta S_{conf} \qquad \textbf{(Equation 1)}$$

Accordingly, the flexibility of the spacer would cause a large loss of conformation entropy so the cooperative effect would be reduced comparing to a rigid spacer. Additionally, the large number of binding ligands would favor the binding events due to the entropy.[63] However, it is still very unrealistic to assume that the spacer has no enthalpic contribution to the binding. The preorganization of the ligand due to the spacer may reduce the enthalpy. What is more, a spacer may directly affect the characteristics of the ligands and the binding affinity.[64] Therefore, in the

future, not only the number of ligands but also the flexibility[65] and spatial proximity of the spacer need to be considered the multivalent system.

It is also very difficult to forecast the binding mode kinetically. In order to assess chelate cooperativity, a bivalent ligand binding to a bivalent receptor event (**Figure 1-5**) was proposed by Ercolani *et al*.[66] Assuming that the number of ligands is in a large excess to the receptors, the first step of the interaction is the monovalent attachment of the ligand BB to protein AA with the association constant 4*K*. The formation of partially bound open complex o-AABB is followed by two possible steps. The other B component of the ligand BB can bind to the o-AABB and the full bound 1:1 cyclic complex are formed through intramolecular binding assoiciation K_{intra}. Alternatively, a second ligand BB can to bind and form a 1:2 crosslinking complex $AA(BB)_2$. Subsequent binding events, such as crosslinking and precipitation, will take place based on various conditions. The microscopic intermolecular association constant *K* accounts for the strength of the binding interaction. Microscopic effective molarity *EM* represents the ease of the intramolecular process. The tendency of a divalent ligand to form the cyclic complex c-AABB is expressed by $K_{intra.}K_{intra}$ can be expressed as ½ *K EM*, where ½ is the statistical factor for the cyclization process. *K* is the microscopic intermolecular association constant, and *EM* is the microscopic effective molarity. The linker with highest values for *EM* are suggested to be perfectly fitting.

The case of the binding of a *n*-valent ligand B to an *n*-valent receptor A to form a 1:1 multicyclic complex c-^{n}A•^{n}B can be derived from the bivalent binding model. It is assumed that the presence of ligands is in large excess of the receptors and the cooperativity is 1. EM values are also regarded as the same among the identical constituent rings. The presence of the intermediate states are not considered because of chelate cooperativity in multivalent binding models. There are the unbound and fully bound species shown in the system (**Figure 1-5**). The factor β depends on

a statistical factor multiplied by the ratio of the *EM* to the ligand concentration, raised to the degree of cyclicity of the assembly. It is evident that although the *EM* is not by itself a measure of chelate cooperativity, it is the key structural parameter on which β is dependent. As the degree of cyclicity is increased, chelate cooperativity becomes more and more sensitive to ligand concentration when $\beta \approx 1$.[66]

In a biological system, the cooperativity α and enhancement factor β are used to explain the multivalent interactions. In the positive cooperativity situation, the binding of the second ligand to the second receptor occurs with a more favorable free energy than the binding of the first ligand to the first receptor, which is not very common. The examples are given in the binding of GM1 to the cholera toxin system, where the binding constant of the first ligand was 4 times lower than the binding constant of the second ligand. Therefore, the binding event was enhanced enthalpically. The negative cooperativity was more common in the polyvalent system. Whitesides and co-workers proposed an enhancement factor β to characterize a multivalent binding effect. Since in many cases, the number of ligand-receptor interactions is unknown and α cannot be generated. The calculation of β is not limited and is derived from the ratio of the binding association constant for the multivalent binding [K_{multi}] of a multivalent ligand to a multivalent receptor with binding association constant [K_{mono}] of a monovalent ligand to a multivalent receptor.[63]

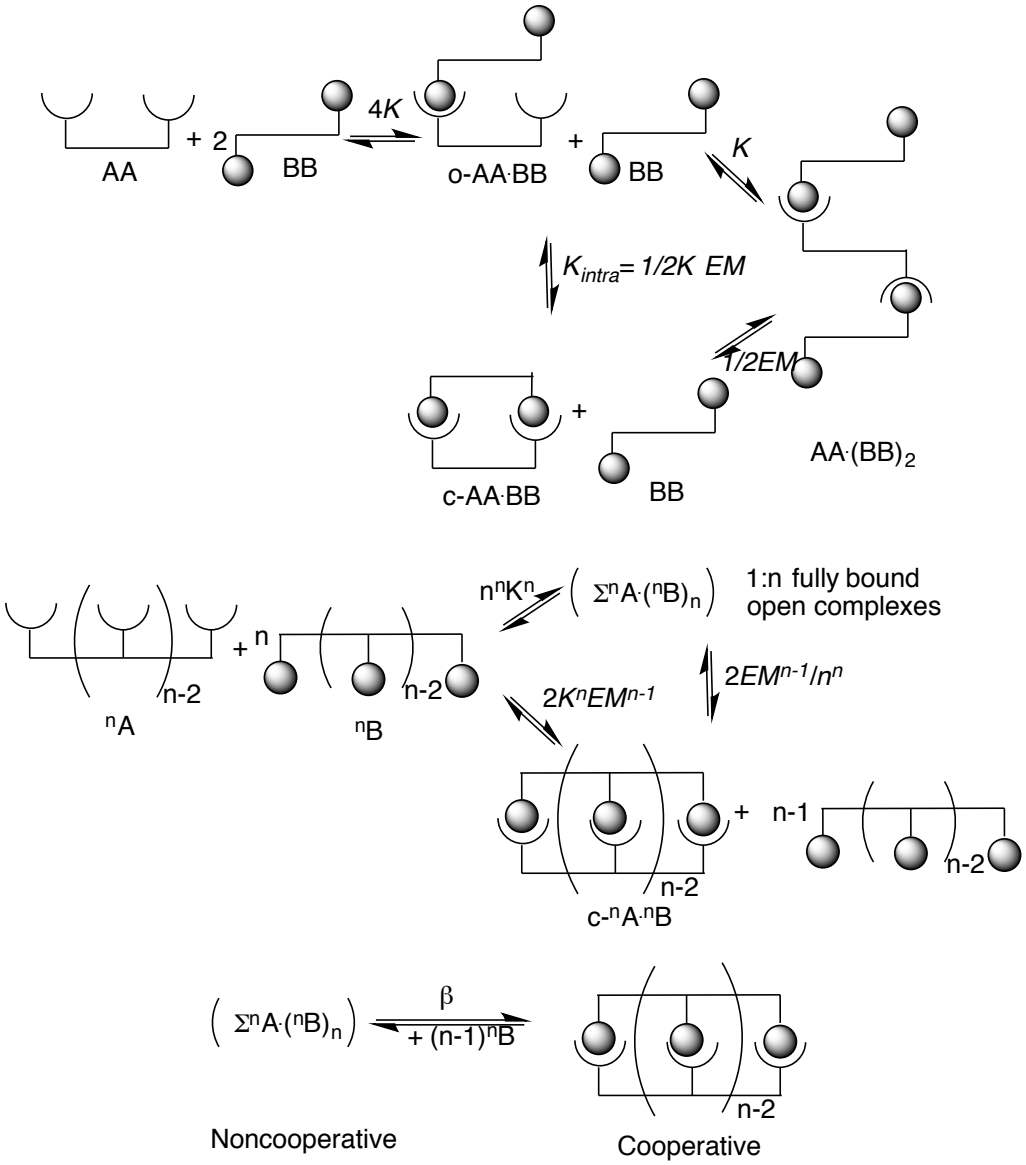

Figure 1-5. Bivalent and Multivalent Binding Models

1.4.2 Current glyconanomaterials

1.4.2.1 Overview of carbohydrate role in biological processes

Glycans, which are compounds that include monosaccharides, oligosaccharides, polysaccharides and their conjugates such as peptidoglycan, glycolipids, and glycoproteins are ubiquitous components of all organisms.[67] Given the enormous diversity of glycans and their complexities of structures in nature, there are two broad biological roles of glycans in nature. Glycans are important structural and modulatory components of living cells. Furthermore, carbohydrate- carbohydrate interactions (CCIs) and carbohydrate-protein interactions (CPIs) play critical roles in many biological process .[68]

The saccharides bind weakly to their receptors and the complexity of the saccharides result in highly variable and unpredictable CCIs and CPIs. In order to increase binding strengths, synthetic glycoconjugates have been widely adopted to develop multivalent systems that mimic the natural complexity of interactions.[69] The study of complexity of glycan roles in CPIs has also been exploited by heterogeneous glycoconjuates.[69] Recent advances in glycoonjuates have demonstrated a particular focus on illustrating the role of glycans as stabilizers of complex architectures. There are various scaffolds shown in **Figure 1-6** to support glycoconjuates, including organic macrocycles,[70-71] dendrimers,[72] nanoparticles,[73] and polymeric backbones.[69] Also, the supramolecular systems could be built based on different individual glycol-clusters.[74] Each scaffold has unique benefits and provides a platform to assemble complex sugar architectures, so that glycoconjugate become an important tool in investigation of glycan-related biological processes.[74]

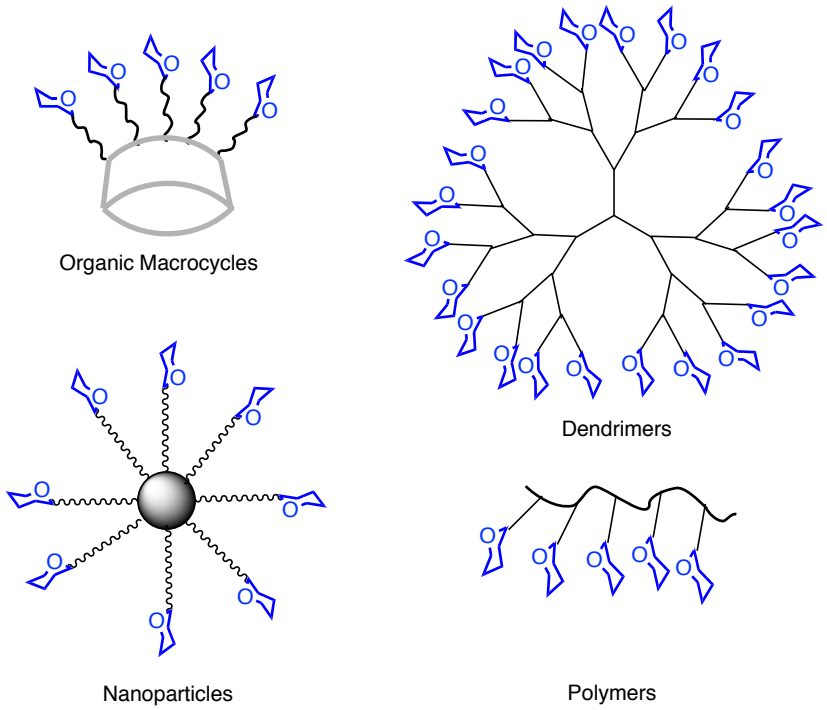

Figure 1-6. Glycoconjugate Structures

1.4.3 Glcyopolymers

1.4.3.1 Overview of glycopolymers

Given that the polymer backbone can display the greatest variation in valency, ligand spacing as well as overall architecture, intense efforts have been exploited in the glycopolymer field based on elegant polymerization developments.[62] Glycopolymer syntheses have been carried out by either polymerization of glycomomers or post-modification of polymers.[60] Living polymerization, such as nitroxide-mediated radical polymerization,[75] atom-transfer radical polymerization (ATRP),[75] reversible addition-fragment chai transfer (RAFT) polymerization,[76] and ring-opening metathesis polymerization (ROMP),[77] provide stratigies to synthesize well-defined glycopolymers with narrow molecular weight. By the combination of living polymerization and click chemistry, different strategies have been developed for the efficient synthesis of glycopolymers.[78]

1.4.3.2 Features of glycopolymers

1.4.3.2.1 Glycopolymer valency and ligand density

The length or the valency of a glycopolymer can affect its functional affinity as well as its ability to cluster receptors.[62] Current living polymerizations provide a tool to predict and control the length of glycopolymers easily.[77, 79] It has been proven that glycopolymers with varied length and valency can affect the signal transmission differently. The optimized length can be determined according to the experimental results. The length of glycopolymer has been suggested to influence lectin binding and ligand-receptor interactions for signal transduction (**Figure 1-7**).[79-81] In the previous studies from our group[57] with varied valency glycopolymers, longer glycopolymers more effectively transmitted signals to induce mouse sperm AE than shorter polymers. Five monosaccharides implicated in mouse sperm acrosomal exocytosis were selected as ligands. Homopolymers with different lengths, 10-mers and 100-mers, were synthesized via ROMP. Their efficacy of AE induction in mouse was dependent on the lengths of the polymers. Only the polymers with sufficient length could induce sperm mouse AE. Therefore, the lengths of polymers can uncover the importance of the valency displayed on the backbone in signal transduction.

Altering the density of glycans on a polymer backbone is another important strategy to affect the glycopolymer functional affinity. Studies employing glycopolymer ligands can complement those using natural glycans, whose variation in density can influence their activity.[82] Generally, there are two ways to alter the density of carbohydrate epitope by inserting a biologically inert monomer. The first method is copolymerization of a monomer bearing the effective epitope with a non-effective epitope. Alternatively, post-polymerization one can functionalize a polymer with the carbohydrate ligand and a biologically inert ligand.[83] The effect of ligand density on the

multivalent events depend on the various system. For example, the advidity and ability of glycopolymers to cluster ConA increased when the density of mannose on the polymer backbone increased.[84]

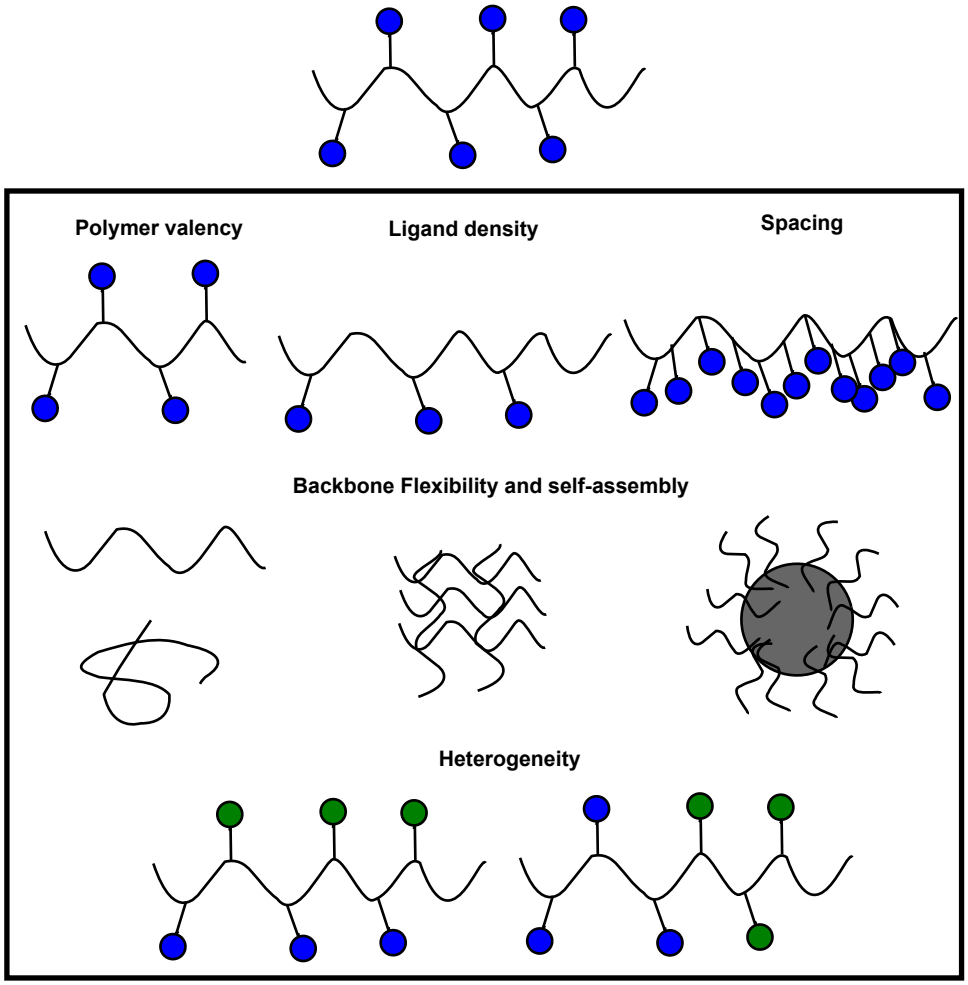

Figure 1-7. Glycopolymer Architecture

1.4.3.2.2 Glycopolymer architecture

Generally, the architecture of polymers includes the rigidity of the polymer and other self-assembled structures.[60] Polymeric structures with various flexibility in backbones can impact their binding affinity to the receptor. Longer and more flexible scaffolds can adjust their structure more

easily to maximized the binding event.[85] Rigid polymers with correct spacing might reduce a decrease in conformational entropy so that the ligands can bind to the receptors more tightly.[62] For example, Miura *et al*[86] demonstrated glycopolymeric hydrogels with different states bind to Con A. The stiff hydrogel showed the weakest binding affinity and the flexible swollen hydrogel binds to ConA more tightly. The flexible backbone allows the linear polymers to self-assemble into micelles, vesicles, nanoparticles and other aggregates.

Despite efficiently imitating functional ligand presentations in terms of valency and density, most of the reported glycoconjuates reflect little inherent heterogeneity of biological systems in the composition. Therefore, the heteroglycopolymers become one of the most useful tools to construct the complexity which mimics the natural biological systems. Then the potential contribution of synergistic or antagonistic effects to molecular recognition events can be estimated.[69] One needs to consider whether the biologically inert motif can bring any supplementary effect because of the hetero-multivalency. For example, the hetero- glycopolymers containing mannose and galactose were synthesized through click chemistry.[78] The competition assay with MC-SPR system were used to examine whether the glycopolymers could inhibit DC-SIGN interactions with HIVgp120. Their study revealed that as mannose composition increased, the avidity and the inhibition increased. Although a saturation effect cannot be ignored, the results may also suggest the existence of synergic interactions involving the galactose.[87] A polymer-supported focused library of hetero-bifunctional ligand has been generated to study the antagonists of cholera toxin. The weak binding ligands revealed the potential to complement the affinity of galactose for cholera toxin by binding to a complementary binding site on the protein surface.[88]

1.5. Synthesis and Characterization of Glycopolymers

1.5.1 Ring-opening metathesis polymerization (ROMP) of glycopolymers

1.5.1.1 Development of synthetic polymers and current advances

There are two general categories of polymerization reactions: chain and step polymerization. A living polymerization is a special chain-growth polymerization with absence of chain-transfer and chain-termination reactions. In an ideal case, the rate of the chain initiation needs to be similar or faster than the rate of propagation, so that the initiator is consumed at the early stages of polymerization and each polymer chain starts to grow at approximately the same time. The monomer should be added irreversibly. When all the monomers are consumed, the active catalyst sites remain intact and can continue to grow if a second monomer is added.

Therefore, in a living system, the polymer molecular weight M_n increases in a linear fashion dependent on monomer conversion. And the final molecular weights can be precisely controlled through the stoichiometry employed. As a result, the living polymer produces a narrow weight distribution, which can be quantified in terms of dispersity index ($Đ_M$). $Đ_M$ is the ratio of weight-average molecular weight M_w, and number-average molecular weight M_n, M_w/M_n. Living systems are characterized by a $Đ_M$ between 1.0 and 1.1. The absence of chain termination and chain transfer provide access to controlled polymer chain growth and well-defined macromolecular architectures, which may be highly valuable in biomedical and biotechnological applications.[89] There are different kinds of living polymerization routes providing various polymer architectures, including living anionic (ROMP), cationic and radical polymerization. Ring-opening metathesis

polymerization catalyzed by ruthenium-catalyst generates low $Đ_M$ and accurate molecular weight linear polymers.

1.5.1.2 Ring-opening metathesis polymerization

Ring-opening metathesis polymerization has emerged as a powerful and broadly used tool to synthesize polymers with numerous applications in biological, electronic and mechanical areas.[90] The catalysts in ROMP are tolerant to many functional groups and the living fashion polymerization allows the synthesis of block copolymers. Ring-opening metathesis polymerization (ROMP) is a chain growth polymerization process where a mixture of cyclic olefins is converted to a polymeric material. The mechanism of ROMP is based on metal-mediated olefin metathesis, with a metal alkylidene intermediate and the unsaturation is conserved. A typical ROMP mechanism has three key steps: 1) initiation, 2) propagation, and 3) termination as shown in **Figure 1-8**.[90] The polymerization is initiated by the coordination of a transition metal alkylidene complex to a cyclic olefin. Subsequently, [2+2] cycloaddition affords a four-membered metallacyclobutane intermediate. The highly strained four-membered ring will effectively form the beginning of a growing polymer chain through a cycloreversion reaction to afford a new metal alkylidene. Even if the resulting complex has increased in size, its reactivity toward cyclic olefins is similar to the initiator. Therefore, analogous steps are repeated during the propagation stage until polymerization ceases. Living ROMP reactions are commonly quenched deliberately through the addition of a specialized reagent, which can selectively remove and deactivate the transition metal from the end of the growing polymer chain, and install a known functional group in place of the metal. Generally, we use ethyl vinyl ether as the quench reagent. The driving force behind the ROMP of

cyclic olefins is the release of strain energy, encompassed by the enthalpic term, ΔH, in the equation ΔG = ΔH- TΔS.

Initiation:

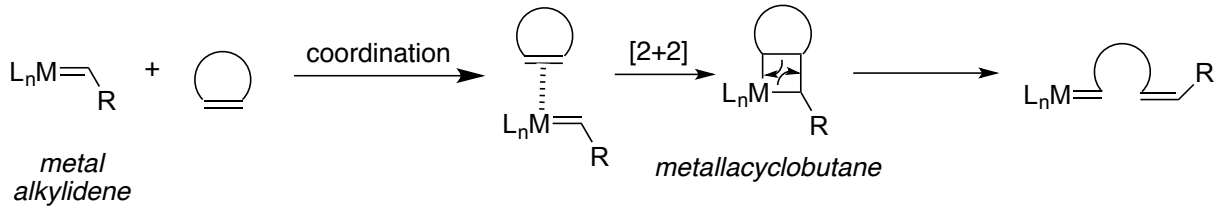

Propagation:

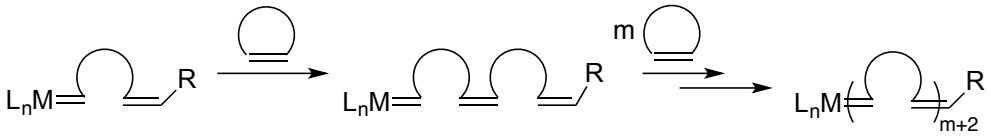

Termination:

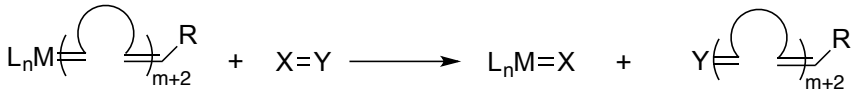

Figure 1-8. Mechanism of a typical ROMP reaction

Monomer concentration and reaction temperature are intimately associated with thermodynamics of ROMP. For every cyclic olefin monomer, there exists a critical monomer concentration above which polymerization will occur at a given temperature. Performing the ROMP at low temperature can mitigate the entropy loss inherent to all polymerizations and drive the reaction to high molecular weight polymer. Low temperatures, however, require catalysts with higher activities. The reaction is driven from monomer to polymer by release of strain associated with the cyclic olefin balanced by entropic penalties. Thus, the most common monomers used in

ROMP are cyclic olefins which possess a considerable degree of strain (> 5 kcal/mol) such as cyclobutene, cyclopentene, cis-cyclooctene, and norbornene (**Figure 1-9**)[91].

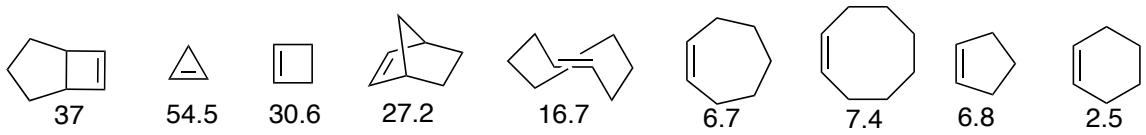

Figure 1-9. Ring strains of common cyclic olefins

Like most late transition metals, Ru shows low oxophilicity, which makes it inherently stable toward many polar functional groups. A new class of Ru-based catalysts was developed including 3rd generation Grubbs catalyst (**Figure 1-10**). This class has NHCs with weakly coordinating pyridines, and so exhibits extremely improved initiation rates. The ROMP reaction with 3rd generation Grubbs catalyst provides highly controlled molecular weights and $Đ_M$ as low as 1.06.

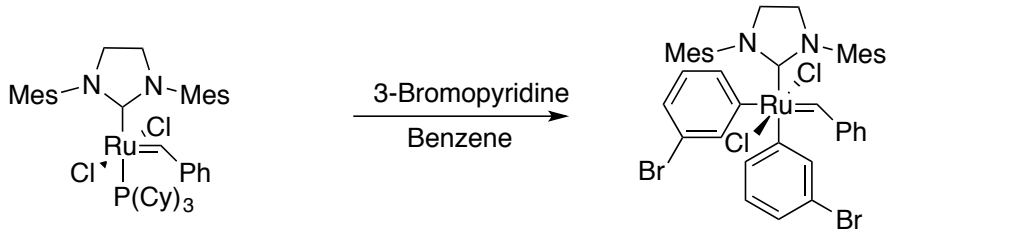

2nd Generation Grubbs Catalyst

3rd Generation Grubbs Catalyst

Figure 1-10. Synthesis of 3rd Generation Grubbs Catalyst

In Sampson's group, ruthenium-catalyzed ROMP has been used for investigating the mechanism of sperm-egg interaction for a long time. Baessler and Lee *et al*[92] have established a family of linear ROMP-derived peptide-displayed polymers to determine the length and spacing requirements for maximal polymer affinity or avidity for the egg. Wu *et al*[57] built a library of homo-glycopolymers to investigate sperm acrosome reaction. Song *et al* [93]has described a new

highly alternating polymerization of cyclobutene 1- carboxylic esters with cyclohexene derivatives by ROMP, which provide a broad scope for synthesis of random, block and alternating copolymers by ROMP.[94]

1.5.2. Small-angle X-ray scattering (SAXS)

Small-angle X-ray scattering (SAXS) is a powerful tool in the study of biological macromolecules and nanocomposites in solution.[95-97] SAXS is a variant of conventional X-ray scattering in which X-ray scattering close to the incident X-ray beam is used to study ordering at longer length-scales (typically 5 to 100 nm). X-ray scattering from a material provides information about the local densities of electrons and atomic nuclei within that material. The advantage of the method allows study of the structure of native particles in near physiological environments and analysis of structural changes in response to variations in external conditions. In modern instruments, the beamstop is often equipped with intensity monitors to record the transmission simultaneously with the scattering pattern. Subsequently, the two-dimensional scattering pattern is radially averaged to obtain the one-dimensional scattering function I(q) as a function of the length of scattering vector, where

$$q=4\pi\sin\theta/\lambda \qquad \textbf{(Equation 1-2)}$$

λ is the wavelength of the incident beam (typically of the order~ 1), and the 2θ is the angle between the incident beam and the scattered radiation.[98]

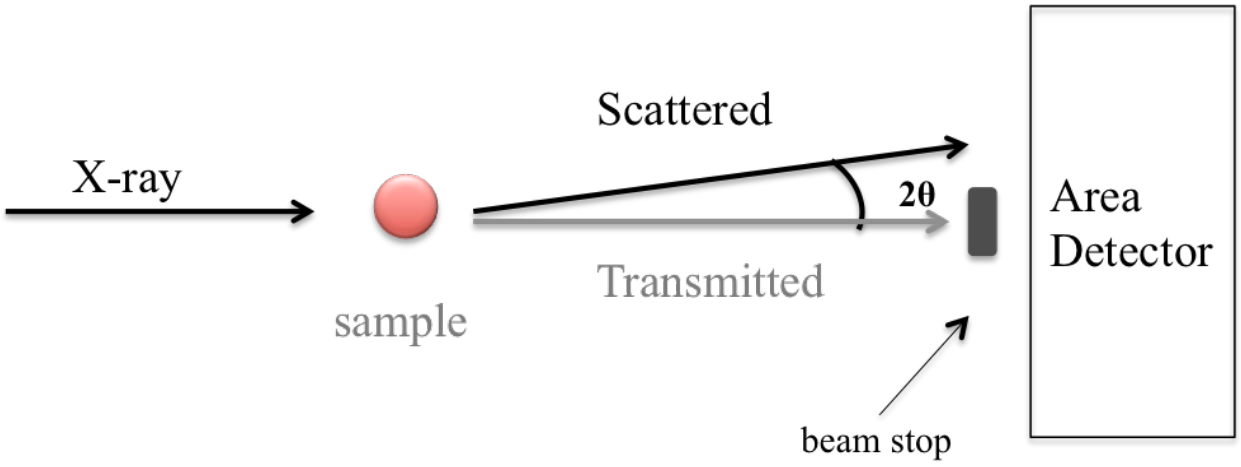

Figure 1-11. Small Angle X-ray Scattering

In a solution state, the scattering data of the whole sample and of the solvent are collected separately. The scattering intensity from the sample is derived from the subtraction of the solvent background ($I_{subtracted}(q) = I(q) - I_{background}(q)$). For those biological samples containing light atoms in which the density is only slightly higher than that of an aqueous buffer, SAXS instruments need to be optimized to provide lowest possible background.[96] In the polydisperse and interacting system, the scattering pattern can be summarized as a linear combination of the different components. For a system containing particles with similar shapes but different sizes, such as micelles, microemulsions, block copolymers or metal nanoparticles, the scattering intensity is the integration of the intensity from the whole system. Thus, the structural parameters of polydisperse systems are obtained by averaging over the whole particles.[95]

The overall parameters can be calculated through some well-developed methods. Guinier analysis[99] has been the most straightforward and important method to analyze the data at the first stage of data analysis. The radius of gyration R_g and the forward scattering $I(0)$ can be determined according to the Guinier equation (**Equation 1-3**):

$$I(q) = I(0) \bullet \exp(-1/3 R_g^2 q^2) \qquad \textbf{(Equation 1-3)}$$

In an ideal system, the Guinier plot ($\ln(I(q))$ vs q^2) should be a linear function, where the intercept gives the $I(0)$ and the slope provides the radius of gyration value R_g. This approximation is valid for reasonably small q values, typically in the range $qR_g < 1.3$. The radius of gyration provides information about aggregations between chains. Other analyses, such as Kratky plots ($q^2 I(q)$ vs q),[100] provide a method to explore chain conformations, for instance, the compactness of the chains and the extent to which they are behaving as Gaussian coils, or rods. More detailed models, such as those developed for polydisperse chains in ideal solvents and with excluded volume interactions, can be fitted if the data are of sufficient quality.

SAXS is often employed as a complementary technique, that when combined with other structural and biochemical methods, allows a fine structural description of particles under investigation. Therefore, the knowledge and practice of SAXS is widely adopted for those studies requiring refined information on function-structure relationships.[97]

Chapter 2 Defining Polymer Backbone Requirements for Activation of Mouse Sperm Acrosomal Exocytosis

2.1 Introduction

Carbohydrate-protein interactions are involved in a wide variety of biological processes, including fertilization[101-103] and implantation,[104] pathogen invasion,[105] immune response,[106-107] and cell growth regulation.[108] Despite weak affinities of individual carbohydrate-protein interactions, multivalent glycoconjugates, such as glycopolymers, glycodendrimers and glyconanoparticles, with multiple carbohydrate ligands can enhance overall binding avidity.[62, 109]

Synthetic glycopolymers provide access to a large variety of overall structures and are popular multivalent glycoconjugates due to their ease of synthesis. Different polymerization strategies provide varying polymer backbone rigidities as well as binding group spacing and density.[62] Flexibility of the polymer scaffold is one of the factors that can affect the biological activity of the glycoconjugate.[85] On the one hand, a rigid polymer with correct spacing may interact with receptors more exactly to avoid a conformational entropy penalty.[62] On the other hand, flexible polymers are more capable of adapting to protein interfaces and of clustering more carbohydrate-binding proteins.[86, 110] Therefore, the effect of the polymer backbone flexibility depends on the receptors engaged and their presented orientations on the backbone.[79]

We are interested in how polymer backbones affect induction of mouse sperm acrosomal exocytosis (AE) by glycopolymers. AE is a key step in mammalian fertilization and only sperm that have undergone AE can participate in the subsequent fertilization steps that lead to sperm–egg fusion.[12] Previous studies in our group[57] and others[42] have found that polynorbornene glycopolymers displaying mannose, fucose, or GlcNAc, or protein displaying mannose, GlcNAc or GalNAc can initiate AE *in vitro*. However, the identity of the sperm receptors remains unknown.

Here, we compare two glycopolymer backbones, polynorbornene and polycyclooctene, displaying the same sugars as inducers of AE. Both polymers are prepared through ruthenium-catalyzed ring-opening metathesis polymerization (ROMP). Polynorbonene backbones are widely adopted in polymer synthesis due to the high ring strain of norbornene and the high polymer rigidity that results from a cyclopentane in the backbone.[90, 111] Functionalized polycyclooctenes are of interest because the backbone can provide a longer interligand spacing along a flexible, acyclic backbone.[112] AE induction activity may be enhanced when the spacing between two ligands is increased, making the binding site more accessible. Moreover, polycyclooctenes are of interest since multiple positions can be substituted with different functional groups on the COE backbone.[113] Comparison of their structures by small angle X-ray scattering (SAXS) in the solution state and their activity as inducers of AE revealed that the polynorbornene backbone with a rigid cylindrical structure forms more effective inducers of AE than the polycyclooctene backbone. Our results demonstrate that activation of AE is dependent on scaffold structure as well as the same pendant sugar.

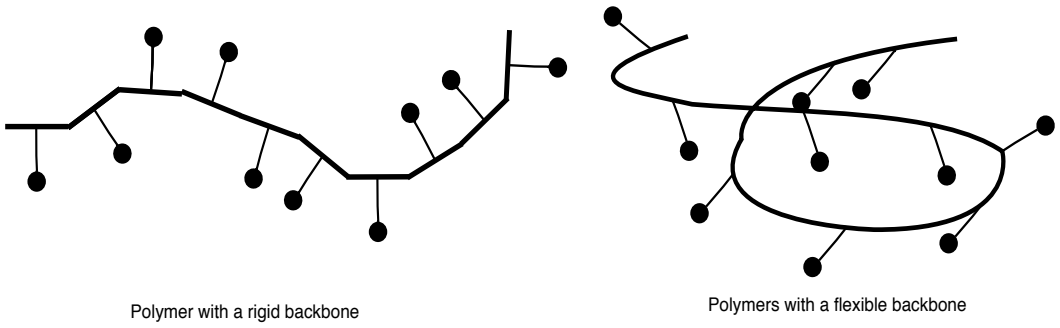

Figure 2-1. Polymers with different backbones

2.2 Results and Discussion

2.2.1 Synthesis of norbornene monomers

The modification of sugar monomers was required to be tolerated in ring-opening metathesis polymerization (ROMP).[90] Acetylated D-glucose and GlcNAc were commercially available and did not require further protection. Acetyl protected D-mannose was prepared by Dr. Linghui Wu. The fully protected L-fucose was synthesized from L-fucose. The synthetic routes to D-glucose and D-mannose norbornene linked monomers were repeated according to the published procedure.[57] Glucose monomer synthesis (**Scheme 2-1**) is taken as an example here. Starting from acetylated glucose, the acetyl group at the anomeric (C1) position is selectively deprotected by hydrazine acetate. In order to attach the linker via an *O*-glycoside linkage, a trichloroacetimidate group was introduced as a glycosyl donor at the C1 position in a basic environment. After the conversion, the modified C1 position underwent nucleophilic substitution by 2-chloroethanol with cleavage of the leaving group trichloroacetimidate to produce compound **6**. The chloride was easily converted to an azide group under Lewis acid mediated conditions. This synthetic route was suitable for synthesis of N_3-mannose (**Scheme 2-2**) and N_3-GlcNAc (**Scheme 2-3**).

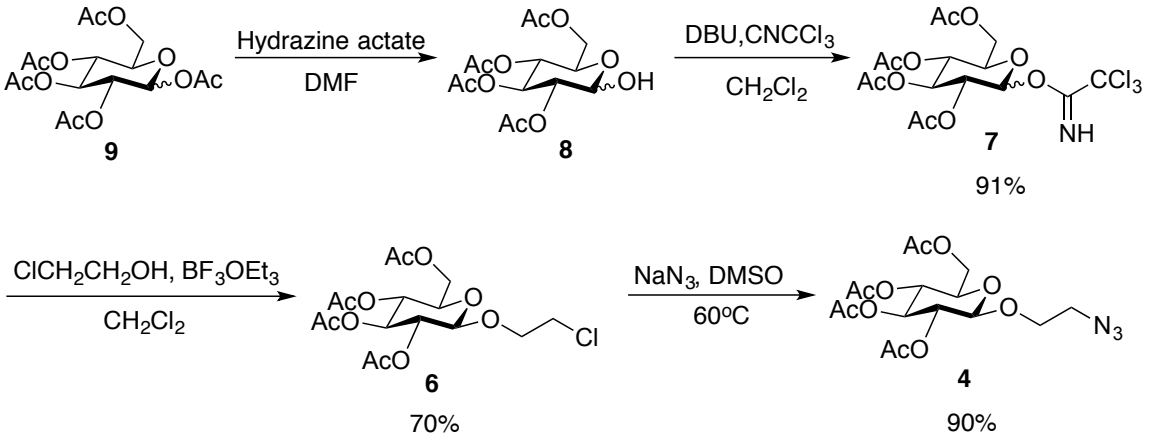

Scheme 2-1. Synthesis of N_3-Glucose

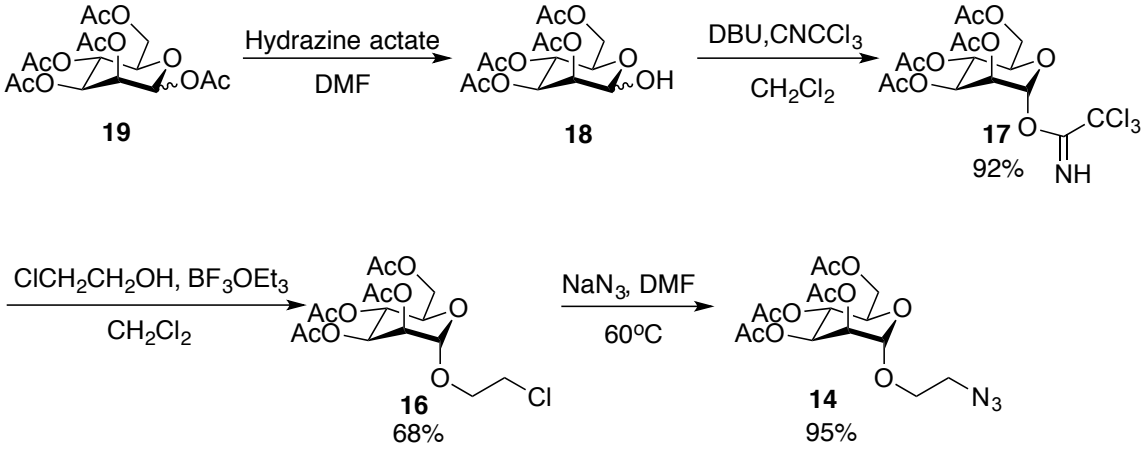

Scheme 2-2. Synthesis of N_3-Mannose

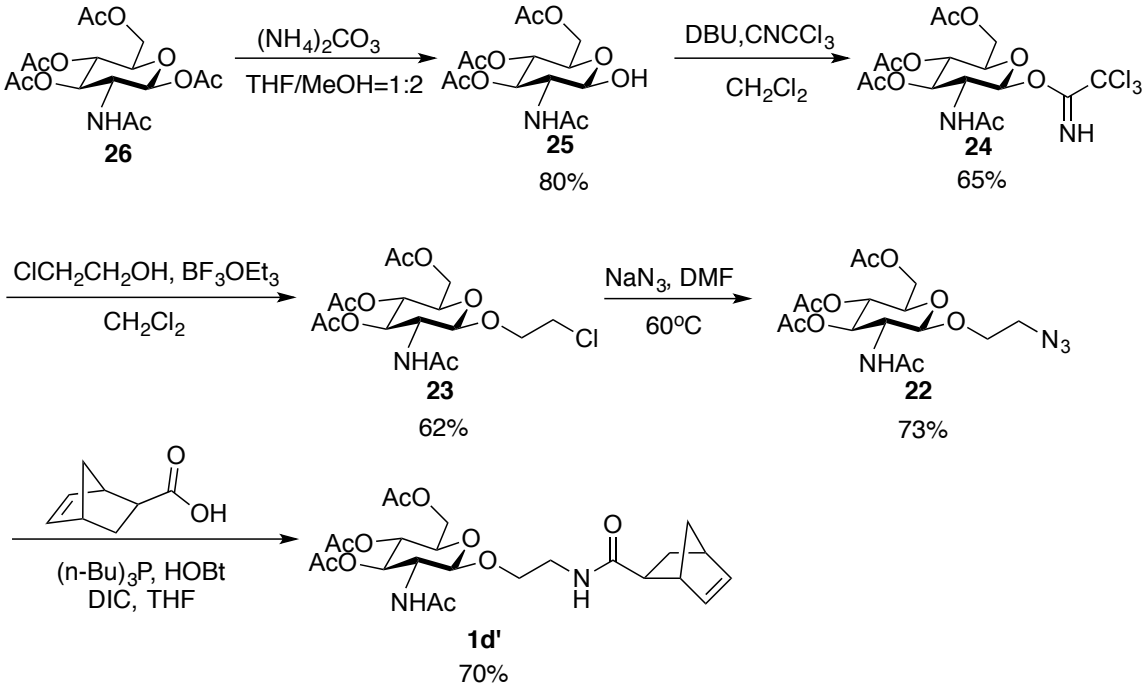

Scheme 2-3. Synthesis of NB-GlcNAc

According to a previous report,[114] the linker was directly added to the C1 position of fully protected sugars using 2-bromoethanol with excess Lewis acid (**Scheme 2-4**). Given that the anomeric carbon is electrophilic, 2-bromoethanol was able to displace the acetyl group. After overnight reaction, the yields were 74%, 75% and 83% for glucose, mannose and L-fucose, respectively. However, in the case of L-fucose, the attachment of bromoethoxy at position C1 was not stereospecific and produced both the α, β isomers in a 1:2 ratio. The β isomer was the desired mammalian saccharides occurring stereochemistry. These isomers could not be purified at this step and the mixture was carried through the whole process. Therefore, extra purification needed to be conducted to separate the two isomers in the last step and the yield was low for this reason. Furthermore, 2-bromoethanol was utilized instead of 2-chloroethanol in the previous synthesis scheme. Because bromide is a better leaving group than chloride, the reaction time was reduced from 3 days to 1 hour. Compared to the previous synthetic route, the modified method involved less steps and provided higher overall yields. This synthetic route was suitable for D-glucose (**Scheme 2-4**), D-mannose (**Scheme 2-5**), and L-fucose (**Scheme 2-6**).

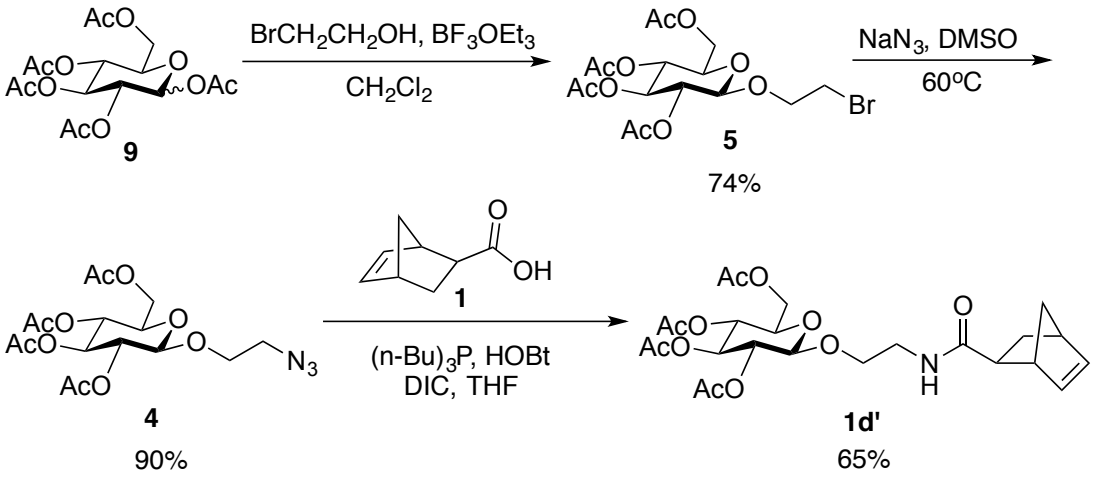

Scheme 2-4. Modified synthetic route to NB-Glucose

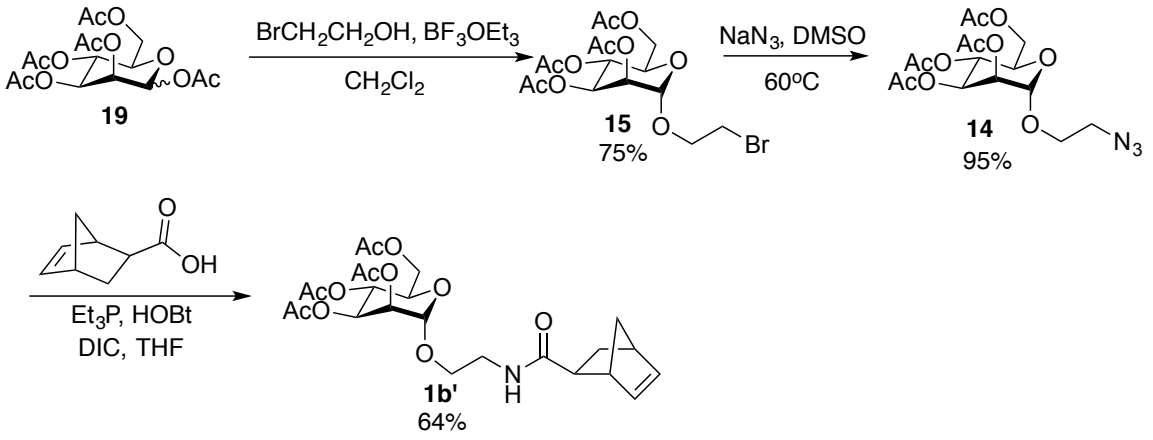

Scheme 2-5. Modified synthetic route to NB-Mannose

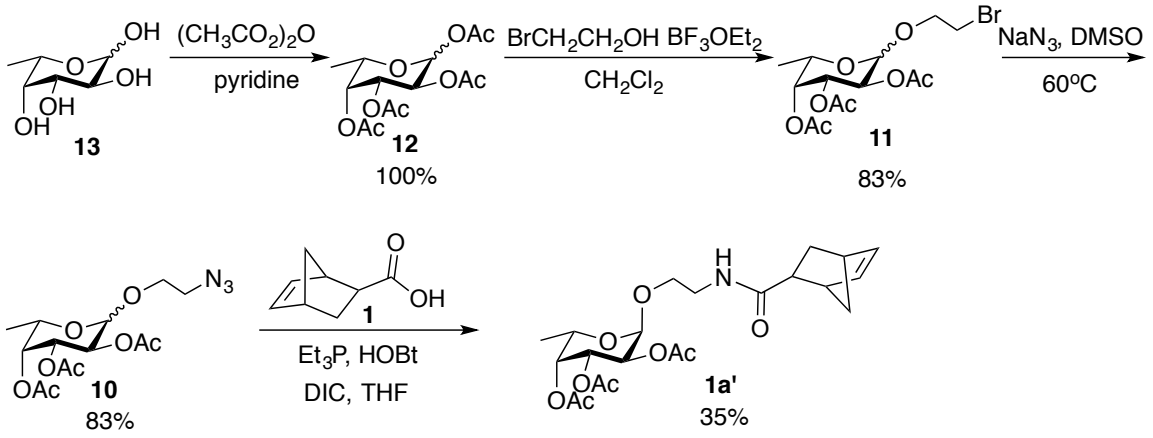

Scheme 2-6. Modified synthetic route to NB-L-Fucose

In the case of GlcNAc, the substitution of the acetyl group by 2-bromoethanol was inhibited because of the neighboring NHAc group at C2. Therefore, we designed another synthetic route for

NB-GlcNAc. In this route, the linker was coupled to the backbone first through conventional coupling reaction by using DIC and DIPEA. The fully protected GlcNAc was prepared as chloroimidate **24**, which presents a better glycosyl donor group at the anomeric position (**Scheme 2-7**). Finally, the sugar was attached to the linker-backbone conjugate **21** through a nucleophilic addition-elimination. However, the yield was relatively low for the last step.

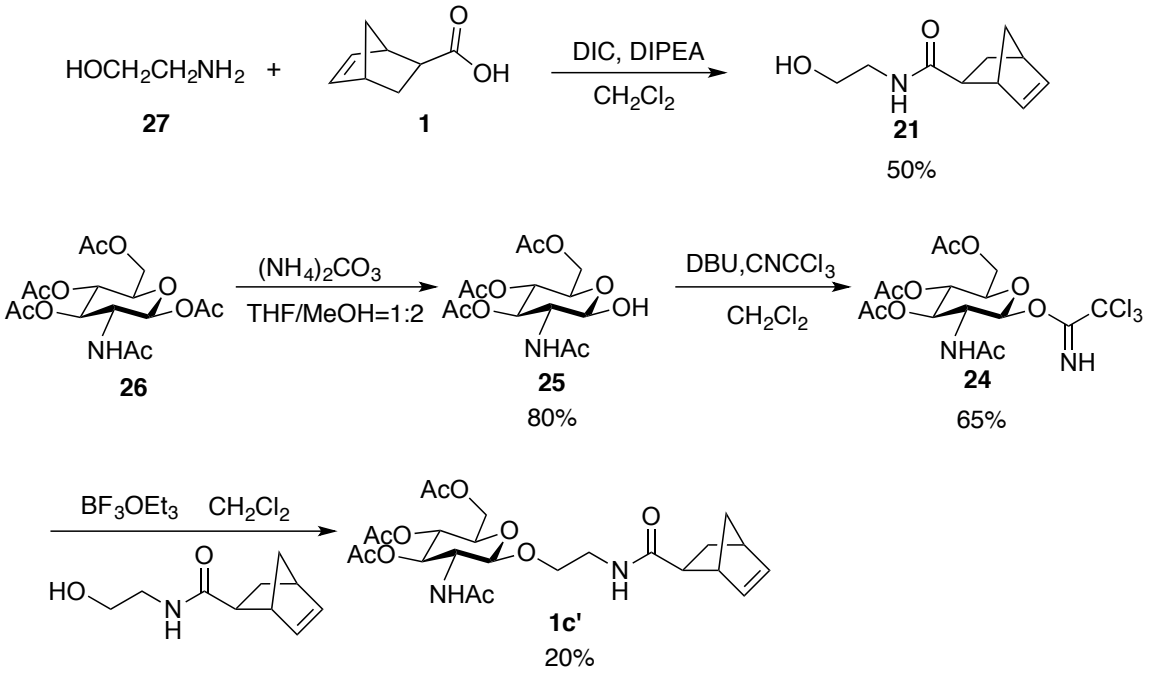

Scheme 2-7. Modified synthesis route to NB-GlcNAc

2.2.2 Synthesis of cyclooctene monomer

4-Cyclooctencarboxylic acid (**2**) was prepared by Dr. Maria Rodolis according to the procedure of Ashby and Coleman.[115] Then, the cyclooctene monomers were synthesized by following similar procedures as for synthesis of norbonene monomers. **Scheme 2-8** illustrates the Staudinger ligation between azide-GlcNAc and cyclooctencarboxylic acid.

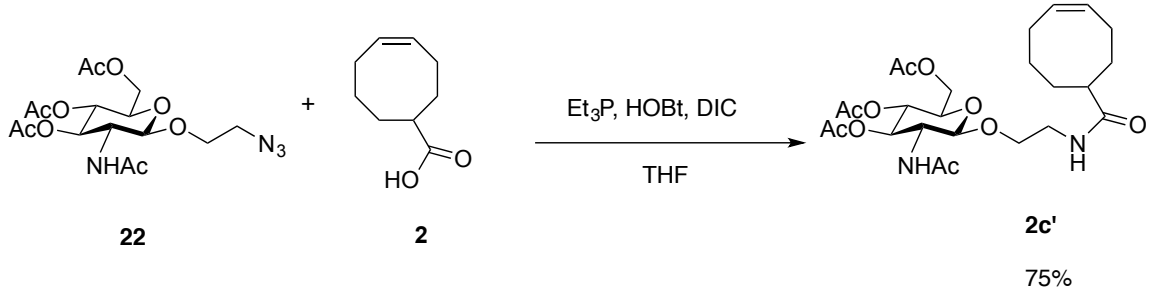

22 **2** **2c'**

75%

Scheme 2-8. Synthesis of COE-GlcNAc

2.2.3 Ring- opening metathesis polymerization(ROMP)

The ROMP of norbornene and cyclooctene polymers (**Scheme 2-9**) was conducted in dry CH_2Cl_2 using a 3rd generation Grubbs catalyst (**3**) at room temperature. Norbornene monomers were polymerized according to the literature.[57] Cyclooctene functionalized at carbon 5 with a sugar moiety proved to be very reactive in ROMP. 100% conversion was achieved in 15-20 minutes at room temperature. Extending reaction times beyond 20 minutes resulted in backbiting and resulted in the formation of shorter polymers. The dispersities were determined by GPC and the results are summarized in **Table 2-1**. In the final step, O-acetyl protecting groups on the sugars were removed via deacetylation under basic conditions. (**Scheme 2-9**)

Table 2-1. Dispersities of poly(**1'**)$_{100}$ and poly(**2'**)$_{100}$. [a] Determined from GPC utilizing a differential refractometer and a multiangle light scattering detector. [b] Data were characterized by Maria Rodolis.

Polymer	M_n^{theor}	M_n[a]	M_w[a]	$Đ_M$[a]
poly(**1a'**)$_{100}$	45497	27982	32676	1.15
poly(**1b'**)$_{100}$	51197	18657	21270	1.14
poly(**1c'**)$_{100}$	51097	30991	36260	1.17
poly(**1d'**)$_{100}$	51197	26880	31450	1.17
poly(**2a'**)$_{100}$[b]	46997	68495	77352	1.13
poly(**2b'**)$_{100}$[b]	52797	43094	53202	1.24
poly(**2c'**)$_{100}$	52697	59639	68235	1.14
poly(**2d'**)$_{100}$[b]	52797	35324	47892	1.36

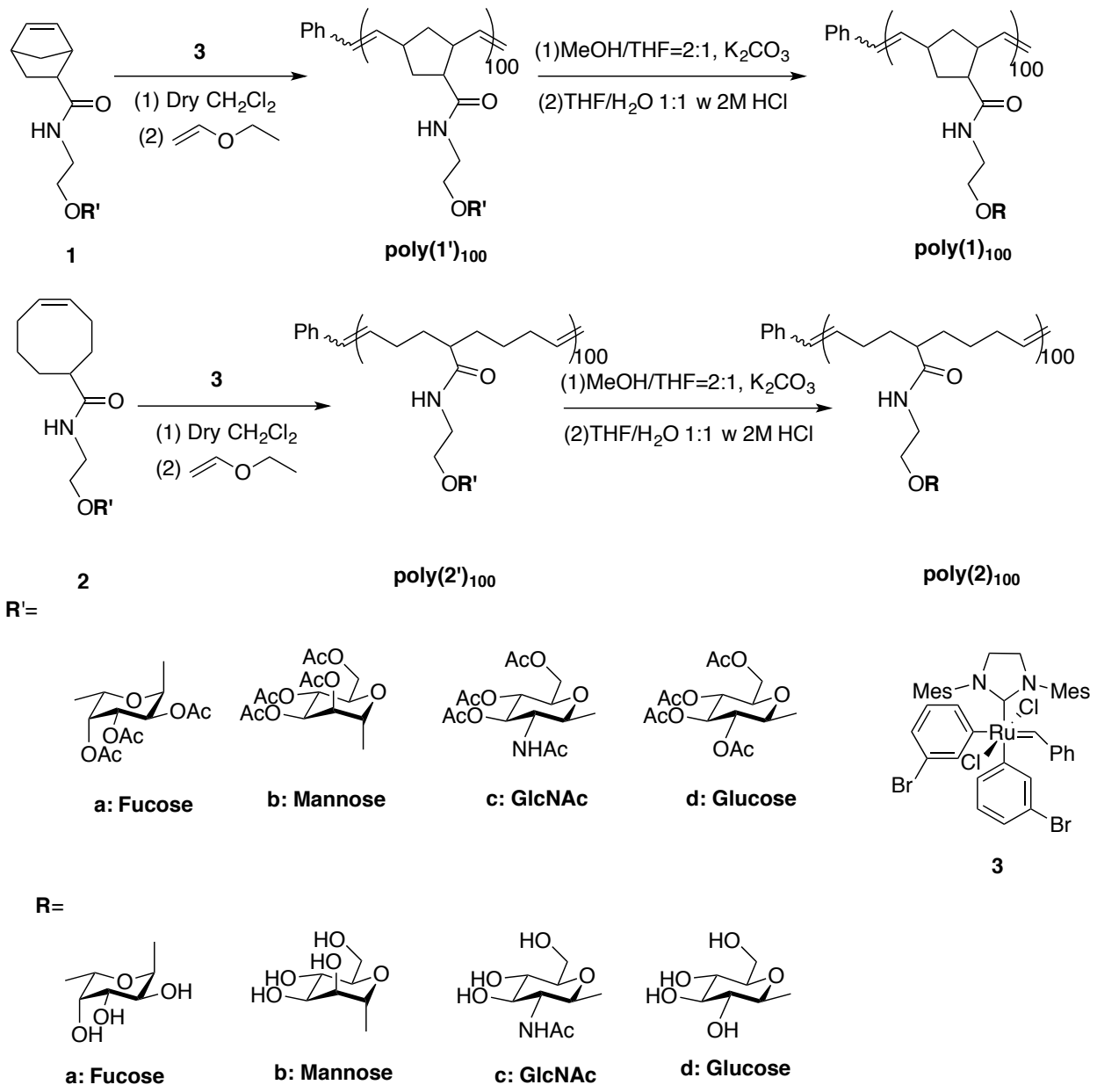

Scheme 2-9. ROMP and deacetylation of NB- and COE- glycopolymers

2.2.4 Comparison of polymer backbones as inducers of mouse sperm acrosome exocytosis.

Our previous studies demonstrated that polynorbornene backbone polymers with fucose, mannose, and GlcNAc ligands activated mouse AE through independent receptors that converge

onto the same intracellular signaling pathways. To further distinguish multivalent structure-activity relationships, we utilized a more flexible polymer backbone with a longer inter-ligand spacing and tested the effect on mouse sperm AE induction.

AE induction was measured at 5 μM, 10 μM, and 20 μM of polymers using the triple stain flow cytometry assay.[58] **Figure 2-2** illustrates the AE induction efficacy of polycyclooctene and polynorbornene displaying fucose, GlcNAc or mannose. Polymers displaying glucose were used as a negative control.

In previous work, we observed that for fucose polymers, poly(**1a**)$_{100}$ AE induction increased as the polymer concentration increased from 5 μM to 10 μM. At higher concentrations of poly(**1a**)$_{100}$, highly cooperative inhibition occurred and the AE induction dropped to around 27%.[57-58] This type of cooperative inhibition is diagnostic of a multivalent activation process that competes poorly with a second monovalent binding event at high concentrations of probe. Mannose and GlcNAc polymers poly(**1b**)$_{100}$ and poly(**1c**)$_{100}$ exhibited similar AE induction plateaus without cooperative inhibition.[57-58]

When these same sugar ligands were displayed on polycyclooctene through the same linker, the AE induction profile was distinct from that of the polynorbornene display. AE induction declined for fucose and GlcNAc cyclooctene backbone polymers. poly(**2a**)$_{100}$ induced less than 20% of AE at 5 μM. Although AE induction continued to increase at higher polymer concentrations, the maximal AE induction reached was about 40%, which was significantly lower than the 100% AE induction observed with poly(**1a**)$_{100}$.

The polycyclooctene displaying GlcNAc followed a similar trend. The level of AE induced by poly(**2c**)$_{100}$ increased when the polymer concentration increased from 5 μM to 20 μM. However,

the maximal AE induction observed with poly(**2c**)$_{100}$ was approximately 20%; significantly lower than the 100% AE induction by poly(**1c**)$_{100}$.[58]

In contrast, induction of AE by mannose cyclooctene polymers exceeded 100% at high concentrations. Although both poly(**1b**)$_{100}$ and poly(**2b**)$_{100}$ displayed strong AE induction, poly(**1b**)$_{100}$ induced an AE plateau of 70%-80% from 5 μM to 20 μM polymer,[58] whereas poly(**2b**)$_{100}$ barely induced AE at 5 μM, and induction increased dramatically upon increasing the polymer concentration to 10 μM and remained at a plateau up to 20 μM.

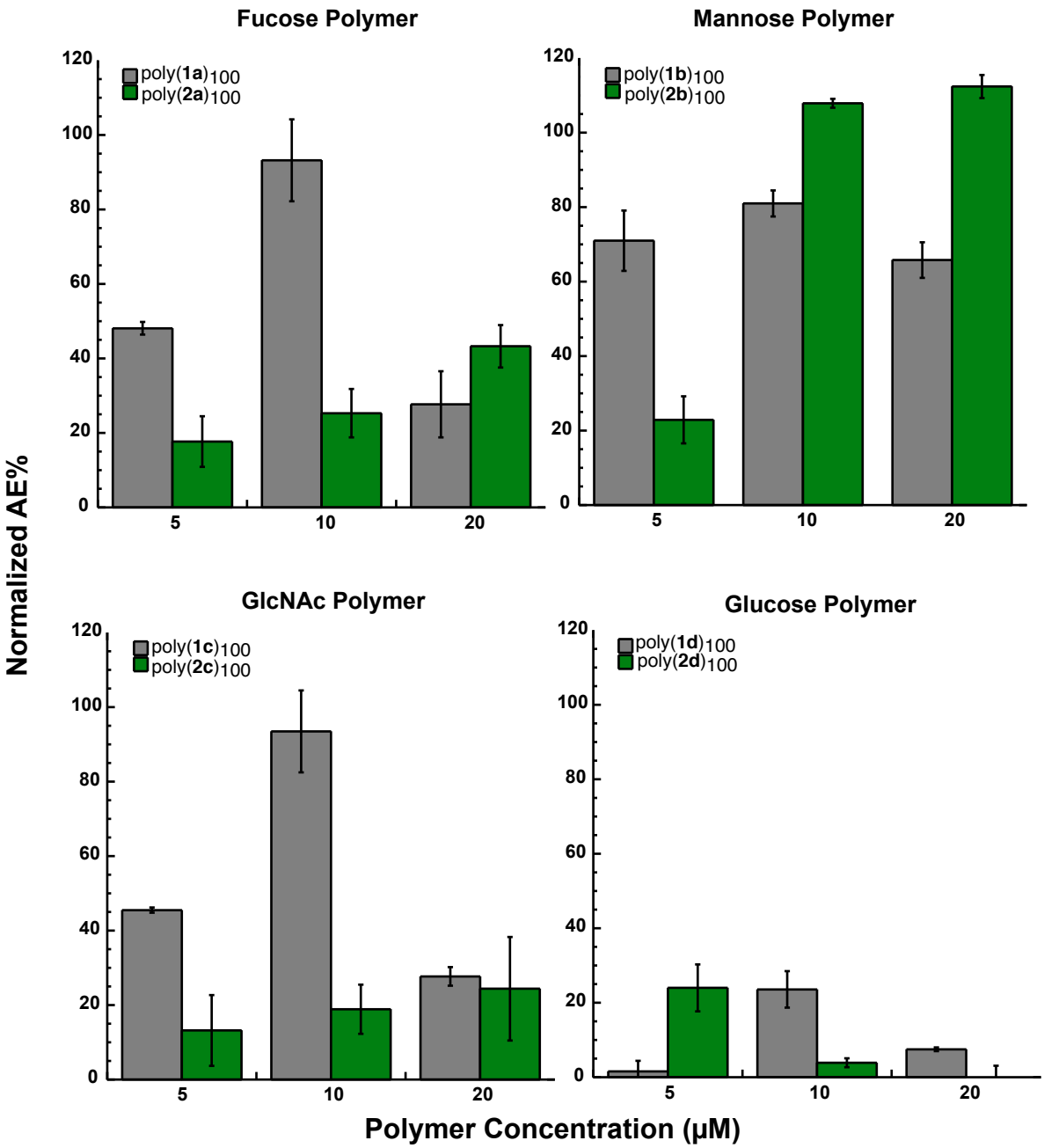

Normalized AE%= (AE% by glycopolymers-AE% by negative control)/(AE% by positive control- AE% by negative control)

Figure 2-2. AE induction by COE and NB backbone polymers

2.2.5 Analysis of glycopolymer solution structures.

We synthesized polycyclooctenes, poly(**2**)$_{100}$, in order to form polymers with longer and more flexible backbones compared to the norbornene backbone used previously. We expected that an enhancement in AE activation would be observed due to greater receptor accessibility.[12,13] However, the flexible backbone in combination with fucose or GlcNAc display reduced rather than enhanced AE induction. Only AE induction by mannose polymers increased. Therefore, we undertook SAXS analysis of the solution polymer conformations to understand the divergent activities of these polymers.

SAXS measurements of norbornene polymers were carried out on 1 wt% of norbornene glycopolymers in both DDI water and M16 medium. M16 medium is the same medium used for AE induction but omitting BSA, which is itself a macromolecule that will scatter X-rays. Spectra were also collected on the DDI water and M16 medium without BSA, and these were used as the background signal and subtracted from the data. To eliminate possible artifacts in fitting parameters from the beamstop in the low *q*-range and points with large uncertainties due to low signal in the high *q* range, SAXS analysis was performed over a *q* range of approximately 0.01Å^{-1} to 0.25Å^{-1}. Although this *q* range is limited, the data will still provide some information on glycopolymer chain conformation as described further below, yielding insight into possible mechanisms for the observed biologically activity.

Preliminary analysis of the norbornene backbone polymers in the mid-*q* range (0.02-0.1Å^{-1}) data without background subtraction yield a power-law dependence of the scattered intensity on q with an exponent close to -1 in the case of glycopolymers in both DDI water (**Figure 2-3A**) and M16 medium (**Figure 2-3B**). The exponent values are summarized in **Table 2-2**. The exponents value of glycopolymers with cyclooctene backbones were found in the range -1.8 to -3. This parameter reflects the polymer conformation. Generally speaking, the rigid rod has an exponent

value around -1. Wherease, the exponent is equal to -1.67 and -2 for swollen coil and a Gaussian chain, respectively. When polymer chains are collapsed, the value is around 3. This suggests a rod-like conformation for the norbornene backbone polymers in solution, while the cyclooctene polymers have a conformation more similar to typical flexible polymers in theta to poor solvents. Thus, an initial analysis of mid-*q* range suggested that the same sugar ligands linked to different polymer backbones access distinct solution structures.

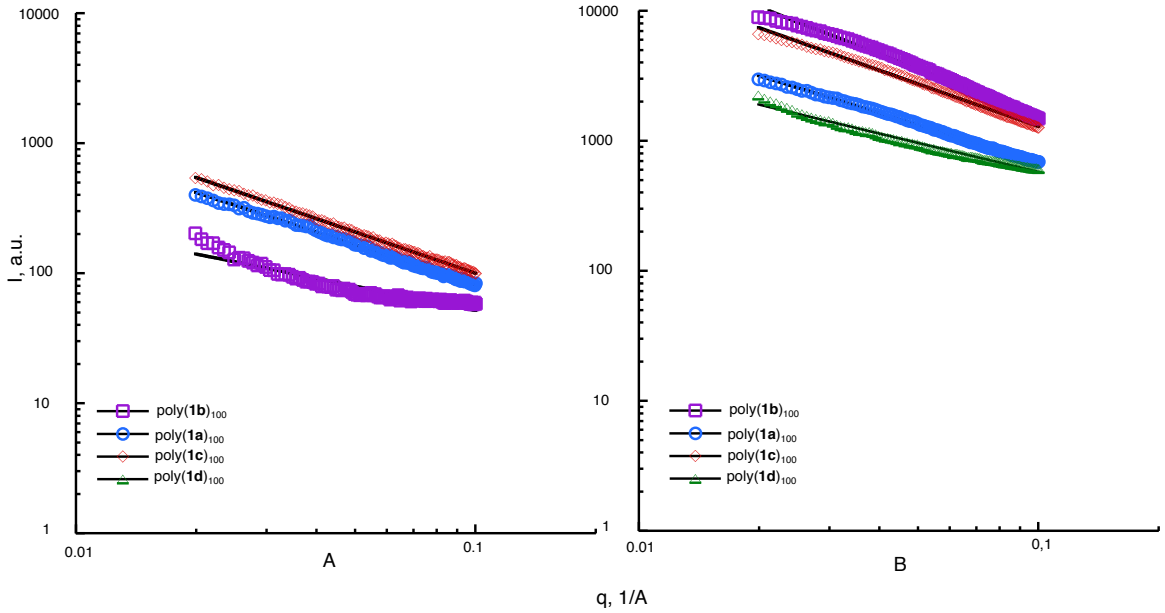

A: polymers in water; B: polymers in M16.

Figure 2-3. Preliminary mid-*q* range analysis of poly(**1**)$_{100}$

Table 2-2 Power-law fitting of poly(**1**)$_{100}$ SAXS data in water and M16.

Polymer	Slope in H_2O	Slope in M16
poly(**1a**)$_{100}$	-1.02	-0.95
poly(**1b**)$_{100}$	-1.20	-1.20
poly(**1c**)$_{100}$	-1.05	-1.09
poly(**1d**)$_{100}$	/	-0.74

In order to optimize the measurement signal, different concentrations of norbornene backbone polymers poly(**1b**)$_{100}$ and poly(**1c**)$_{100}$ were tested. The scattering data are shown in **Figure 2-4**. The comparisons between 0.75 wt%. 1.0 wt% and 1.5 wt% of poly(**1b**)$_{100}$ demonstrated that the scattering intensity decreased at the lowest concentration (**Figure 2-4A**). There were no significant qualitative differences as concentration changes for poly(**1c**)$_{100}$ (**Figure 2-4B**). The intermediate *q*-range analysis indicated that the slopes of all the polymers were close to 1 (**Figure 2-5** and **Table 2-3**). Therefore, all the samples may be fit to cylinder models. After background subtraction, no dips in intensity at low *q* for higher concentrations were observed for either polymers type (**Figure 2-4C, D**). Therefore, there were no strong repulsions between chains at these testes concentrations. However, there was a slight increase in intensity for poly(**1c**)$_{100}$ at 1.5 wt%, which was probably caused by aggregation of polymers.

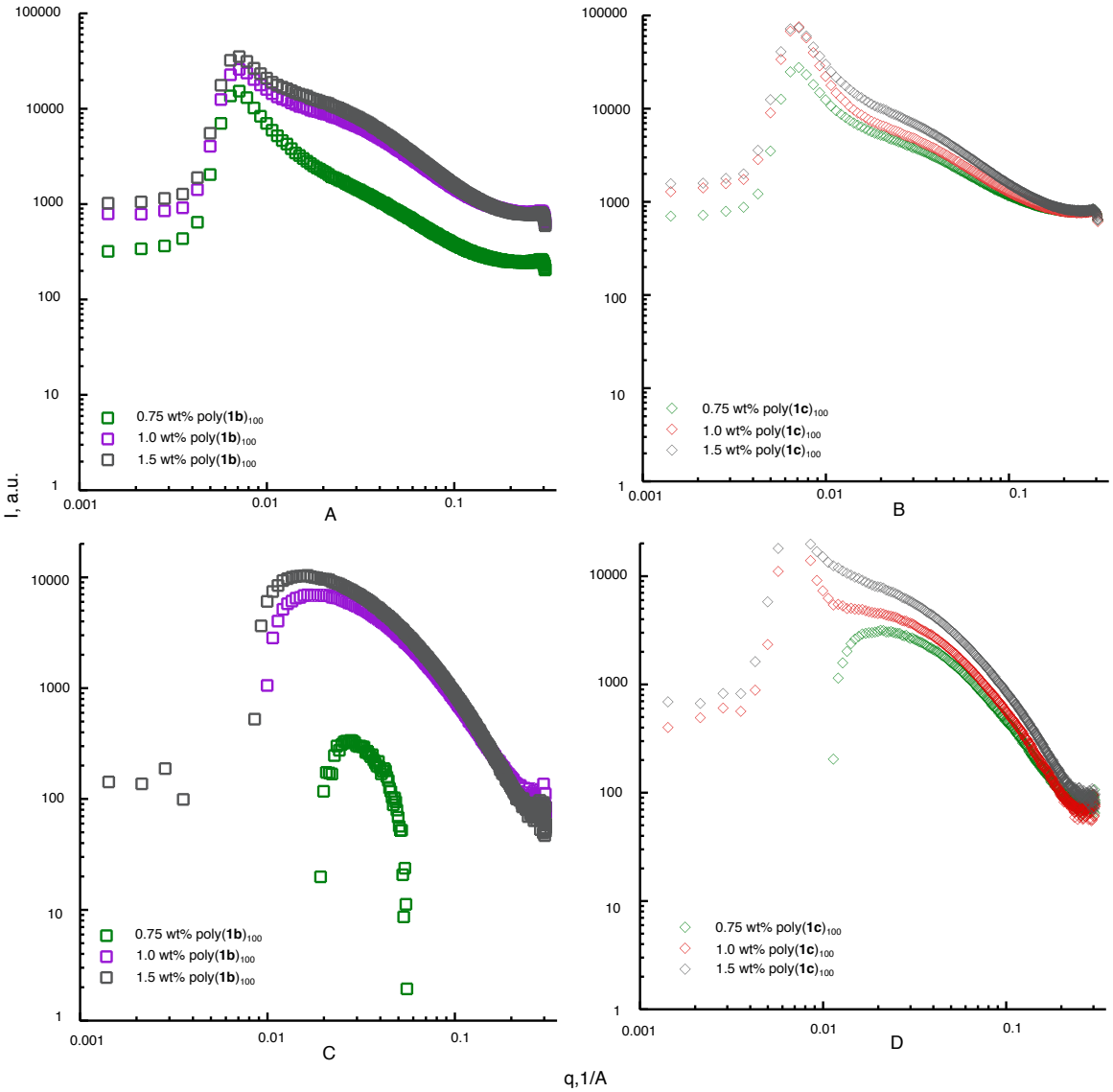

A: poly(**1b**)$_{100}$ at three different concentrations; B: poly(**1c**)$_{100}$ at three different concentrations;
C: poly(**1b**)$_{100}$ after background subtraction; D: poly(**1c**)$_{100}$ at three different concentrations;

Figure 2-4. Concentration study in SAXS

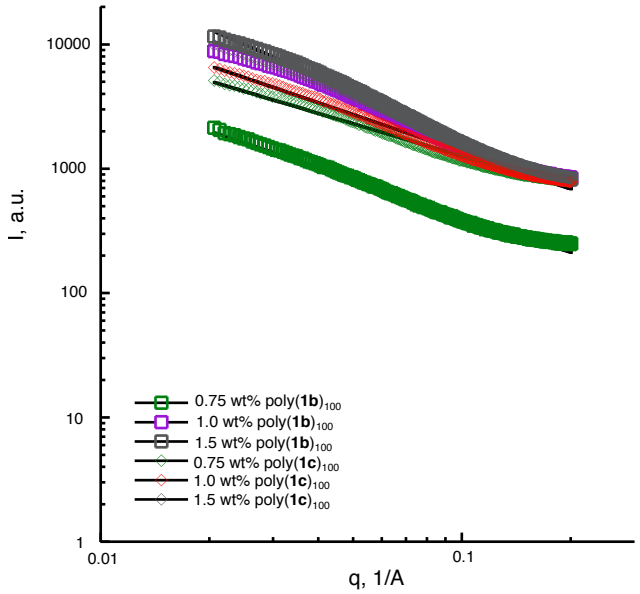

Figure 2-5. Intermediate q range analysis of polymers at different concentrations

Table 2-3 Power-law fitting of poly(**1**)$_{100}$ SAXS data at different concentrations

Polymer	Exponent
0.75 wt% poly(**1b**)$_{100}$	-1.11
1.0 wt% poly(**1b**)$_{100}$	-1.18
1.5 wt% poly(**1b**)$_{100}$	-1.43
0.75 wt% poly(**1c**)$_{100}$	-1.04
1.0 wt% poly(**1c**)$_{100}$	-1.05
1.5 wt% poly(**1c**)$_{100}$	-1.30

Figures **2-5** and **2-6** show SAXS data for the glycopolymers with polynorbornene and polycyclooctene backbones, respectively. The two data sets display a qualitatively different dependence on *q*, suggesting different conformations of the glycopolymers with the two different backbones.

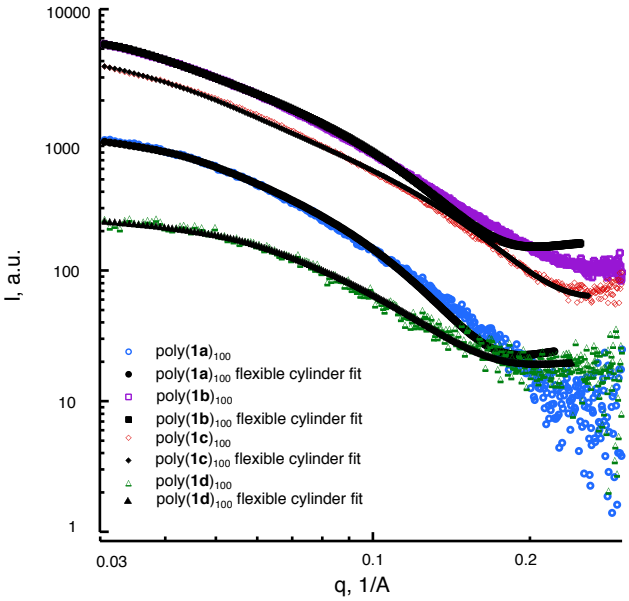

Figure 2-6. SAXS data for glycopolymers with polynorbornene backbones and fits to flexible cyldiner model. Black lines represent results from data fitting.

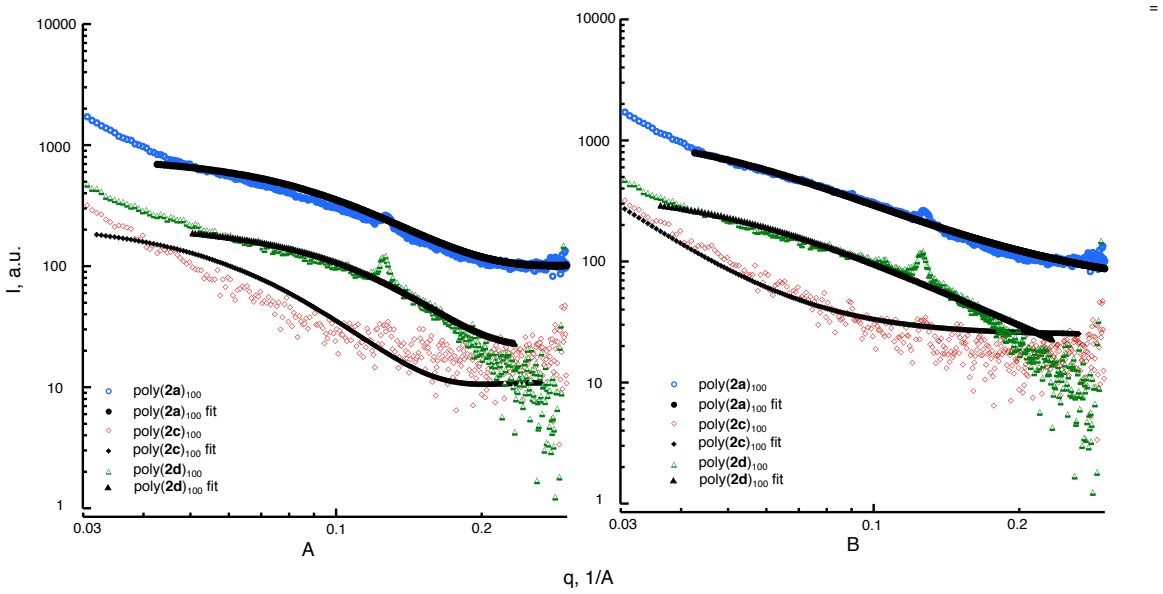

Figure 2-7. SAXS data for glycopolymers with polycyclooctene backbones, and fits to polymer excluded volume model (right) and flexible cylinder model (left). Black lines represent results from data fitting.

A more detailed data analysis was conducted for both glycopolymers. Based on the initial slope value analysis, the norbornene backbone polymers were fit to the flexible cylinder model, which describes a chain. This model includes the contour length L and radius R comprised of a series of locally stiff segments of length l_p, where $2l_p$ is the Kuhn length. The results are summarized in **Table 2-4**. The polymers with norbornene backbone all had similar structures with a contour length in the range of 70-220 Å, a radius of 14-20 Å, and a Kuhn length of 60-100 Å. The Kuhn lengths obtained from data fitting are large, indicating that these polymers are quite rigid. Although this result is somewhat unexpected, it is consistent with the findings of Pesek *et al.,* who examined bottlebrush polymers with a norbornene backbone of similar length as our systems, and with polystyrene side chains (PNb(PS)).[116] They performed SANS studies of these polymers in deuterated toluene and attempted to fit the data with a variety of different models. They also find that their systems are well-described by the flexible cylinder models and obtain contour lengths that are similar to what we have found.

Table 2-4 Flexible cylinder model fit of poly(NB)s. [a] Fitting errors are less than 0.01.

Polymer	Contour length (Å)	Kuhn length (Å)	Radius (Å)
poly(**1a**)$_{100}$	107.17 ± 0.24	73.06 ± 0.18	19.90 ± 0.02
poly(**1b**)$_{100}$	144.46 ± 0.04	93.11 ± 0.03	18.72 ± 0.003[a]
poly(**1c**)$_{100}$	219.37 ± 0.17	59.82 ± 0.10	14.10 ± 0.01
poly(**1d**)$_{100}$	70.41 ± 0.82	56.64 ± 0.78	18.48 ± 0.08

COE-backbone polymers were fit to both the flexible cylinder model mentioned above, as well as a model developed for flexible polymer chains with excluded volume interactions, first described by Benoit and later put in analytical form by Hammouda.[117-118] This model includes the polymer radius of gyration, R_g, and a parameter m that is related to the excluded volume parameter, ν, as $m = 1/\nu$. The results are shown in **Figure 2-7**. All polymers show some excess scattering at

low q that is not captured by either model, but since this region is also affected by scattering from the beamstop, it is difficult to discern if this indicates aggregation of chains into larger structures. Accordingly, we focus on fitting data in the mid- to high-q range to obtain information about chain conformation. Fits to the flexible cylinder model for these polymers were performed in order to facilitate direct comparison of parameters for the two series of polymers; however, it is clear that the polymer excluded volume model provides a better fit to the data. It is not possible to fit both series of polymers with the polymer excluded volume model, as this model will not reproduce the rigid rod limit.[118]

Results (**Table 2-5**) from the fits to the flexible cylinder model result in values for L and R that are similar to the norbornene polymers (L = 80 – 170 Å, R = 14 – 20 Å), although it should be noted that there is significant uncertainty in the largest value of the contour length, which was obtained for the cyclooctene polymer with GlcNAc groups due to noise in the data. However, all of these systems show much smaller values for the Kuhn length, in the range 7 – 20 Å, as compared to the norbornene backbone polymers. This is consistent with the cyclooctene backbone polymers having a more flexible structure. Fits to the polymer excluded volume model indicate a radius of gyration of 28 – 30 Å for the COE polymers with glucose and fucose groups. As expected, the radius of gyration is much smaller than the contour length of the polymer obtained from fits to the flexible cylinder model, again consistent with a much more flexible chain conformation. The value of R_g for the cyclooctene polymer with GlcNAc groups is quite large, 220 Å, although again this should be interpreted with caution as there is greater noise in the data for this sample. The values of the parameter m range from 1.8 – 1.9 for the cyclooctene polymers with glucose and fucose groups, to 2.8 for the polymer with GlcNAc groups. We would expect values for the parameter m of 1.67 for flexible polymer chains swollen by a good solvent, 2 for chains in a theta solvent, and

values close to 3 for chains that are collapsed in a poor solvent. The results indicate that the cyclooctene polymers with glucose and fucose groups are behaving as if in a moderately good to theta solvent, with a conformation that is close to an ideal random walk. However, the cyclooctene polymer with GlcNAc groups appears to have a more compact, collapsed configuration.

Table 2-5 Flexible cylinder and excluded volume model fit of poly(COE)s. [a] Fitting errors are less than 0.01.

Polymer	Contour length (Å)	Kuhn length (Å)	Radius (Å)	m	R_g (Å)
poly(**2a**)$_{100}$	78.60 ± 3.22	19.65 ± 0.03	13.53 ± 0.03	1.94 ± 0.005[a]	30.69 ± 0.06
poly(**2c**)$_{100}$	168.69 ± 47.14	20.00 ± 0.07	18.91 ± 0.30	2.85 ± 0.001[a]	222.08 ± 0.03
poly(**2d**)$_{100}$	97.60 ± 5.59	6.83 ± 0.06	13.99 ± 0.10	1.80 ± 0.02	28.27 ± 0.11

Earlier studies of polynorbornene backbone conformations focused on characterization of polymers on a surface or in the molten state. The chain conformations exhibited high degrees of heterogeneity. For example, diblock copolymer of norbornene and organometallic derivatives of norbornene or polyacetylene exhibited different conformations in the film state, including spherical, cylindrical or lamellar morphology, depending on the diblock compositions and molecular weights. For norbornene backbone brush copolymers containing polylactide (PLA) and poly(n-butyl acrylate) (PnBA) side chain, the polymer assembled in a highly ordered lamellar state, with extended backbone conformation.[119-121] These results provide an estimate of the single-molecule size, but do not provide information on their solution-state structures. We conclude that the sugars on our polymers serve to block aggregation of norbornyl chains, and help to maintain a flexible cylinder conformation in solution. These structures are analogous to the bottlebrush polymers of Pesak *et al* in which the brushes serve to prevent aggregation, where with increase in the length of brushes the conformation transited from spherical particles to cylinders.[116]

Glycoconjugate conformations have been investigated by SAXS analysis for maltpentaose-carrying polystyrene (PVM5A) and PVLA with PT in water .[122-123] These glycopolymers are often found to self-assemble into nanoparticles, micelles, vesicles, or tubular aggregates due to the amphiphilic nature of the polymers.[74] All of these polymers have flexible backbones, analogous to our polycyclooctene glycopolymers.

Our SAXS comparative analysis of the polynorbornene and polycyclooctene glycopolymers indicates that different types of activating receptor complexes are formed with each sugar ligand. Polycyclooctene mannose are the most effective AE inducers. Our results suggest that large clusters of mannose receptors are important for mannose ligand signaling. In contrast, large clusters do not enhance the AE efficacy of fucose and GlcNAc, and the effective dose range of fucose activation is very narrow. These data suggest that a single relatively rigid polymer can stabilize receptor dimers by displaying the correct spacing for fucose or GlcNAc binding.

2.3 Conclusion

A series of glycopolymers based on a polycyclooctene backbones was synthesized. These glycopolymers were compared to previously prepared polynorbornene glycopolymers as inducers of mouse sperm acrosomal exocytosis. According to SAXS analyses, the glycopolymers with polynorbornene backbones form flexible cylinders in cell medium. However, glcopolymers with polycyclooctene backbones are significantly less rigid and have conformations typical of polymer chains in a theta to poor solvent. The cylinder conformations are requisite for efficient acrosomal exocytosis induction by fucose and GlcNAc polymers. In contrast, the conformations adopted by glycopolymers with polycyclooctene enhanced mannose induction of AE. Thus, the appropriate choice of polymer backbone for optimal cellular activation is dependent on the receptor that is

engaged. Our results further support that there are independent receptors on the mouse sperm cell surface for different sugar ligands which can be engaged to induce acrosomal exocytosis.

Chapter 3 Understanding the Effects of Ligand Density and Heterostructures on Mouse Sperm Acrosomal Exocytosis

3.1 Introduction

Acrosomal exocytosis (AE) in spermatozoa is a critical step for successful mammalian fertilization.[40] The AE leads to the release of acrosomal proteins and modification of the sperm head morphology. After AE, the sperm are ready for sperm-egg membrane fusion in the following step.[11] Carbohydrates on mouse ZP3 play an important role in sperm AE.[124] Previous studies have demonstrated that both sugar termini and protein backbones are necessary for induction of AE in mouse. However, the exact role of these sugars in the redundant signaling pathways to induce AE is still largely unknown.[47] In the previous studies in our group, Wu *et al* successfully designed and synthesized novel glycopolymers, which were utilized to study sperm AE.[57] These synthetic glycopolymers with a multivalent display of mannose, GlcNAc or fucose mimicked the biological function of physiological AE inducer and activated the sperm AE in a dose-dependent manner.[57] The studies also revealed the three sugar polymers could activate AE independently. Furthermore, the ligand-receptor binding triggered AE through convergent signaling pathways.[57] Later on, the studies of AE induction by these glycopolymers over a larger concentration range by flow cytometry suggested that each polymer had a distinct dose response curve.[58] The results further proved that each sugar had its distinctive binding site or active site on the sperm cell surface. However, the experiments were conducted with homopolymers that present a single sugar ligand. Hence, the structures barely reflect the complexity of glycosides present in nature.[69] Therefore, AE induction by heterogeneous presentations of these sugar ligands in the polymer structures are interesting and necessary to investigate.

Recent research on synthetic polymers has contributed to unraveling the mechanism of glycan-protein recognition processes.[62] Typically, these systems incorporate several copies of identical

sugar motifs attached to the polymer scaffold as we reported in previous studies.[57-58] However, natural oligosaccharides and polysaccharides consist of a variety sugars, which cannot be mimicked by a homopolymer structure.[69] The synthesis of hetero-glycopolymers featuring well-defined macromolecular architectures are an informative tool to tune affinity and selectivity towards a specific set of receptors.

In this paper, the study between sugar ligand and receptors on sperm cell surface is designed with heteroglycopolymers (**Figure 3-1**). First, random copolymers (**Figure 3-1a**) were synthesized through copolymerization of the biologically inert ligand glucose with effective ligands. Thus, the ligand densities of effective ligands on the backbone were tuned from 100% to 50% or 10%. The AE induction by these random copolymers was compared with induction by their corresponding homopolymers. Our results demonstrate that a low density of ligands presentation was more optimal for mouse AE activation. Second, block copolymers (**Figure 3-1b**) with two effective binding blocks were synthesized to investigate whether any synergetic effect occurred with the "multi-domain" structure. These block copolymers do not show any enhancement in AE activations compared to their corresponding block copolymers with one active block and one inactive block.

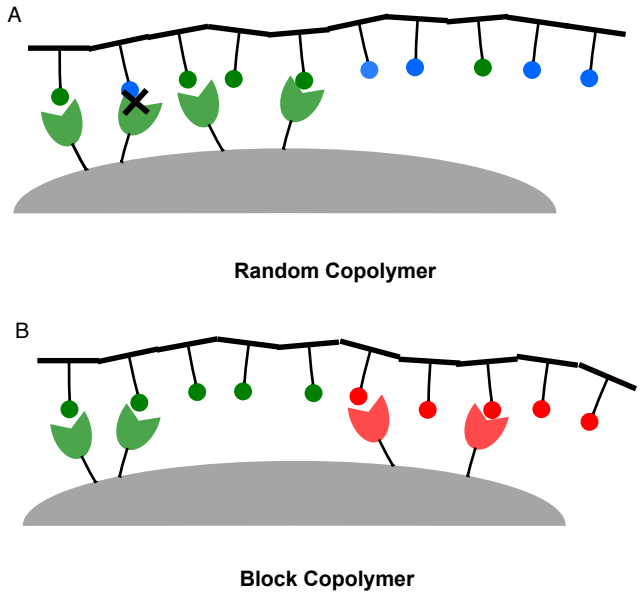

Figure 3-1. Heteropolymer architectures. A: Random copolymer. B: Block copolymer

3.2 Results and Discussion

3.2.1 Synthesis and characterization of protected heteroglycopolymers.

According to the previous procedures established in our group, four sugar norbornene monomers were successfully synthesized.[57] Based on our assay studies, fucose, mannose, GlcNAc sugar ligands were regarded as effective ligands and glucose was considered as a non-effective ligand.[57-58] The random copolymers containing effective ligands and glucose in 10:90 or 50:50 ratio, were synthesized in CH_2Cl_2 with catalyst $(H_2IMes)(3\text{-Br-pyr})_2Cl_2Ru{=}CHPh$ (**3**) (**Scheme 3-1a**). The block copolymers were prepared by sequential copolymerization of the two effective monomers. After the polymerization of the first monomer had reached completion, the second monomer was added to the reaction mixture (**Scheme 3-1b**). After all monomers were consumed, the polymerizations were quenched with excess ethyl vinyl ether, followed by precipitation in cold ether. The structures of the copolymers were confirmed by ^1H NMR analysis. The number-average

molecular weights (M_n), the weight average molecular weights (M_w) and dispersity index ($Đ_M$) of polymers were characterized by GPC utilizing a differential refractometer and a multi-angle light scattering detector (**Table 3-1**).

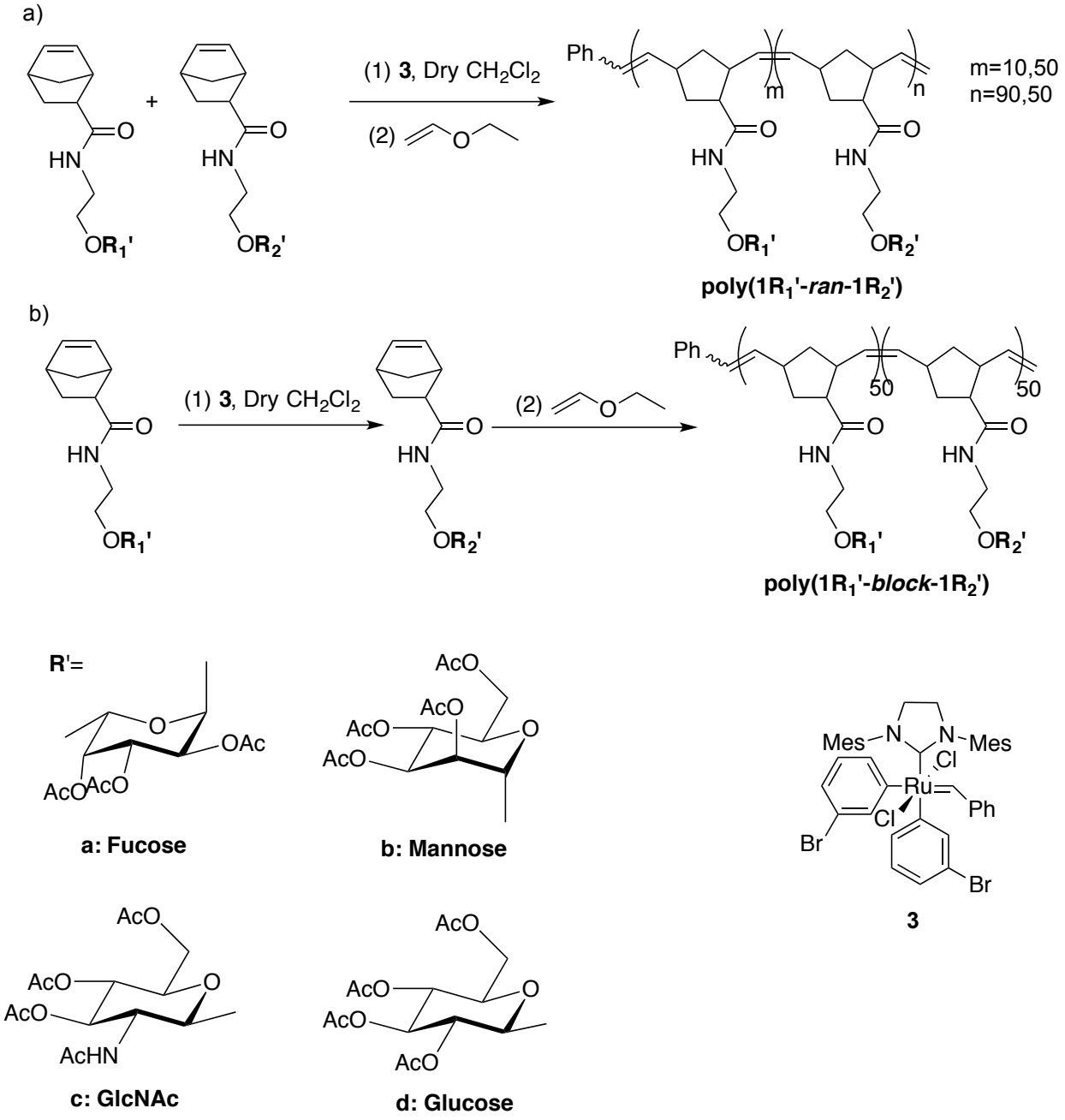

Scheme 3-1. ROMP of random and block copolymers

The polymers with fully protected sugars were deprotected by treating with excess K_2CO_3 in MeOH/THF followed by neutralization with a THF/H_2O/HCl cocktail mixture (**Scheme 3-2**). The deprotected polymers were purified by dialysis and stored in H_2O as stock solution. The removal of the protecting acetyl groups was confirmed by ^1H NMR.

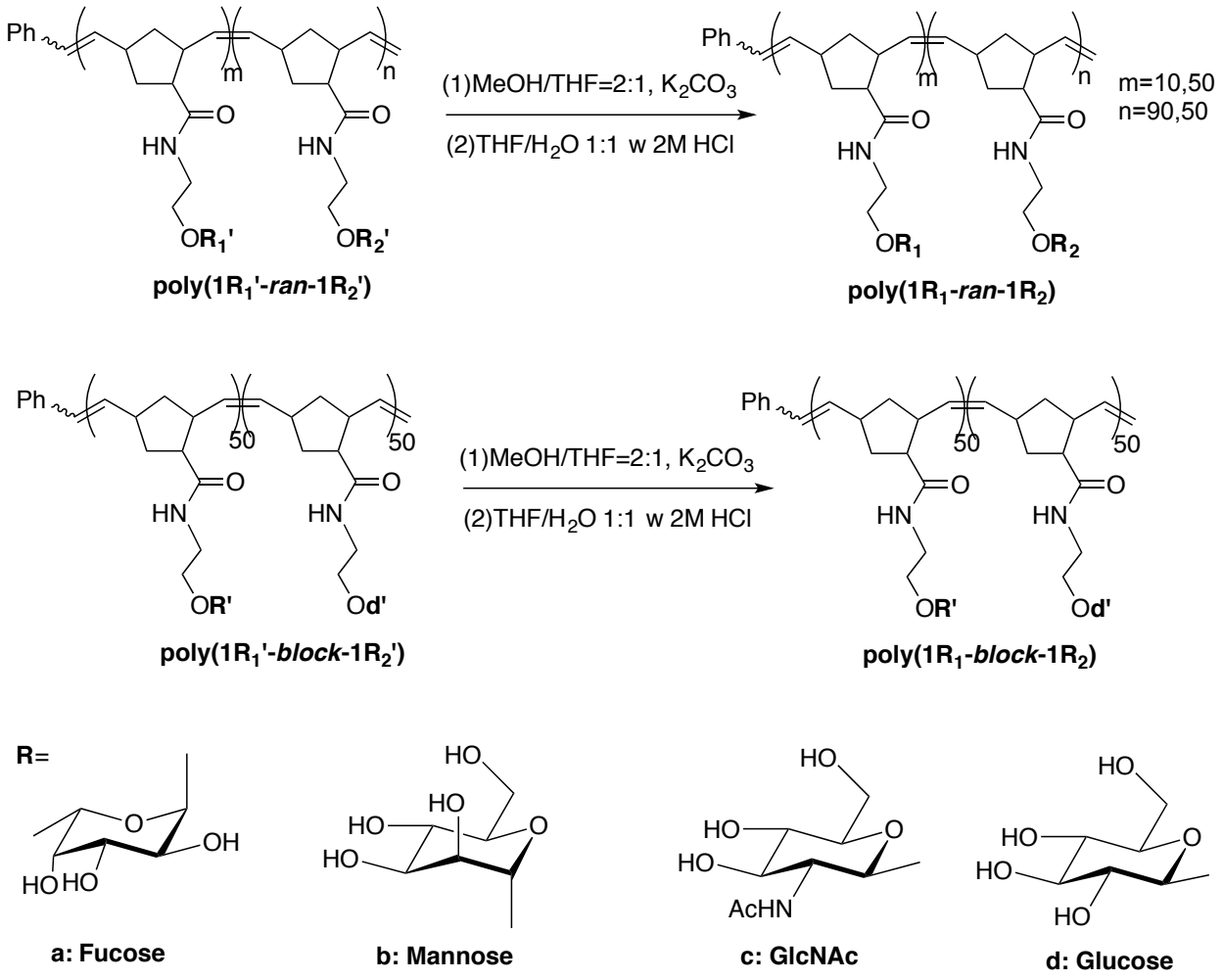

Scheme 3-2 Deacetylation of heteroglycopolymers

Table 3-1 Random and Block Copolymers Characterization Data. [a]Theoretical molecular weights were calculated based on the catalyst-to-monomer ratio assuming full conversion. [b]Determined from GPC in THF utilizing a differential refractometer and a multiangle light scattering detector.

Polymer	$^{a}M_n^{theor}$	M_n	M_w	$Đ_M$
poly(**1a'**$_{50}$-*ran*-**1d'**$_{50}$)	48347	62865	66510	1.06
poly(**1a'**$_{10}$-*ran*-**1d'**$_{90}$)	50627	45894	49565	1.08
poly(**1b'**$_{50}$-*ran*-**1d'**$_{50}$)	51197	17774	18357	1.03
poly(**1b'**$_{10}$-*ran*-**1d'**$_{90}$)	51197	13921	16329	1.17
poly(**1c'**$_{50}$-*ran*-**1d'**$_{50}$)	51147	61784	64626	1.05
poly(**1c'**$_{10}$-*ran*-**1d'**$_{90}$)	51187	33141	39106	1.18
poly(**1b'**$_{50}$-*block*-**1a'**$_{50}$)	48347	19009	19437	1.02
poly(**1b'**$_{50}$-*block*-**1c'**$_{50}$)	51147	40514	40919	1.01
poly(**1a'**$_{50}$-*block*-**1c'**$_{50}$)	48297	60150	73383	1.22
poly(**1a'**$_{50}$-*block*-**1d'**$_{50}$)	48347	60128	96725	1.61
poly(**1b'**$_{50}$-*block*-**1d'**$_{50}$)	51197	88890	160002	1.80
poly(**1c'**$_{50}$-*block*-**1d'**$_{50}$)	51147	43729	45765	1.05

3.2.2 SAXS characterization of heteropolymers.

Small angle X-ray scattering (SAXS) was used to obtain information about copolymer conformation in water and cell medium. SAXS measurements of norbornene polymers at 1 wt% were carried out in M16 medium without BSA (**Figure 3-2**). The intermediate *q* range (0.02-0.1Å^{-1}) data without background subtraction was first fitted to generate the exponent values. The exponent values are summarized in **Table 3-2**. This parameter reflects the polymer conformation. Generally speaking, the rigid rod has an exponent value around -1. Whereas, the exponent is equal to -1.67 and -2 for a swollen coil and a Gaussian chain, respectively. When the polymer chains are collapsed, the exponent is around -3. The exponent values of random and block polymers in water

were about -1.01 to -1.20, close to -1. The exponent values for these polymers in M16 remained close to -1. These data suggest a rod-like conformation for the random and block copolymers in solution.

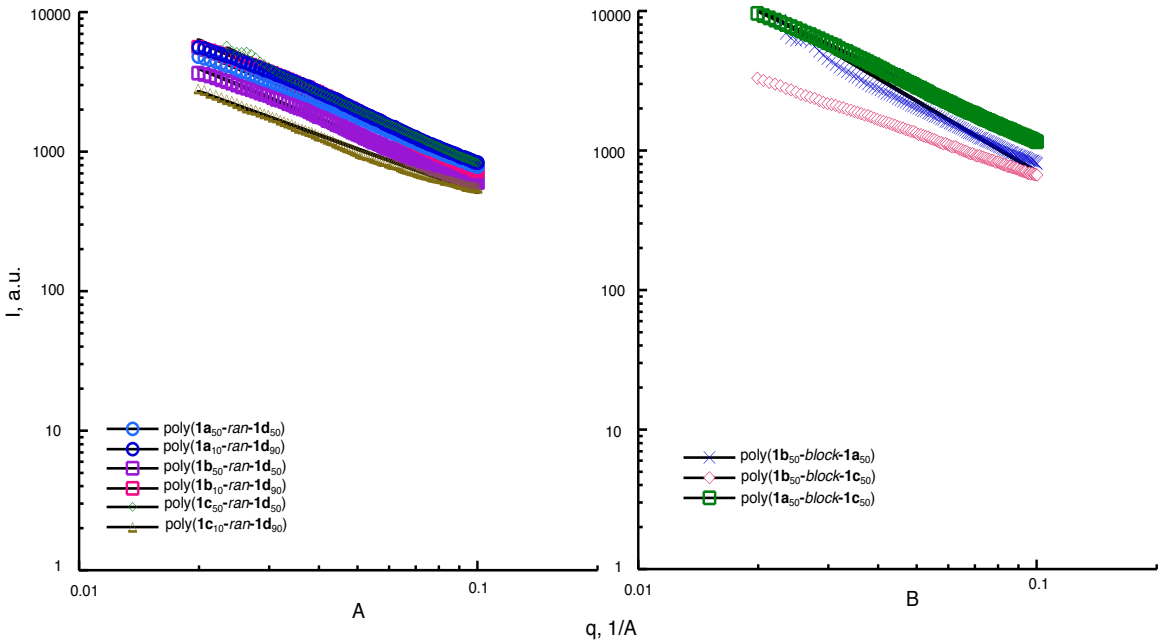

Figure 3-2. Intermediate *q*-range analysis of random and block copolymers. A: random polymers; B: block polymers.

Table 3-2 Power-law fitting of random and block copolymers SAXS data in M16

Polymer	Exponent
poly(**1a**$_{50}$-*ran*-**1d**$_{50}$)	-1.18
poly(**1a**$_{10}$-*ran*-**1d**$_{90}$)	-1.25
poly(**1b**$_{50}$-*ran*-**1d**$_{50}$)	-1.19
poly(**1b**$_{10}$-*ran*-**1d**$_{90}$)	-1.33
poly(**1c**$_{50}$-*ran*-**1d**$_{50}$)	-1.33
poly(**1c**$_{10}$-*ran*-**1d**$_{90}$)	-1.03
poly(**1b**$_{50}$-*block*-**1a**$_{50}$)	-1.44
poly(**1b**$_{50}$-*block*-**1c**$_{50}$)	-1.00
poly(**1a**$_{50}$-*block*-**1c**$_{50}$)	-1.35

Spectra were also collected on the M16 medium without BSA, and this was used as the background signal and was subtracted from the data. To eliminate possible artifacts in fitting parameters from the beamstop in the low q range and points with large uncertainties due to low signal in the high q range, SAXS detailed analysis was performed over a q range of approximately 0.01 $Å^{-1}$ to 0.25 $Å^{-1}$. Although this q range is limited, the data still provide some information on glycopolymer chain conformation as described further below, yielding insight into possible mechanisms for the observed biological activity.

Figures 3-3 and **3-4** show SAXS data for random and block copolymers, respectively. Based on the initial slope value analysis, the random and block polymers were fit to the flexible cylinder model which describes a chain. The flexible cylinder model includes the contour length L and radius R comprised of a series of locally stiff segments of length l_p, where $2l_p$ is the Kuhn length. The results are summarized in **Table 3-3**. The random polymers all had similar structures with a contour length in the range of 70-220 Å, a radius of 17-22 Å, and a Kuhn length of 56-200 Å. The Kuhn lengths obtained from the data fitting are large, indicating that these polymers are quite rigid. It is consistent with the findings for polynorbornene backbone homopolymers described in Chapter 2.

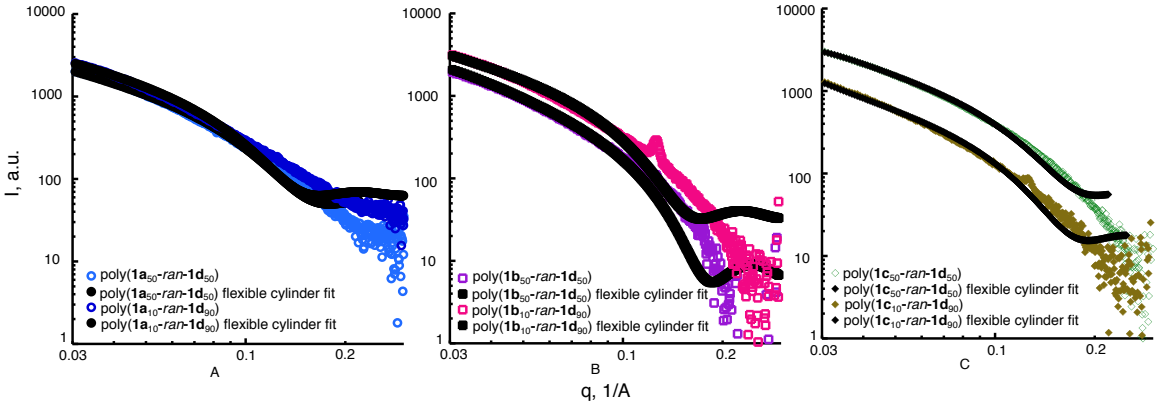

Figure 3-3. SAXS data for random copolymers and fits to flexible cylinder model. Black lines represent results from data fitting. A: fucose polymers. B: mannose polymers. C: GlcNAc polymers.

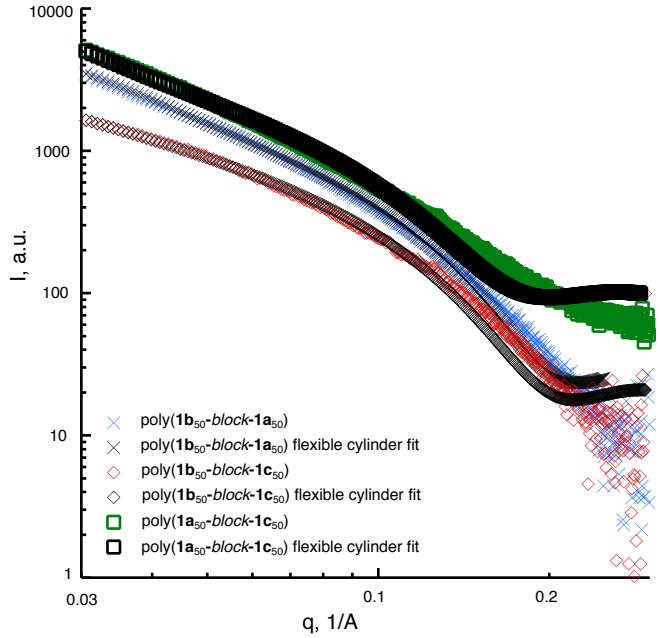

Figure 3-4. SAXS data for block copolymers and fits to flexible cylinder model. Black lines represent results from data fitting.

Table 3-3 Flexible cylinder fit for random and block copolymers. A Fitting errors were less than 0.01.

Polymer	Contour length (Å)	Kuhn length (Å)	Radius (Å)
poly(**1a**$_{10}$-*ran*-**1d**$_{90}$)	274.97 ± 0.0001[a]	68.75 ± 0.06	17.73 ± 0.01
poly(**1a**$_{50}$-*ran*-**1d**$_{50}$)	175.45 ± 0.06	141.35 ± 0.11	21.40 ± 0.01
poly(**1b**$_{10}$-*ran*-**1d**$_{90}$)	254.27 ± 0.08	196.77 ±0.12	22.25 ± 0.004[a]
poly(**1b**$_{50}$-*ran*-**1d**$_{50}$)	70.41 ± 0.82	56.64 ± 0.78	18.48 ± 0.08
poly(**1c**$_{10}$-*ran*-**1d**$_{90}$)	403.67 ± 0.33	130.73 ± 0.19	20.02 ± 0.01
poly(**1c**$_{50}$-*ran*-**1d**$_{50}$)	158.41 ± 0.08	99.80 ± 0.06	18.89 ± 0.01
poly(**1b**$_{50}$-*block*-**1a**$_{50}$)	323.79 ± 0.0001[a]	80.96 ± 0.05	17.06 ± 0.01
poly(**1b**$_{50}$-*block*-**1c**$_{50}$)	251.3 ± 1.33	182.49 ± 0.96	17.32 ± 0.01
poly(**1a**$_{50}$-*block*-**1c**$_{50}$)	417.87 ± 0.00007[a]	104.48 ± 0.03	19.16 ± 0.004[a]

3.2.3 Effect of heteroglycopolymers on acrosomal exocytosis.

We examined the effect of heteroglycopolymers on sperm AE by flow cytometry assay.[58] The results for random copolymers were compared to those for their corresponding homopolymers (**Figure 3-5**). We fitted the AE results obtained with random copolymers to a double sigmoidal model (**Figure 3-6**). The fitted dose response constants for random copolymers are summarized in **Table 3-4**.

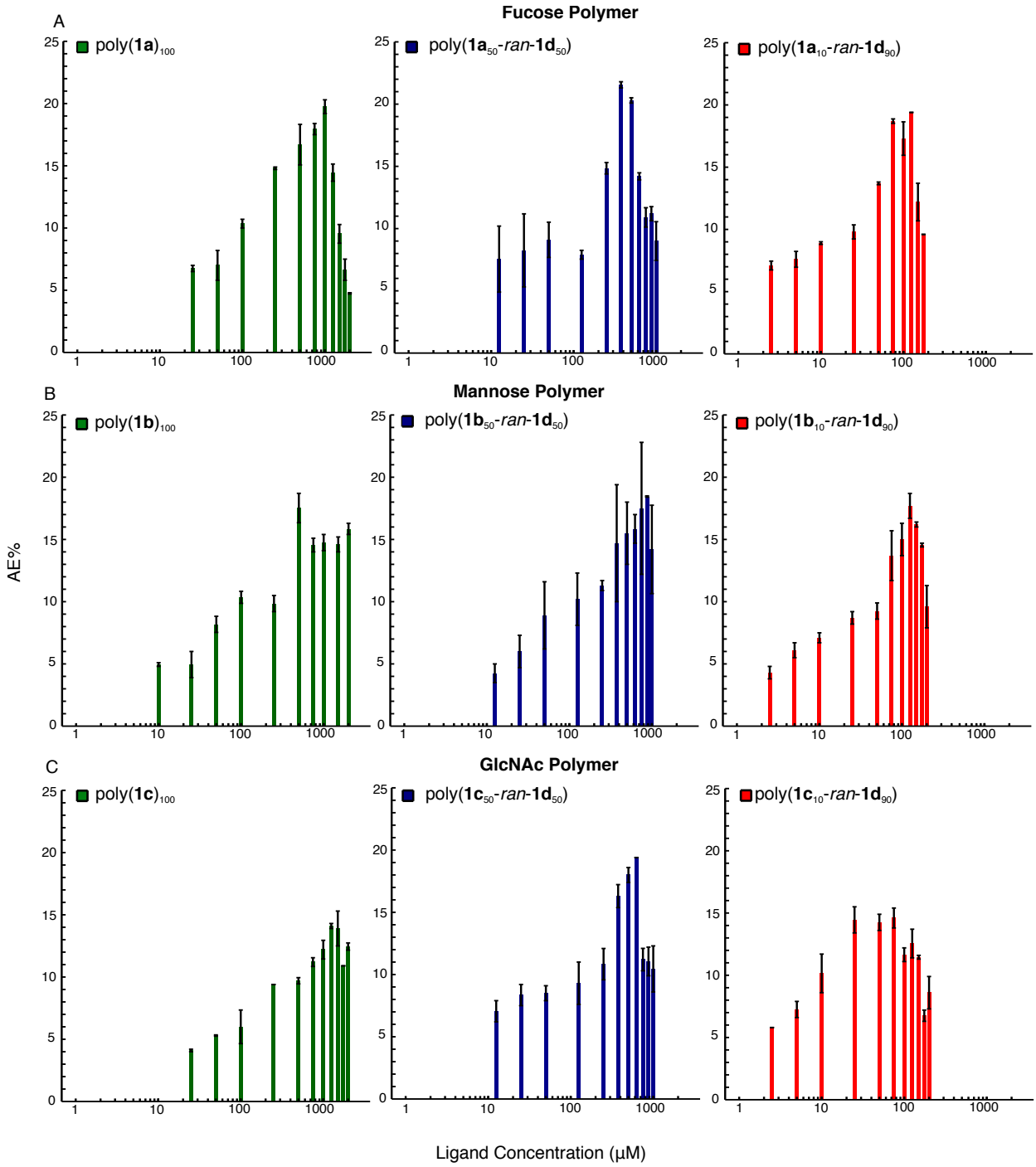

Figure 3-5. AE inductions by random copolymers compared to their homopolymer counterpart. A: fucose polymer comparison. B: mannose polymer comparison. C: GlcNAc polymers comparison. Green bars represent homopolymers, blue bars represent random copolymers with active 50% ligand density, and red bars represent random copolymers with active 10% ligand density.

For fucose random polymers (**Figure 3-6A**), both of the random copolymers induce the maximal AE, which was approximately 19%. Previous studies with fucose homopolymer revealed that the EC_{50} was 160 ± 1.1 μM (in ligand concentration). The EC_{50} for poly(**1a**$_{50}$-*ran*-**1d**$_{50}$) is 247 ± 12.5 μM. Whereas, the EC_{50} was reduced to 47 ± 1.2 μM for poly(**1a**$_{10}$-*ran*-**1d**$_{90}$). With the increase of the ligand concentrations, poly(**1a**$_{50}$-*ran*-**1d**$_{50}$) and poly(**1a**$_{10}$-*ran*-**1d**$_{90}$) also showed asymmetric activation curve with highly cooperative inhibition arms.

Random mannose copolymers demonstrated no loss in potency with decreasing ligand density (**Figure 3-6b**). The EC_{50} for poly(**1b**$_{50}$-*ran*-**1d**$_{50}$) was 185 μM, which is comparable to that of poly(**1b**)$_{100}$. Poly(**1b**$_{10}$-*ran*-**1d**$_{90}$) exhibited a relatively low EC_{50} value of 65 μM. Furthermore, there was no inhibition arm for poly(**1b**$_{50}$-*ran*-**1d**$_{50}$) and poly(**1b**)$_{100}$ rather than poly(**1b**$_{10}$-*ran*-**1d**$_{90}$).

The same trends of activation curve trend were found for GlcNAc random polymers (**Figure 3-6C**). Poly(**1c**$_{50}$-*ran*-**1b**$_{50}$) provided a relatively wide activation platform the same as poly(**1c**)$_{100}$. Moreover, the EC_{50} of the two polymers were approximately the same. However, poly(**1c**$_{10}$-*ran*-**1b**$_{90}$) followed a bell-shaped response, showing inhibition at high concentrations around 100 μM ligand. Furthermore, the low density polymer could not induce maximal AE activation.

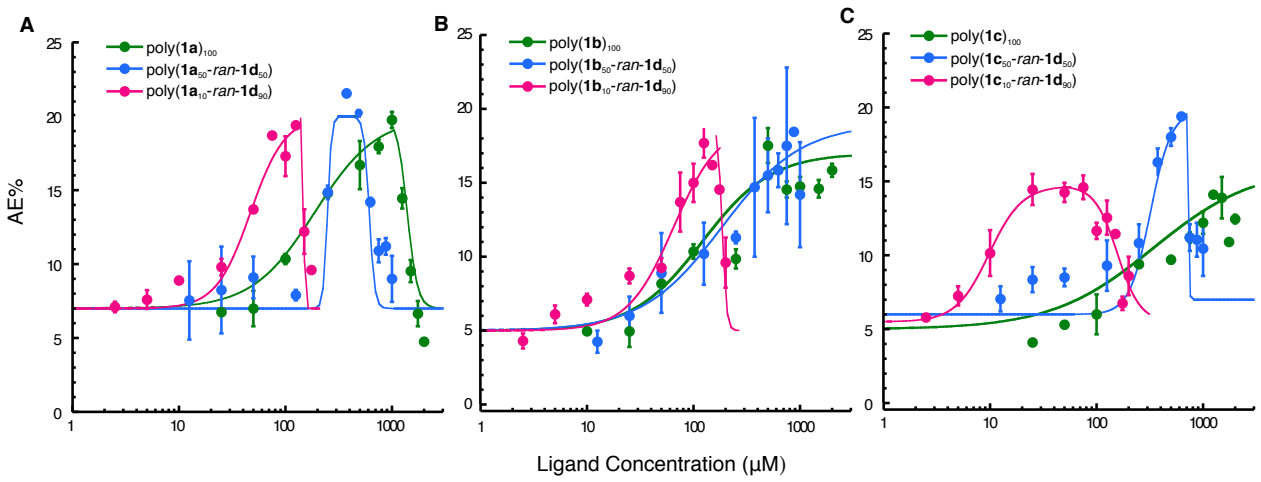

Figure 3-6. AE induction by random copolymers compared to their homopolymers with curve fit. A: fucose polymer comparison. B: mannose polymer comparison. C: GlcNAc polymer comparison. Green circles represent homopolymers, blue circles represent random copolymers with 50% active ligand density, and red bars represent random copolymers with 10% active ligand density.

Table 3-4 Dose responses for polymer inducers of AE. [a] Data are fits described in experimental methods. Errors are the standard error of the fit. [b] Data are extracted from previous report. [c] ND: not determined. [d] Fitting errors are large.

Polymer	EC_{50} (μM)[a]	IC_{50} (μM)[a]	Slope[a]
poly(**1a**)$_{100}$	160 ± 1.1[b]	1350 ± 1.0[b]	1.5 ± 0.2[b], -9.5±3.0[b]
poly(**1a**$_{10}$-*ran*-**1d**$_{90}$)	47 ± 1.2	148	2.7 ± 1.2, -69.9[d]
poly(**1a**$_{50}$-*ran*-**1d**$_{50}$)	247± 12.5	611± 1.1	23.1[d], -17.3 ± 27.4
poly(**1b**)$_{100}$	120 ± 1.7[b]	ND[b,c]	1.3 ± 0.8[b]
poly(**1b**$_{10}$-*ran*-**1d**$_{90}$)	65 ± 1.6	186 ± 2.4	2 ± 1.3, -21.4 ± 188
poly(**1b**$_{50}$-*ran*-**1d**$_{50}$)	185 ± 1.7	ND[c]	1.2 ± 0.8
poly(**1c**)$_{100}$	341 ± 2.2[b]	ND[b,c]	0.9 ± 0.6[b]
poly(**1c**$_{10}$-*ran*-**1d**$_{90}$)	10 ± 1.1	157 ±1.8	2.8 ± 0.8, -4.1± 5.4
poly(**1c**$_{50}$-*ran*-**1d**$_{50}$)	320 ± 1.1	ND	4.4 ± 1.5, ND

The models of AE activation by homopolymers were proposed by Rodolis *et al*[58] based on the ligand-induced receptor dimerization activation model. Assuming that the ligand concentration is in large excess relative to receptor, the binding-activation steps take place in two consecutive step. In the first step, the polymer ligands bind to the first receptor arm and form a R-L complex. In the following step, the second intra ligand is in close proximity to the RL complex and forms the RLR complex. Upon increasing ligand concentration, the monovalent formation of RL competes with the bivalent formation of RLR, leading to a symmetric bell-curve response. Activation arms were observed for fucose, mannose and GlcNAc polymers. However, fucose homopolymers also showed a highly cooperative inhibition arm. Therefore, formation of an inactive complex RLR* was proposed to explain the loss of symmetry in the bell curve.[58] For random copolymers systems, the possible binding events are more complicated. Asymmetric inhibition curves were also observed for all the fucose polymers, as well as mannose for polymer poly(**1b**$_{10}$-*ran*-**1d**$_{90}$). In addition to proposed inactive complex, the asymmetric inhibition arm may be caused by incorrect inter-ligand spaces present in the homo- and random copolymers. Poly(**1c**$_{10}$-*ran*-**1d**$_{90}$), however, had a symmetric binding profile.

In our next series of experiments, we tested block copolymers as AE inducers Block copolymers, including poly(**1a**$_{50}$-*block*-**1d**$_{50}$), poly(**1b**$_{50}$-*block*-**1d**$_{50}$) and poly(**1c**$_{50}$-*block*-**1d**$_{50}$), contained 50 copies of effective ligand and 50 copies of non-effective ligand. AE induction by poly(**1b**$_{50}$-*block*-**1d**$_{50}$) (**Figure 3-7 green bar**) and poly(**1c**$_{50}$-*block*-**1d**$_{50}$) (**Figure 3-7 red bar**) decreased at high ligand concentration, which were different from their homopolymers. The results indicated that a longer polymer may be required for mannose and GlcNAc ligand to induce AE induction at high concentration.

Block copolymers containing two effective-ligand blocks, for which each effective ligand had 50 copies, were compared to their corresponding block copolymers containing 50 copies of effective ligands and 50 copies of non-effective ligands in **Figure 3-7** and **Figure 3-8**. The AE response to poly(**1b**$_{50}$-*block*-**1a**$_{50}$) (**Figure 3-7A**, **Figure 3-8A**) the response to pattern of the poly(**1a**$_{50}$-*block*-**1d**$_{50}$), where AE induction decreased dramatically at high ligand concentration. The results suggested that activation by poly(**1b**$_{50}$-*block*-**1a**$_{50}$) is dominated by fucose ligand. Similarly, activation by poly(**1b**$_{50}$-*block*-**1c**$_{50}$) (**Figure 3-7B**, **Figure 3-8B**) is dominated by GlcNAc ligand. Therefore, the signaling pathway induced by mannose ligand is inhibited by activation of fucose or GlcNAc ligand signaling pathway. However, AE activation by poly(**1a**$_{50}$-*block*-**1c**$_{50}$) did not decrease at high concentrations as seen for poly(**1a**$_{50}$-*block*-**1d**$_{50}$) and poly(**1c**$_{50}$-*block*-**1d**$_{50}$). The results imply that the signaling pathways induced by fucose and GlcNAc can cross-talk.

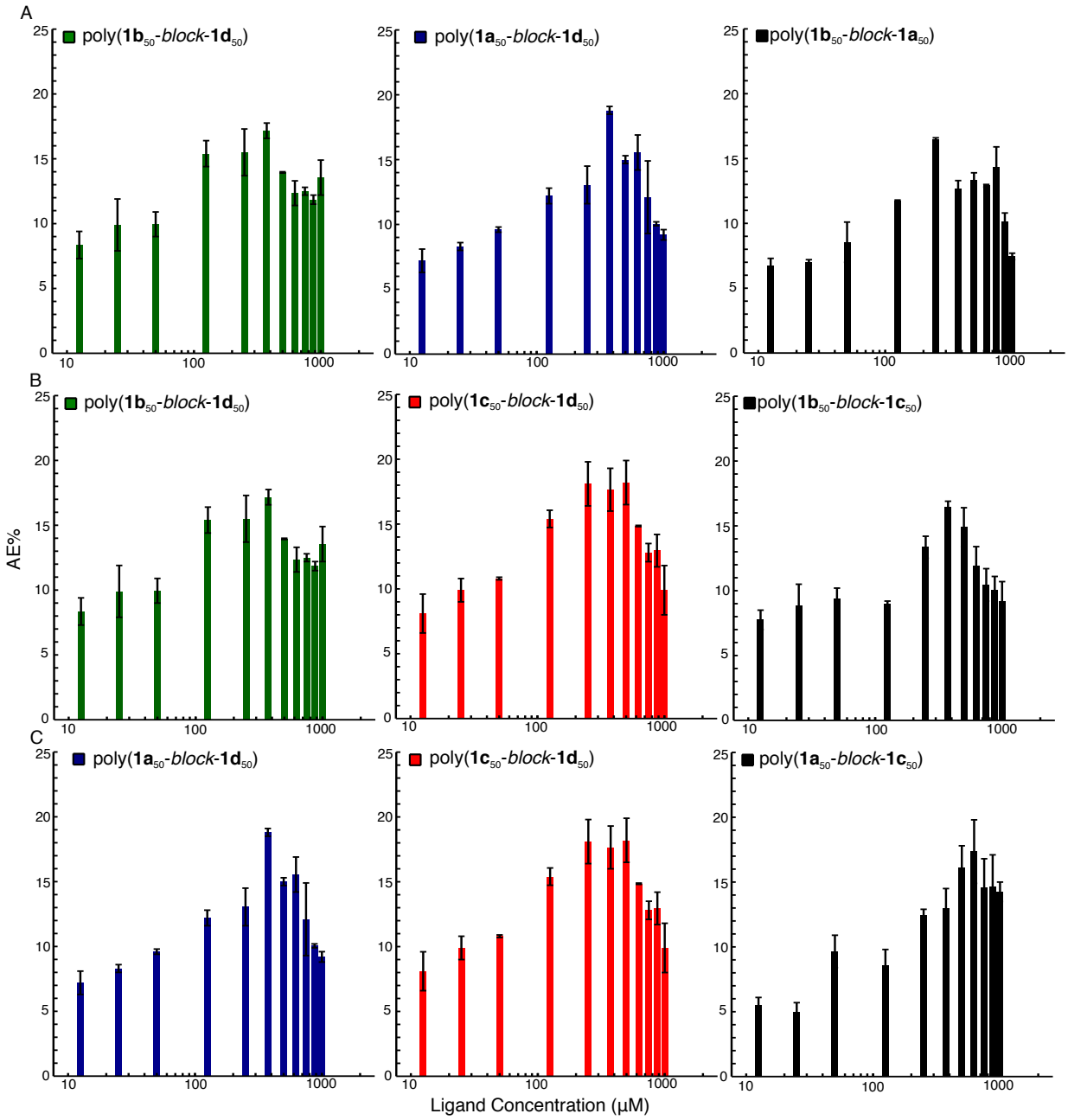

Figure 3-7. AE inductions by block copolymers. A: mannose and fucose block copolymers comparison. B: mannose and GlcNAc block copolymers comparison. C: fucose and GlcNAc block copolymers comparison.

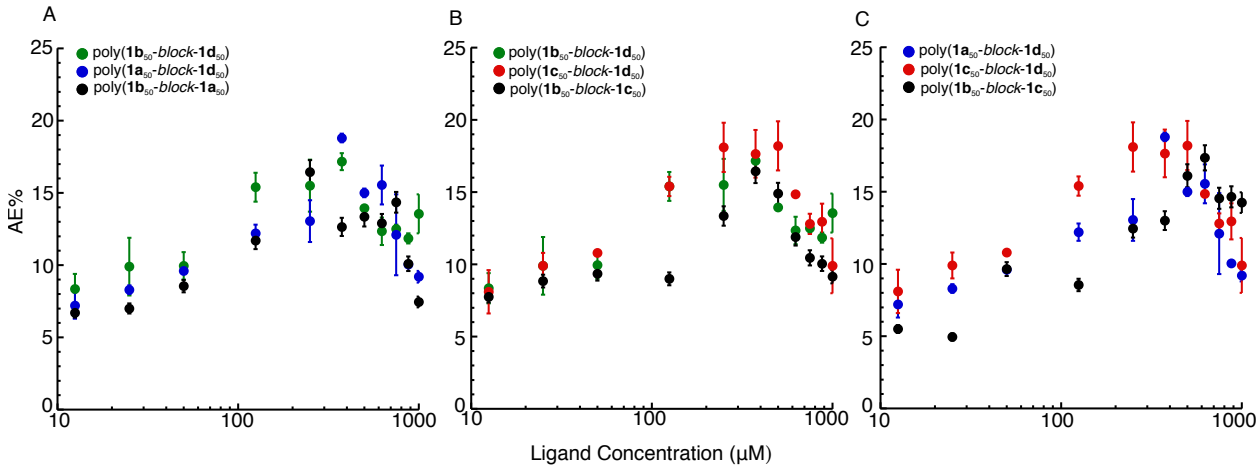

Figure 3-8. AE inductions by block copolymers (scattering plot). A: mannose and fucose block copolymers comparison. B: mannose and GlcNAc block copolymers comparison. C: fucose and GlcNAc block copolymers comparison.

3.2.4 AE induction tested by fluorescence microscopy assay.

3.2.4.1 Comparison of random copolymers with their corresponding homopolymers sugar pairs.

AE activation by random copolymers and block copolymers was also tested by sperm fluorescence microscopy assay following the published procedure.[57] Calcium ionophore A23187 and PBS were treated as the positive and negative control, respectively. All the experimental results were normalized as described in the experimental method section. First, the random polymers were compared to pairs of their corresponding homopolymer where the effective ligand concentrations were the same (**Figure 3-9**). Thus, 10 μM poly(**1**-*ran*-**1d**$_{90}$) was compared to the combination of 1 μM poly(**1**)$_{100}$ and 9 μM poly (**1d**)$_{100}$. 10μM poly(**1**-*ran*-**1d**$_{50}$) was compared to the combination of 5 μM poly(**1**)$_{100}$ and 5 μM poly (**1d**)$_{100}$.

As expected, the activation of AE varied in two conditions. For mannose polymers (**Figure 3-9B**), when sperm were incubated with the homopolymer pairs, normalized AE was approximately

10%, which was similar to the single poly(**1b**)$_{100}$ activity. Whereas, the normalized AE activated by poly(**1b**$_{10}$-*ran*-**1d**$_{90}$) reached 57%. Similar results were observed for fucose (**Figure 3-9A**) and GlcNAc (**Figure 3-9C**) polymers. The normalized AE% was much higher than that activated by the homopolymer pairs. The normalized AE percentages for poly(**1**-*ran*-**1d**$_{50}$) were comparable to the combination of the homopolymer pairs. The results suggest that lowering the ligand density of sugar ligands does not reduce the activation of AE. In contrast, the potency of the ligand, on a per ligand basis, was enhanced dramatically. The results are consistent with our studies by flow cytometry assay.

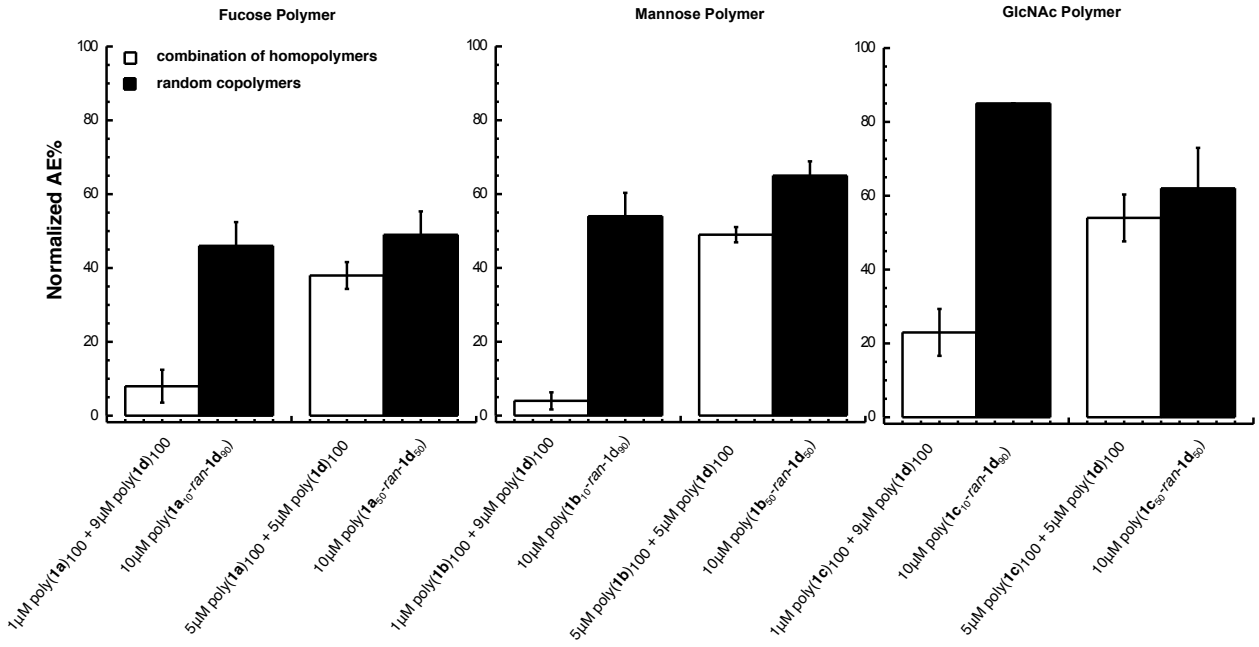

Figure 3-9. AE induction by random copolymers compared to their corresponding homopolymer pairs.

3.2.4.2 AE induction by random and block copolymers.

In the next experiment, random copolymers were tested at three different concentrations. The results were normalized and are summarized in **Figure 3-10** and **3-11**. Random copolymers also

activated AE in a dose-dependent manner, but the pattern was different from their homopolymers. When the concentration of poly(**1b**)$_{100}$ was 1 μM, there was little activation of AE. However, when the non-effective ligand was added, random polymers could activate the acrosome reaction even at a low concentration of polymer. Poly(**1b**$_{10}$-*ran*-**1d**$_{90}$) and poly(**1b**$_{50}$-*ran*-**1d**$_{50}$) induce 69% and 38% AE at 1 μM (**Figure 3-11B**), which suggested no concentration threshold for random copolymers. Similar results were observed for random fucose (**Figure 3-11A**) and GlcNAc (**Figure 3-11C**) polymers. At 5 μM and 10 μM, random copolymers with 10% and 50% ligand densities displayed similar AE activation abilities. The results from fluorescence microscopy assay suggested that the random copolymers with lower density ligands could activate AE as well as their homopolymers, which is consistent with the results obtained from the flow cytometry assay.

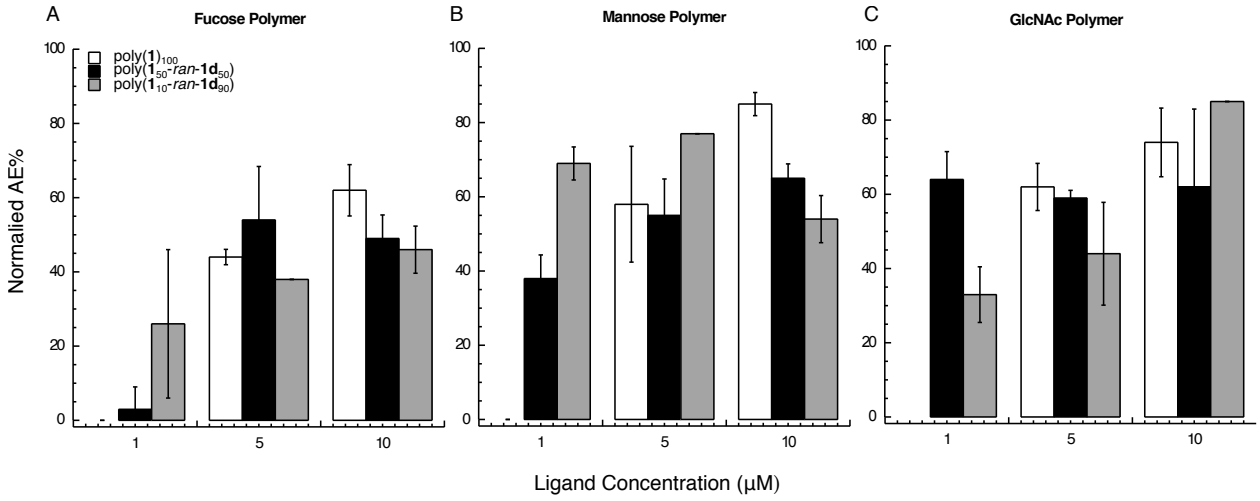

Figure 3-10. Random copolymers induce AE in a dose-dependent manner. A: fucose polymers. B: mannose polymers. C: GlcNAc polymers

The block copolymers built with two effective ligands were tested at different concentrations. In previous studies, when two different homopolymers were combined in the sperm assay at a relatively low concentration, for example, 2.5 μM poly(**1b**)$_{100}$ plus 2.5 μM poly(**1a**)$_{100}$, they only enhance AE activation slightly. The results suggested that there were different binding sites for the different sugar ligands. When the two homopolymers were mixed at low concentration, they

could not enhance AE. However, when two effective ligands are present as blocks on a single backbone, AE percentage increases dramatically at a low concentration (1 μM). However, the AE activation was not enhanced at 5 μM and 10 μM compared to the homopolymers. These results indicated that there was no concentration threshold for block copolymers, unlike random copolymers. Furthermore, there were no synergetic effects from the multiblock construction.

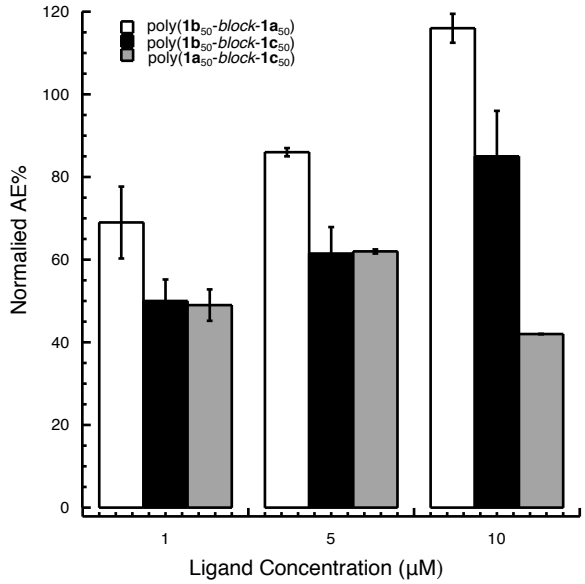

Figure 3-11. Block copolymers induce AE in a dose-dependent manner

3.2.4. Immunoblotting of anti-PKA and anti-pY by controls and polymers

3.2.4.1 Comparison between different cell media (WH and M16) with anti-pPKA

We compared the phosphorylation of protein kinase A (PKA) in three different cell media. The M16 medium was the cell medium used for both fluorescence microscopy assay and flow cytometry assay. The other two media tested were Whitten's HEPES (WH) medium[125] as well as TYH. Both of the cell media are very commonly used in sperm assays. Sperm were incubated in WH for 60 minutes and prepared for SDS-PAGE gel and immunoblotting with two different methods. Lanes 1-4 in **Figure 3-12A** were pellets from membrane purification. Lane 5 represents

pellets collected directly after incubation. Protein bands of 250 kD, 125 kD and three bands from 37 kD and 50 kD were observed in WH medium. Without membrane purification, the protein bands were not clear enough to see.

Since the sperm after membrane purification showed clear bands, the different components after purification (**Figure 3-12B**) were loaded on a SDS-PAGE gel. Additionally, the M16 medium and M16 with calcium ionphore (A23187) were compared in this experiment. Lanes 1-3 were pellets after 10,000 *g* centrifugation, lanes 4-6 were after 1,000*g* centrifugation and lanes 7,8 were supernatant. In sperm fluorescence microscopy assay, M16 medium was the negative control and A23187 was the positive control. Therefore, in the immunoblotting experiment, sperm incubated in those two conditions were compared. But unlike in the fluorescence microscopy assay, there were no differences between lane 5 and lane 6 or lane 7 and lane 8, which mean although A23187 could induce more AE, it probably did not alter the phosphorylation of PKA during the process.

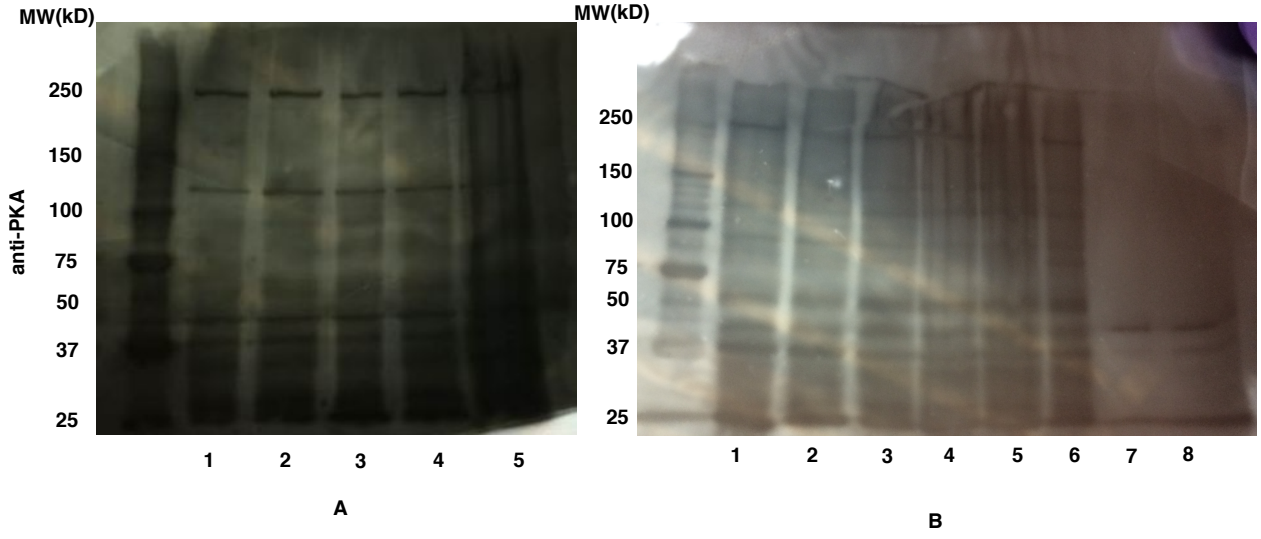

A: phosphorylation of protein kinase A (PKA) in WH cell medium
Lane 1-2: 10μL, 15μL pellet after 10,000 *g* centrifugation;
Lane 3-5: 10μL, 15μL pellet after 10,000 *g* centrifugation or 15μL pellet after 1,000 *g* centrifugation and centrifugation again after mixing with SDS buffer
B: phosphorylation of protein kinase A (PKA) in both WH and M16 cell media
Lane 1-3: pellet after 10,000 *g* centrifugation 1-WH medium; 2-M16 medium; 3- M16 medium with A23187;
Lane 4-6: pellet after 1,000 *g* centrifugation 4-WH medium; 5-M16 medium; 6- M16 medium with A23187;
Lane 7-8: supernatant 7-M16 medium; 8- M16 medium with A23187

Figure 3-12. Phosphorylation of PKA in different cell media

In contrast, A23187 may change the phosphorylation of PKA at some earlier time point which we did not observe.

3.2.4.2 Kinetic study of phosphorylation of PKA and tyrosine phosphorylation in sperm acrosomal exocytosis

Our immunofluorescence assay suggested that the sperm required 30 minutes to capacitate before acrosomal exocytosis. In the kinetic study of sperm AE, we incubated the sperm to get capacitated for 30 minutes. Then A23187 or PBS was added into the cell medium. Sperm samples at different time points after capacitation were collected. The time frames used were from 1 min to 30 min in order to observe the kinetics in phosphorylation of both PKA (**Figure 3-13 left**) and tyrosine kinase (**Figure 3-13 right**). These time frames were consistent with our fluorescence microscopy assay. Still, we could barely see the differences in phosphorylation of PKA in sperm treated with (**lane 1-4**) or without (**lane 5-8**) A23187 in **Figure 3-13 left** at 1 min, 7 min, 15 min and 30 min after capacitation. Similar trends were observed in the phosphorylation of tyrosine kinase, where no differences between samples treated with or without A23187 were observed. The strongest band was 116 kD, which is hexokinase and will not change during whole process. Other bands from 40 kD to 100 kD could barely be seen. The results were different from previous results reported on Tanotel *et al*'s paper. We proposed that the phosphorylation may take place in a very short time frame (less than one minute) after we added the A23187 or PBS.

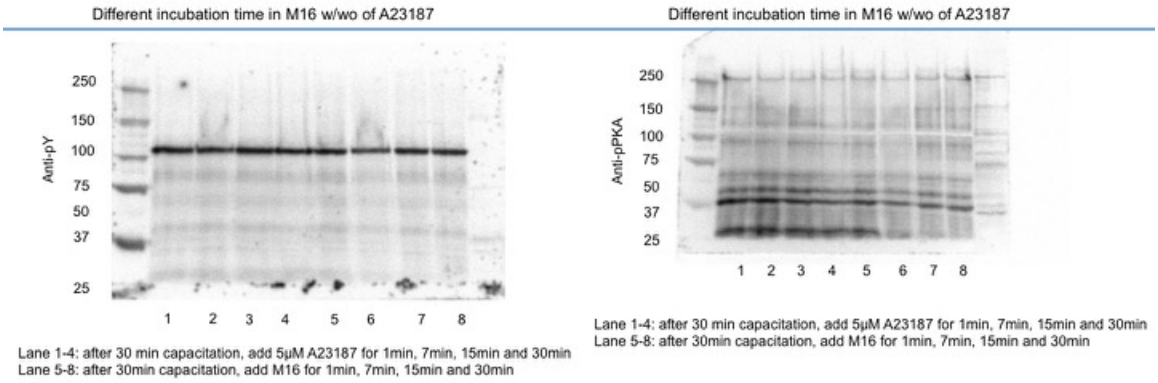

Figure 3-13. Kinetic studies of phosphorylation of tyrosine kinase (left) and protein kinase A (right).

Therefore, four different block copolymers (10 μM) were added to treat the sperm samples. After one minute, the samples were collected and the phosphorylation results are shown in **Figure 3-14**. However, the polymers and 5 μM A23187 did not change the phosphorylation of PKA substrates.

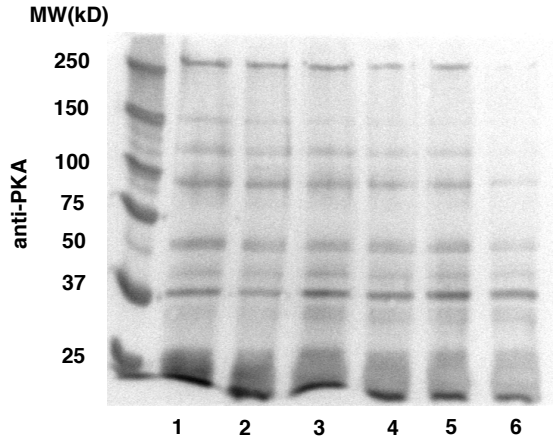

Lane 1-6: 5 μM A23187, 10 μM poly(**1b**$_{50}$-*block*-**1a**$_{50}$), 10 μM poly(**1b**$_{50}$-*block*-**1c**$_{50}$), 10 μM poly(**1c**$_{50}$-*block*-**1d**$_{50}$), 10 μM poly(**1b**$_{50}$-*block*-**1d**$_{50}$), PBS

Figure 3-14. Phosphorylation of PKA induced by different block copolymers

3.2.4.3. Optimization of experimental conditions

Since no differences in positive and negative controls was observed in previous experiments, more conditions have been tried and modified. We changed the medium from M16 to TYH. Also,

the incubation time for the anti-pY experiment was extended to 90 minutes and the incubation time for anti-pPKA was shortened to 30 minutes.

Condition 1. THY medium and time scales changed The sperm were allowed to stand for 5 min in HTYH (non-capacitation) and then were collected by centrifugation for 5 min at 550*g*. The pellets were resuspended in TYH and incubated for different times.[126] Lanes 1-6 showed the sperm incubated in the TYH for 15 min, 30 min, 45 min, 60 min, 90 min and 120 min. After incubation and wash with PBS, the pellets were resuspended in with water and treated with SDS loading buffer. However, the samples were aggregated in the gel, due to DNA from the sperm chromatin that got loose. Therefore, the gel did not show 116 kD bands in the anti-pY experiments. Upon shortening the time for anti-pPKA experiments, there were still no differences between negative and positive control because of the loose DNA.

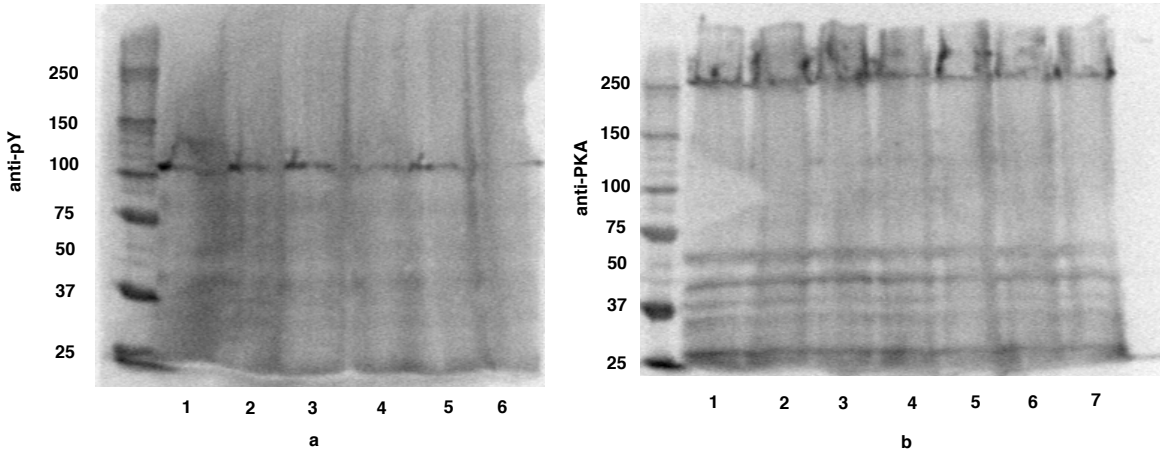

A: phosphorylation of tyrosine kinase in TYH
Lane 1-6: 15 min, 30 min, 45 min, 60 min, 90 min and 120 min
B: phosphorylation of protein kinase A(PKA) in TYH
Lane 1-5: 1 min, 3 min, 5 min, 7 min and 10 min in TYH; Lane 6-7: 5 min in TYH + 2 min or 5 min after addition of A23187

Figure 3-15. Kinetics study of phosphorylation of PKA and tyrosine kinase in TYH

Condition 2. Comparison of TYH and HTYH media. Since HCO_3^- plays a vital role in sperm activation, HTYH medium without bicarbonate was set as negative control. Sperm were incubated in TYH (capacitation condition) and HTYH (non-cap) for 1 min, 3 min and 10 min. There were

no differences between both conditions for phosphorylation of tyrosine kinase (**Figure 3-16a**) and phosphorylation of PKA (**Figure 3-16b**).

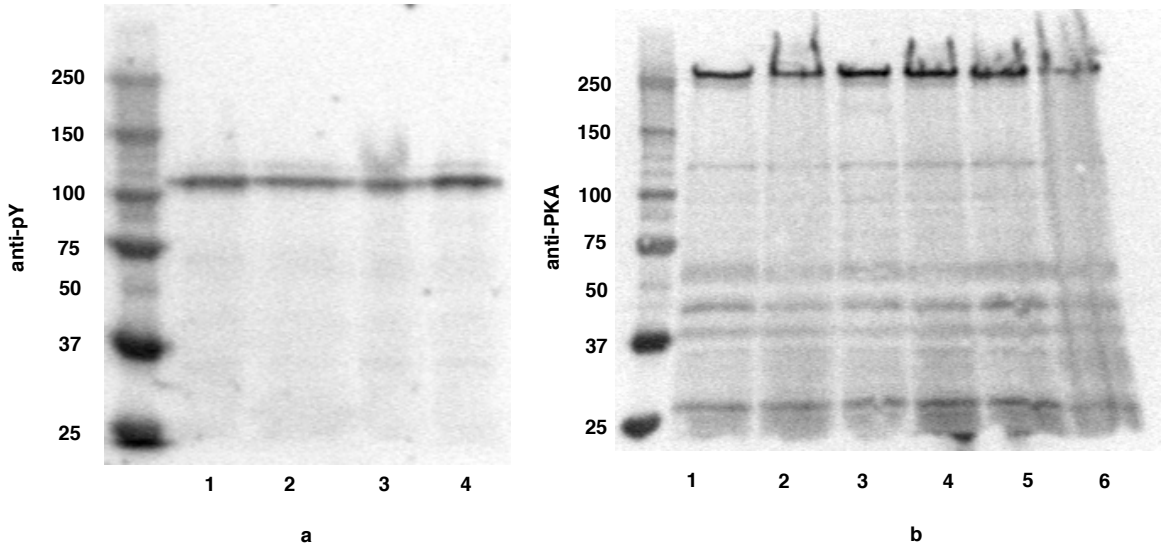

A: phosphorylation of tyrosine kinase in TYH and HTYH
Lane 1-2: 60 min in TYH and HTYH; Lane 3-5: 90 min in TYH and HTYH
B: phosphorylation of protein kinase A(PKA) in TYH and HTYH
Lane 1-3: 1min, 3min, 10min in TYH; Lane 4-6: 1min, 3min, 10min in HTYH
Figure 3-16. Phosphorylation of PKA and tyrosine kinase A in different cell media

Condition 3. Different loading sample concentrations. Sperm were incubated in TYH for different times and diluted 5- or 10- fold at 10 min or 30 min. Sperm incubated for 30 min and 60 min gave more bands around 150 kD- 250 kD. If diluted samples were used, clear bands but not strong intensities were obtained. band but not that strong. Therefore, 2-fold dilution was used tried in the following experiment.

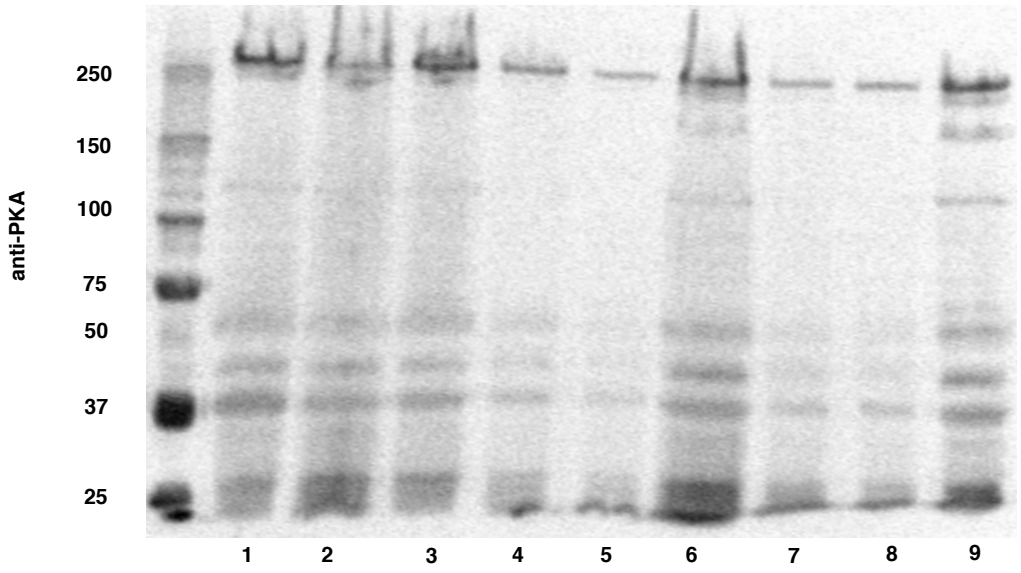

Lane 1-2: 1 min, 3min; Lane 3-5: 10 min, 10 min (5-fold dilution), 10 min (10-fold dilution);
Lane 6-8: 30 min, 30 min (5-fold dilution), 30 min (10-fold dilution); Lane 9: 60 min

Figure 3-17. Kinetics study in phosphorylation of PKA in TYH with diluted samples

Condition 4. Different cell lysis method. Because there was some aggregation in the gels, another cell lysis method before loading the gel was used. The sperm samples were diluted 2-fold. 500 μL sperm after incubation were centrifuged at 3000 rpm for 5min and washed with PBS. The pellets were treated with 20 μL RIPA with protease and phosphatase inhibitor on ice for 1 hour. Then the samples were centrifuged at 10,000 *g* for 5 min at 4°C. Both supernatant and pellets were saved for SDS- PAGE. The samples were resuspended in 20 μL 2× SDS loading buffer and boiled for 5 min.

The first four lanes were supernatant samples and there were only two bands around 120kD. The last four lanes were pellet samples, which means that most tyrosine phosphorylation proteins were membrane binding proteins. However, there were no differences between TYH and HTYH.

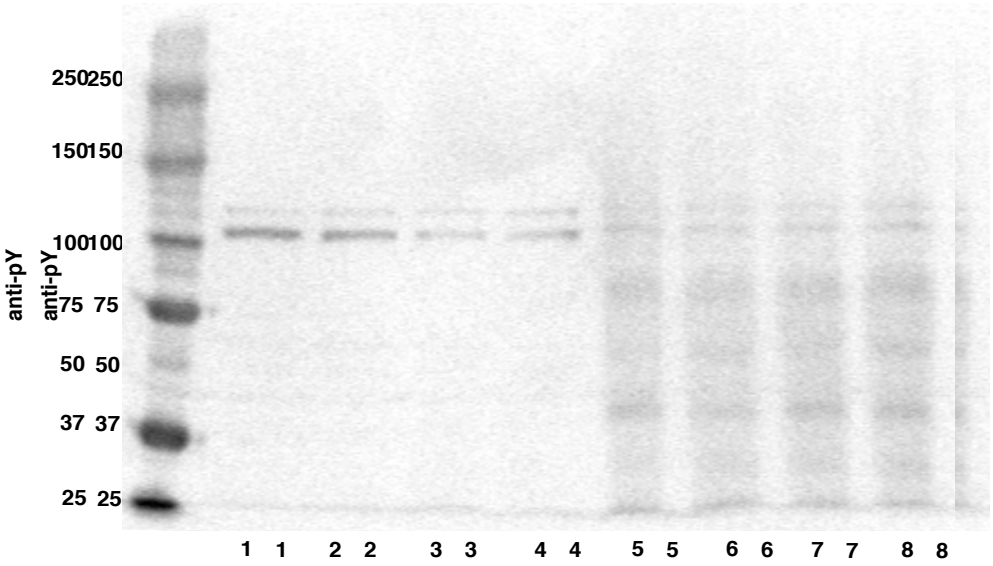

Lane 1-2: 30 min, 60 min in TYH(supernatant); Lane 3-4: 30 min, 60 min in HTYH(supernatant);
Lane 5-6: 30 min, 60 min in TYH(pellet); Lane 7-8: 30 min, 60 min in HTYH(pellet)

Figure 3-18. Kinetics study phosphorylation of tyrosine kinase in TYH with new cell lysis method.

The phosphorylation of PKA was also tested with a new cell lysis method. Different time points from 1 min to 60 min in TYH or HTYH with only the pellets of the sperm samples were analyzed (**Figure 3-19**). However, there were no differences between TYH and HTYH.

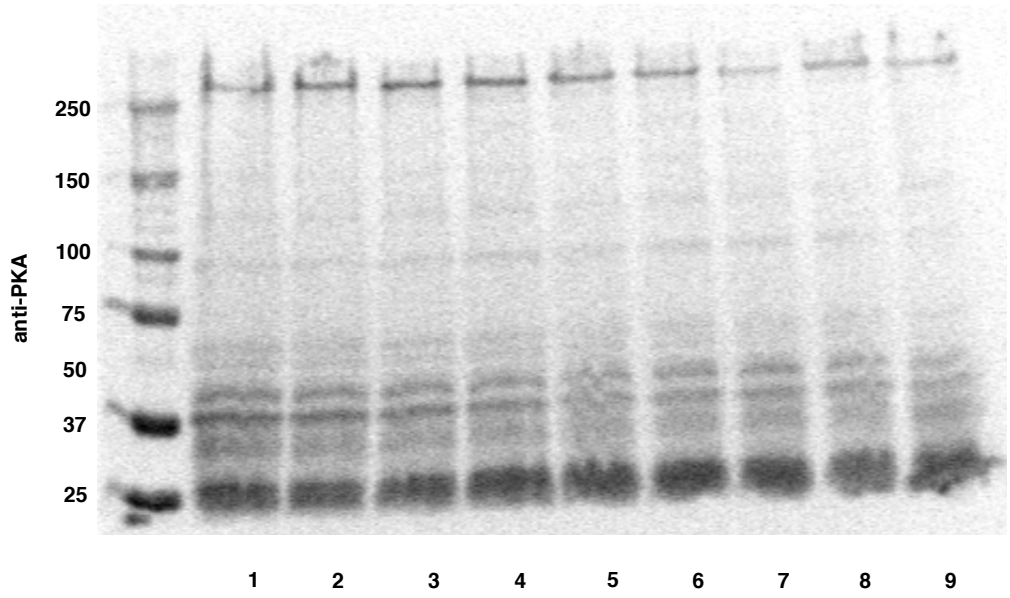

Lane 1-7: 1min, 3min. 5min, 10min, 30min, 45min, 60min in TYH (pellet)
Lane 8-9: 30min, 60min in HTYH (pellet)

Figure 3-19. Kinetic study of phosphorylation of PKA in TYH with new cell lysis method.

Poly(**1b**$_{50}$-*block*-**1a**$_{50}$) was used in the assay to compare with negative control. In **Figure 3-20**, after 30 min capacitation, the tyrosine phosphorylation increased by poly(**1b**$_{50}$-*block*-**1a**$_{50}$) after 5 min (lane5) and continued until 30 min (lane7). However, without block copolymers, the tyrosine phosphorylation increased to a maximum at 30 min (lane4). The results showed that poly(**1b**$_{50}$-*block*-**1a**$_{50}$) could make tyrosine phosphorylation happen faster.

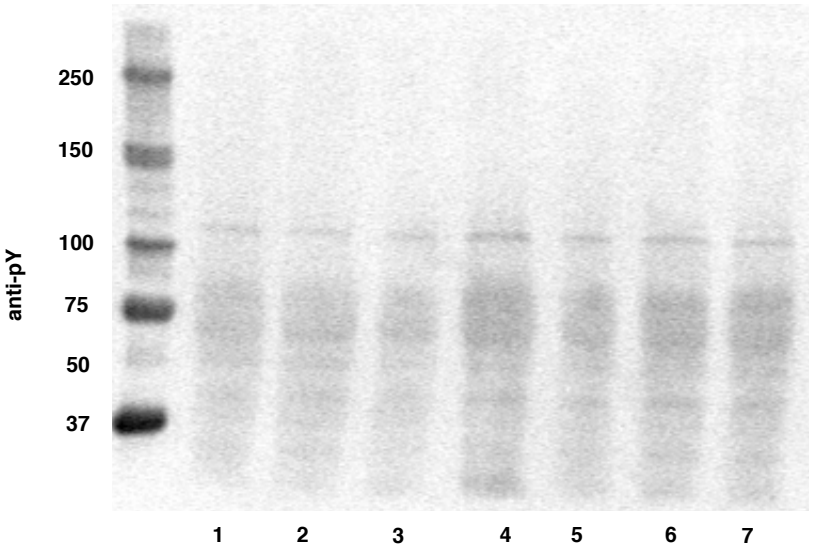

Lane 1-4: 0 min, 5 min. 15 min and 30 min in TYH (pellet);
Lane 5-7: 5 min, 15 min and 30 min in TYH (pellet) with poly(**1b**$_{50}$-*block*-**1a**$_{50}$)
Figure 3-20. Kinetics study phosphorylation of tyrosine in TYH with or without polymers

3.3 Conclusions

In summary, a series of random glycopolymers with varing saccharide densities as well as block copolymers presenting of two effective motifs were synthesized by ring-opening metathesis polymerization (ROMP). The conformations of these random and block copolymers were confirmed to be flexible cylinders by SAXS. A wide concentration range of induction by random glycopolymers was measured. The lowest density fucose and mannose polymers tested were most active on a per-sugar basis, highlighting the complexity of these interactions. The 50% ligand

density was more optimal for AE induction by GlcNAc polymers. Furthermore, the block polymer structure with two effective motifs showed that fucose and GlcNAc would dominate the AE induction when combined with mannose ligand. The activation curve of block copolymers with fucose and GlcNAc suggested crosstalk between signaling pathway. The best polymer structure for a particular lectin is not necessarily the optimum structure for other lectins, even those with the same carbohydrate specificity. Given the importance of AE in mammalian fertilization, glycopolymers with different structures will be a useful tool to study this complicated process. Future work will be focused on the development of glycopolymers with optimized inter-ligand space and gaining a thorough understanding of the ligand-receptor events in AE activation.

Our synthetic glycopolymers have demonstrated AE induction in wild-type mice sperm. In the future work, the sperm from transient mice with various gene knock-outs will be tested with our glycopolymers probes to further study the molecular mechanism of AE. For example, studies have indicated that the $Zp3r^{-/-}$ mice sperm undergo normal AE compared to wild-type sperm triggered by A23187.[39] However, A23187 is a non-physiological inducer and the normal AE of deficient sperm may affected by the redundancy of AE process. Therefore, our glycopolymers can induce AE as a physiological inducer, the different AE percentages between deficient sperm and wild-type sperm are expected, and the role of Zp3r/sp56 receptors in the ZP-induced AE can be better understood. Other gene knock-out mice sperm with deficient cell surface receptors, such as CD46[127] and CatSper[128], can also be tested by our glycopolymers in order to investigate their roles in ZP-induced AE.

Since sialyl-$Lewis^X$ oligosaccharide is predominant terminal sequence on human ZP and the precise glycoprotein that activates AE in human sperm is still unknown, our norbornyl glycopolymers are potential inducers of AE in human sperm.[44] These glycopolymers will be

screened with human sperm from fertile donors to identify sperm glycoprotein receptors required for human fertility. The flow cytometry approach by using glycopolymers with effective ligands will be applied to screen the sperm AE function in certain cases of human male infertility.

Chapter 4 Experimental Methods

4.1 Synthesis of Glycopolymers

4.1.1 Synthesis of glycomonomers

Materials. Sugars and other chemicals used were purchased from Advanced Chem Tech. (Louisville, KY), Sigma-Aldrich (Milwaukee, WI) or Fisher Scientific, Inc. (Springfield, NJ). CH_2Cl_2, DMF, CH_3OH, benzene, THF and EtO_2 were dried in a GlassContour solvent pushstill dispensing system (SG Water USA LLC, Nashua, NH); pyridine, hexane, acetone, ethyl acetate and dimethyl sulfide were used without further purification. $(H_2IMes)(3\text{-}BrPyr)_2Cl_2Ru{=}CHPh$ **3**, was prepared according to the literature.[129] All reactions were carried out under an N_2 atmosphere in oven-dried glassware unless otherwise specified. Moisture and oxygen-sensitive reagents were handled in glovebox.

General Methods. Analytical thin layer chromatography (TLC) was performed with precoated silica gel plates (60F254), flash chromatography was performed with silica gel-60 (230–400 mesh) and Combi-Flash chromatography with RediSep normal phase silica columns (Teledyne Isco, silica gel-60, 230–400 mesh). TLC spots were detected by UV and by staining with 10% phosphomolybdic acid (PMA) in ethanol. The usual workup mentioned in the following syntheses was three washes of the organic layer with 5% (w/v) aq $NaHCO_3$, followed by three washes with 1N aq HCl, and drying of the organic layer over Na_2SO_4. Bruker 400M Hz and Bruker 500MHz NMR instruments were used to perform NMR analyses. ^{1}H-NMR spectra are reported as chemical shift in parts per million (multiplicity, coupling constant in Hz, integration) and were acquired in $CDCl_3$ unless otherwise noted, ^{1}H-NMR data are assumed to be first order.

2,3,4,6-tetra-*O*-acetyl-D-glucopyranosyl trichloroacetimidate 7. To a solution of compound **8** (0.75 mmol, 260 mg) in dry CH_2Cl_2 (7.5 mL) was added trichloroacetonenitrile (7.5 mmol, 0.75

mL) and DBU (0.075 mmol, 11μL).[130] After stirring for 3h at rt, the mixture was concentrated. The crude oil was purified by chromatography (ethyl acetate: hexane = 3:7, v/v, combiflash) to yield **7** as a colorless oil (334 mg, Yield: 91%). The NMR spectra is in agreement with a previous report. ^{1}H NMR (600 MHz, $CDCl_3$): δ 8.69 (s, 1H), 6.56 (d, *J* = 3.7 Hz, 1H), 5.57 (t, *J* = 9.9 Hz, 1H), 5.18 (t, *J* = 9.9 Hz, 1H), 5.14 (dd, *J* = 10.2, 3.7 Hz, 1H), 4.27 (dd, *J* = 12.4, 4.2 Hz, 1H), 4.22 (ddd, *J* = 10.3, 4.2, 2.1 Hz, 1H), 4.13 (dd, *J* = 12.5, 2.2 Hz, 1H), 2.08 (s, 3H), 2.05 (s, 3H), 2.03 (s, 3H), 2.02 (s, 3H).

1-Chloroethyl-2,3,4,6-tetra-*O*-acetyl-α-D-glucopyranoside 6. To a cooled solution of compound **7** (0.457 mmol, 225mg) and 2-chloroethanol (2.286 mmol, 0.153 mL) in dry CH_2Cl_2 (4.5 mL) was added BF3-etherate (0.09 mmol, 8.5μL).[131] The solution was stirred for 3h at -80 °C, and worked-up. The crude oil was concentrated and purified by chromatography (ethyl acetate: hexane = 4:6, v/v, combiflash) to yield **6** as a white solid (158 mg, Yield: 70%). The NMR spectra is in agreement with a previous report. ^{1}H NMR (600 MHz, $CDCl_3$): δ 5.21 (dd, *J* = 10.1, 9.0 Hz, 1H), 5.08 (t, *J* = 9.7 Hz, 1H), 5.04 -4.98 (m, 1H), 4.57 (dd, *J* = 8.1, 1.1 Hz, 1H), 4.26 (dd, *J* = 12.4, 4.8 Hz, 1H), 4.15 (dd, *J* = 12.3, 2.4 Hz, 1H), 4.09 (dt, *J* = 10.8, 5.2 Hz, 1H), 3.80-3.73 (m, 1H), 3.71 (ddd, *J* = 9.9, 4.8, 2.4 Hz, 1H), 3.65-3.59 (m, 2H), 2.09 (d, *J* = 1.2 Hz, 3H), 2.06 (d, *J* = 1.1 Hz, 3H), 2.02 (s, 3H), 2.00 (d, *J* = 1.0 Hz, 3H).

1-Bromoethyl-2,3,4,6-tetra-O-acetyl-α-D-glucopyranoside 5. Boron trifluoride etherate (4.88 mmol, 556 mg) was added to a solution of **9** (0.977 mmol, 381 mg) and 2-bromoethanol (1.99 mmol) in dry CH_2Cl_2 (5mL). The reaction mixture was stirred in the dark under a nitrogen atmosphere for 16h. After work-up, the mixture was purified by chromatography (ethyl acetate: hexane = 1: 1, v/v, combiflash) to yield **5** as a white solid (213 mg, Yield: 74%). The NMR spectra is in agreement with a previous report.[132] ^{1}H-NMR (400 MHz, $CDCl_3$): δ 5.19-5.23 (t, J = 9.5,

1H), 5.05-5.10 (t, J = 9.8, 1H), 4.98-5.02 (t, J = 9.4, 1H), 4.56-4.58 (d, J = 8.0, 1H), 4.23-4.27 (dd, J = 12.3, 4.8, 1H), 3.78-3.84 (m, 1H), 3.69-3.73 (m, 1H), 3.43-3.47 (m, 2H), 3.63 (t, J = 10.0, 5.0, 2H), 2.08 (s, 3H), 2.06 (s, 3H), 2.02 (s, 3H), 2.00 (s, 3H).

1-Azidoethyl-2,3,4,6-tetra-O-acetyl-α-D-glucopyranoside 4. To a solution of compound **5** (0.222 mmol, 101 mg) in dry DMSO (8 mL) was added sodium azide (1.332 mmol, 87 mg). Then the reaction mixture was stirred for 1 h at 60 °C. After work-up the mixture was concentrated and purified by chromatography (ethyl acetate: hexane = 4: 6, v/v, combiflash) to yield **4** as a white solid (88 mg, Yield: 95%). The NMR spectra is in agreement with a previous report.[133] ^{1}H-NMR (400 MHz, $CDCl_3$): δ 5.17-5.22 (t, J = 9.5, 1H), 5.05-5.10 (t, J = 9.5, 1H),4.98- 5.02 (t, J = 9.4, 1H), 4.57-4.59 (d, J = 8.0, 1H), 4.21-4.25 (dd, J = 12.3, 4.8, 1H), 3.99-4.03 (m, 1H), 3.65-3.72 (m, 2H), 3.44-3.50 (m, 1H), 3.24-3.30 (m, 2H), 2.06 (s, 3H), 2.02 (s, 3H), 2.00 (s, 3H), 1.98 (s, 3H).

1-Aminoethyl-2,3,4,6-tetra-*O*-acetyl-α-D-glucopyranosylbicyclo[2.2.1]hept-5-ene-exo-2-carboxamide 1d'. The synthesis of **1d'** was performed following previous procedures.[57] **4** (0.816 mmol, 340 mg) and **1** (1.468 mmol, 202 mg) were combined with HOBt • H_2O (1.468 mmol, 225 mg) and dried for more than 1 h in vacuum. This mixture was dissolved in dry THF (8 mL) under N_2 and cooled to 0 °C. Then N,N'-Diisopropylcarbodiimide (1.468 mmol, 230 µL) was added and the solution was stirred for 10 min, followed by the addition of triethylphosine (1.756 mmol, 197 µL) and stirred for 1 h at 0 °C. The reaction mixture was stirred for 16 h at rt. After work-up, the mixture was concentrated and purified by chromatography (acetone: methylene chloride = 1:4, v/v, combiflash) to yield **1d'** as a white solid (271 mg, Yield: 65%). The NMR spectra is in agreement with a previous report.[57] ^{1}H NMR (400 MHz, $CDCl_3$): δ 6.08-6.14 (m, 2H), 5.98 (s, 1H), 5.17-5.22 (t, J = 9.5, 1H), 5.04-5.09 (m, 1H), 4.96-5.00 (t, J = 8.0, 1H), 4.50-4.52 (d, J=8.0, 1H), 4.22-4.28 (m, 1H), 4.11-4.13 (m, 1H), 3.82-3.86 (m, 1H), 3.69-3.73 (m, 2H), 3.42-3.45 (m,

2H), 2.90 (s, 2H), 2.07 (s, 3H), 2.03-2.04 (m, 3H), 2.02 (s, 3H), 2.00 (s, 3H), 1.86-1.91 (m, 1H), 1.67-1.70 (m, 1H), 1.24-1.34 (m, 2H).

Tetra-acetyl-α-L-fucopyranose 12. To a solution of L-fucose **13** (2.65 mmol, 436 mg) in pyridine (26 mL) was added DMAP (0.265 mmol, 32.4 mg). The solution was cooled to 0°C and fresh Ac_2O (13 mL) was added, the mixture allowed to stir for 2 h at 0°C. After the reaction was complete, the mixture was concentrated and diluted with 40 mL toluene, extracted with aq 1M HCl and 5% aq $NaHCO_3$ solution three times, dried with Na_2SO_4 and concentrated to yield as a colorless oil (881 mg, Yield: 100%). The NMR spectra is in agreement with a previous report.[130] ^{1}H-NMR (500 MHz, $CDCl_3$): δ 6.22 (d, J = 3.3 Hz, 1H), 5.41 – 5.07 (m, 2H), 4.33 – 4.06 (m, 1H), 2.11 (s, 1H), 2.07 (s, 3H), 2.04 (s, 3H), 1.90 (d, J = 7.8 Hz, 6H), 1.05 (d, J = 6.5 Hz, 3H).

1-Bromoethyl-2,3,4-tri-*O*-acetyl-L-fucopyranoside 11. Compound **11** was synthesized following the same procedure to prepare **5** and the product was obtained a mixture of α and β diastereomers (Yield: 83%). The mixture was used for the next step without further separation. ^{1}H-NMR (500 MHz, $CDCl_3$): δ 5.49-4.71 (m, 3.7H), 4.41 (d, J = 7.9 Hz, 0.3H), 4.22-4.12 (m, 0.7 H), 4.07 (dt, J = 11.0, 5.4 Hz, 0.3H), 3.88 (dt, J = 11.5, 5.7 Hz, 0.7H), 3.79 (t, J = 5.7 Hz, 1.6H), 3.77-3.63 (m, 1.3H), 3.40 (td, J = 5.8, 1.3 Hz, 3.6H), 2.92 (s, 0.7H), 2.06 (d, J = 5.2 Hz, 3H), 1.97 (d, J = 4.5 Hz, 3H), 1.87 (d, J = 3.4 Hz, 3H), 1.11 (d, J = 6.4 Hz, 1H), 1.03 (d, J = 6.5 Hz, 2H).

1-Azidoethyl-2,3,4-tri-*O*-acetyl-α-L-fucopyranoside 10. Compound **10** was synthesized following the same procedure to prepare **4** (Yield: 83%). ^{1}H-NMR (500 MHz, $CDCl_3$): δ 5.46-5.23 (m, 1.4H), 5.23-5.13 (m, 0.7H), 5.08 (d, J = 9.9 Hz, 1.4H), 4.98 (dd, J = 10.5, 3.5 Hz, 0.3H), 4.50 (d, J = 7.9 Hz, 0.3H), 4.14 (qd, J = 6.6, 1.5 Hz, 0.7H), 4.12-3.95 (m, 0.6H), 3.92-3.73 (m, 1H), 3.60 (dddd, J = 28.7, 10.6, 7.2, 4.2 Hz, 1H), 3.52-3.20 (m, 2H), 2.12 (d, J =4.5 Hz, 3H), 2.08

– 1.97 (m, 3H), 1.93 (d, J = 2.3 Hz, 3H), 1.26 – 1.15 (m, 1H), 1.11 (d, J = 6.5 Hz, 2H).

1-Aminoethyl-2,3,4-tri-*O*-acetyl-α-L-fucopyranosyl bicyclo [2.2.1] hept-5-ene-exo-2-carbox-amide 1a'. Compound **1a'** was synthesized following the same procedure to prepare **1d'** (Yield: 35%). ^{1}H NMR (500 MHz, $CDCl_3$): δ 6.17 (dd, *J* = 5.9, 2.8 Hz, 1H), 6.13 (ddd, *J* = 11.1, 5.7, 3.0 Hz, 1H), 5.94 (s, 1H), 5.38 (dt, *J* = 10.9, 3.4 Hz, 1H), 5.31 (s, 1H), 5.17 (ddd, *J* = 10.8, 3.7, 1.0 Hz, 1H), 5.08 (t, *J* = 3.1 Hz, 1H), 4.16 (dq, *J* = 8.5, 7.1, 6.1 Hz, 1H), 3.79 (m, 1H), 3.53 (m, 3H), 2.94 (dt, *J* = 5.2, 2.6 Hz, 2H), 2.19 (s, 3H), 2.09 (d, *J* = 7.0 Hz, 3H), 2.02 (s, 3H), 1.94 (dt, *J* = 10.9, 3.6 Hz, 1H), 1.73 (d, *J* = 8.3 Hz, 1H), 1.44 – 1.31 (m, 2H), 1.17 (dd, *J* = 6.6, 2.6 Hz, 3H).

2,3,4,6-tetra-*O*-acetyl-D-mannopyranosyl trichloroacetimidate 17. Compound **17** was synthesized following the same procedure to prepare **7** from **18** (Yield: 92%). The NMR spectra is in agreement with a previous report. ^{1}H NMR (400 MHz, $CDCl_3$): δ 6.17-6.18 (d, *J* = 1.6 Hz, 1H), 5.40 – 5.28 (m, 3H), 4.20 – 4.16 (m, 1H), 4.10 – 4.00 (m, 2H), 2.10 (s, 3H), 1.98 (s, 3H), 1.97 (s, 3H), 1.91 (s, 3H).

1-Chloroethyl-2,3,4,6-tetra-*O*-acetyl-α-D-mannopyranoside 16. Compound **16** was synthesized following the same procedure to prepare **6** (Yield: 68%). ^{1}H NMR (400 MHz, $CDCl_3$): δ 5.27 – 5.18 (m, 3H), 4.80 (d, *J* = 1.2 Hz, 1H), 4.21-- 4.17 (dd, *J* = 12.3, 5.5 Hz, 1H), 4.07 – 4.03 (m, 2H), 3.89—3.83 (dt, *J* = 11.5, 5.8 Hz, 1H), 3.78—3.73 (dt, *J* = 11.2, 5.9 Hz, 1H), 3.64—3.64 (t, *J* = 5.6 Hz, 2H), 2.08 (s, 3H), 2.03 (s, 3H), 1.98 (s, 3H), 1.92 (s, 3H).

1-Bromoethyl-2,3,4,6-tetra-O-acetyl-α-D-mannopyranoside 15. Compound **15** was synthesized following the same procedure to prepare **5** from **19** (Yield: 84%). ^{1}H-NMR (400 MHz, $CDCl_3$): δ 5.23-5.31 (m, 3H), 4.84 (s, 1H), 4.20-4.25 (dd, J= 12.68, 5.80, 1H), 4.08-4.11 (m, 2H), 3.82-3.97 (m, 2H), 3.47-3.50 (t, J = 5.96, 2H), 2.12 (s, 3H), 2.06 (s, 3H), 2.01 (s, 3H), 1.95 (s, 3H).

1-Azidoethyl-2,3,4,6-tetra-O-acetyl-α-D-mannopyranoside 14. Compound **14** was synthesized following the same procedure to prepare **4** (Yield: 95%). ^{1}H-NMR (400 MHz, $CDCl_3$): δ 5.27-5.35 (m, 3H), 4.88 (s, 1H), 4.27-4.31 (dd, J= 12.3, 5.4, 1H), 4.11-4.15 (dd, J=12.3,2.3,1H), 4.03-4.07 (m, 1H), 3.80-3.90 (m, 1H), 3.65-3.70 (m, 1H), 3.45-3.53 (m, 1H), 2.16 (s, 3H), 2.11 (s, 3H), 2.05 (s, 3H), 2.00 (s, 3H).

1-Aminoethyl-2,3,4,6-tetra-O-acetyl-α-D-mannopyranosyl bicyclo[2.2.1]hept-5-ene-exo-2-carboxamide 1b'. Compound **1b'** was synthesized following the same procedure to prepare **1d'** (Yield: 64%). ^{1}H-NMR (400 MHz, $CDCl_3$): δ 6.12-6.17 (m, 2H), 5.98-6.00 (m, 1H), 5.26-5.38 (m, 3H), 4.86 (s, 1H), 4.26-4.31 (ddd,J=12.24, 5.60, 2.20, 1H), 4.11-4.15 (dd, J = 12.24, 2.48, 1H), 3.96-4.01 (m, 1H), 3.79-3.84 (m, 1H), 3.43-3.63 (m, 3H), 2.95 (s, 2H), 2.18 (s, 3H), 2.12(s, 3H), 2.07 (s, 3H), 2.03 (s, 3H), 1.87-1.98 (m, 1H), 1.71-1.74(t, J = 6.80, 1H), 1.37-1.39 (m, 2H).

(1-Hydroxyl)-2-acetamido-3,4,6-tri-O-acetyl-D-glucopyranose 25. To a solution of compound **26** (1.171 mmol, 389 mg) and ammonium carbonate (4.683 mmol, 450mg) dry THF/MeOH (4:8mL) was added and the mixture was stirred at rt for 16h. The mixture was concentrated and then diluted with EtOAc, and the organic layer was extracted with cold brine, dried with Na_2SO_4 and concentrated to yield **25** as a colorless oil (325 mg, Yield: 80%).[134.1]^{1}H-NMR (500 MHz, $CDCl_3$): δ 6.08-6.11 (d, J = 9.3, 1H), 5.23-5.32 (m, 2H), 5.10-5.14 (t, J = 9.5, 1H), 4.20-4.30 (m, 3H), 4.05-4.13 (m, 3H), 2.09 (s, 3H), 2.02 (d, J = 3.6, 6H), 1.97 (s, 3H),1.25 (s, 3H).

2-Acetamido-3,4,6-tri-*O*-acetyl-2-deoxy-D-glucopyranosyl trichloroacetimidate 24. Compound **24** was synthesized following the same procedure to prepare **7**. Yield: 65%. ^{1}H-NMR (600 MHz, $CDCl_3$): δ 8.81 (s, 1H), 6.37 (d, J = 3.1, 1H), 5.67-5.71 (d, J = 8.7, 1H), 5.23-5.28 (m,

2H), 4.53-4.58 (m, 1H), 4.23-4.28 (dd, J = 12.9, 4.6, 1H), 4.11-4.13 (d, J = 10.3, 2H), 2.08 (s, 3H), 2. 06 (d, J = 3.4, 6H), 1.94 (s, 3H), 1.26(s, 3H).

1-Chloroethyl-2-Acetamido-3,4,6-tri-*O*-acetyl-2-deoxy-β-D-glucopyranoside 23. Compound **23** was synthesized following the same procedure to prepare **5**. Yield: 62%. 1H NMR (600 MHz, $CDCl_3$): δ 5.50 (d, *J* = 8.9 Hz, 1H), 5.34—5.27 (m, 1H), 5.08 (t, *J* = 9.7 Hz, 1H), 4.77 (dd, *J* = 8.4, 0.9 Hz, 1H), 4.26 (dd, *J* = 12.3, 4.7 Hz, 1H), 4.16—4.08 (m, 2H), 3.87 (dt, *J* = 10.5, 8.7 Hz, 1H), 3.77 (ddd, *J* = 11.0, 6.8, 5.8 Hz, 1H), 3.71 (ddd, *J* = 10.1, 4.8, 2.4 Hz, 1H), 3.64 (ddd, *J* = 6.1, 4.9, 1.0 Hz, 2H), 2.09 (s, 3H), 2.03 (d, *J* = 5.7, 6H), 1.97 (s, 3H).

1-Azidoethyl-2-acetamido-3,4,6-tri-*O*-acetyl-2-deoxy-β-D-glucopyranoside 22. Compound **22** was synthesized following the same procedure to prepare **4**. Yield: 73%. 1H NMR (500 MHz, $CDCl_3$): δ 5.60 (d, *J* = 8.6 Hz, 1H), 5.38 (dd, *J* = 10.6, 9.3 Hz, 1H), 5.09 (t, *J* = 9.7 Hz, 1H), 4.85 (d, *J* = 8.3 Hz, 1H), 4.27 (dd, *J* = 12.3, 4.8 Hz, 1H), 4.17 (dd, *J* = 12.3, 2.4 Hz, 1H), 4.06 (ddd, *J* = 10.9, 4.8, 3.3 Hz, 1H), 3.83 (dt, *J* = 10.8, 8.5 Hz, 1H), 3.78—3.68 (m, 2H), 3.52 (ddd, *J* = 13.4, 8.6, 3.2 Hz, 1H), 3.28 (ddd, *J* = 13.5, 4.7, 3.2 Hz, 1H), 2.10 (s, 3H), 2.05 (d, *J* = 3.4 Hz, 6H), 1.97 (s, 3H).

N-(2-hydroxyethyl)bicyclo[2.2.1]hept-5-ene-2-carboxamide 21. Yield: 50%. ^{1}H-NMR (400 MHz, $CDCl_3$): δ 6.74 (s, 1H), 6.11 (dd, J = 15.0, 3.0 Hz, 2H), 4.19 (s,1H), 3.68 (d,J = 3.6 Hz, 2H), 3.39 (q, J = 5.2 Hz, 2H), 2.91 (d, J = 3.4 Hz, 2H), 2.07 (dd, J = 4.6 Hz, 1H), 1.87 (dt, J =11.4 Hz, 1H), 1.67 (d, J = 8.2 Hz, 1H), 1.34 (dd, J = 8.9 Hz, 2H).

Aminoethyl-2-acetamido-3,4,6-tri-*O*-acetyl-2-deoxy-β-D-glucotopyranosyl bicycle [2.2.1] hept-5-ene-exo-2-carboxamide 1c'. The NMR spectra is in agreement with a previous report.[57] Yield: 20%. 1H NMR (400 MHz, $CDCl_3$): δ 6.25 (d, *J* = 4 Hz, 1H), 6.22 – 6.01 (m, 3H), 5.19 (td,

J = 9.9, 4.7 Hz, 1H), 5.08 (td, *J* = 9.6, 2.7 Hz, 1H), 4.58 (d, *J* = 8.4 Hz, 1H), 4.26 (dt, *J* = 12.7, 5.0 Hz, 1H), 4.14 (dd, *J* = 12.2, 2.2 Hz, 1H), 3.96 (tq, *J* = 8.7, 3.9 Hz, 1H), 3.86 (ddt, *J* = 9.9, 6.5, 3.3 Hz, 1H), 3.70 (ddd, *J* = 10.0, 5.2, 2.4 Hz, 2H), 3.58 – 3.49 (m, 1H), 3.39 (m, 1H), 2.91 (s, 2H), 2.08 (d, *J* = 1.7 Hz, 3H), 2.04 (d, *J* = 4.6 Hz, 6H), 1.95 (d, *J* = 10.7 Hz, 3H), 1.90 (m, 1H), 1.70 (t, *J* = 8.0 Hz, 1H), 1.38 – 1.22 (m, 3H).

2a'[1]. Compound **2a'** was synthesized following the same procedure to prepare **1d'**. Yield: 65%. ^{1}H NMR (500 MHz, CD_2Cl_2) δ 7.78 (d, *J* = 8.4 Hz, 1H), 7.63 (dd, *J* = 24.2, 8.0 Hz, 1H), 7.41 – 7.21 (m, 2H), 6.05 – 5.92 (m, 1H), 5.64 – 5.45 (m, 2H), 5.28 – 5.10 (m, 2H), 5.06 – 4.88 (m, 3H), 4.79 (t, *J* = 5.4 Hz, 1H), 4.09 – 3.95 (m, 1H), 3.80 – 3.58 (m, 3H), 3.45 – 3.23 (m, 3H), 2.34 – 2.21 (m, 1H), 2.18 – 1.89 (m, 12H), 1.88 (s, 3H), 1.85 – 1.72 (m, 2H), 1.70 – 1.45 (m, 5H), 1.34 – 1.08 (m, 3H), 1.01 (dd, *J* = 21.4, 6.5 Hz, 14H). ^{13}C NMR (126 MHz, $CDCl_3$) δ 178.0, 170.8, 170.4, 130.9, 130.8, 129.8, 96.6, 77.5, 77.4, 77.2, 71.3, 71.2, 71.1, 70.3, 68.30, 68.07, 67.96, 67.79, 67.76, 65.01, 64.80, 45.7, 42.3, 39.1, 32.7, 30.5, 29.8, 28.3, 26.18, 26.1, 24.3, 23.7, 21.0, 20.9, 20.8, 16.0, 1.2.

2b'[2]. Compound **2b'** was synthesized following the same procedure to prepare **1d'**. Yield: 75%. ^{1}H NMR ($CDCl_3$, 500 MHz,) δ 5.90 (q, *J* = 5.9 Hz, 1H), 5.63 (dtd, *J* = 19.9, 10.8, 9.9, 3.8 Hz, 2H), 5.30 – 5.17 (m, 3H), 4.76 (s, 1H), 4.21 (dd, *J* = 12.3, 5.6 Hz, 1H), 4.10 – 4.00 (m, 1H), 3.90 (t, *J* = 7.7 Hz, 1H), 3.86 – 3.66 (m, 1H), 3.47 (tt, *J* = 8.1, 3.6 Hz, 2H), 3.39 – 3.29 (m, 1H), 2.34 (dtt, *J* = 14.1, 8.9, 4.4 Hz, 1H), 2.21 (dp, *J* = 12.5, 6.5, 6.0 Hz, 1H), 2.18 – 1.80 (m, 18H), 1.63 (ddt, *J* = 38.7, 15.2, 6.9 Hz, 5H), 1.35 (tt, *J* = 15.3, 6.1 Hz, 1H), 1.20 (t, *J* = 7.1 Hz, 1H), 1.07 (d, *J* = 6.5 Hz, 2H). ^{13}C NMR ($CDCl_3$, 126 MHz) δ 178.1, 171.2, 170.7, 170.1, 169.7, 157.2, 130.7, 129.8,

[1] The compound was synthesized and 1H NMR characterized by Maria Rodolis.
[2] The compound was synthesized and characterized by Maria Rodolis.

97.7, 77.5, 77.4, 77.2, 69.4, 69.1, 68.7, 67.4, 66.2, 62.5, 60.5, 45.5, 42.0, 38.9, 32.7, 32.5, 30.5, 30.3, 28.1, 26.0, 24.2, 23.6, 20.9, 20.8, 20.7, 14.2, 1.1.

2c'. Compound **2c'** was synthesized following the same procedure to prepare **1d'**.Yield: 75%. ^{1}H NMR ($CDCl_3$, 500 MHz) δ 7.77 (dd, *J* = 73.8, 8.3 Hz, 1H), 7.40 (dt, *J* = 26.6, 7.3 Hz, 1H), 6.49 (dd, *J* = 19.2, 8.4 Hz, 1H), 6.23 (dt, *J* = 32.0, 6.6 Hz, 1H), 5.73 – 5.51 (m, 3H), 5.17 (t, *J* = 10.0 Hz, 1H), 5.04 (q, *J* = 9.7 Hz, 2H), 4.85 – 4.73 (m, 0H), 4.61 (t, *J* = 8.2 Hz, 1H), 4.31 (td, *J* = 10.0, 3.6 Hz, 0H), 4.20 (ddd, *J* = 17.5, 12.3, 4.8 Hz, 1H), 4.08 (dd, *J* = 19.1, 12.5 Hz, 2H), 3.94 (ddt, *J* = 18.7, 9.5, 4.6 Hz, 1H), 3.80 (q, *J* = 9.3, 8.1 Hz, 1H), 3.73 – 3.59 (m, 2H), 3.59 – 3.37 (m, 2H), 3.30 (qd, *J* = 13.3, 11.4, 6.2 Hz, 1H), 2.33 (ddt, *J* = 14.6, 9.7, 5.4 Hz, 1H), 2.23 (q, *J* = 8.0, 7.5 Hz, 2H), 2.11 (p, *J* = 6.6 Hz, 3H), 2.05 (d, *J* = 4.8 Hz, 6H), 1.98 (dd, *J* = 10.9, 4.2 Hz, 10H), 1.93 (s, 3H), 1.83 (dq, *J* = 13.6, 4.4 Hz, 1H), 1.74 – 1.52 (m, 6H), 1.42 – 1.12 (m, 6H), 1.11 – 1.01 (m, 1H), 0.82 (dp, *J* = 26.5, 6.8 Hz, 2H). ^{13}C NMR ($CDCl_3$, 126 MHz) d 178.7, 171.9, 169.4, 130.6, 129.6, 129.5, 128.4, 126.7, 125.7, 117.9, 110.8, 101.0, 97.8, 77.4, 77.3, 77.1, 72.6, 71.9, 71.3, 68.4, 68.1, 67.8, 62.1, 54.3, 51.6, 45.5, 45.3, 42.2, 39.0, 32.5, 30.4, 30.3, 30.2, 29.7, 29.3, 28.0, 25.9, 24.1, 23.4, 23.0, 22.7, 20.7, 20.6, 19.4, 18.9, 14.1, 5.5.

2d'[3]. Compound **2d'** was synthesized following the same procedure to prepare **1d'**.Yield: 85%. ^{1}H NMR ($CDCl_3$, 500 MHz) δ 5.87 (q, *J* = 5.1 Hz, 1H), 5.60 (dq, *J* = 31.0, 9.0 Hz, 2H), 5.14 (t, *J* = 9.5 Hz, 1H), 4.96 (dt, *J* = 44.2, 9.4 Hz, 2H), 4.58 (d, *J* = 7.9 Hz, 1H), 4.46 (d, *J* = 7.9 Hz, 1H), 4.20 (dd, *J* = 12.4, 4.9 Hz, 1H), 4.11 – 3.96 (m, 2H), 3.78 (qd, *J* = 11.9, 10.1, 6.1 Hz, 2H), 3.64 (dddd, *J* = 19.6, 14.5, 10.1, 5.4 Hz, 2H), 3.36 (dtt, *J* = 16.8, 11.4, 6.6 Hz, 2H), 2.32 (dtd, *J* = 14.4, 9.2, 5.0 Hz, 1H), 2.22 – 1.79 (m, 19H), 1.72 – 1.51 (m, 4H), 1.31 (tq, *J* = 13.4, 6.3 Hz, 1H), 1.19 (t, *J* = 7.0

[3] The compound was synthesized and characterized by Maria Rodolis.

Hz, 1H), 1.05 (d, J = 6.5 Hz, 4H). ^{13}C NMR ($CDCl_3$, 125 MHz,) δ 178.0, 171.2, 170.6, 170.2, 169.5, 157.3, 130.6, 129.7, 100.9, 95.9, 77.5, 77.4, 77.2, 72.7, 71.9, 71.4, 70.7, 69.2, 68.7, 68.3, 67.6, 67.4, 61.9, 60.4, 45.5, 41.8, 39.0, 32.5, 30.4, 30.3, 28.1, 26.0, 24.2, 23.6, 21.0, 20.8, 20.7, 20.6, 20.3, 14.2, 1.0.

4.1.2 Ring-opening metathesis of polymerization (ROMP) of glycopolymers

The general method of ROMP was as follows:[57] monomer catalyst and solvent were thoroughly dried before use. Monomer **1a-b** or **2a-b** (0.04 mmol, 19.6 mg) was dissolved in 0.674 mL CH_2Cl_2. To the reaction was added 3rd generation Grubbs catalyst (**3**) (0.4 μmol, 0.340 mg). Random polymers preparation. Monomer (10 eq, 90 eq and 50 eq) and catalyst (1 eq) were mixed in solvent CH_2Cl_2 to achieve a final concentration of total monomer of 57 μM and allowed to react at rt. The reaction was monitored by TLC and immediately quenched with ethyl vinyl ether. Ethyl vinyl ether (100 μL) was added to quench the reaction when it was done. The mixture was stirred for an additional 30 min. Poly(**1**)$_{100}$ was isolated by precipitation with cold Et_2O to yield 100-mers as light yellow sticky oils. Poly(**2**)$_{100}$ was purified by column chromatography (100% ethyl acetate or 100% isopropyl alcohol).

Purified poly(**1**)$_{100}$ was dissolved in filtered THF (about 1.3 mg/mL). An aliquot (100 μL) of the polymer solution was injected and analyzed by gel permeation chromatography and static light scattering. Elution was performed at 0.7 mL/min with THF. UV signals were measured at 220 nm and 256 nm at 30 ^{o}C. Narrowly dispersed polystyrene standards from Sigma Aldrich were used as molecular weight calibrants. The number average and weighted average molecular weights were calculated from the chromatogram. For $Đ_M$ (dispersity index) determination of poly(**2**)$_{100}$, the polymers were dissolved in $CHCl_3$ (0.5 mg/mL). An aliquot (100 μL) of the polymer solution was

injected and analyzed by gel permeation chromatography using a Phenogel column (300 x 7.80 mm, 5 μm, linear mixed bed, 0-40k MW range).

poly(**1a'**)$_{100}$: Yield after purification: 65%.^{1}H NMR (500 MHz, $CDCl_3$): δ 5.75-6.47 (m), 4.89-5.56 (with max at 5.06, 5.15, 5.30, 5.34), 4.15 (br s), 3.25-3.94 (with max at 3.38, 3.54, 3.76), 3.07 (br s), 2.70 (br s), 2.26-2.47 (m), 1.78-2.24 (with max at 2.02, 2.09, 2.19), 1.63 (br s), 1.28 (br s), 1.16 (br s), 0.72-0.99 (with max at 0.90).

poly(**1b'**)$_{100}$: Yield after purification: 92%. ^{1}H NMR (500 MHz, $CDCl_3$): δ 5.85-6.3 (m), 5.10-5.50 (with max at 5.23, 5.27, 5.34), 4.80 (br s), 4.26 (br s), 4.09 (br s), 3.96 (br s), 3.75 (br s), 3.52 (br s), 3.02 (br s), 2.68 (br s), 2.33 (br s), 1.73-2.24 (with max at 2.00, 2.05, 2.10, 2.15), 1.60 (br s), 1.05-1.27 (m).

poly(**1c'**)$_{100}$: Yield after purification: 81%. ^{1}H NMR (500 MHz, $CDCl_3$): δ 6.01-6.62 (m), 5.14-5.54 (with max at 5.22, 5.31), 5.08 (br s), 4.48-4.96 (m), 4.27 (br s), 4.15 (br s), 2.84-4.06 (with max at 2.92, 2.99, 3.37, 3.54, 3.69, 3.80, 3.87, 3.98), 2.66 (br s), 2.38 (br s), 1.76-2.20 (with max at 1.91, 1.96, 2.04, 2.09), 1.62 (br s), 0.97-1.48 (with max at 1.16, 1.27, 1.35).

poly(**1d'**)$_{100}$ Yield after purification: 75%. ^{1}H NMR (500 MHz, $CDCl_3$): δ 5.78-6.0 (m), 5.23-5.48 (with max at 5.28, 5.32), 5.20 (br s), 5.07 (br s), 4.96 (br s), 4.55 (br s), 4.28 (br s), 4.13 (br s), 3.84 (br s), 3.63-3.77 (with max at 3.70, 3.75), 3.18-3.62 (with max at 3.30, 3.50, 3.53), 3.03 (br s), 2.67 (br s), 2.20-2.37 (with max at 2.37, 2.33), 1.90-2.20 (with max at 1.94, 2.02, 2.05, 2.10, 2.19), 1.75 (br s), 1.60 (br s), 0.97-1.39 (m).

poly(**1a'**$_{50}$-*ran*-**1d'**$_{50}$): Yield after purification: 92%. ^{1}H NMR (400 MHz, $CDCl_3$): δ 6.09 (br s), 5.63-4.86 (m), 4.53 (br s), 4.27 (br s), 4.20-4.02 (m), 3.95-3.22 (m), 3.17-2.51(with max at 3.17, 2.92, 2.84), 2.51-1.75 (with max 2.41, 2.19, 2.14, 1.83), 1.73 (br s), 1.39-1.02 (with max at

1.26,1.11).

poly(**1a'**$_{10}$-*ran*-**1d'**$_{90}$): Yield after purification: 73%. ^{1}H NMR (400 MHz, $CDCl_3$): δ 5.93 (br s), 5.54-4.79 (m), 4.54 (br s), 4.26 (br s), 4.13 (d), 3.96-3.20(with max 3.52, 3.31), 3.02 (br s), 2.68 (br s), 2.40-1.80 (with max 2.28, 2.17, 2.10,2.03), 1.72 (br s), 1.58 (br s), 1.38-0.90 (with max 1.26, 1.14).

poly(**1b'**$_{50}$-*ran*-**1d'**$_{50}$): Yield after purification: 97%. ^{1}H NMR (500 MHz, $CDCl_3$): δ 5.78-6.40 (m), 5.20-5.50 (with max at 5.23, 5.27, 5.32), 5.07 (br s), 4.96 (br s), 4.80 (br s), 4.55 (br s), 4.26 (br s), 4.13 (br s), 3.96 (br s), 3.84 (br s), 3.63-3.77 (with max at 3.70, 3.75), 3.18-3.62 (with max at 3.30, 3.50, 3.53), 3.03 (br s), 2.67 (br s), 2.20-2.37 (with max at 2.37, 2.33), 1.73-2.24 (with max at 1.94, 2.00, 2.02, 2.05, 2.10, 2.15, 2.19), 1.60 (br s), 0.97-1.39 (m).

poly(**1b'**$_{10}$-*ran*-**1d'**$_{90}$): Yield after purification: 98%. ^{1}H NMR (500 MHz, $CDCl_3$): δ 5.78-6.40 (m), 5.20-5.50 (with max at 5.23, 5.27, 5.32), 5.07 (br s), 4.96 (br s), 4.80 (br s), 4.55 (br s), 4.26 (br s), 4.13 (br s), 3.96 (br s), 3.84 (br s), 3.63-3.77 (with max at 3.70, 3.75), 3.18-3.62 (with max at 3.30, 3.50, 3.53), 3.03 (br s), 2.67 (br s), 2.20-2.37 (with max at 2.37, 2.33), 1.73-2.24 (with max at 1.94, 2.00, 2.02, 2.05, 2.10, 2.15, 2.19), 1.60 (br s), 0.97-1.39 (m).

poly(**1c'**$_{50}$-*ran*-**1d'**$_{50}$): Yield after purification: 96%. ^{1}H NMR (400 MHz, $CDCl_3$): δ 6.41-5.75 (m), 5.75-5.30 (br s), 4.72 (br s), 4.56 (br s), 4.26 (br s), 4.13 (br s), 4.00-3.12 (with max 3.57, 3.52), 2.99 (br s), 2.61 (br s), 2.32 (br s), 2.19-1.40 (with max 1.86, 1.82, 1.64), 1.40-0.93 (m), 0.96-0.78 (m).

poly(**1c'**$_{10}$-*ran*-**1d'**$_{90}$): Yield after purification: 89%. ^{1}H NMR (400 MHz, $CDCl_3$): δ 5.91 (br s), 5.56 – 4.89 (m), 4.69 (br s), 4.54 (br s), 4.26(br s), 4.13 (d), 3.91 – 3.17 (m), 3.01 (br s), 2.67 (br s), 2.50-1.79 (m, with max 2.20), 1.63(br s), 1.37 – 0.94 (m),4.84 – 4.73 (m).

poly(**1b'**$_{50}$-*block*-**1a'**$_{50}$): Yield after purification: 86%. ^{1}H NMR (500 MHz, $CDCl_3$): δ 6.32 – 5.68 (m), 5.53 – 4.91 (m), 4.80 (dd), 4.26 (br s), 4.10(br s), 3.86 (br s), 3.87 – 3.13 (m), 3.03 (d, J = 15.0 Hz), 2.68 (br s), 2.47 – 1.72 (with max 2.21, 2.17), 1.58 (br s), 1.32 – 1.00 (m).

poly(**1b'**$_{50}$-*block*-**1c'**$_{50}$) Yield after purification: 92%. ^{1}H NMR (400 MHz, $CDCl_3$): δ 6.67 – 5.80 (m), 5.51 – 4.88 (m), 4.80 (br s), 4.59 (br s), 4.25 (br s), 4.11 (t, J = 14.0 Hz), 4.03 –2.66(with max 3.14,2.96), 2.66 (br s), 2.35 (br s), 2.24 – 1.75 (m), 1.65 (br s), 1.40 – 0.98 (m).

poly(**1a'**$_{50}$-*block*-**1c'**$_{50}$) Yield after purification: 100%. ^{1}H NMR (400MHz, $CDCl_3$): δ 6.38 – 5.71 (m), 5.47 – 4.86 (m), 4.79 (br s), 4.26 (m), 4.13 (t, J = 9.2 Hz), 4.03 -3.16 (with max 3.92, 3.87, 3.79, 3.61, 3.52, 3.36), 3.16 – 2.83 (m), 2.69 (br s), 2.26-1.88 (with max 2.17, 2.11), 1.72-1.40(with max 1.72, 1.60), 1.40-0.88(with max 1.26, 1.13, 0.88).

poly(**1a'**$_{50}$-*block*-**1d'**$_{50}$) Yield after purification: 89%. ^{1}H NMR (400 MHz, $CDCl_3$): δ 5.92 (br s), 5.54 – 4.80 (m), 4.53 (dd), 4.29 (br s), 4.20 – 4.10 (m), 3.90-3.15 (with max 3.82, 3.78, 3.51, 3.34), 3.03 (br s), 2.69 (br s), 2.27-1.92 (with max 2.17, 2.12), 1.72(br s), 1.60 (d), 1.26 (br s), 1.14 (q).

poly(**1b'**$_{50}$-*block*-**1d'**$_{50}$): Yield after purification: 89%. ^{1}H-NMR (400 MHz, $CDCl_3$): δ 6.31 – 5.70 (m), 5.39 – 5.12 (m), 5.07 (t), 4.96 (t), 4.88 (br, s), 4.53 (br s), 4.27 (br s), 4.11 (t), 3.97 (br s), 3.90 – 3.61 (with max 3.61,3.38, 3.32), 3.02 (br s), 2.68 (br s), 2.46 -1.86 (m), 1.60 (br s).

poly(**1c'**$_{50}$-*block*-**1d'**$_{50}$): Yield after purification: 65%. ^{1}H NMR (400 MHz, Chloroform-*d*): δ 6.41 – 5.75 (m), 5.75-5.30 (br s), 4.72 (br s), 4.56 (br s), 4.26 (br s), 4.13 (br s), 4.00 -3.12(with max 3.57, 3.52), 2.99 (br s), 2.61 (br s), 2.32 (br s), 2.19 –1.40 (with max 1.86, 1.82, 1.64), 1.40 – 0.93 (m), 0.96 – 0.78 (m).

poly(**2a'**)$_{100}$[4]: ^{1}H NMR ($CDCl_3$, 400 MHz,) δ 5.57 – 5.21 (m), 5.14 (d, *J* = 10.7 Hz), 5.04 (s), 4.12 (d, *J* = 8.0 Hz), 3.93 – 3.23 (m), 2.77 – 2.46 (m), 2.16 (s), 2.06 (s), 1.77 – 1.16 (m), 1.14 (d, *J* = 6.4 Hz), 0.96 – 0.68 (m).

poly(**2b'**)$_{100}$[5]: ^{1}H-NMR (CD_2Cl_2,500 MHz) δ 6.25 – 5.70 (br), 5.30 (q, *J* = 10.6), 5.22 (s), 5.12 (t, *J* = 9.5 Hz), 4.96 (t, *J* = 9.0 Hz), 4.83 (dt, *J* = 18.6, 9.2 Hz), 4.49 (t, *J* = 8.2 Hz), 4.15 (dq, *J* = 12.7, 7.3, 6.0 Hz), 4.04 (dq, *J* = 12.7, 7.4, 6.9 Hz), 3.75 (dd, *J* = 9.8, 5.0 Hz), 3.69 – 3.54 (m), 3.34 (dtd, *J* = 18.3, 13.3, 7.0 Hz), 2.04 (dd, *J* = 23.0, 10.2 Hz), 1.97 (s), 1.91 (d, *J* = 14.1 Hz), 1.64 – 1.15 (m), 0.79 (q, *J* = 12.7, 9.6 Hz).

poly(**2c'**)$_{100}$: ^{1}H NMR ($CDCl_3$, 500 MHz) δ 6.00 (t, *J* = 5.6 Hz), 5.93 – 5.76 (m), 5.65 (dddd, *J* = 22.8, 16.2, 8.6, 4.3 Hz), 5.23 – 5.11 (m), 5.07 (td, *J* = 9.7, 6.7 Hz), 4.59 (dd, *J* = 10.2, 8.2 Hz), 4.22 (ddd, *J* = 20.7, 12.3, 4.8 Hz), 4.16 – 4.04 (m), 3.95 (dtt, *J* = 15.4, 7.3, 3.6 Hz), 3.83 (tdd, *J* = 9.7, 6.4, 3.4 Hz), 3.66 (ddtt, *J* = 16.9, 13.4, 7.2, 3.4 Hz), 3.52 (dddt, *J* = 27.4, 14.1, 6.3, 3.6 Hz), 3.33 (ddddd, *J* = 22.3, 18.2, 11.5, 7.5, 4.4 Hz), 2.48 – 2.30 (m), 2.30 – 2.20 (m), 2.15 (d, *J* = 7.9 Hz), 2.08 (d, *J* = 3.6 Hz), 2.05 – 1.99 (m), 1.98 (s), 1.95 (s), 1.89 (td, *J* = 10.7, 5.5 Hz), 1.79 – 1.55 (m), 1.45 – 1.29 (m), 1.24 (d, *J* = 2.4 Hz).

poly(**2d'**)$_{100}$[6]: ^{1}H NMR (CD_2Cl_2, 500 MHz) δ 5.38 – 5.10 (m), 4.74 (t, *J* = 5.0 Hz), 4.16 (dq, *J* = 9.2, 5.2, 3.7 Hz), 3.99 (d, *J* = 12.4 Hz), 3.94 – 3.86 (m), 3.71 (tt, *J* = 10.1, 5.3 Hz), 3.56 – 3.25 (m), 2.18 – 1.85 (m), 1.64 – 1.41 (m), 1.42 – 1.07 (m).

[4] The compound was synthesized and characterized by Maria Rodolis.
[5] The compound was synthesized and characterized by Maria Rodolis.
[6] The compound was synthesized and characterized by Maria Rodolis.

4.1.3 Deacetylation of protected polymers

The general method of deacetylation was as follows[135]: the protected polymer was dissolved in MeOH/THF 2:1 (2 mL) and to this solution was added K_2CO_3 and the reaction stirred for 20-30 min. The reactions were quenched by a solution of THF/H_2O containing 1N HCl (3.52 mL) and allowed to stir for 30–60 min. The solvents were removed in vacuum, followed by dialysis to afford the deprotected polymer as a white powder.

poly(**1a**)$_{100}$: Yield after purification: 33%. ^{1}H NMR (400 MHz, D_2O): δ 5.03—5.40 (m), 4.15—4.36 (m), 3.10—3.90 (with max at 3.40, 3.54, 3.61, 3.64), 2.12—3.08 (with max at 2.39, 2.60, 2.98), 1.45—2.21 (with max at 1.56, 2.01), 1.0—1.40 (with max at 1.11, 1.16).

poly(**1b**)$_{100}$: Yield after purification: 67%. ^{1}H NMR (600 MHz, D_2O): δ 5.12—5.43 (m), 4.77 (m), 3.17—3.92 (with max at 3.26, 3.51, 3.68, 3.77, 3.84), 2.29—3.17 (with max at 2.42, 2.94), 1.48—2.13 (with max at 1.59, 1.91), 1.13 (br s).

poly(**1c**)$_{100}$: Yield after purification: 81%. ^{1}H NMR (600 MHz, D_2O): δ 5.02—5.40 (m), 4.38 (br s), 3.66—3.83 (with max at 3.73, 3.78, 3.80), 3.47—3.66 (with max at 3.51, 3.57, 3.62), 3.32 (br s), 3.15 (br s), 2.86 (m), 2.42—2.66 (with max at 2.33, 2.57), 1.91 (br s), 1.52 (br s).

poly(**1d**)$_{100}$: Yield after purification: 60%. ^{1}H NMR (500 MHz, D_2O): δ 5.08—5.50 (m), 4.34 (br s), 3.85 (br s), 3.66 (br s), 3.18—3.50 (with max at 3.73, 3.78, 3.80), 2.20—3.10 (with max at 2.40, 2.68, 2.98), 1.30—2.10 (with max at 1.59, 1.98), 1.09 (br s).

poly(**1a**$_{50}$-*ran*-**1d**$_{50}$): Yield after purification: 41%. ^{1}H NMR (500 MHz, D_2O): δ 5.39 (br s), 4.47 (br s), 4.11 – 2.22 (m), 1.82 (d), 1.38 – 0.98 (m).

poly(**1a**$_{10}$-*ran*-**1d**$_{90}$): Yield after purification: 60%. ^{1}H-NMR (500 MHz, D_2O): δ 5.36 (br s), 4.41 (br s), 4.09 – 2.28 (m), 2.24 – 1.37 (m), 1.35 – 0.94 (m).

poly(**1b**$_{50}$-*ran*-**1d**$_{50}$): Yield after purification: 60%. ^{1}H NMR (500 MHz, D_2O) δ 5.34 (s, 3H), 4.75 – 4.64 (m, 21H), 3.85 (s, 2H), 3.71 – 3.61 (m, 7H), 3.52 (s, 1H), 3.41 (s, 1H), 3.33 (s, 4H), 3.21 (s, 1H), 2.93 (s, 2H), 2.41 (s, 1H), 1.58 (s, 2H), 1.14 – 1.09 (m, 1H).

poly(**1b**$_{10}$-*ran*-**1d**$_{90}$): Yield after purification: 30%. ^{1}H NMR (500 MHz, D_2O): δ 5.41 (br s), 4.42 (br s), 4.08 – 2.24 (m), 1.84 (m).

poly(**1c**$_{50}$-*ran*-**1d**$_{50}$): Yield after purification: 88%. ^{1}H NMR (500 MHz, D_2O): δ 5.39 (br s), 4.77 (br s), 4.49 (br s), 4.41 (br s), 3.88-2.12 (with max 3.76, 3.64, 3.53, 3.47, 3.44, 3.35, 3.27, 2.99, 2.46), 2.12 – 1.99 (m), 1.97 – 1.93 (m), 1.62 (br s), 0.86 (br s), 0.62 (br s).

poly(**1c**$_{10}$-*ran*-**1d**$_{90}$): Yield after purification: 40%. ^{1}H NMR (500 MHz, D_2O): δ 5.37 (br s), 4.41 (br s), 4.05 – 2.14 (m), 2.14 – 1.34 (m), 1.24 (t).

poly(**1b**$_{50}$-*block*-**1a**$_{50}$): Yield after purification: 35%. ^{1}H NMR (500 MHz, D_2O): δ 5.41 (br s), 4.79 (br s), 4.05 – 3.19 (m), 3.18 – 2.28(m), 2.26 – 1.46 (m), 1.23 (br s).

poly(**1b**$_{50}$-*block*-**1c**$_{50}$): Yield after purification: 81%. ^{1}H NMR (500 MHz, D_2O): δ 5.40 (br s), 4.49 (br s), 4.05 – 2.20 (m), 2.16 – 1.76 (m), 1.64 (br s), 1.20 (br s).

poly(**1a**$_{50}$-*block*-**1c**$_{50}$): Yield after purification: 31%. ^{1}H NMR (500 MHz, D_2O) δ 5.32 (s, 8H), 4.69 (d, J = 5.0 Hz, 1H), 4.43 (s, 2H), 3.83 (s, 2H), 3.80 – 3.63 (m, 8H), 3.62 (s, 5H), 3.58 – 3.50 (m, 1H), 3.47 (s, 3H), 3.40 – 3.31 (m, 12H), 2.91 (s, 4H), 2.39 (s, 4H), 1.96 (dd, J = 7.2, 3.1 Hz, 7H), 1.90 (s, 3H), 1.56 (s, 5H), 1.16 – 1.08 (m, 9H), 1.01 (s, 12H).

poly(**1a**$_{50}$-*block*-**1d**$_{50}$): Yield after purification: 21%. ^{1}H NMR (500 MHz, D_2O): δ 5.40 (br s), 4.79 (br s), 4.43 (br s), 4.11 – 3.22 (m), 2.76 (br s), 2.20 – 1.46 (m), 1.20 (br s).

poly(**1b**$_{50}$-*block*-**1d**$_{50}$): Yield after purification: 43%. ^{1}H NMR (500 MHz, D_2O): δ 5.41 (br s), 4.42 (br s), 4.08 – 2.24 (m), 1.84 (m).

poly(**1c**$_{50}$-*block*-**1d**$_{50}$): Yield after purification: 73%. ^{1}H-NMR (500 MHz, D_2O): δ 5.40 (br s), 4.47 (br s), 4.04 – 3.13 (m), 3.13 – 2.17 (m), 2.17 – 1.40 (m), 1.40 – 0.98 (m).

poly(**2a**)$_{100}$: ^{1}H NMR (500 MHz, D_2O) δ 5.46 (s), 4.92 – 4.73(m), 4.01(s), 3.85 –3.75(m), 3.74 – 3.37(m), 2.31(s), 2.25 – 2.01(m), 1.66 – 1.21(m), 1.11 (s).

poly(**2b**)$_{100}$: ^{1}H NMR (500 MHz, D_2O) δ d 5.64 (s), 5.38 (s), 5.22 (d, J = 11.7 Hz), 4.96 – 4.89 (m), 4.71 – 4.64 (m), 4.11 – 4.07 (m), 3.79 (s), 3.71 – 3.58 (m), 3.54 (s), 3.40 (s), 2.74 – 2.67 (m), 2.66 – 2.58 (m), 2.40 – 2.26 (m), 2.17 – 1.98 (m), 1.98 – 1.83 (m), 1.68 – 1.55 (m), 1.38 – 0.97 (m).

poly(**2c**)$_{100}$: ^{1}H NMR (500 MHz, D_2O) δ 5.81– 5.71 (m), 5.45 (s), 5.20 – 4.60 (m), 4.57 – 4.51 (m), 3.95 – 3.64 (m), 3.56 – 3.29 (m), 2.43 – 2.36 (m), 2.24 – 1.92 (m), 1.79 –1.56 (m), 1.46 – 1.21 (m).

poly(**2d**)$_{100}$[7]: ^{1}H NMR (500 MHz, D_2O) δ 5.41 – 5.34 (m), 4.89 – 4.82 (m), 4.77 (d, *J* = 18.9 Hz), 4.38 (dd, *J* = 7.4, 3.2 Hz), 3.87 (dd, *J* = 28.5, 10.5 Hz), 3.77 – 3.55 (m), 3.37 (dtd, *J* = 53.2, 20.6, 18.8, 9.5 Hz), 3.20 (t, *J* = 8.6 Hz), 2.24 (d, *J* = 14.4 Hz), 1.95 (s), 1.56 (s), 1.41 (s), 1.27 (s).

[7] The compound was synthesized and characterized by Maria Rodolis.

4.1.4 Small angle X-ray scattering (SAXS)

Small Angle X-ray Scattering (SAXS). Small-angle X-ray scattering (SAXS) measurements were conducted on a Bruker Nanostar U in the high resolution configuration (Brookhaven National Lab, Brookhaven, NY). The wavelength of the beam is 0.15418 with Cu rotating anode source. The nomial distance from sample to detector (Vantec 2000 area detector) was 1.1 m and the actual distance was calibrated with silver behenate before the measurements. Deprotected glycopolymer solutions were prepared at the indicated concentrations and loaded into quartz capillary (diameter 0.1 mm). The capillary was fixed in the sample holder and scattering data for each sample was collected for 18 h.

4.2 Sperm treatment and biological assay

General Methods. All experiments performed on mice were approved by the Stony Brook University IACUC (Protocol 0616) and were conducted in accordance with the National Institute of Health and the United States Department of Agriculture guidelines. Chemical for assay buffer were purchased from Sigma-Aldrich Fisher Scientific and VWR. The culture media will be prepared regarding to the reference.[57-58]

4.2.1 Sperm flow cytometry assay

Materials. DMSO and A23187 calcium ionophore were purchased from Sigma-Aldrich. A23187 stock solution (1 mg/mL) was prepared by dilution with DMSO. Propidium iodide was purchased from Fisher Scientific. Alexa Fluor® 488 soybean trypsin inhibitor (SBTI) and SYTO-

17 were purchased from Life Technologies. All chemicals for assay buffers were purchased from Sigma-Aldrich, Fisher Scientific and VWR. Fluorescent stains propidium iodide (PI) was dissolved in water (2.4 mM) and stored at -20°C. Alexa Fluor® 488 soybean trypsin inhibitor (SBTI) was dissolved in water (1 mg/mL) and stored at -20 °C in 40 μL aliquots. SYTO-17 was diluted in DMSO (1 mM) and stored at -20 °C. Stock solutions of deprotected glycopolymers were stored in DDI water at -20 °C at a polymer concentration of 100 mM.

Sperm treatment. Sperm were isolated by force from the cauda epididymis of two 9- to 12-week-old CD-1 male breeders (Charles River) in a phenol red-free M16 medium (2.57 mM $CaCl_2$) (6 mL) supplemented with 0.3% BSA (w/v). The sperm suspension was then gently pipetted into a polypropylene culture tube (12 mm × 75 mm) and incubated for 10 min at 25 °C. Then the concentration of sperm concentration was assessed by haemocytometer and motility was examined by phase-contrast microscopy (20X). Aliquots (125 μL) containing about 2.5×10^6 sperm were subsequently diluted to a final volume of 250 μL (1.25×10^7 sperm/mL). The sperm suspension was incubated for another 15 min to get additional capacitation at 25 °C. A 250 μL solution containing SYTO 17 (2.5 μL), SBTI (1 μL) and either A23187 (5 mM, positive control), glycopolymer (0.5 mM~ 30 mM, sample), or Dulbecco's Phosphate-Buffered Saline (PBS, negative control) was added to the 250 μL sperm suspension to a final volume of 500 μL. The mixture was kept at 0°C in the dark for 15 min and then 20 min in the dark at rt. Samples were centrifuged for 5 min at 500 *g*, and the resulting pellet was re-dissolved with 500 ml of a PBS solution containing PI (24 mM), SBTI (2 mg/mL) and SYTO-17 (5 mM). Samples were re-suspended at 1 min intervals and allowed to incubate for 20 min at 25 °C before flow cytometric analysis.

Flow cytometry assay. Flow cytometry Analyses were performed on a Becton Dickinson LSR Fortessa system in combination with the BD-FACSDiva™ Software Version 8. SYTO-17 stained all cellular events and was excited at 640 nm and detected at 670/30 nm. PI stained all nonviable cells and was excited at 561 nm and detected at 582/15 nm. Alexa Fluor® 488 SBTI stained all cells that have undergone acrosome exocytosis and was excited at 488 nm and detected at 530/30 nm. These three stains have minimal emission overlap. Utilizing the forward and sideways scatter, small debris was gated out of analyses. As previously reported, additional gating was necessary to remove noncellular events which displayed similar scatter characteristics to sperm. Events which exhibited weak SYTO-17 and PI staining (weak DNA content) were gated out before acrosome integrity and viability could be determined. Viability and acrosome integrity was measured at a flow rate of 600 cells/sec for 1 min.

Statistical analysis. The acrosome integrity of live sperm was normalized to PBS (negative control) and 5 mM A23187 (positive control). Only live sperm were included in the analysis and each experiment was conducted in biological triplicate. Normalized AE% was calculated using [AE% of glycopolymers -AE% of negative control]]/[AE% positive control-AE% negative control]. Data represent mean ± SEM of at least three independent experiments when compared to the negative control. EC_{50} and IC50 were obtained by fitting sigmoidal model using GraphPad.

4.2.2 Sperm fluorescence microscopy assay

Isolation and capacitation of sperm. Sperm were isolated from cauda epididymis and vas deferens of two 10 to 12-week-old ICR male breeders (Taconic, NJ) in M16 medium with 0.3% BSA (3 mL). The sperm suspension was then pipette to the bottom of a polypropylene culture tube (12 × 75 mm) and incubated at 37 °C for 30 min under 5% CO_2 in air. Once the incubation was

complete, the sperm motility was examined by phase-contrast microscopy. Only samples of capacitated sperm displaying >70% motility were used in subsequent experiments. The concentration of sperm was accessed by hemocytometer.

Sperm treatment. Aliquots (20 μL) containing 5×10^5 capacitated sperm were transferred to microcentrifuge tubes with glycopolymers, negative and positive controls, at 37°C under 5% CO_2 for 30 min based on the time-course study. After incubation, the sperm were pelleted by centrifugation at 800 *g* for 7 min. The supernatant was removed by pipette and the pelleted sperm were washed once by 40 μL PBS and fixed with 40 μL70% ethanol. After incubated at 4 °C for 30 min, the sperm were pelleted and washed twice with 40 μL PBS. The final pellet was resuspended in 40 μL of DDI water. Aliquots (10 μL) of each sample were transferred to cover slips on 6-well plate and air-dried.

Assessment of Sperm Acrosome Reaction. 10 μL Rhodamine labeled peanut agglutinin (PNA) (Vector labs) at concentration of 10 μg/mL was incubated with fixed sperm on cover slips for 10 min at room temperature in dark. After washed with 3 mL DDI water (three times of 10 min each), the cover slips were covered on SuperFrost Plus microscope slides (Fisher Scientific, Suwanee, GA) over a drop (6 μL) of mounting medium Vectashield (Vector labs), sealed with nail polish, and the acrosomal status was assessed by reverse fluorescent microscope. Sperm that displayed continuous red fluorescence along their acrosomal arcs were scored as acrosome-intact; those that displayed no red fluorescence or punctuate fluorescence were determined as acrosome-reacted. The slides were coded, and counted blindly; all experiments were conducted at least three times. Each time, three independent replicates of each test group were analyzed, and 200 sperm from each replicate were counted. In the event that treatment with a negative control resulted in higher than 15% acrosome-reacted sperm, data from the entire experiment were discarded.

4.2.3 SDS-PAGE and immunoblotting

Sperm preparation and membrane purification. Toyoda-Yokoyama-Hosi (standard TYH) medium is consisting of 119.37mM NaCl, 4.78 mM KCl, 1.71mM $CaCl_2$, 1.19mM $KHPO_4$, 1.19 mM $MgSO_4$, 25.07mM $NaHCO_3$, 1mM Na-pyruvate, 5.56 mM glucose, 5mg/mL BSA, 50μg/mL streptomycin sulfate and 75μg/mL penicillin G potassium at pH 7.4 when equilibrated with 5% CO2. H-TYH uses Na·HEPES instead of $NaHCO_3$ and PVA instead of BSA to let the sperm swim out but not underdo capacitation. After treatment, sperm were collected by centrifugation, washed in 1 ml of phosphate-buffered saline (PBS), resuspended in Laemmli sample buffer without β-mercaptoethanol, and boiled for 5 min. After centrifugation, 5% β-mercaptoethanol was added to the supernatants, and the mixture was boiled again for 5 min.[126]

Alternatively, mouse sperm (2×10^6 cells) were homogenized using 10 strokes with a homogenizer in TE buffer (50 mM Tris-HCl, pH 7.5, 1 mM EDTA) supplemented with protease inhibitors and phosphatase inhibitor (Bio-Rad). After homogenization, the sample was sonicated three times for 15 s on ice with 1-min intervals. Cell debris was pelleted (1,000 ×*g* for 10 min at 4 °C), and the supernatant was centrifuged at 10,000×*g* for 10 min at 4 °C. The final pellet, which contained the membrane fraction, was resuspended in sample buffer and used for SDS-PAGE and immunoblotting.[50]

Another method is that the sperm were isolated, purified, and lysed on ice for 30 min in a weak RIPA lysis buffer [50 mmol Tris-HCl/L, pH 7.4, 150 mmol NaCl/L, 1% (v/v) NP40, 0.25% (w/v) sodium deoxycholate] containing a protease inhibitor cocktail and 50 μg PMSF/mL. The sperm lysates were mixed with an equal volume of 2×SDS loading buffer (approximately 40 μL) containing 200 mmol/L DTT and boiled for 5 min for western blotting analysis.[136]

SDS-PAGE and immunoblotting. Protein extracts equivalent to 1–2 × 10^6 sperm per lane were subjected to 10% SDS-PAGE gel and electro-transferred to PVDF membranes (Bio-Rad) at 250 mA for 120 min on ice. Membranes were blocked with 5% fat-free milk in TBS containing 0.1% Tween 20 (T-TBS). For anti-pY and anti-pPKA immunodetections, membranes were blocked with 5% BSA in T-TBS. Antibodies were diluted in T-TBS as follows: 1/10,000 for anti-PY (clone 4G10), 1/5,000 for anti-pPKA (clone 100G7E). Secondary antibodies were diluted 1/10,000 in T-TBS and developed using an enhanced chemiluminescence detection kit (Bio-Rad) according to the manufacturer's instructions. When necessary, PVDF membranes were stripped at 60 °C for 15 min in the stripping buffer. (20 mL of 20% SDS, 12.5mL of 1M Tris-HCl, pH=6.8 and 150 µL β-mercaptoethanol in 200 mL ddi water)

References

1. Sharlip ID, J. J., Belker AM, Lipshultz LI, Sigman M, Thomas AJ, Schlegel PN, Howard SS, Nehra A, Damewood MD, Overstreet JW, Sadovsky R Best practice policies for male infertility. *Fertil. Steril.* **2002,** *77* (5), 873-882.
2. Agarwal, A.; Mulgund, A.; Hamada, A.; Chyatte, M. R. A unique view on male infertility around the globe. *Reprod. Biol. Endocrinol.* **2015,** *13*, 37.
3. Ferré-Ybarz, L.; Basagaña, M.; Coroleu, B.; Bartolomé, B.; Cisteró-Bahima, A. Human seminal plasma allergy and successful pregnancy. *J. Investig. Allergol. Clin. Immunol.* **2006,** *16* (5), 314- 316.
4. van der Westerlaken, L.; Naaktgeboren, N.; Verburg, H.; Dieben, S.; Helmerhorst, F. M. Conventional in vitro fertilization versus intracytoplasmic sperm injection in patients with borderline semen: a randomized study using sibling oocytes. *Fertil. Steril.* **2006,** *85* (2), 395-400.
5. Pizzol, D.; Ferlin, A.; Garolla, A.; Lenzi, A.; Bertoldo, A.; Foresta, C. Genetic and molecular diagnostics of male infertility in the clinical practice. *Frontiers in Bioscience* **2014,** *19*, 291- 303.
6. Calvo, L.; Dennison-Lagos, L.; Banks, S. M.; Dorfmann, A.; Thorsell, L. P.; Bustillo, M.; Schulman, J. D.; Sherins, R. J. Acrosome reaction inducibility predicts fertilization success at in-vitro fertilization. *Hum. Reprod.* **1994,** *9* (10), 1880-1886.
7. Katsuki, T.; Hara, T.; Ueda, K.; Tanaka, J.; K., O. Prediction of outcomes of assisted reproduction treatment using the calcium ionophore-induced acrosome reaction. *Hum. Reprod.* **2005,** *20* (2), 469-475.
8. Rahman, M. S.; Pang, M. G. Sperm Biology: Towards Understanding Global Issue of Male Infertility. *Austin Andrology* **2016,** *1* (1), 1003.
9. Evans, J. P. Sperm-egg interaction. *Annu. Rev. Physiol.* **2012,** *74*, 477-502.
10. Wassarman, P. M.; Florman, H. M. Cellular mechanisms during mammalian fertilization. *Handbook of Physiology: section 14- Cell Physiology* **1997**, 885-938.
11. Yanagimachi, R. The physiology of reproduction. **1994**, 189-317.
12. Wassarman, P. M. Mammalian Fertilization: molecular aspects of gamete adhesion, exocytosis, and fusion. *Cell* **1999,** *96* (2), 175- 183.
13. Lishko, P. V.; Kirichok, Y.; Ren, D.; Navarro, B.; Chung, J. J.; Clapham, D. E. The control of male fertility by spermatozoan ion channels. *Annu. Rev. Physiol.* **2012,** *74*, 453-75.
14. Visconti, P. E.; Krapf, D.; de la Vega-Beltran, J. L.; Acevedo, J. J.; Darszon, A. Ion channels, phosphorylation and mammalian sperm capacitation. *Asian J. Androl.* **2011,** *13* (3), 395-405.
15. Eliasson, R. Cholesterol in human semen. *Biochem. J.* **1966,** *98*.
16. De Jonge, C. Biological basis for human capacitation. *Hum. Reprod. Update* **2005,** *11* (3), 205-14.
17. Zeng, Y.; Oberdorf, J. A.; Florman, H. M. pH regulation in mouse sperm: identification of Na+-, Cl−-, and HCO3- dependent and arylaminobenzoate-dependent regulatory mechanisms and characterization of their roles in sperm capacitation. *Dev. Bio.* **1996,** *173* (2), 510-520.
18. Carr, D. W.; Acott, T. S. Intracellular pH regulates bovine sperm motility and protein phosphorylation. *Biol. Reprod.* **1989,** *41*, 907-920.

19. Visconti, P. E.; Moore, G. D.; Bailey, J. L.; Leclerc, P.; Connors, S. A.; Pan, D.; Olds-Clarke, P.; Kopf, G. S. Capacitation of mouse spermatozoa II. Protein tyrosine phosphorylation and capacitation are regulated by a cAMP-dependent pathway. *Development* **1995,** *121*.
20. Visconti, P. E.; Bailey, J. L.; Moore, G. D.; Pan, D.; Olds-Clarke, P.; Kopf, G. S. Capacitation of mouse spermatozoa I. Correlation between the capacitation state and protein tyrosine phosphorylation. *Development* **1995,** *121*, 1129-1137.
21. Abou-haila, A.; Tulsiani, D. R. Signal transduction pathways that regulate sperm capacitation and the acrosome reaction. *Arch. Biochem. Biophys.* **2009,** *485* (1), 72-81.
22. Tsai, P. S.; Brewis, I. A.; van Maaren, J.; Gadella, B. M. Involvement of complexin 2 in docking, locking and unlocking of different SNARE complexes during sperm capacitation and induced acrosomal exocytosis. *PLoS One* **2012,** *7* (3), e32603.
23. Sosa, C. M.; Pavarotti, M. A.; Zanetti, M. N.; Zoppino, F. C.; De Blas, G. A.; Mayorga, L. S. Kinetics of human sperm acrosomal exocytosis. *Mol. Hum. Reprod.* **2015,** *21* (3), 244-54.
24. Buffone, M. G.; Rodriguez-Miranda, E.; Storey, B. T.; Gerton, G. L. Acrosomal exocytosis of mouse sperm progresses in a consistent direction in response to zona pellucida. *J. Cell. Physiol.* **2009,** *220* (3), 611-20.
25. Ferrer, M.; Rodriguez, H.; Zara, L.; Yu, Y.; Xu, W.; Oko, R. MMP2 and acrosin are major proteinases associated with the inner acrosomal membrane and may cooperate in sperm penetration of the zona pellucida during fertilization. *Cell Tissue Res.* **2012,** *349* (3), 881- 895.
26. Mao, H. T.; Yang, W. X. Modes of acrosin functioning during fertilization. *Gene* **2013,** *526* (2), 75-9.
27. Bianchi, E.; Doe, B.; Goulding, D.; Wright, G. J. Juno is the egg Izumo receptor and is essential for mammalian fertilization. *Nature* **2014,** *508* (7497), 483-7.
28. Ebensperger, C.; Barros, C. Changes at the hamster oocyte surface from the germinal vesicle stage to ovulation. *Mol. Reprod. Dev.* **1984,** *9* (4), 387-397.
29. Johnson, M. H.; Eager, D.; Muggleton- Harris, A.; Grave, H. M. Mosaicism in organisation concanavalin A receptors on surface membrane of mouse egg. *Nature* **1975,** *257*, 321-322.
30. Evans, J. P. The molecular basis of sperm‐oocyte membrane interactions during mammalian fertilization. *Hum. Reprod. Update* **2002,** *8* (4), 297- 311.
31. Cho, C.; Bunch, D. O.; Faure, J.; Goulding, E. H.; Eddy, E. M.; Primakoff, P.; Myles, D. G. Fertilization defects in sperm from mice lacking fertilin β. *Science* **1998,** *281*, 1857-1859.
32. Chen, H.; Sampson, N. S. Mediation of sperm-egg fusion: evidence that mouse egg alpha6beta1, integrin is the receptor for sperm fetilin beta. *Chem. Biol.* **1999,** *6* (1), 1-10.
33. Kaji, K.; Oda, S.; Shikano, T.; Ohnuki, T.; Uematsu, Y.; Sakagami, J.; Tada, N.; Miyazaki, S.; Kudo, A. The gamete fusion process is defective in eggs of Cd9-deficient mice. *Nat. Genet.* **2000,** *24* (3), 279-282.
34. Inoue, N.; Ikawa, M.; Isotani, A.; Okabe, M. The immunoglobulin superfamily protein Izumo is required for sperm to fuse with eggs. *Nature* **2005,** *434* (7030), 234-238.
35. Georgadaki, K.; Khoury, N.; Spandidos, D. A.; Zoumpourlis, V. The molecular basis of fertilization (Review). *Int. J. Mol. Med.* **2016,** *38* (4), 979-86.
36. Wassarman, P. M.; Jovine, L.; Qi, H.; Williams, Z.; Darie, C.; Litscher, E. S. Recent aspects of mammalian fertilization research. *Mol Cell Endocrinol* **2005,** *234* (1-2), 95-103.
37. Alberts B, J. A., Lewis J, et al. Molecular Biology of the Cell. 4th edition. **2002**.
38. WASSARMAN, J. D. B. A. P. M. Identification of a ZP3-binding protein on acrosome-intact mouse sperm by photoaffinity crosslinking. *Proc. Natl. Acad. Sci.* **1990,** *87*, 5563-5567.

39. Muro, Y.; Buffone, M. G.; Okabe, M.; Gerton, G. L. Function of the acrosomal matrix: zona pellucida 3 receptor (ZP3R/sp56) is not essential for mouse fertilization. *Biol. Reprod.* **2012,** *86* (1), 1-6.
40. Wassarman, P. M. Mammalian fertilization: molecular aspects of gamete adhesion, exocytosis, and fusion. *Cell* **1999,** *96*, 175-183.
41. Jeffrey, D. B.; Wassarman, P. M. Galactose at the nonreducing terminus of O-linked oligosaccharides of mouse egg zona pellucida glycoprotein ZP3 is essential for the glycoprotein's sperm receptor activity. *Proc. Natl. Acad. Sci. U S A* **1988,** *85*, 6778-6782.
42. Loeser, C. R.; Tulsiani, D. R. P. The role of carbohydrate in the induction of the acrosome reaction in mouse spermatozoa. *Biol. Reprod.* **1999,** *60*, 94-101.
43. Hanna, W. F.; Kerr, C. L.; Shaper, J. H.; Wright, W. W. Lewis X-containing neoglycoproteins mimic the intrinsic ability of zona pellucida glycoprotein ZP3 to induce the acrosome reaction in capacitated mouse sperm. *Biol. Reprod.* **2004,** *71* (3), 778-89.
44. Pang, P. C.; Chiu, P. C.; Lee, C. L.; Chang, L. Y.; Panico, M.; Morris, H. R.; Haslam, S. M.; Khoo, K. H.; Clark, G. F.; Yeung, W. S. Human sperm binding is mediated by the sialyl-LewisX oligosaccharide on the zona pellucida. *Science* **2011,** *333* (6050), 1761-1765.
45. Johnston, D. S.; Wright, W. W.; Shaper, J. H.; Hokke, C. H.; Van den Eijnden, D. H.; Joziasse, D. H. Murine sperm-zona binding, a fucosyl residue is required for a high affinity sperm-binding ligand. *J. Biol. Chem.* **1998,** *273*, 1888-1895.
46. Buffone, M. G.; Hirohashi, N.; Gerton, G. L. Unresolved questions concerning mammalian sperm acrosomal exocytosis. *Biol. Reprod.* **2014,** *90* (5), 112.
47. Gupta, S. K.; Bhandari, B. Acrosome reaction: relevance of zona pellucida glycoproteins. *Asian J. Androl.* **2011,** *13* (1), 97-105.
48. Ward, C. R.; Storey, B. T.; Kopf, G. S. Activation of a Gi protein in mouse sperm membranes by solubilized proteins of the zona pellucida, the egg's extracellular matrix. *J. Biol. Chem.* **1992,** *267* (20), 14061- 14067.
49. Ward, C. R.; Storey, B. T.; Kopf, G. S. Selective activation of Gil and Gi2 in mouse sperm by the zona pellucida, the egg's extracellular matrix. *J. Bio. Chem.* **1994,** *269* (18), 13254- 13258.
50. Wertheimer, E.; Krapf, D.; de la Vega-Beltran, J. L.; Sanchez-Cardenas, C.; Navarrete, F.; Haddad, D.; Escoffier, J.; Salicioni, A. M.; Levin, L. R.; Buck, J.; Mager, J.; Darszon, A.; Visconti, P. E. Compartmentalization of distinct cAMP signaling pathways in mammalian sperm. *J. Biol. Chem.* **2013,** *288* (49), 35307-20.
51. Naz, R. K.; Rajesh, P. B. Role of tyrosine phosphorylation in sperm capacitation / acrosome reaction. *Reprod. Biol. Endocrinol.* **2004,** *2*, 75.
52. Walensky, L. D.; Snyder, S. H. Inositol 1,4,5-Trisphosphate receptors selectively localized to the acrosomes of mammalian sperm. *J. Cell Bio.* **1995,** *130*, 857- 869.
53. Arnoult, C.; Cardullo, R. A.; Lemos, J. R.; Florman, H. M. Activation of mouse sperm T-type Calcium channels by adhesion to the egg zona pellucida. *Proc. Natl. Acad. Sci. U. S. A.* **1996,** *93*, 13004- 13009.
54. Ganguly, A.; Bukovsky, A.; Sharma, R. K.; Bansal, P.; Bhandari, B.; Gupta, S. K. In humans, zona pellucida glycoprotein-1 binds to spermatozoa and induces acrosomal exocytosis. *Hum. Reprod.* **2010,** *25* (7), 1643-56.
55. Jose, O.; Hernandez-Hernandez, O.; Chirinos, M.; Gonzalez-Gonzalez, M. E.; Larrea, F.; Almanza, A.; Felix, R.; Darszon, A.; Trevino, C. L. Recombinant human ZP3-induced sperm acrosome reaction: evidence for the involvement of T- and L-type voltage-gated calcium channels. *Biochem. Biophys. Res. Commun.* **2010,** *395* (4), 530-4.

56. Florman, H. M.; Christophe Arnoult; Kazam, I. G.; Li, C.; O'Toole, C. M. B. A perspective on the control of mammalian fertilization by egg-activated ion channels in sperm- a tale of two channels. *Bio. Repro.* **1998,** *59*, 12-16.
57. Wu, L.; Sampson, N. S. Fucose, mannose, and beta-N-acetylglucosamine glycopolymers initiate the mouse sperm acrosome reaction through convergent signaling pathways. *ACS Chem. Biol.* **2014,** *9* (2), 468-475.
58. Rodolis, M. T.; Huang, H.; Sampson, N. S. Glycopolymer induction of mouse sperm acrosomal exocytosis shows highly cooperative self-antagonism. *Biochem. Biophys. Res. Commun.* **2016,** *474* (3), 435-440.
59. Lee, Y. C.; Lee, R. T. Carbohydrate-protein interactions: basis of glycobiology *Acc. Chem. Res.* **1995,** *28* (8), 321-327.
60. Ting, S. R. S.; Chen, G.; Stenzel, M. H. Synthesis of glycopolymers and their multivalent recognitions with lectins. *Polym. Chem.* **2010,** *1* (9), 1392.
61. Miura, Y. Design and synthesis of well-defined glycopolymers for the control of biological functionalities. *Polym. J.* **2012,** *44* (7), 679-689.
62. Kiessling, L. L.; Grim, J. C. Glycopolymer probes of signal transduction. *Chem. Soc. Rev.* **2013,** *42* (10), 4476-4491.
63. Mammen, M.; Choi, S.; Whitesides, G. M. Polyvalent interactions in biological systems: implications for design and use of multivalent ligands and inhibitors. *Angrew. Chem. Int. Ed.* **1998,** *37*, 2754-2794.
64. Fasting, C.; Schalley, C. A.; Weber, M.; Seitz, O.; Hecht, S.; Koksch, B.; Dernedde, J.; Graf, C.; Knapp, E. W.; Haag, R. Multivalency as a chemical organization and action principle. *Angrew. Chem. Int. Ed.* **2012,** *51* (42), 10472-98.
65. Weber, M.; Bujotzek, A.; Haag, R. Quantifying the rebinding effect in multivalent chemical ligand-receptor systems. *J. Chem. Phys.* **2012,** *137* (5), 054111.
66. Ercolani, G.; Schiaffino, L. Allosteric, chelate, and interannular cooperativity: a mise au point. *Angrew. Chem. Int. Ed.* **2011,** *50* (8), 1762-8.
67. Kiessling, L. L.; Splain, R. A. Chemical approaches to glycobiology. *Annu. Rev. Biochem.* **2010,** *79*, 619-53.
68. Varki, A.; Lowe, J. B. Chapter 6 Biological roles of glycans. *Essentials of Glycobiology. 2nd edition*.
69. Jimenez Blanco, J. L.; Ortiz Mellet, C.; Garcia Fernandez, J. M. Multivalency in heterogeneous glycoenvironments: hetero-glycoclusters, -glycopolymers and -glycoassemblies. *Chem. Soc. Rev.* **2013,** *42* (11), 4518-31.
70. Sansone, F.; Casnati, A. Multivalent glycocalixarenes for recognition of biological macromolecules: glycocalyx mimics capable of multitasking. *Chem. Soc. Rev.* **2013,** *42* (11), 4623-39.
71. Fulton, D. A.; Stoddart, J. F. Neoglycoconjugates based on cyclodextrins and calixarenes. *Bioconjugate Chem.* **2001,** *12* (5), 655-672.
72. Roy, R.; Shiao, T. C.; Rittenhouse-Olson, K. Glycodendrimers- versatile tools for nanotechnology. *Braz. J. Pharm. Sci.* **2013,** *49*.
73. Marradi, M.; Chiodo, F.; Garcia, I.; Penades, S. Glyconanoparticles as multifunctional and multimodal carbohydrate systems. *Chem. Soc. Rev.* **2013,** *42* (11), 4728-45.
74. Delbianco, M.; Bharate, P.; Varela-Aramburu, S.; Seeberger, P. H. Carbohydrates in supramolecular chemistry. *Chem. Rev.* **2016,** *116* (4), 1693-1752.

75. Vazquez-Dorbatt, V.; Lee, J.; Lin, E. W.; Maynard, H. D. Synthesis of glycopolymers by controlled radical polymerization techniques and their applications. *ChemBiochem* **2012,** *13* (17), 2478-87.
76. Ghadban, A.; Albertin, L. Synthesis of glycopolymer architectures by reversible-deactivation radical polymerization. *Polymers* **2013,** *5* (2), 431-526.
77. Fraser, C.; Grubbs, R. H. Synthesis of glycopolymers of controlled molecular weight by ring-opening metathesis polymerization using well-defined functional group tolerant tuthenium carbene catalystst. *Macromolecules* **1995,** *28* (21), 7248- 7255.
78. Ladmiral, V.; Mantovani, G.; Clarkson, G. J.; Cauet, S.; Irwin, J. L.; M., H. D. Synthesis of neoglycopolymers by a combination of "click chemistry" and living radical polymerization. *J. Am. Chem. Soc.* **2006,** *128* (14), 4823- 4830.
79. Kanai, M.; Mortell, K. H.; Kiessling, L. L. Varying the size of multivalent ligands: the dependence of concanavalin A binding on neoglycopolymer length. *J. Am. Chem. Soc.* **1997,** *119* (41), 9931-9932.
80. Kiessling, L. L.; Gestwicki, J. E.; Strong, L. E. Synthetic multivalent ligands in the exploration of cell-surface interactions. *Curr. Opin. Struct. Biol.* **2000,** *4*, 696-703.
81. Puffer, E. B.; Pontrello, J. K.; Hollenbeck, J. J.; Kink, J. A.; Kiessling, L. L. Activating B cell signaling with defined multivalent ligands. *ACS Chem. Bio.* **2007,** *2* (4), 252-262.
82. Dam, T. K.; Brewer, C. F. Lectins as pattern recognition molecules: the effects of epitope density in innate immunity. *Glycobiology* **2010,** *20* (3), 270-9.
83. Burns, J. A.; Gibson, M. I.; Becer, C. R. Glycopolymers via post- polymerization modification techniques. *Functional polymers by post-polymerization modification: concepts, guidelines and applications.* **2014**.
84. Gestwicki, J. E.; Cairo, C. W.; Strong, L. E.; Oetjen, K. A.; Kiessling, L. L. Influencing receptor-ligand binding mechanisms with multivalent ligand architecture. *J. Am. Chem. Soc.* **2002,** *124*, 14922-14933.
85. Kiessling, L. L.; Strong, L. E.; Gestwicki, J. E. Principles for multivalent ligand design. *Annu. Rep. Med. Chem.* **2000,** *35*, 321-330.
86. Hoshino, Y.; Nakamoto, M.; Miura, Y. Control of protein-binding kinetics on synthetic polymer nanoparticles by tuning flexibility and inducing conformation changes of polymer chains. *J. Am. Chem. Soc.* **2012,** *134* (37), 15209-15212.
87. Becer, C. R.; Gibson, M. I.; Geng, J.; Ilyas, R.; Wallis, R.; Mitchell, D. A.; Haddleton, D. M. High-affinity glycopolymer binding to human DC-SIGN and disruption of DC-SIGN Interactions with HIV envelope glycoprotein. *J. Am. Chem. Soc.* **2010,** *132*, 15130-15132.
88. Tran, H. A.; Kitov, P. I.; Paszkiewicz, E.; Sadowska, J. M.; Bundle, D. R. Multifunctional multivalency: a focused library of polymeric cholera toxin antagonists. *Org. Biomol. Chem.* **2011,** *9* (10), 3658-71.
89. Grainne Black, D. M., and Wilhelm Risse Living Ring-Opening Olefin Metathesis Polymerization. *Hand book of Metathesis: Catalyst Development* **2008**.
90. Bielawski, C. W.; Grubbs, R. H. Living ring-opening metathesis polymerization. *Prog. Polym. Sci.* **2007,** *32* (1), 1-29.
91. Schleyer, P. v. R.; E., W. J.; Blanchard, K. R. Evaluation of strain in hydrocarbons. The strain in adamantane and its origin. *J. Am. Chem. Soc.* **1970,** *92* (8), 731-732.
92. Baessler, K. A.; Lee, Y.; Sampson†, N. S. Beta 1 integrin is an adhesion protein for sperm binding to eggs. *ACS Chem. Biol. 4* (5), 357-366.

93. Song, A.; Parker, K. A.; Sampson, N. S. Synthesis of copolymers by alternating ROMP (AROMP). *J. Am. Chem. Soc.* **2009,** *131*, 3444-3445.
94. Parker, K. A.; Sampson, N. S. Precision synthesis of alternating copolymers via ring-opening polymerization of 1-substituted cyclobutenes. *Acc. Chem. Res.* **2016,** *49* (3), 408-17.
95. Svergun, D. I.; Koch, M. H. J. Small-angle scattering studies of biological macromolecules in solution. *Rep. Prog. Phyis.* **2003,** *66*, 1735- 1782.
96. Blanchet, C. E.; Svergun, D. I. Small-angle X-ray scattering on biological macromolecules and nanocomposites in solution. *Annu. Rev. Phys. Chem.* **2013,** *64*, 37-54.
97. Di Cola, E.; Grillo, I.; Ristori, S. Small angle X-ray and neutron scattering: powerful tools for studying the structure of drug-loaded liposomes. *Pharmaceutics* **2016,** *8* (2).
98. Feigin, L. A.; Svergun, D. I. Structure analysis by small-angle X-ray and neutron scattering. *New York: Plenum* **1987**.
99. Guinier, A. La diffraction des rayons X aux tr`es petits angles; application a l'´etude de ph´enom`enes ultramicroscopiques. *Ann. Phys.(Paris)* **1939,** *12*, 161-237.
100. Doniach, S. Changes in biomolecular conformation seen by small angle X-ray scattering. *Chem. Rev.* **2001,** *101* (1763-1778).
101. Schröter, S.; Osterhoff, C.; McArdle, W.; Ivell, R. The glycocalyx of the sperm surface. *Hum. Reprod. Update* **1999,** *5* (4), 302-313.
102. Pang, P.; Chiu, P. C. N.; Lee, C.; Chang, L.; Panico, M.; Morris, H. R.; Haslam, S. M.; Khoo, K.; Clark, G. F.; Yeung, W. S. B.; Dell, A. Human sperm binding is mediated by the sialyl-Lewis(x) oligosaccharide on the zona pellucida. *Science* **2011,** *333* (6050), 1761-1764.
103. Florman, H. M.; Wassarman, P. M. O-Linked oligosaccharides of mouse egg ZP3 account for its sperm receptor activity. *Cell* **1985,** *41* (1), 313-324.
104. Genbacev, O. D.; Prakobphol, A.; Foulk, R. A.; Krtolica, A. R.; Ilic, D.; Singer, M. S.; Yang, Z.; Kiessling, L. L.; Rosen, S. D.; Fisher, S. J. Trophoblast L-selectin mediated adhesion at the maternal-fetal interface. *Science* **2003,** *299* (5605), 405-408.
105. Kwon, D. S.; Gregorio, G.; Bitton, N.; Hendrickson, W. A.; Littman, D. R. DC-SIGN-mediated internalization of HIV is required for trans-enhancement of T cell infection. *Immunity* **2002,** *16*, 135-144.
106. Rabinovich, G. A.; van Kooyk, Y.; Cobb, B. A. Glycobiology of immune responses. *Ann. N. Y. Acad. Sci.* **2012,** *1253*, 1-15.
107. van Kooyk, Y.; Rabinovich, G. A. Protein-glycan interactions in the control of innate and adaptive immune responses. *Nat. Immunol.* **2008,** *9* (6), 593-601.
108. Lichtenstein, R. G.; Rabinovich, G. A. Glycobiology of cell death: when glycans and lectins govern cell fate. *Cell Death Differ.* **2013,** *20* (8), 976-986.
109. Choi, S. Synthetic multivalent molecules: concepts and biomedical applications. **2004**.
110. Hasegawa, T.; Kondoh, S.; Matsuura, K.; Kobayashi, K. Rigid helical poly(glycosyl phenyl isocyanide)s: synthesis, conformational analysis, and recognition by lectins. *Macromolecules* **1999,** *32* (20), 6595-6603.
111. Lee, Y.; Sampson, N. S. Romping the cellular landscape: linear scaffolds for molecular recognition. *Curr. Opin. Struct. Biol.* **2006,** *16* (4), 544-550.
112. Hillmyer, M. A.; Laredo, W. R.; Grubbs, R. H. Ring-opening metathesis polymerization of functionalized cyclooctenes by a ruthenium-based metathesis catalyst. *Macromolecules* **1995,** *28* (18), 6311- 6316.

113. Zhang, J.; Matta, M. E.; Hillmyer, M. A. Synthesis of sequence-specific vinyl copolymers by regioselective ROMP of multiply substituted cyclooctenes. *ACS Macro Lett.* **2012,** *1* (12), 1383-1387.
114. Hayes, W.; Osborn, H. M. I.; Osborne, S. D.; Rastall, R. A.; Romagnoli, B. One-pot synthesis of multivalent arrays of mannose mono- and disaccharides. *Tetrahedron* **2003,** *59* (40), 7983-7996.
115. Alonso-Villanueva, J.; Vilas, J. L.; Moreno, I.; Laza, J. M.; Rodríguez, M.; León, L. M. ROMP of functionalized cyclooctene and norbornene derivatives and their copolymerization with cyclooctene. *J. Macromol. Sci., Part A* **2011,** *48* (3), 211-218.
116. Pesek, S. L.; Li, X.; Hammouda, B.; Hong, K.; Verduzco, R. Small-angle neutron scattering analysis of bottlebrush polymers prepared via grafting-through polymerization. *Macromolecules* **2013,** *46* (17), 6998-7005.
117. Benoit, H. *Comptes Rendus* **1957,** *245*, 2244-2247.
118. Hammouda, B. SANS from homogeneous polymer mixtures - a unified overview. *Advances in Polym. Sci* **1993,** *106*, 87-133.
119. Sankaran, V.; Cohen, R. E.; Cummins, C. C.; Schrock, R. R. Morphology of diblock copolymers of norbornene and organometallic derivatives of norbornene. *Macromolecules* **1991,** *24* (25), 6664-6669.
120. Saunders, R. S.; Cohen, R. E.; Schrock, R. R. Synthesis and characterization of diblock copolymer films containing self-assembled polyacetylene structures. *Macromolecules* **1991,** *24* (20), 5599-5605.
121. Xia, Y.; Olsen, B. D.; Kornfield, J. A.; Grubbs, R. H. Efficient synthesis of narrowly dispersed brush copolymers and study of their assemblies: the importance of side chain arrangement. *J. Am. Chem. Soc.* **2009,** *131* (51), 18525-18532.
122. Wataoka, I.; Urakawa, H.; Kobayashi, K.; Akaike, T.; Schmidt, M.; Kajiwara, K. Structural characterization of glycoconjugate polystyrene in aqueous solution. *Macromolecules* **1999,** *32*, 1816-1821.
123. Fukuda, T.; Inoue, Y.; Koga, T.; Matsuoka, M.; Miura, Y. Encapsulation of polythiophene by glycopolymer for water-soluble nanowire. *Chem. Lett.* **2011,** *40* (8), 864-866.
124. Benoff, S. Carbohydrates and fertilization: an overview. *Mol. Hum. Reprod.* **1997,** *3* (7), 599-637.
125. Krapf, D.; Arcelay, E.; Wertheimer, E. V.; Sanjay, A.; Pilder, S. H.; Salicioni, A. M.; Visconti, P. E. Inhibition of Ser/Thr phosphatases induces capacitation-associated signaling in the presence of Src kinase inhibitors. *J. Biol. Chem.* **2010,** *285* (11), 7977-85.
126. Tateno, H.; Krapf, D.; Hino, T.; Sanchez-Cardenas, C.; Darszon, A.; Yanagimachi, R.; Visconti, P. E. Ca2+ ionophore A23187 can make mouse spermatozoa capable of fertilizing in vitro without activation of cAMP-dependent phosphorylation pathways. *Proc. Natl. Acad. Sci. U. S. A.* **2013,** *110* (46), 18543-8.
127. Inoue, N.; Ikawa, M.; Nakanishi, T.; Matsumoto, M.; Nomura, M.; Seya, T.; Okabe, M. Disruption of mouse CD46 causes an accelerated spontaneous acrosome reaction in sperm. *Mol. Cell. Biol.* **2003,** *23* (7), 2614-2622.
128. Navarrete, F. A.; Alvau, A.; Lee, H. C.; Levin, L. R.; Buck, J.; Leon, P. M.; Santi, C. M.; Krapf, D.; Mager, J.; Fissore, R. A.; Salicioni, A. M.; Darszon, A.; Visconti, P. E. Transient exposure to calcium ionophore enables in vitro fertilization in sterile mouse models. *Sci. Rep.* **2016,** *6*, 33589.

129. Love, J. A.; Morgan, J. P.; Trnka, T. M.; Grubbs, R. H. A practical and highly active ruthenimu- based catalyst that effects the cross metathesis of acrylonitrile *Angrew. Chem. Int. Ed.* **2002,** *41* (21), 4035- 4036.
130. Feketea, A.; Gyergyóia, K.; Kövérb, K. E.; Bajzaa, I.; Lipták, A. Preparation of the pentasaccharide hapten of the GPL of Mycobacterium avium serovar 19 by achieving the glycosylation of a tertiary hydroxyl group. *Carbohydr. Res.* **2006,** *341* (10), 1312-21.
131. Gu, L.; Luo, P. G.; Wang, H.; Meziani, M. J.; Lin, Y.; Veca, L. M.; Cao, L.; Lu, F.; Wang, X.; Quinn, R. A.; Wang, W.; Zhang, P.; Lacher, S.; Sun, Y. Single-walled carbon nanotube as a unique scaffold for the multivalent display of sugars. *Biomacromolecules* **2008,** *9*, 2408-2418.
132. Dasgupta, S.; Rajput, V. K.; Roy, B.; Mukhopadhyay, B. Lanthanum trifluoromethane-sulfonate-catalyzed facile synthesis of per-O-acetylated sugars and their one-pot conversion to S-aryl and O-alkyl/aryl glycosides. *J. Carbohyd. Res.* **2007,** *26* (2), 91- 106.
133. Paterson, S. M.; Clark, J.; Stubbs, K. A.; Chirila, T. V.; Baker, M. V. Carbohydrate-based crosslinking agents: Potential use in hydrogels. *J. Polym. Sci., Part A: Polym. Chem.* **2011,** *49* (20), 4312-4315.
134. Chittaboina, S.; Hodges, B.; Wang, B. A facile route for the regioselective deacetylation of peracetylated carbohydrates at anomeric position. *Lett. Org. Chem.* **2006,** *3*, 35-38.
135. Murphy, J. J.; Furusho, H.; Paton, R. M.; Nomura, K. Precise synthesis of poly(macromonomer)s containing sugars by repetitive ROMP and their attachments to poly(ethylene glycol): Synthesis, TEM analysis and their properties as amphiphilic block fragments. *Chem. Eur. J.* **2007,** *13* (32), 8985-8997.
136. Fang, P.; Xu, W.; Li, D.; Zhao, X.; Dai, J.; Wang, Z.; Yan, X.; Qin, M.; Zhang, Y.; Xu, C.; Wang, L.; Qiao, Z. A novel acrosomal protein, IQCF1, involved in sperm capacitation and the acrosome reaction. *Andrology* **2014**.

Appendix

Checklist for compounds.

Compound	Reference	^{1}H NMR	^{13}C NMR	GPC	SAXS
1a'	57	√			
1b'	57	√	√		
1c'	57	√			
1d'	57	√	√		
2a'	57	√[a]	√		
2b'	57	√[a]	√[a]		
2c'	57	√	√		
2d'	57	√[a]	√[a]		
poly(**1a'**)$_{100}$	57	√		√	
poly(**1b'**)$_{100}$	57	√		√	
poly(**1c'**)$_{100}$	57	√		√	
poly(**1d'**)$_{100}$	57	√		√	
poly(**2a'**)$_{100}$		√[a]		√[a]	
poly(**2b'**)$_{100}$		√[a]		√[a]	
poly(**2c'**)$_{100}$		√[a]		√	
poly(**2d'**)$_{100}$		√[a]		√[a]	
poly(**1a'**$_{50}$-*ran*-**1d'**$_{50}$)		√		√	
poly(**1a'**$_{10}$-*ran*-**1d'**$_{90}$)		√		√	
poly(**1b'**$_{50}$-*ran*-**1d'**$_{50}$)		√		√	
poly(**1b'**$_{10}$-*ran*-**1d'**$_{90}$)		√		√	

[a] The compounds were characterized by Maria Rodolis.

poly(**1c'**$_{50}$-*ran*-**1d'**$_{50}$)		√	√	
poly(**1c'**$_{10}$-*ran*-**1d'**$_{90}$)		√	√	
poly(**1b'**$_{50}$-*block*-**1a'**$_{50}$)		√	√	
poly(**1b'**$_{50}$-*block*-**1c'**$_{50}$)		√	√	
poly(**1a'**$_{50}$-*block*-**1c'**$_{50}$)		√	√	
poly(**1a'**$_{50}$-*block*-**1d'**$_{50}$)		√	√	
poly(**1b'**$_{50}$-*block*-**1d'**$_{50}$)		√	√	
poly(**1c'**$_{50}$-*block*-**1d'**$_{50}$)		√	√	
poly(**1a**)$_{100}$	57	√		√
poly(**1b**)$_{100}$	57	√		√
poly(**1c**)$_{100}$	57	√		√
poly(**1d**)$_{100}$	57	√		√
poly(**2a**)$_{100}$		√		√
poly(**2b**)$_{100}$		√		√
poly(**2c**)$_{100}$		√		√
poly(**2d**)$_{100}$		√[a]		√
poly(**1a**$_{50}$-*ran*-**1d**$_{50}$)		√		√
poly(**1a**$_{10}$-*ran*-**1d**$_{90}$)		√		√
poly(**1a**$_{50}$-*ran*-**1d**$_{50}$)		√		√
poly(**1a**$_{10}$-*ran*-**1d**$_{90}$)		√		√
poly(**1a**$_{50}$-*ran*-**1d**$_{50}$)		√		√
poly(**1a**$_{50}$-*block*-**1b**$_{50}$)		√		√
poly(**1a**$_{50}$-*block*-**1b**$_{50}$)		√		√
poly(**1a**$_{50}$-*block*-**1b**$_{50}$)		√		√
poly(**1a**$_{50}$-*block*-**1b**$_{50}$)		√		√

poly(**1a**$_{50}$-*block*-**1b**$_{50}$)	√	√

	Parameter	Value
1	Data File Name	C:/ Documents and Settings/ User/ Desktop/ NMR 500/ NB-L-fucose-32-33-hh-07182013/ 1/ fid
2	Title	NB-L-fucose-32-33-hh-07182013.1.fid
3	Origin	Bruker BioSpin GmbH
4	Spectrometer	spect
5	Solvent	CDCl3
6	Temperature	298.1
7	Pulse Sequence	zg30
8	Experiment	1D
9	Probe	5 mm CPPBBO BB-1H/ 19F/ D Z-GRD Z122624/ 0008
10	Number of Scans	16
11	Receiver Gain	32
12	Relaxation Delay	1.0000
13	Pulse Width	12.0000
14	Modification Date	2013-07-18T15:13:46
15	Spectrometer Frequency	499.89
16	Spectral Width	10000.0
17	Lowest Frequency	-1929.5
18	Nucleus	1H
19	Acquired Size	32768
20	Spectral Size	65536

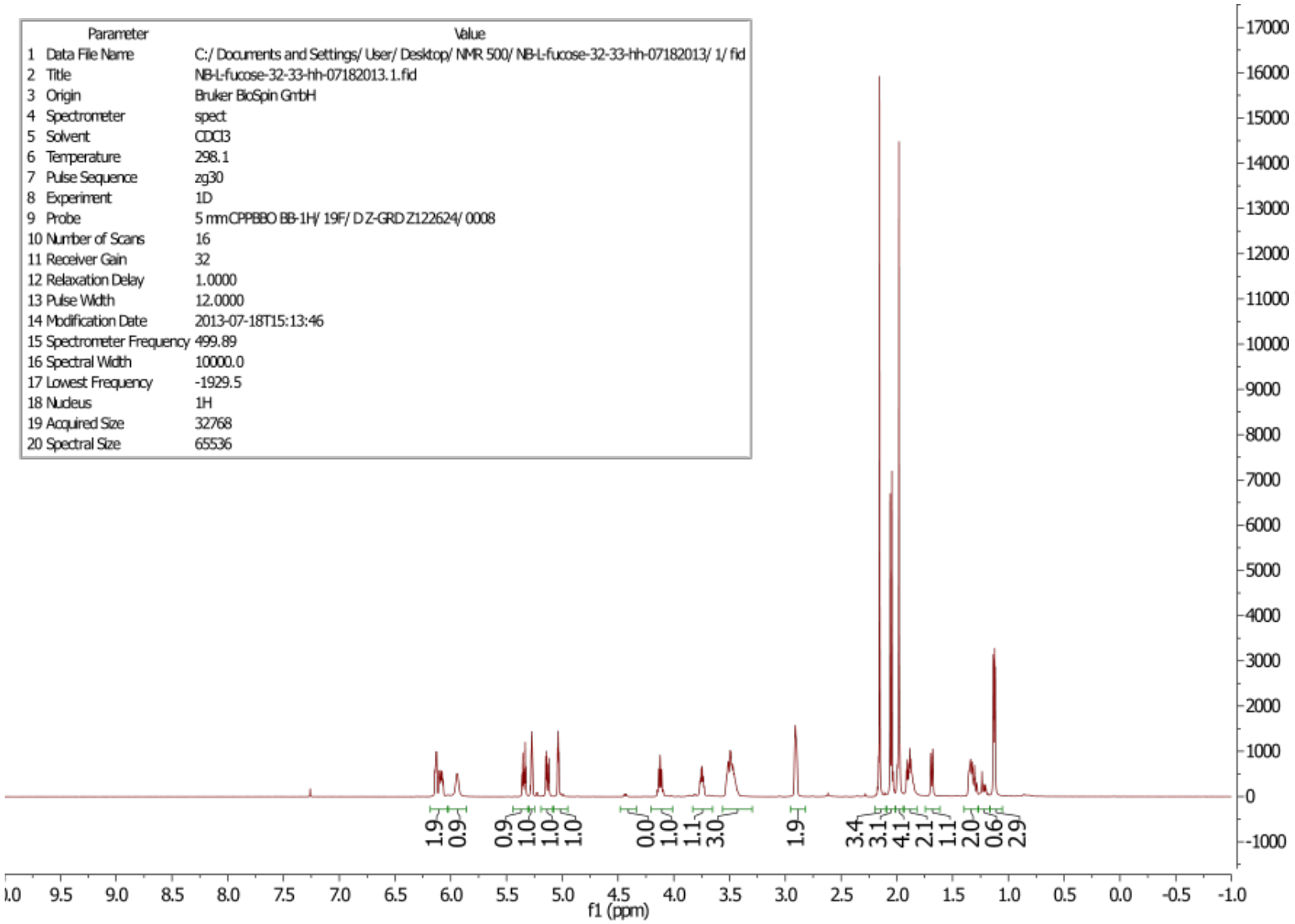

^{1}H NMR of **1a'**

Parameter	Value
1 Data File Name	C:/ Documents and Settings/ User/ Desktop/ nmr400/ NB-mannose-hh-07032012/ 1/ fid
2 Title	NB-mannose-hh-07032012.1.fid
3 Origin	Bruker BioSpin GmbH
4 Spectrometer	spect
5 Solvent	CDCl3
6 Temperature	298.2
7 Pulse Sequence	zg30
8 Experiment	1D
9 Probe	5 mm PABBO BB/ 19F-1H/ D Z-GRD Z116098/ 0058
10 Number of Scans	16
11 Receiver Gain	32
12 Relaxation Delay	1.0000
13 Pulse Width	10.1000
14 Modification Date	2012-07-03T17:40:54
15 Spectrometer Frequency	399.83
16 Spectral Width	8223.7
17 Lowest Frequency	-1651.1
18 Nucleus	1H
19 Acquired Size	32768
20 Spectral Size	65536

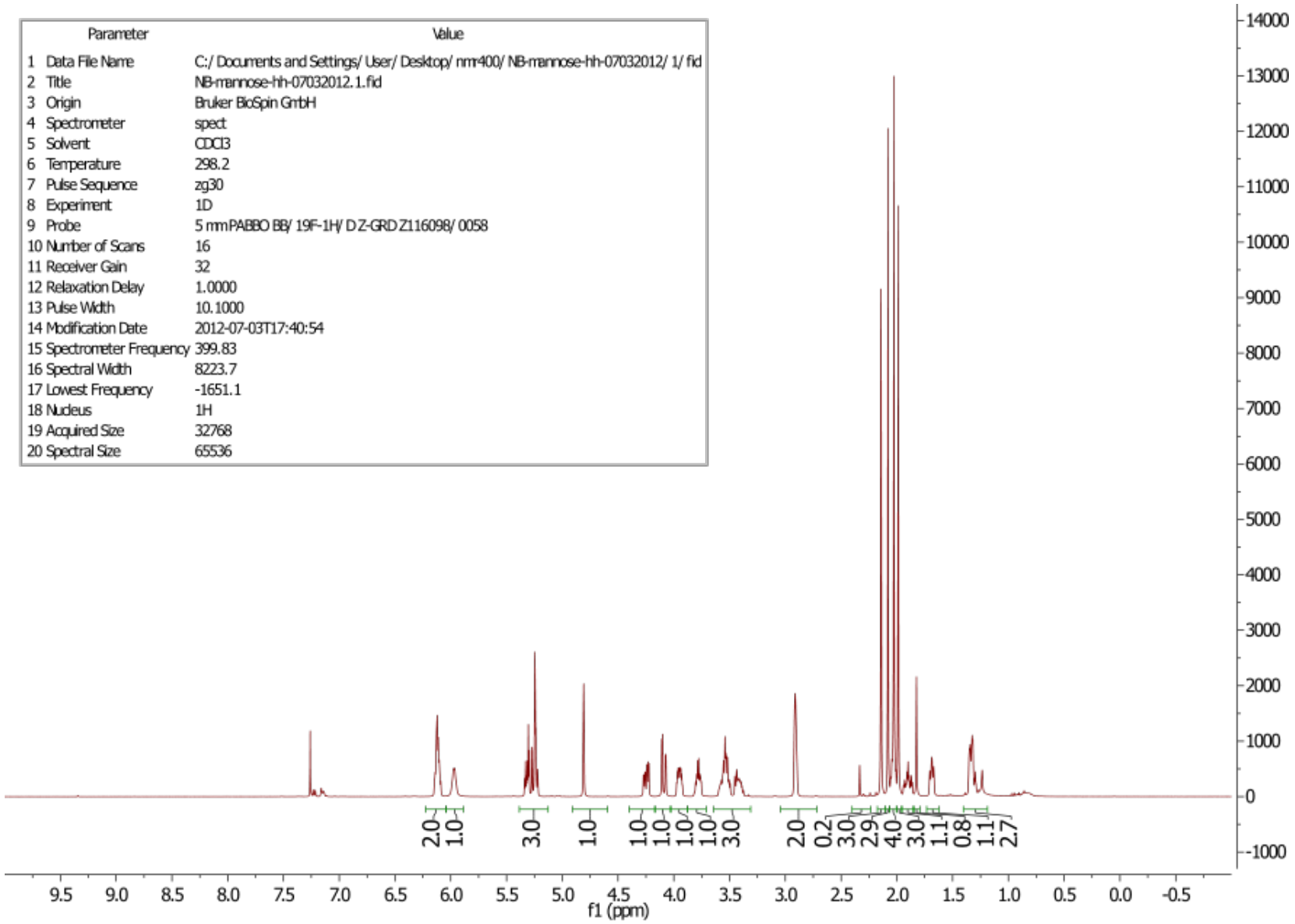

^{1}H NMR of **1b'**

	Parameter	Value
1	Data File Name	C:/ Documents and Settings/ User/ Desktop/ NMR 500/ nb-glcnac-hh-05152014/ 1/ fid
2	Title	nb-glcnac-hh-05152014.1.fid
3	Origin	Bruker BioSpin GmbH
4	Spectrometer	spect
5	Solvent	CDCl3
6	Temperature	298.2
7	Pulse Sequence	zg30
8	Experiment	1D
9	Probe	5 mm CPPBBO BB-1H/ 19F/ D Z-GRD Z122624/ 0008
10	Number of Scans	16
11	Receiver Gain	32
12	Relaxation Delay	1.0000
13	Pulse Width	12.0000
14	Modification Date	2014-05-15T12:51:16
15	Spectrometer Frequency	499.89
16	Spectral Width	10000.0
17	Lowest Frequency	-1919.4
18	Nucleus	1H
19	Acquired Size	32768
20	Spectral Size	65536

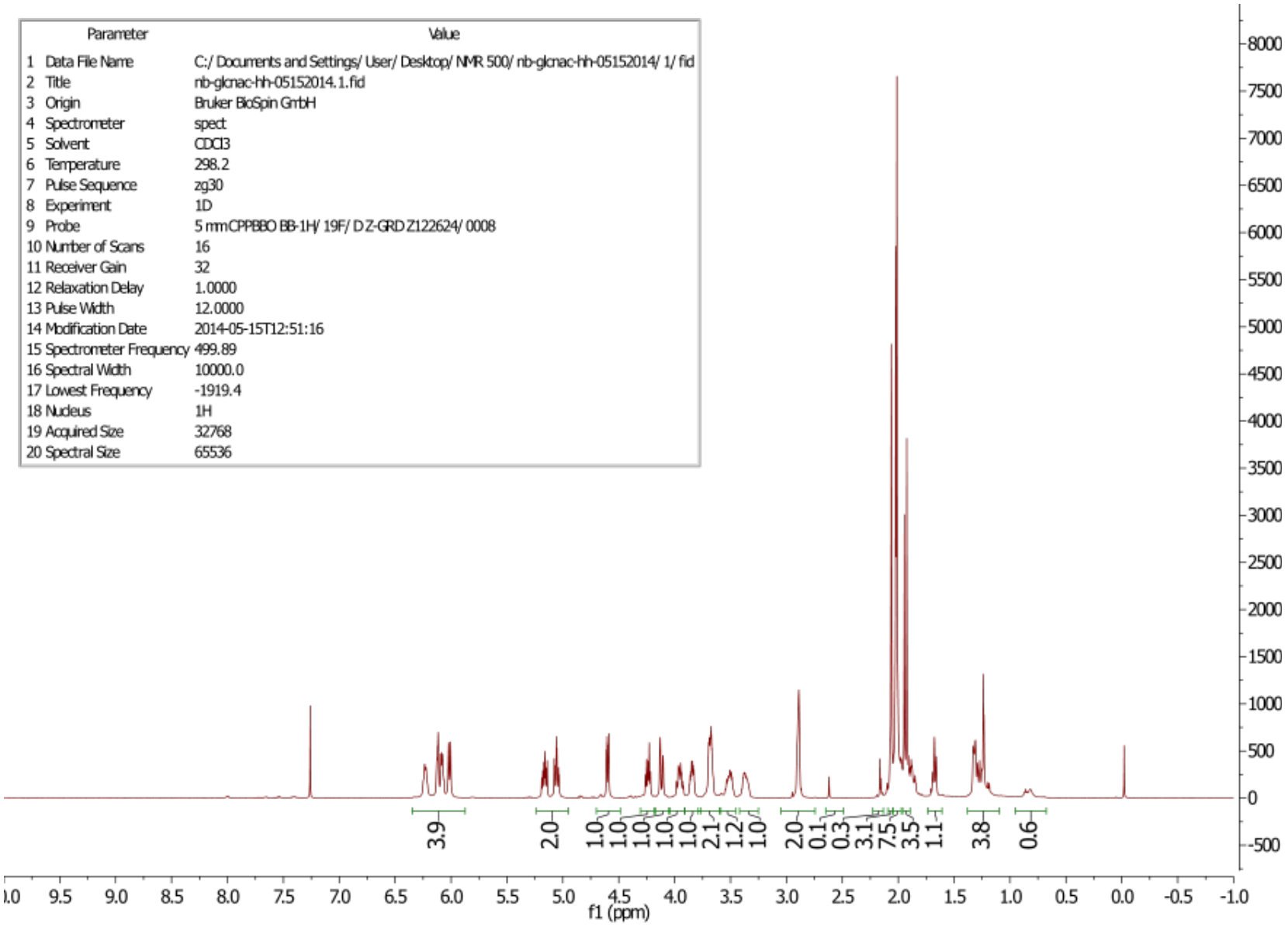

^{1}H NMR of **1c'**

	Parameter	Value
1	Data File Name	C:/ Documents and Settings/ User/ Desktop/ nmr400/ nb-glucose-hh-08032012/ 1/ fid
2	Title	nb-glucose-hh-08032012.1.fid
3	Origin	Bruker BioSpin GmbH
4	Spectrometer	spect
5	Solvent	CDCl3
6	Temperature	298.2
7	Pulse Sequence	zg30
8	Experiment	1D
9	Probe	5 mm PABBO BB/ 19F-1H/ D Z-GRD Z116098/ 0058
10	Number of Scans	16
11	Receiver Gain	32
12	Relaxation Delay	1.0000
13	Pulse Width	10.1000
14	Modification Date	2012-08-03T13:26:08
15	Spectrometer Frequency	399.83
16	Spectral Width	8223.7
17	Lowest Frequency	-1651.1
18	Nucleus	1H
19	Acquired Size	32768
20	Spectral Size	65536

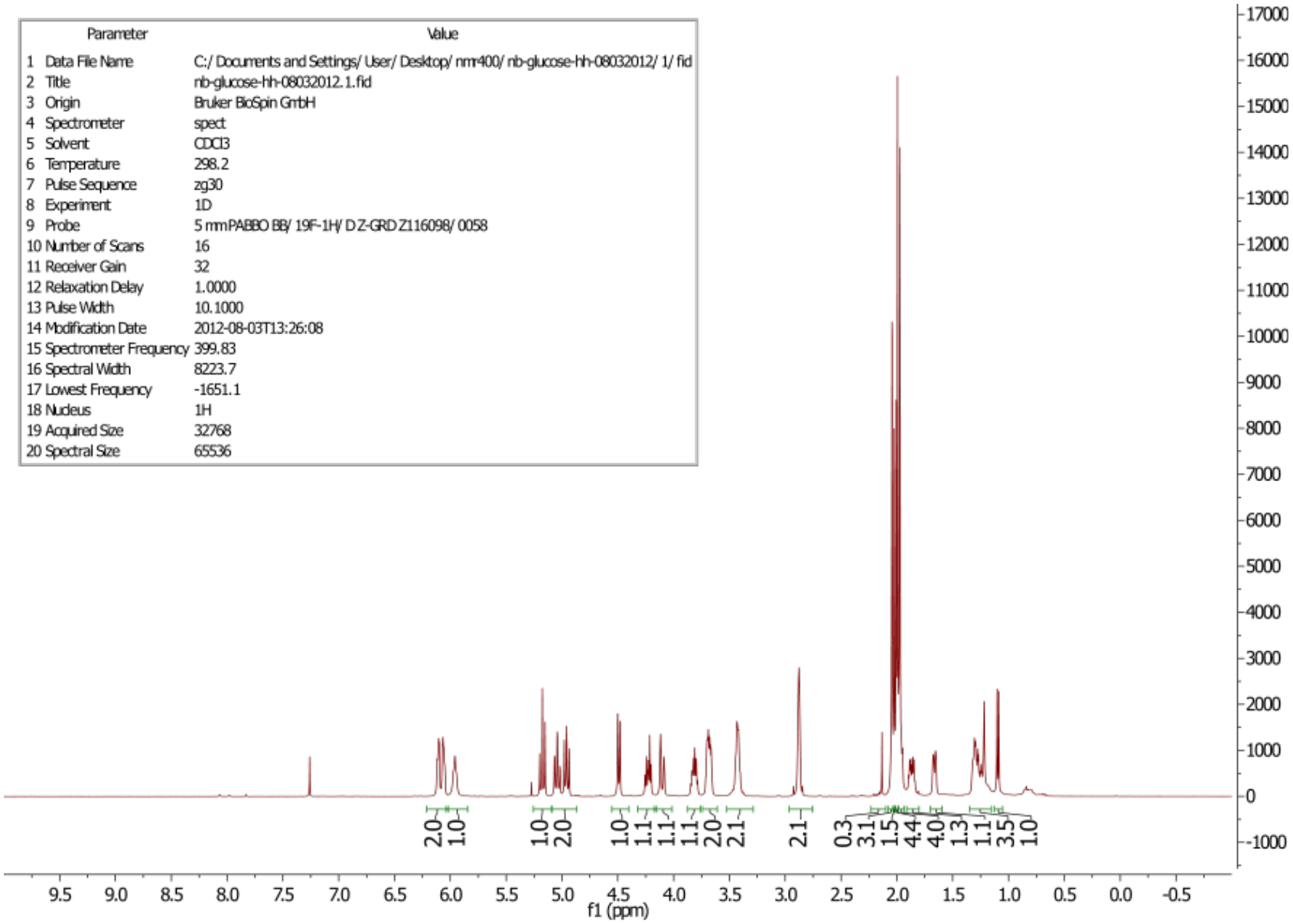

^{1}H NMR of **1d'**

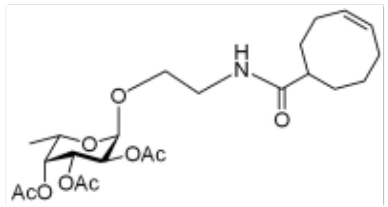

2a'

^{1}H NMR of **2a'**

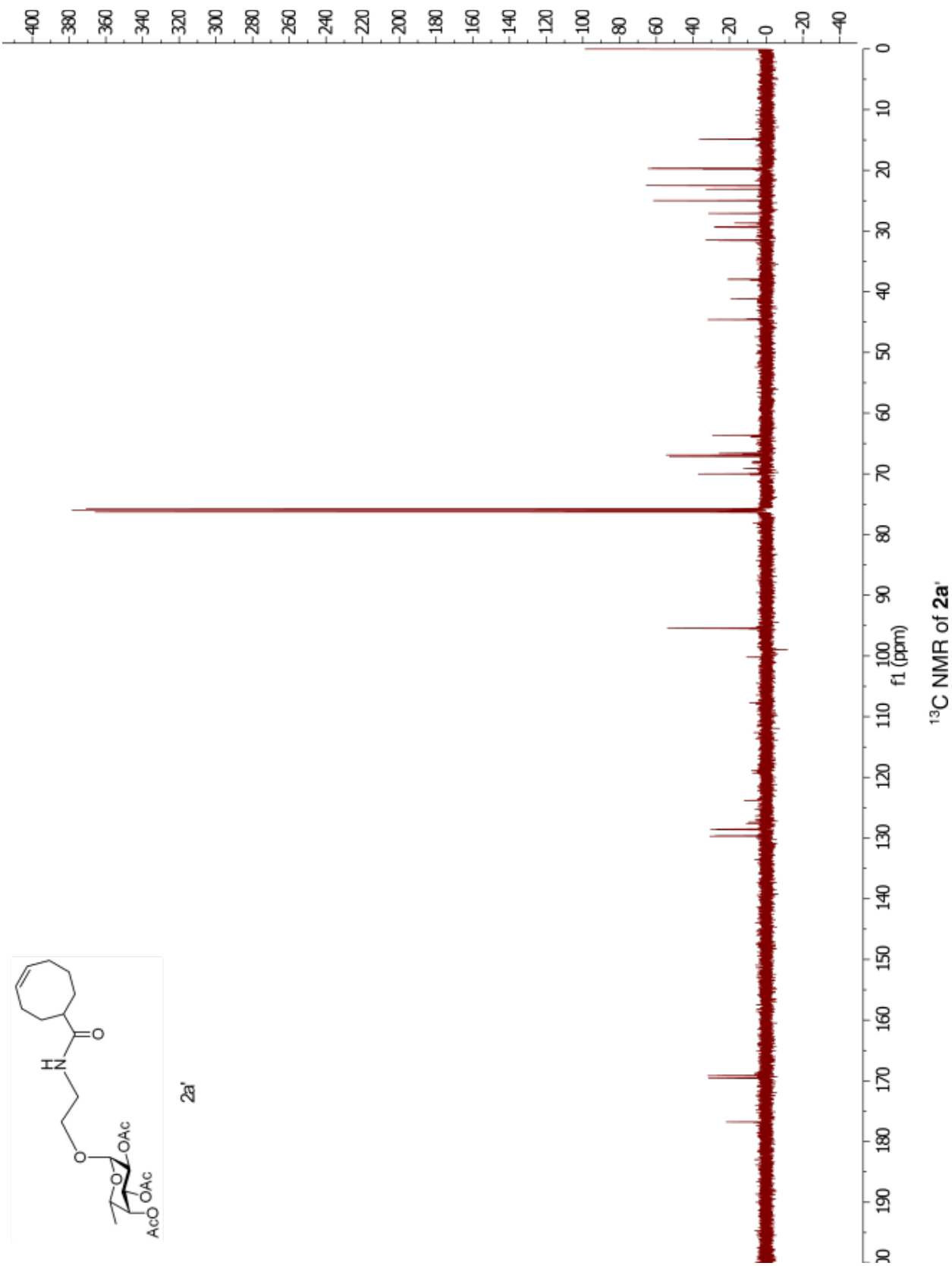
2a'
f1 (ppm)
^{13}C NMR of **2a'**

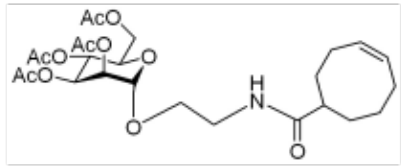

2b'

^{1}H NMR of **2b'**

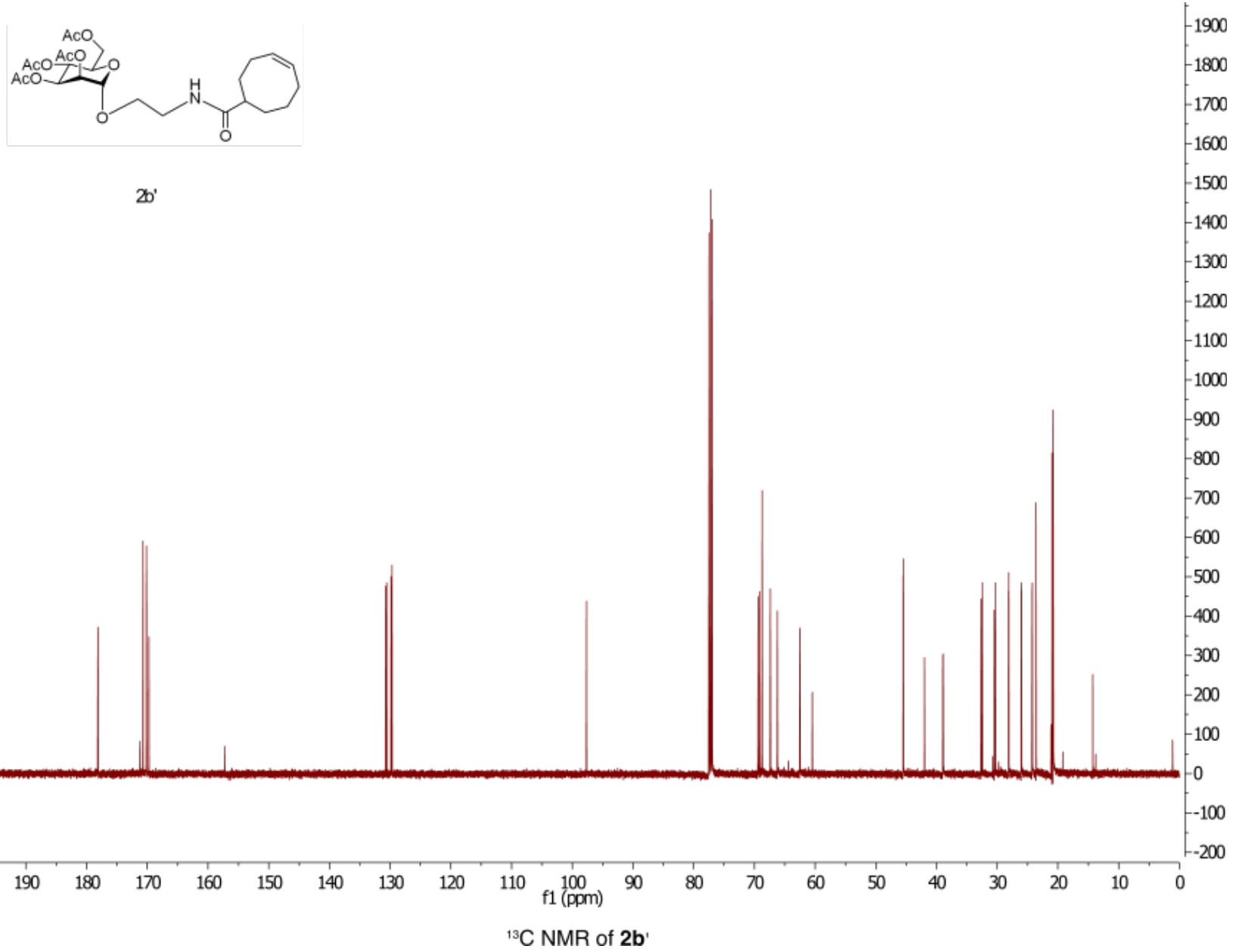
AcO
AcO
AcO
AcO
O
H
N
O
O
2b'
1900
1800
1700
1600
1500
1400
1300
1200
1100
1000
900
800
700
600
500
400
300
200
100
0
-100
-200
190
180
170
160
150
140
130
120
110
100
90
80
70
60
50
40
30
20
10
0
f1 (ppm)

^{13}C NMR of **2b'**

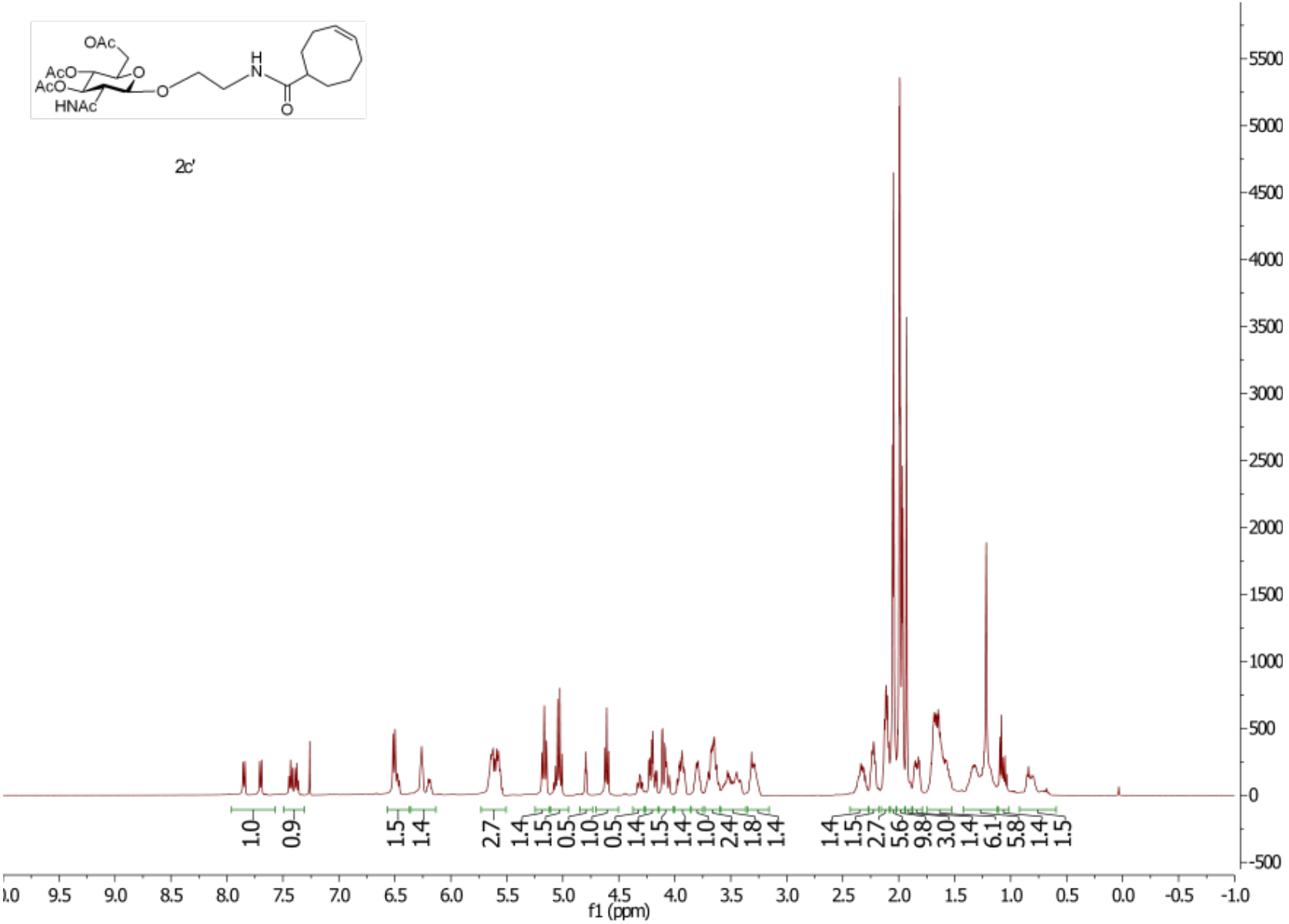
OAc
AcO
AcO
HNAc
O
O
H
N
O
2c'
5500
5000
4500
4000
3500
3000
2500
2000
1500
1000
500
0
-500
1.0 0.9 1.5 1.4 2.7 1.4 1.5 0.5 1.0 0.5 1.4 1.5 1.4 1.0 2.4 1.8 1.4 1.4 1.5 2.7 5.6 9.8 3.0 1.4 6.1 5.8 1.4 1.5
9.5 9.0 8.5 8.0 7.5 7.0 6.5 6.0 5.5 5.0 4.5 4.0 3.5 3.0 2.5 2.0 1.5 1.0 0.5 0.0 -0.5 -1.0
f1 (ppm)

^{1}H NMR of **2c'**

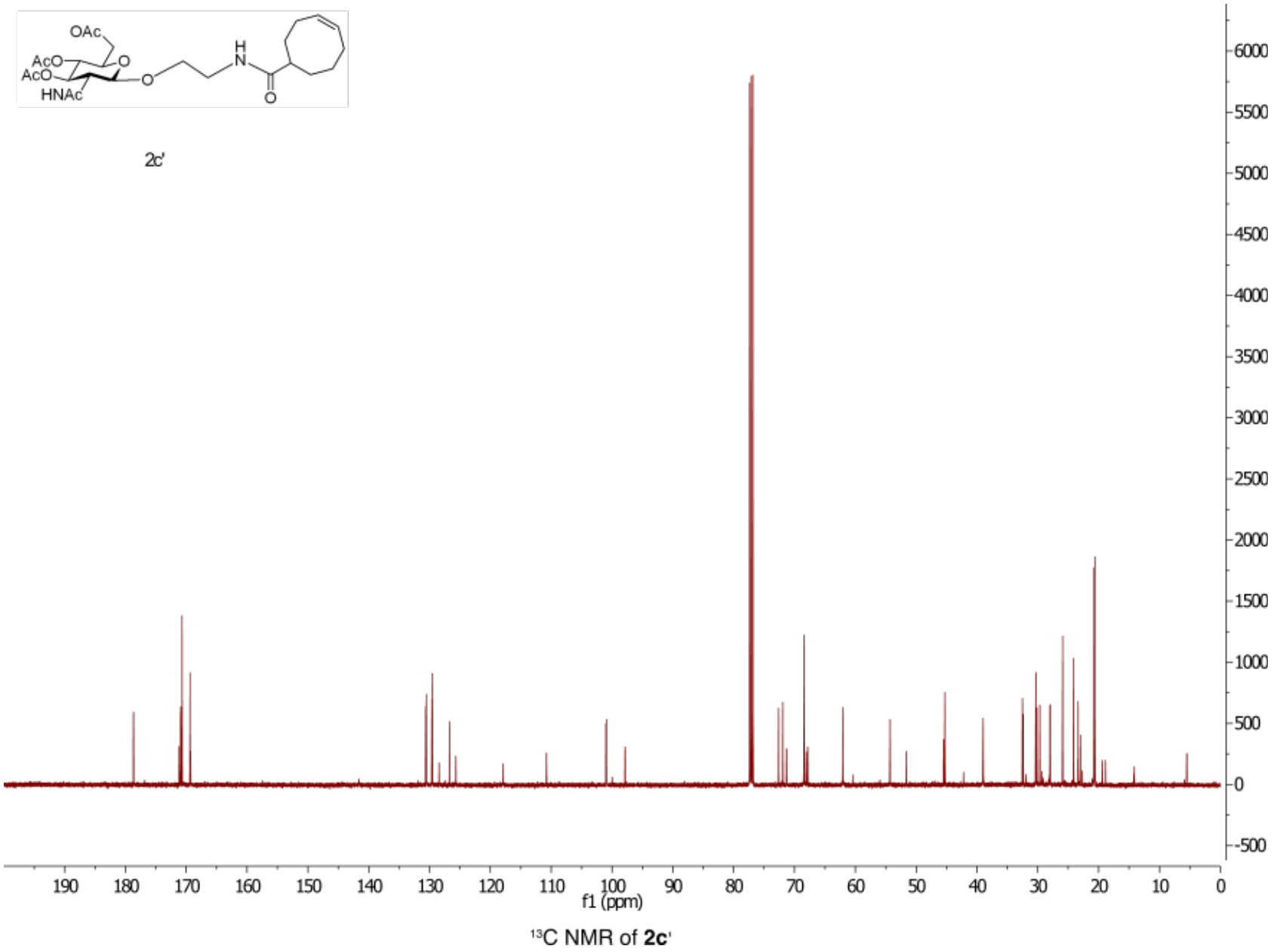
OAc
AcO
AcO
HNAc
O
H
N
O
2c'
6000
5500
5000
4500
4000
3500
3000
2500
2000
1500
1000
500
0
-500
190
180
170
160
150
140
130
120
110
100
90
80
70
60
50
40
30
20
10
0
f1 (ppm)

^{13}C NMR of **2c'**

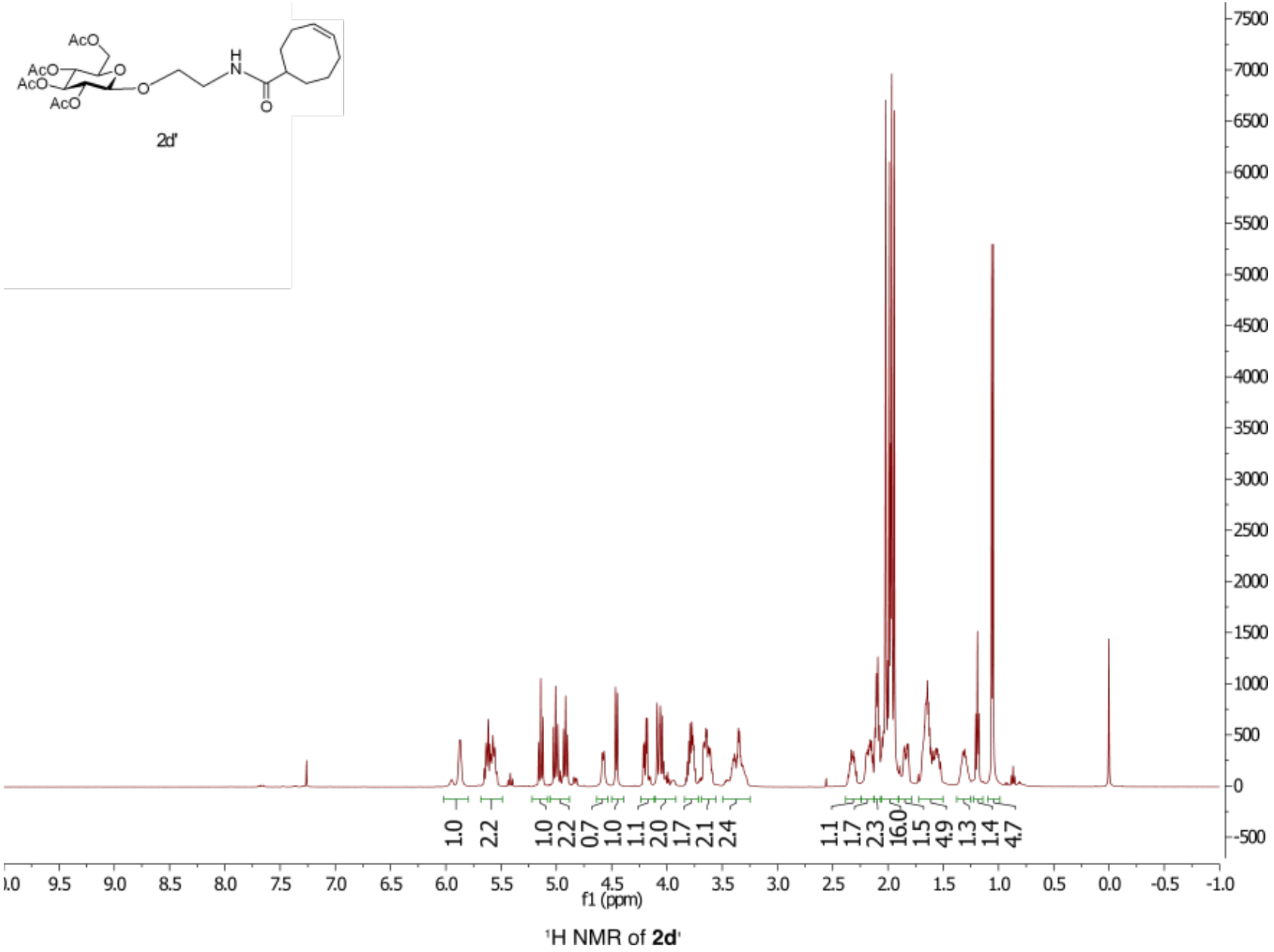
AcO
AcO
AcO
AcO
O
H
N
O
2d'
7500
7000
6500
6000
5500
5000
4500
4000
3500
3000
2500
2000
1500
1000
500
0
-500
1.0 2.2 1.0 2.2 0.7 1.0 1.1 2.0 1.7 2.1 2.4 1.1 1.7 2.3 16.0 1.5 4.9 1.3 1.4 4.7
9.5 9.0 8.5 8.0 7.5 7.0 6.5 6.0 5.5 5.0 4.5 4.0 3.5 3.0 2.5 2.0 1.5 1.0 0.5 0.0 -0.5 -1.0
f1 (ppm)

^{1}H NMR of **2d'**

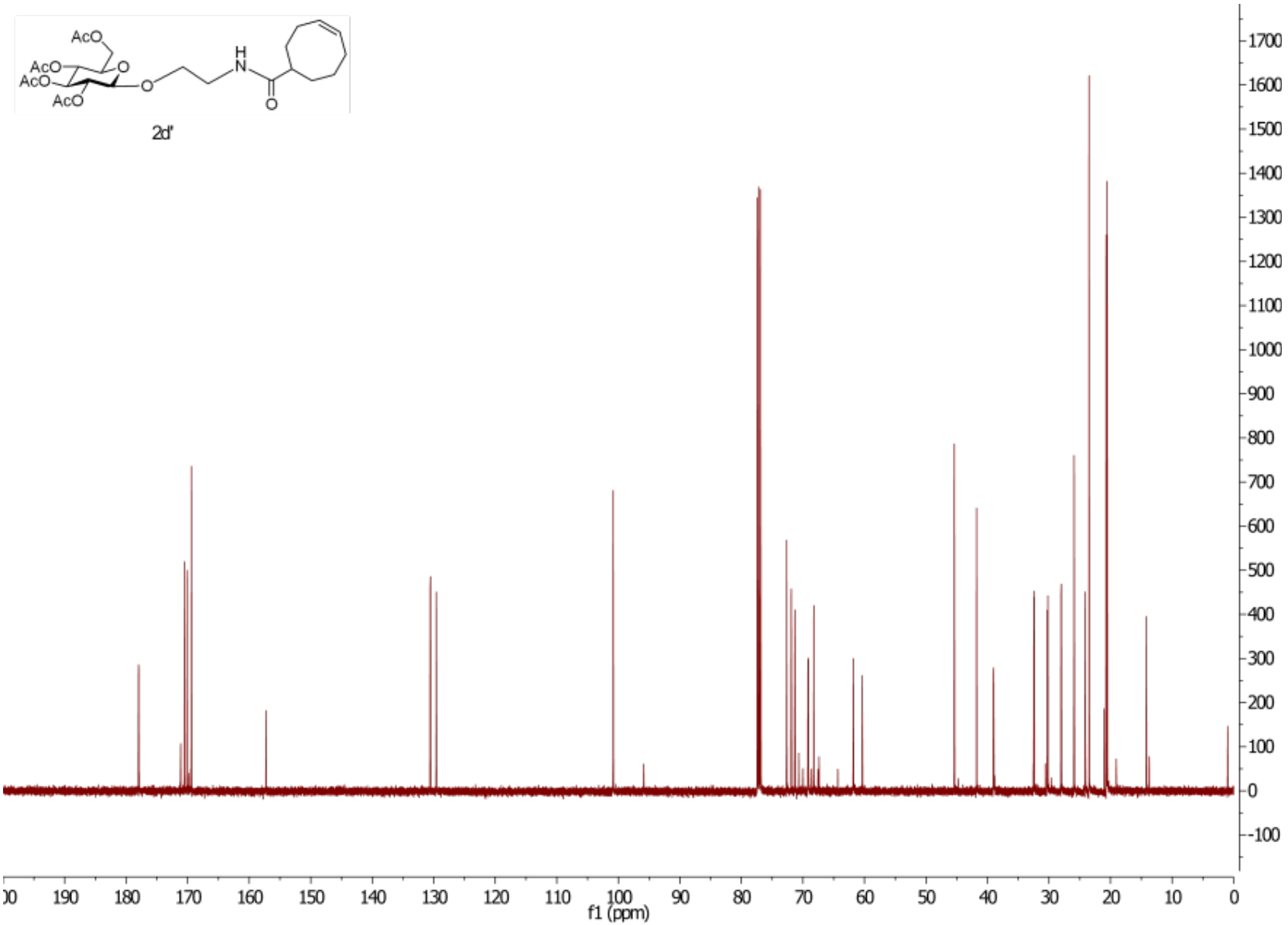
AcO
AcO
AcO
AcO
O
H
N
O
2d'
1700
1600
1500
1400
1300
1200
1100
1000
900
800
700
600
500
400
300
200
100
0
-100
190
180
170
160
150
140
130
120
110
100
90
80
70
60
50
40
30
20
10
0
f1 (ppm)

^{13}C NMR of **2d'**

	Parameter	Value
1	Data File Name	C:/ Documents and Settings/ User/ Desktop/ nmr400/ poly-(L-fuocose)100-1-hh-07232013/ 1/ fid
2	Title	poly-(L-fuocose)100-1-hh-07232013.1.fid
3	Origin	Bruker BioSpin GmbH
4	Spectrometer	spect
5	Solvent	CDCl3
6	Temperature	298.2
7	Pulse Sequence	zg30
8	Experiment	1D
9	Probe	5 mm PABBO BB/ 19F-1H/ D Z-GRD Z116098/ 0058
10	Number of Scans	19
11	Receiver Gain	32
12	Relaxation Delay	1.0000
13	Pulse Width	10.1000
14	Modification Date	2013-07-23T15:18:12
15	Spectrometer Frequency	399.83
16	Spectral Width	8223.7
17	Lowest Frequency	-1651.1
18	Nucleus	1H
19	Acquired Size	32768
20	Spectral Size	65536

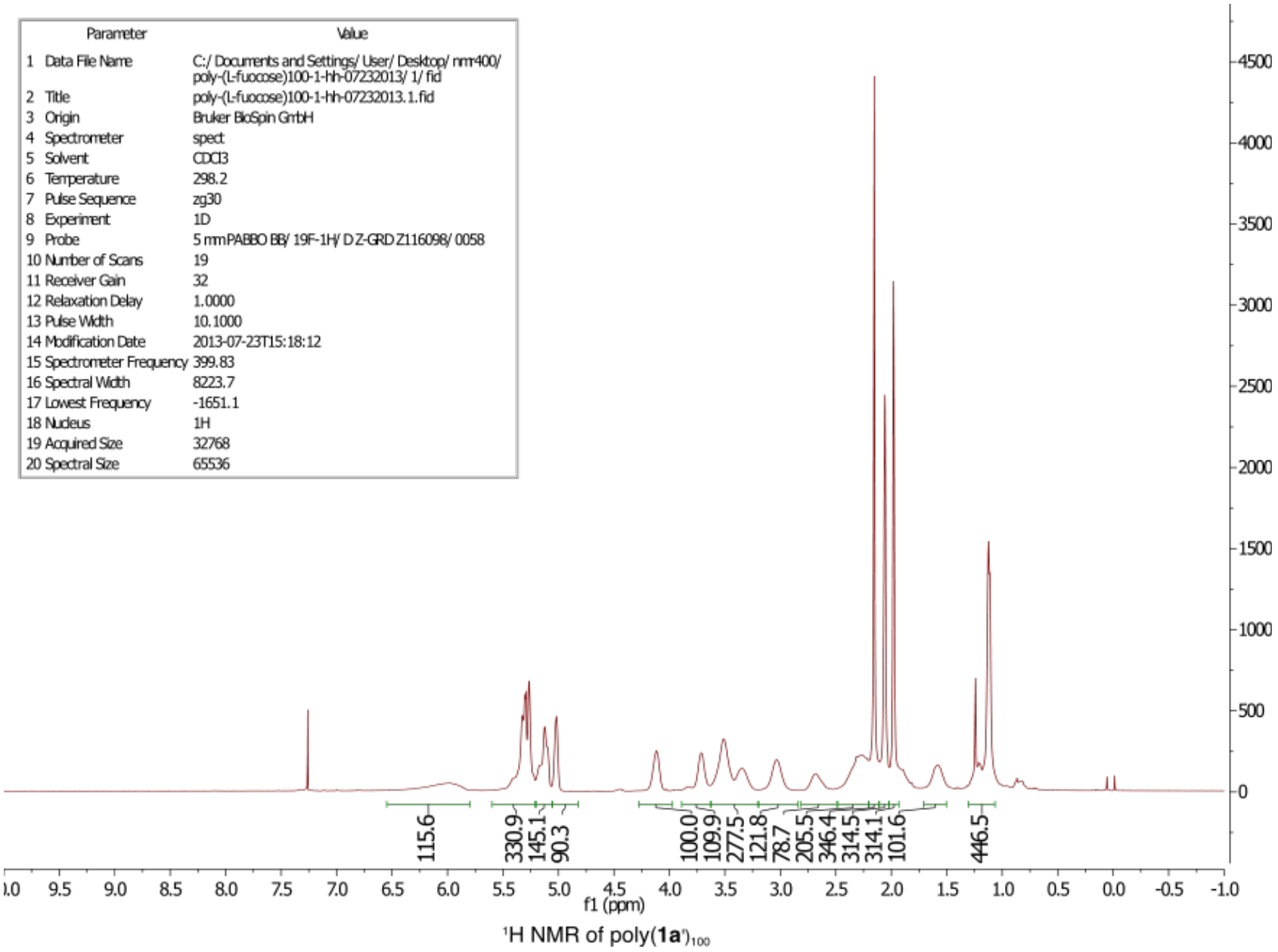

^{1}H NMR of poly(**1a**')$_{100}$

Parameter	Value
1 Data File Name	C:/ Documents and Settings/ User/ Desktop/ NMR 500/ NB-Mannose 100mer-1 hh09272012/ 1/ fid
2 Title	NB-Mannose 100mer-1 hh09272012.1.fid
3 Origin	Bruker BioSpin GmbH
4 Spectrometer	spect
5 Solvent	CDCl3
6 Temperature	298.2
7 Pulse Sequence	zg30
8 Experiment	1D
9 Probe	5 mm CPPBBO BB-1H/ 19F/ D Z-GRD Z122624/ 0008
10 Number of Scans	44
11 Receiver Gain	32
12 Relaxation Delay	1.0000
13 Pulse Width	12.0000
14 Modification Date	2012-09-27T12:50:10
15 Spectrometer Frequency	499.89
16 Spectral Width	10000.0
17 Lowest Frequency	-1913.0
18 Nucleus	1H
19 Acquired Size	32768
20 Spectral Size	65536

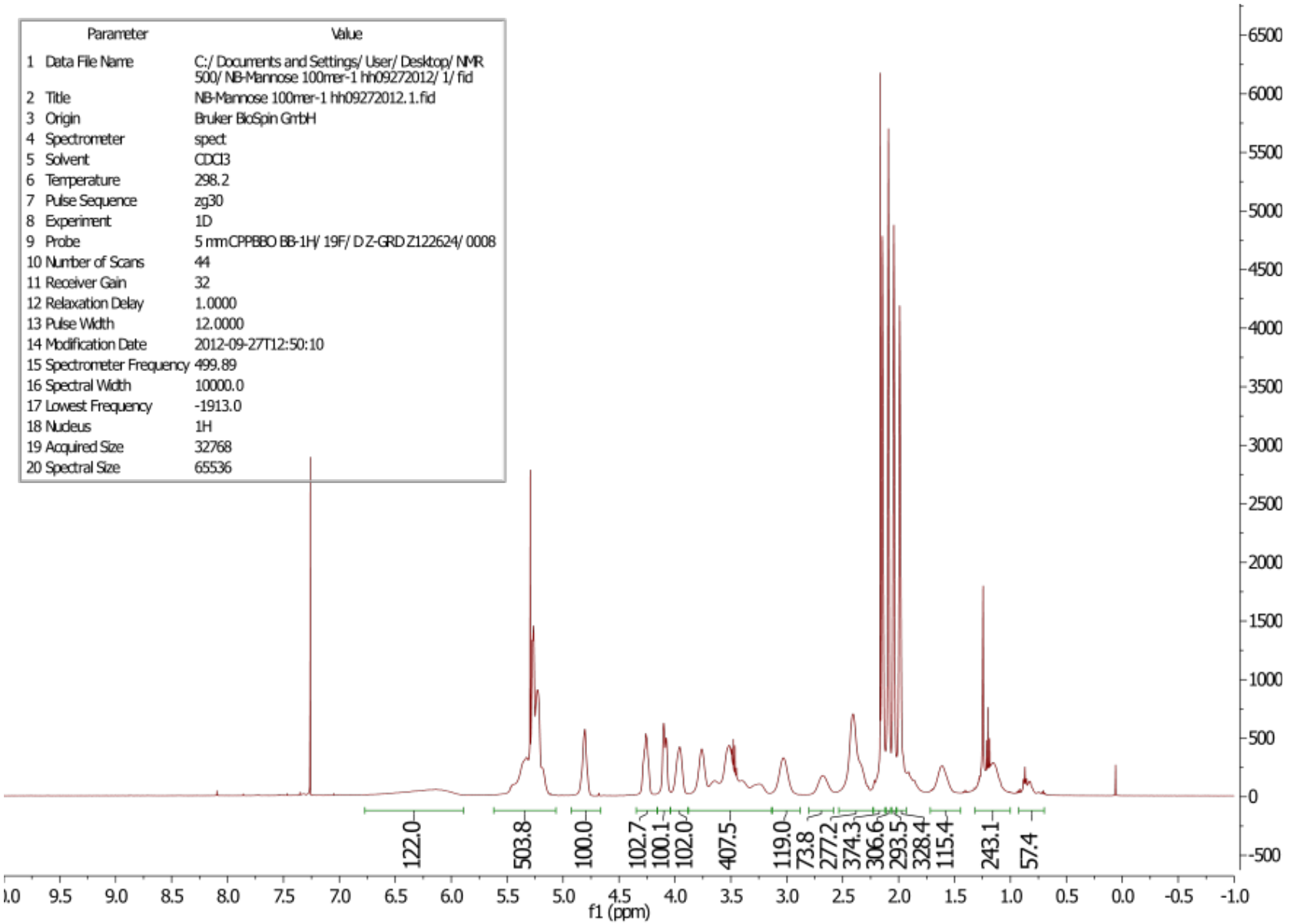

^{1}H NMR of poly(**1b**')$_{100}$

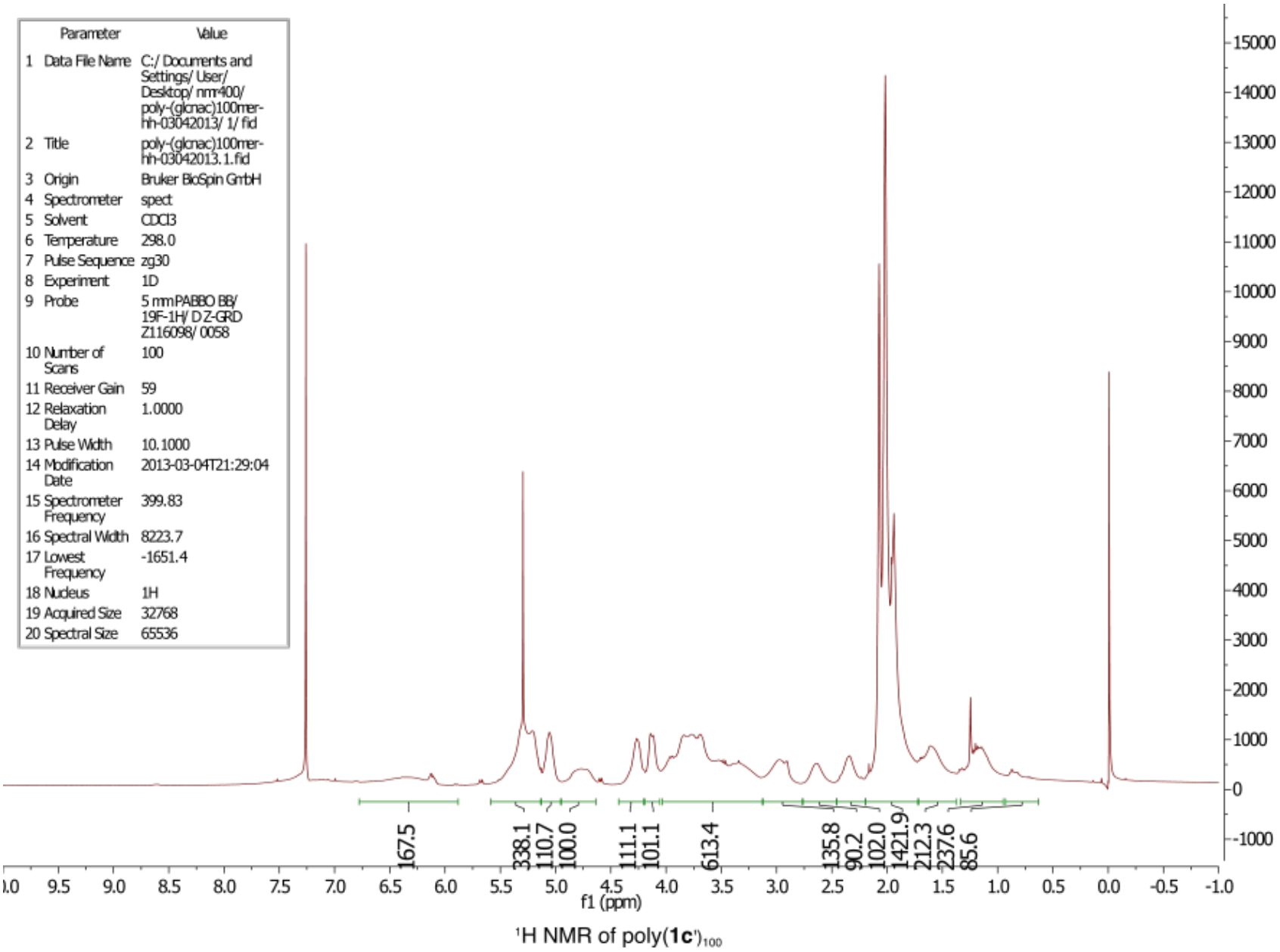

^{1}H NMR of poly(**1c**')$_{100}$

	Parameter	Value
1	Data File Name	C:/ Documents and Settings/ User/ Desktop/ nmr400/ nb-glucose-100mer-1-hh-09042012/ 1/ fid
2	Title	nb-glucose-100mer-1-hh-09042012.1.fid
3	Origin	Bruker BioSpin GmbH
4	Spectrometer	spect
5	Solvent	CDCl3
6	Temperature	298.1
7	Pulse Sequence	zg30
8	Experiment	1D
9	Probe	5 mm PABBO BB/ 19F-1H/ D Z-GRD Z116098/ 0058
10	Number of Scans	16
11	Receiver Gain	66
12	Relaxation Delay	1.0000
13	Pulse Width	10.1000
14	Modification Date	2012-09-04T16:34:28
15	Spectrometer Frequency	399.83
16	Spectral Width	8223.7
17	Lowest Frequency	-1651.3
18	Nucleus	1H
19	Acquired Size	32768
20	Spectral Size	65536

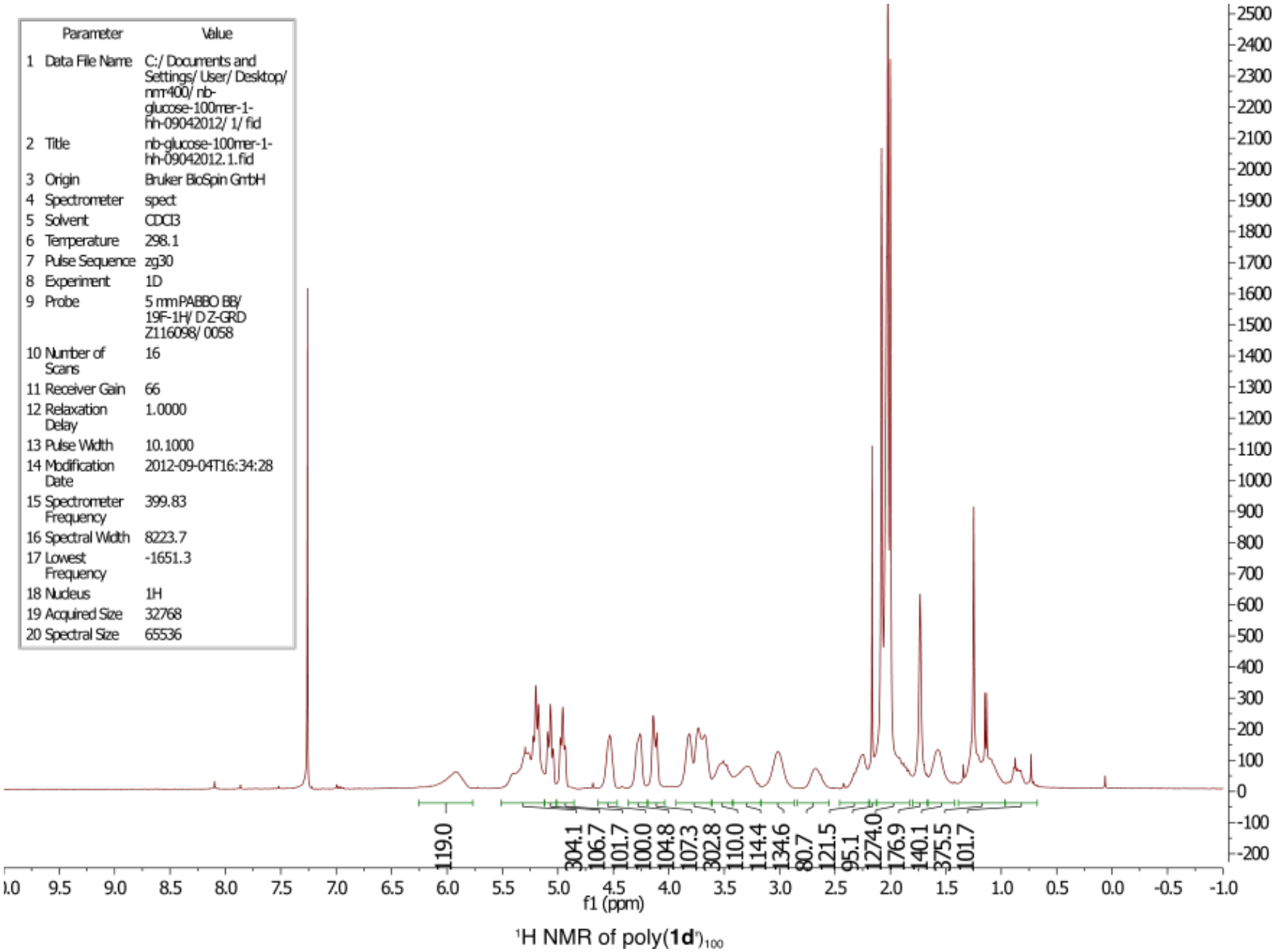

^{1}H NMR of poly(**1d**')$_{100}$

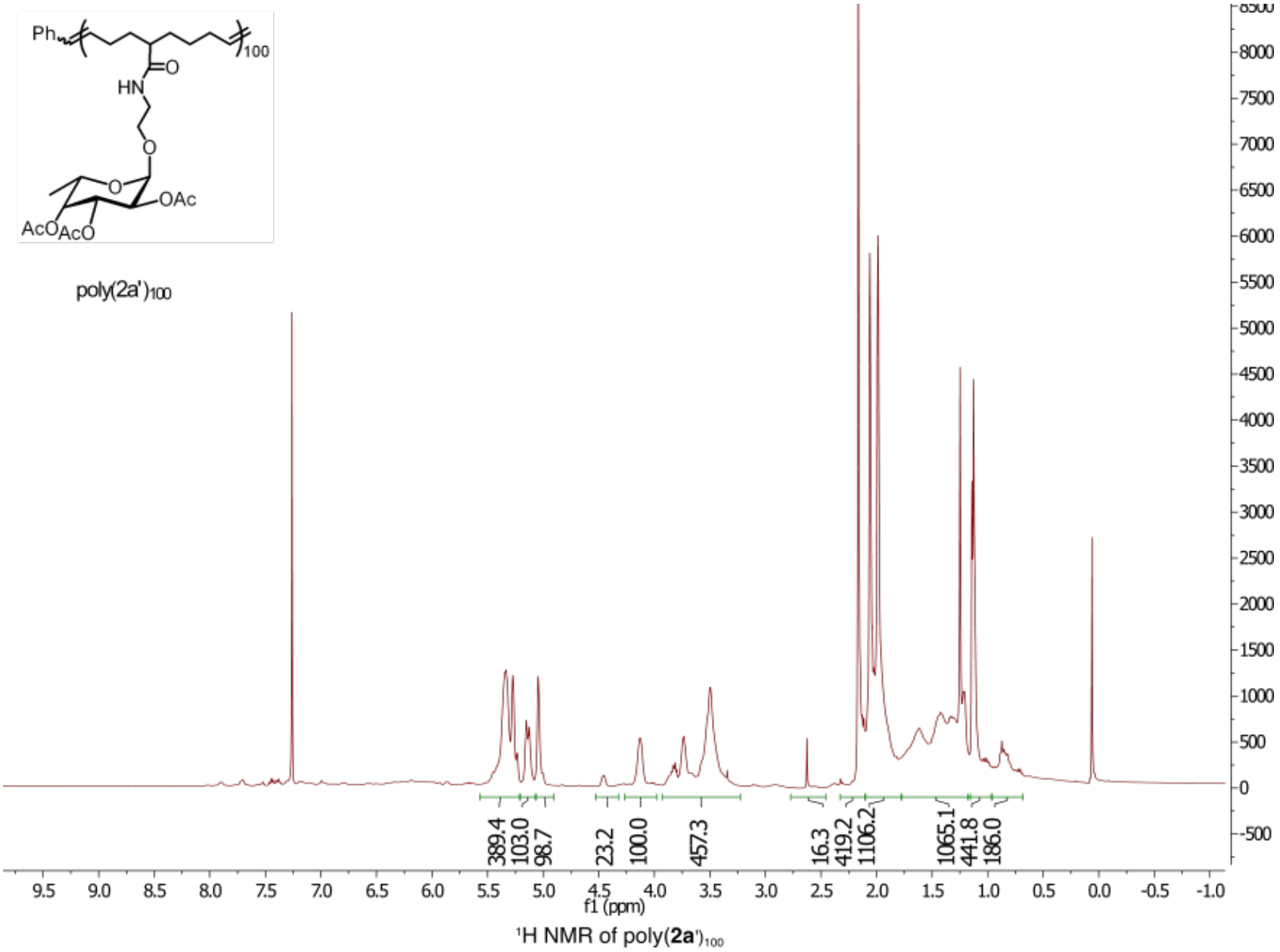
Ph
100
O
HN
O
O
OAc
AcO
AcO
poly(2a')100
389.4
103.0
98.7
23.2
100.0
457.3
16.3
419.2
1106.2
1065.1
441.8
186.0
f1 (ppm)
¹H NMR of poly(2a')100

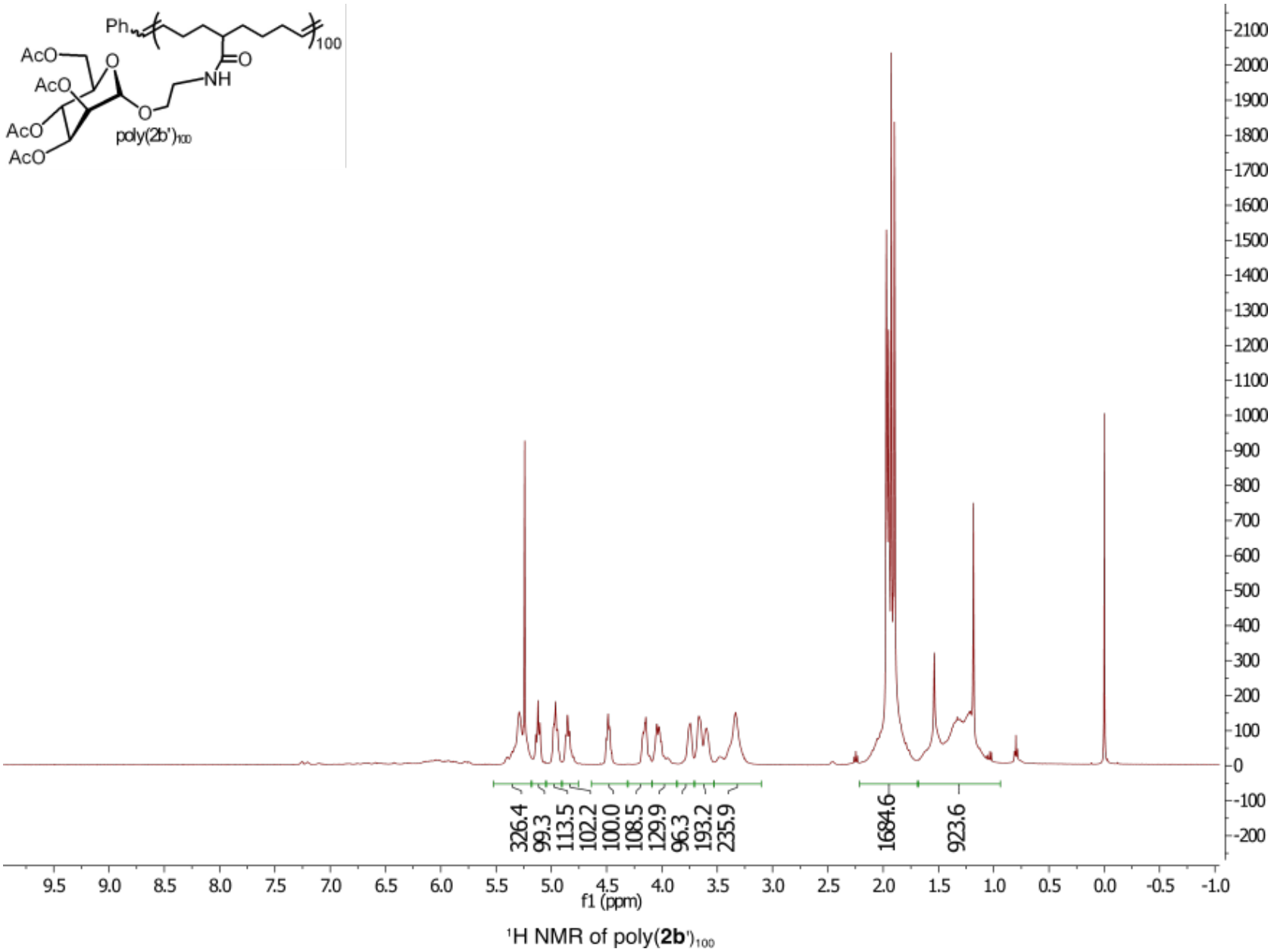

^{1}H NMR of poly(**2b**')$_{100}$

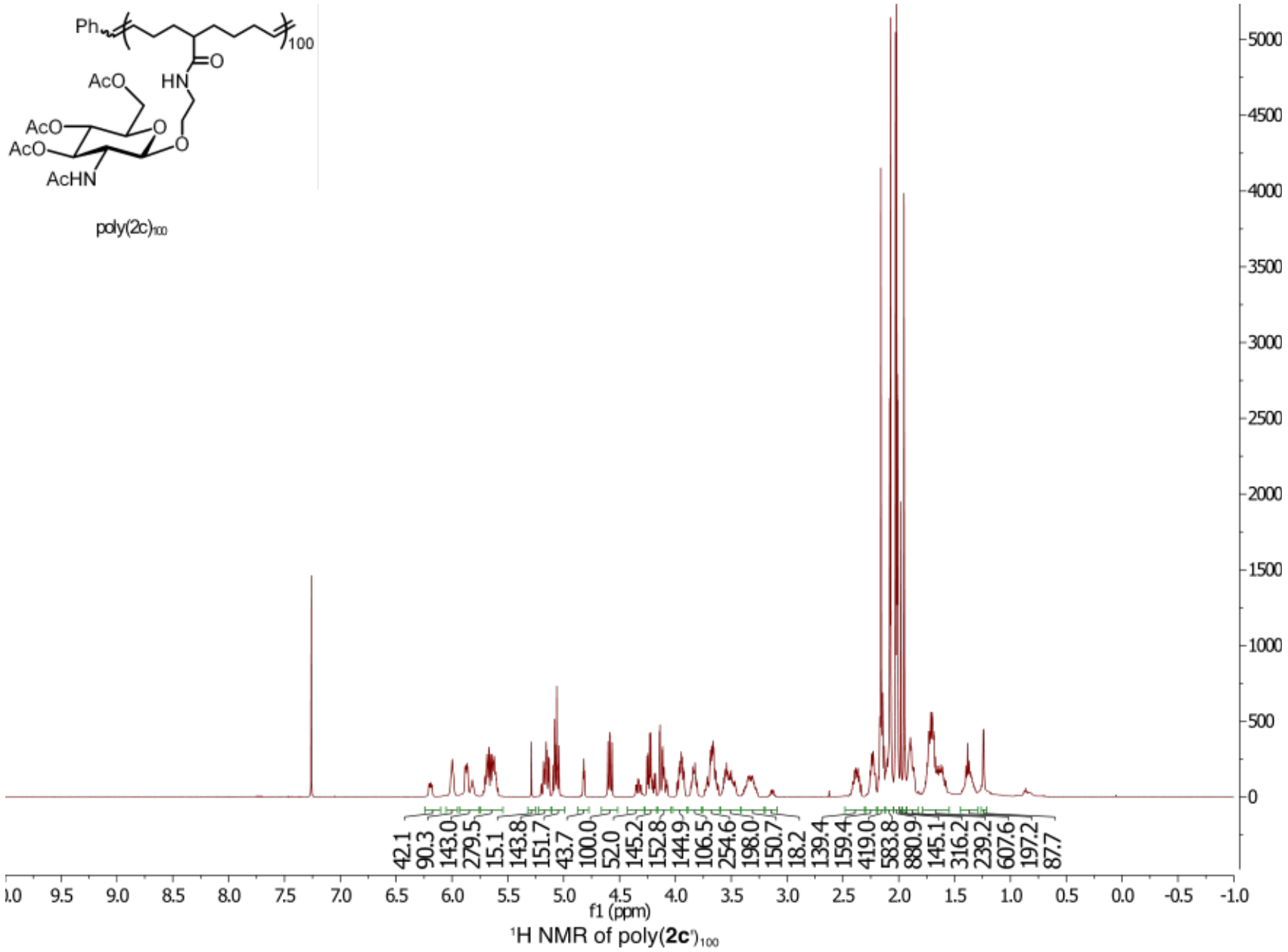
Ph
100
O
HN
AcO
AcO
AcO
O
O
AcHN
poly(2c)100
5000
4500
4000
3500
3000
2500
2000
1500
1000
500
0
42.1
90.3
143.0
279.5
15.1
143.8
151.7
43.7
100.0
52.0
145.2
152.8
144.9
106.5
254.6
198.0
150.7
18.2
139.4
159.4
419.0
583.8
880.9
145.1
316.2
239.2
607.6
197.2
87.7
9.5
9.0
8.5
8.0
7.5
7.0
6.5
6.0
5.5
5.0
4.5
4.0
3.5
3.0
2.5
2.0
1.5
1.0
0.5
0.0
-0.5
-1.0
f1 (ppm)
1H NMR of poly(2c')100

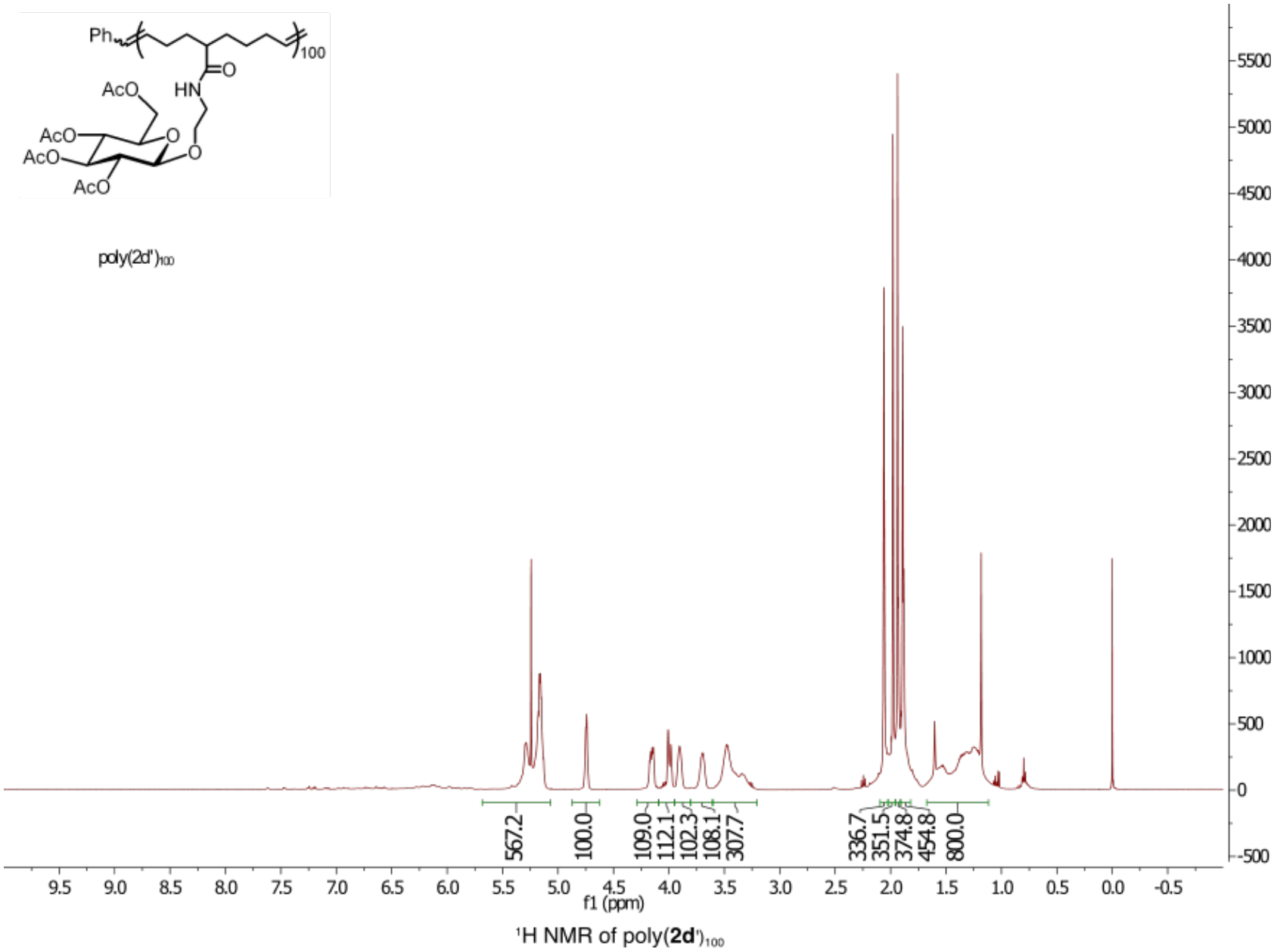

^{1}H NMR of poly(**2d'**)$_{100}$

	Parameter	Value
1	Data File Name	E:/ nmr400/ R-(fuc50/ Glc50)-2-05272014-hh/ 1/ fid
2	Title	Glc50)-2-05272014-hh.1.fid
3	Origin	Bruker BioSpin GmbH
4	Spectrometer	spect
5	Solvent	CDCl3
6	Temperature	298.1
7	Pulse Sequence	zg30
8	Experiment	1D
9	Probe	5 mm PABBO BB/ 19F-1H/ D Z-GRD Z116098/ 0058
10	Number of Scans	64
11	Receiver Gain	75
12	Relaxation Delay	1.0000
13	Pulse Width	10.1000
14	Modification Date	2014-05-27T12:57:46
15	Spectrometer Frequency	399.83
16	Spectral Width	8223.7
17	Lowest Frequency	-1651.1
18	Nucleus	1H
19	Acquired Size	32768
20	Spectral Size	65536

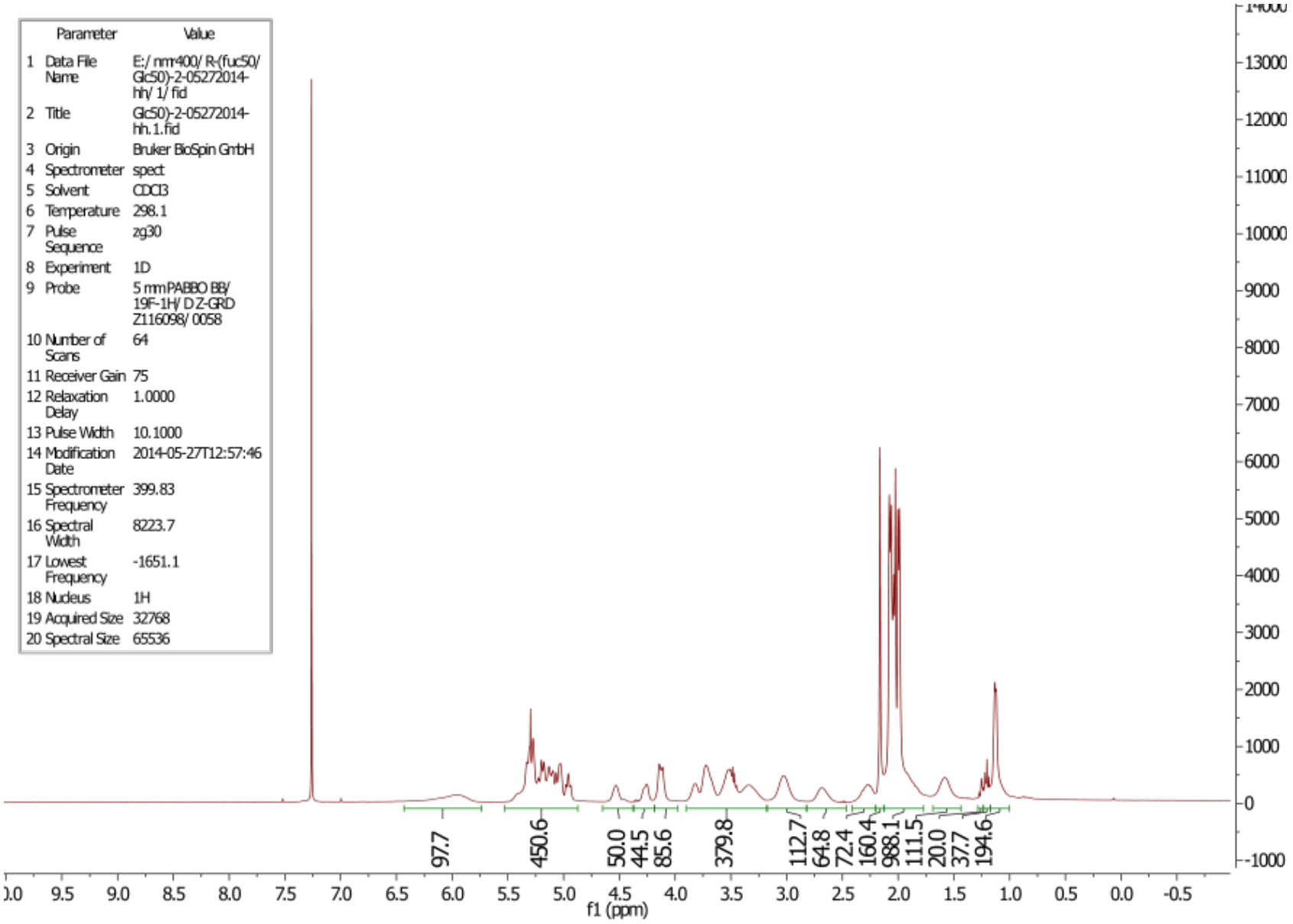

^{1}H NMR poly(**1a**'$_{50}$-*ran*-**1d**'$_{50}$)

	Parameter	Value
1	Data File Name	E:/ nmr400/ Ran(man50/ ran-(fuc10/ glc90)-hh-04232014-1/ 1/ fid
2	Title	glc90)-hh-04232014-1.1.fid
3	Origin	Bruker BioSpin GmbH
4	Spectrometer	spect
5	Solvent	CD2Cl2
6	Temperature	298.2
7	Pulse Sequence	zg30
8	Experiment	1D
9	Probe	5 mm PABBO BB/ 19F-1H/ D Z-GRD Z116098/ 0058
10	Number of Scans	16
11	Receiver Gain	66
12	Relaxation Delay	1.0000
13	Pulse Width	10.1000
14	Modification Date	2014-04-23T17:43:52
15	Spectrometer Frequency	399.83
16	Spectral Width	8223.7
17	Lowest Frequency	-1642.7
18	Nucleus	1H
19	Acquired Size	32768
20	Spectral Size	65536

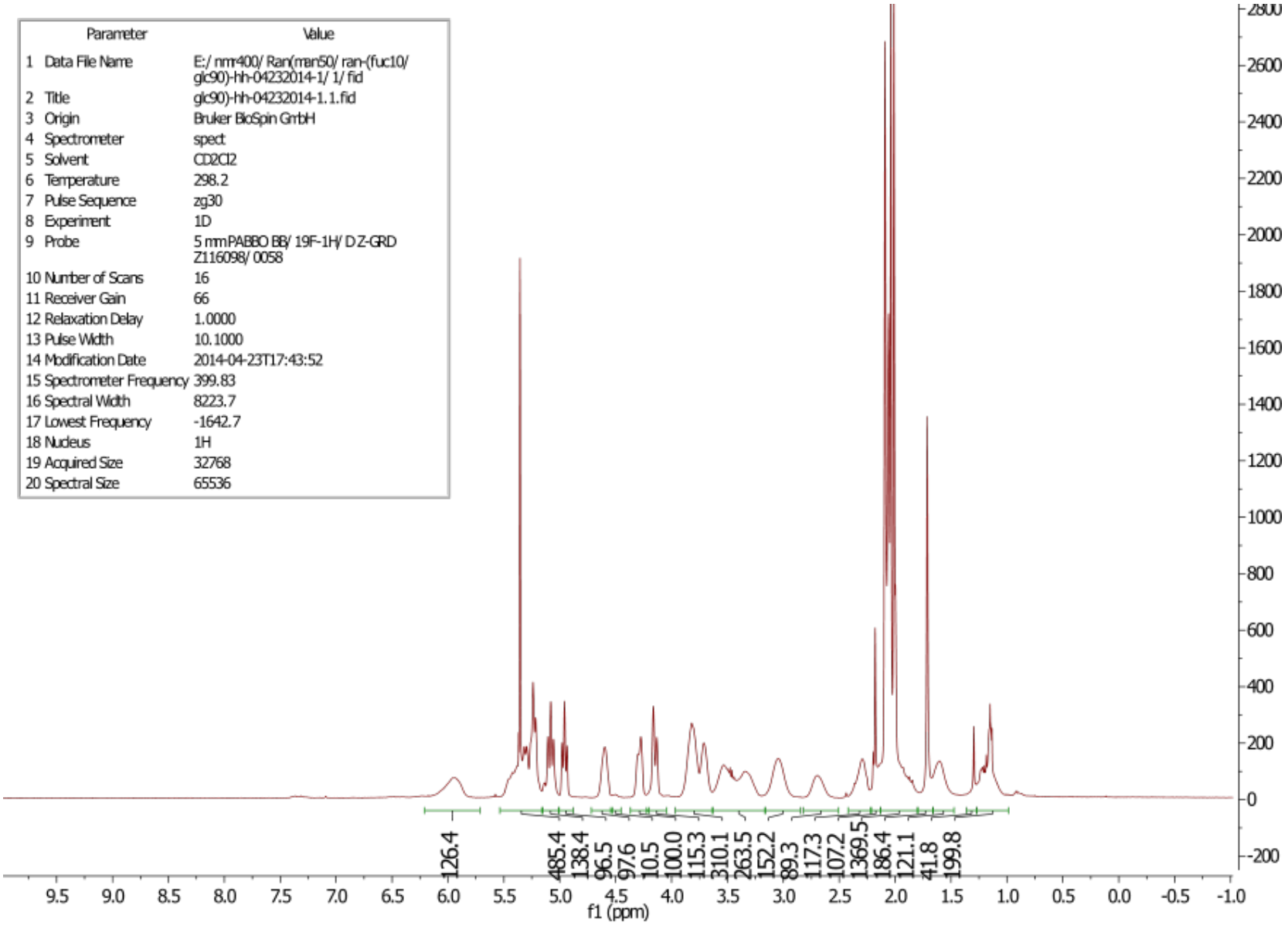

^{1}H NMR poly(**1a**'$_{10}$-*ran*-**1d**'$_{90}$)

	Parameter	Value
1	Data File Name	C:/ Documents and Settings/ User/ Desktop/ nmr400/ Ran(man50/ glc50)-hh-04232014-4/ 1/ fid
2	Title	glc50)-hh-04232014-4.1.fid
3	Origin	Bruker BioSpin GmbH
4	Spectrometer	spect
5	Solvent	CD2Cl2
6	Temperature	298.1
7	Pulse Sequence	zg30
8	Experiment	1D
9	Probe	5 mm PABBO BB/ 19F-1H/ D Z-GRD Z116098/ 0058
10	Number of Scans	16
11	Receiver Gain	32
12	Relaxation Delay	1.0000
13	Pulse Width	10.1000
14	Modification Date	2014-04-23T17:30:28
15	Spectrometer Frequency	399.83
16	Spectral Width	8223.7
17	Lowest Frequency	-1642.7
18	Nucleus	1H
19	Acquired Size	32768
20	Spectral Size	65536

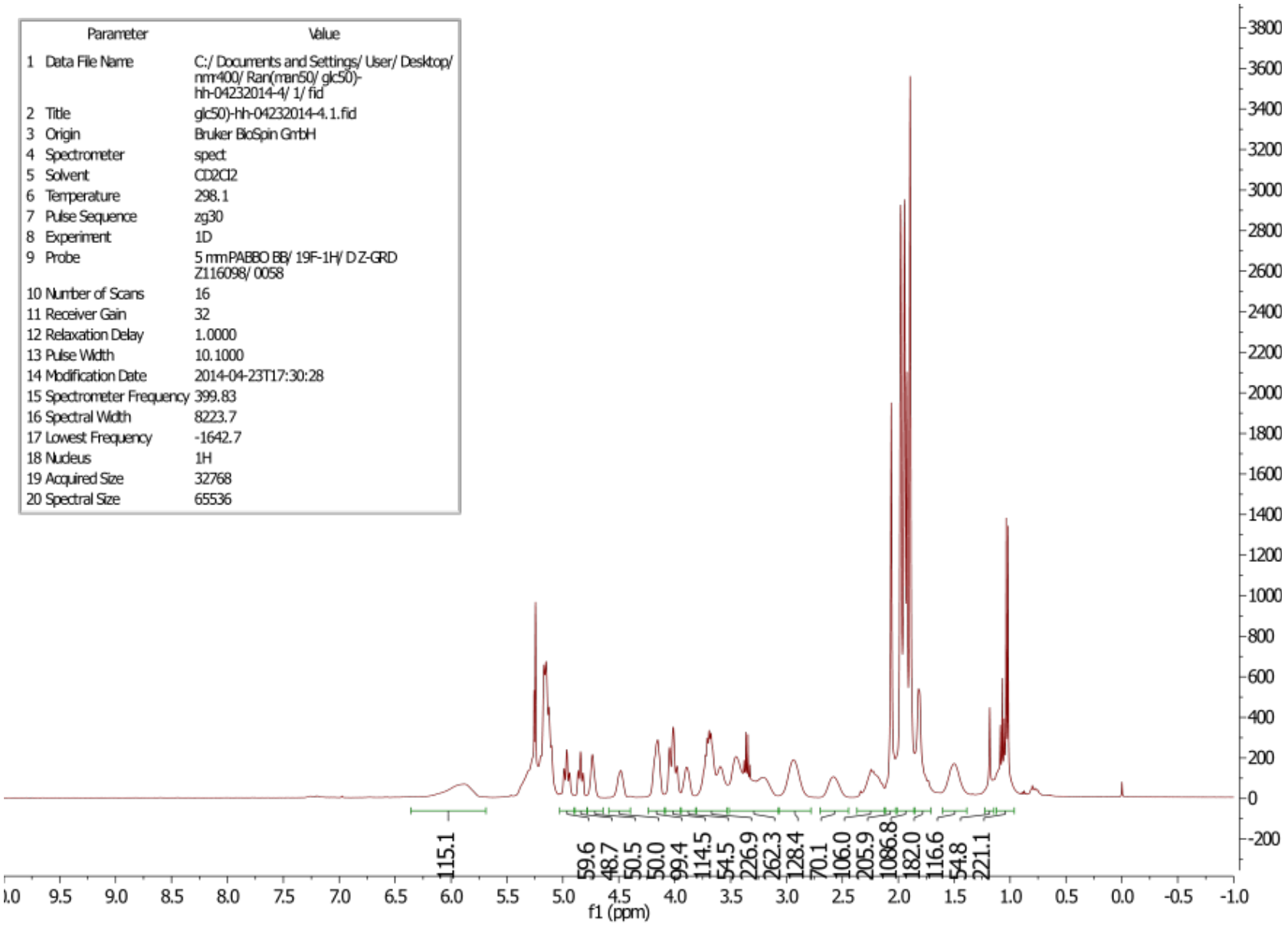

^{1}H NMR poly(**1b**'$_{50}$-*ran*-**1d**'$_{50}$)

	Parameter	Value
1	Data File Name	C:/ Documents and Settings/ User/ Desktop/ NMR 500/ Ran-(Glu90/ Man10) 100mer -trace-10252012-hh-1/ 1/ fid
2	Title	Man10) 100mer -trace-10252012-hh-1.1.fid
3	Origin	Bruker BioSpin GmbH
4	Spectrometer	spect
5	Solvent	CD2Cl2
6	Temperature	298.1
7	Pulse Sequence	zg30
8	Experiment	1D
9	Probe	5 mm CPPBBO BB-1H/ 19F/ D Z-GRD Z122624/ 0008
10	Number of Scans	1388
11	Receiver Gain	32
12	Relaxation Delay	1.0000
13	Pulse Width	12.0000
14	Modification Date	2012-10-25T14:24:52
15	Spectrometer Frequency	499.89
16	Spectral Width	10000.0
17	Lowest Frequency	-1913.0
18	Nucleus	1H
19	Acquired Size	32768
20	Spectral Size	65536

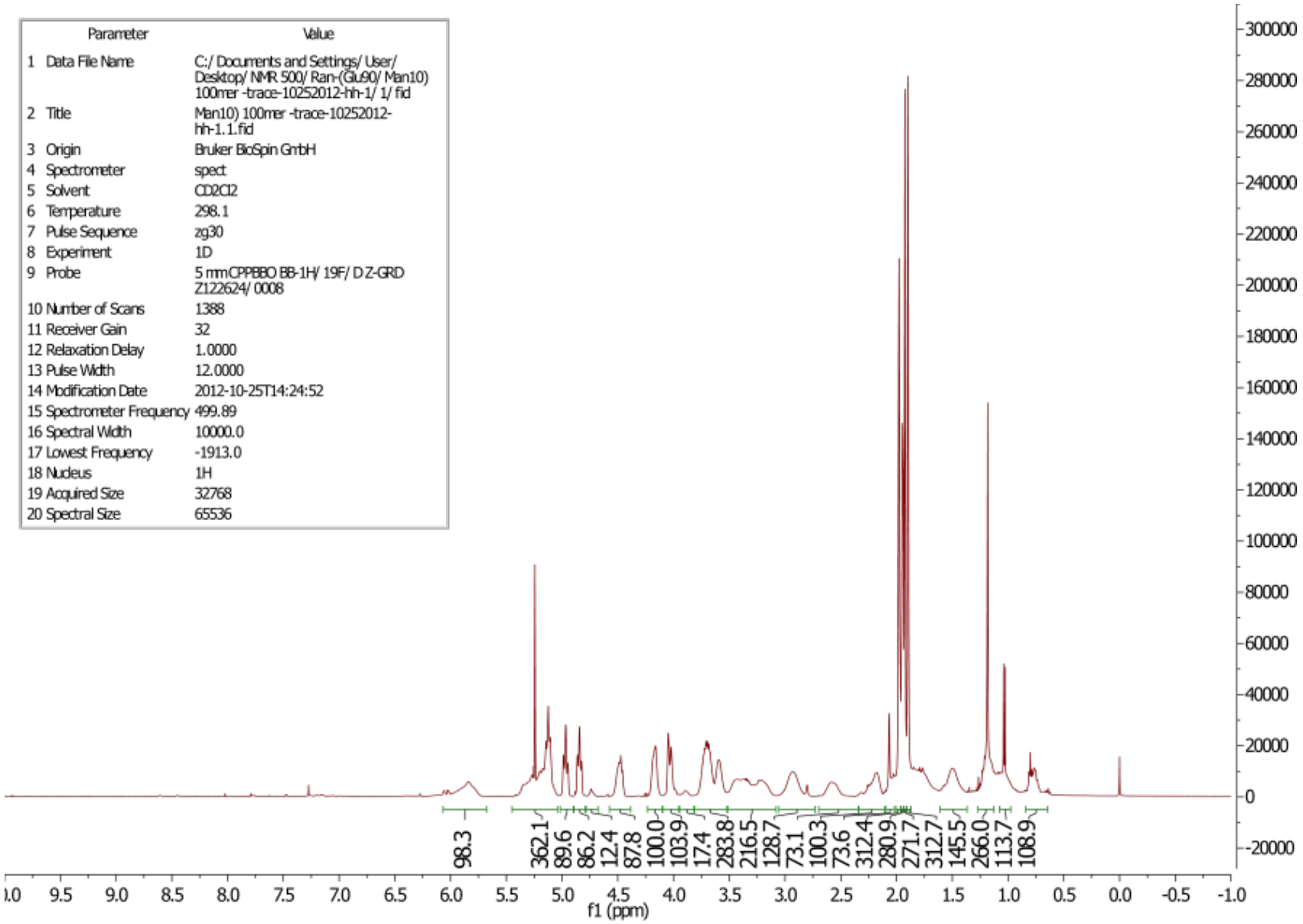

^{1}H NMR poly(**1b'**$_{10}$-*ran*-**1d'**$_{90}$)

	Parameter	Value
1	Data File Name	C:/ Documents and Settings/ User/ Desktop/ nmr400/ ran-(glc50/ glcnac50)-1-hh-03072013/ 1/ fid
2	Title	glcnac50)-1-hh-03072013.1.fid
3	Origin	Bruker BioSpin GmbH
4	Spectrometer	spect
5	Solvent	CDCl3
6	Temperature	298.0
7	Pulse Sequence	zg30
8	Experiment	1D
9	Probe	5 mm PABBO BB/ 19F-1H/ D Z-GRD Z116098/ 0058
10	Number of Scans	75
11	Receiver Gain	66
12	Relaxation Delay	1.0000
13	Pulse Width	10.1000
14	Modification Date	2013-03-07T18:51:12
15	Spectrometer Frequency	399.83
16	Spectral Width	8223.7
17	Lowest Frequency	-1651.3
18	Nucleus	1H
19	Acquired Size	32768
20	Spectral Size	65536

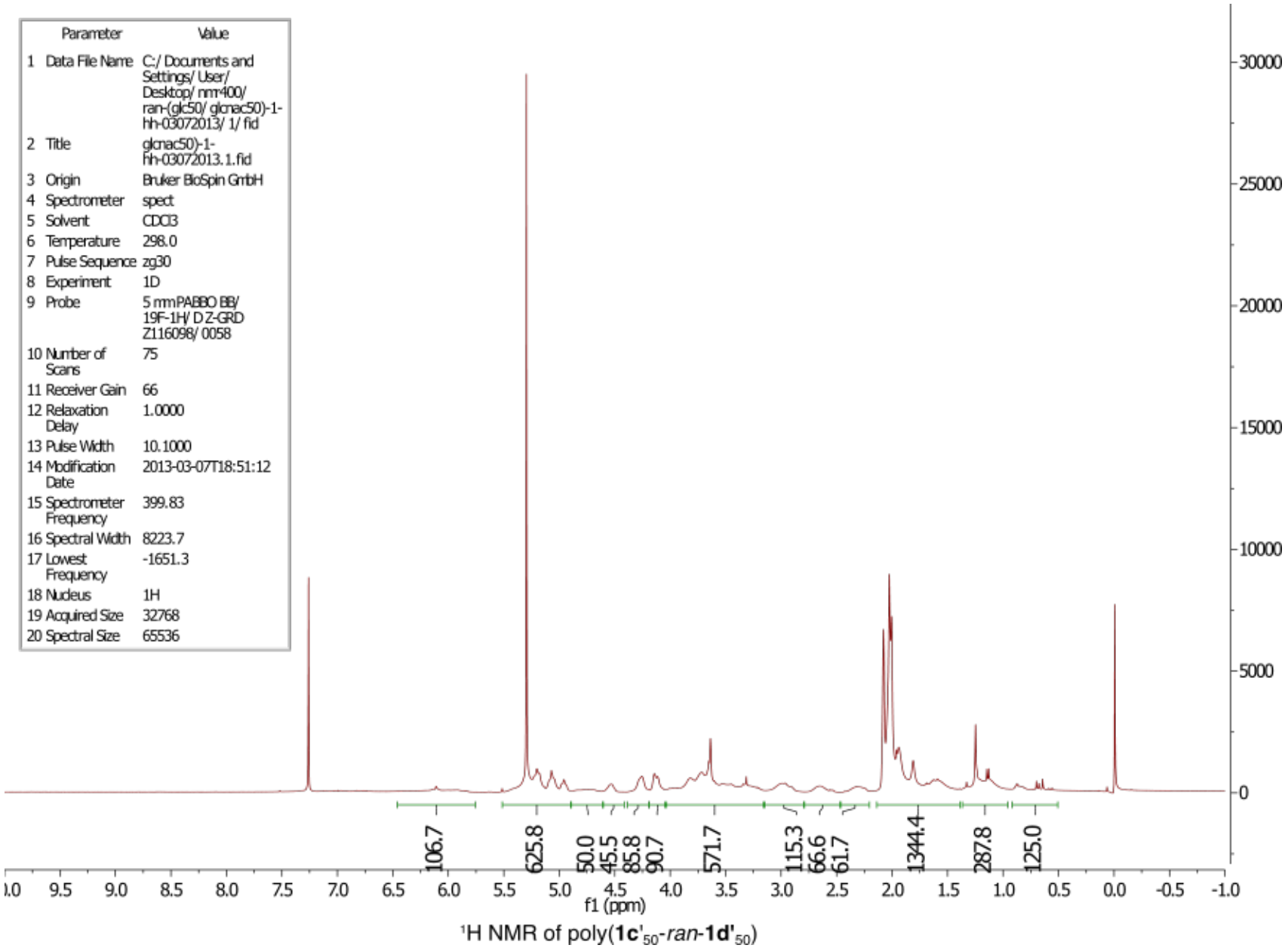

^{1}H NMR of poly(**1c**'$_{50}$-*ran*-**1d**'$_{50}$)

	Parameter	Value
1	Data File Name	E:/ nmr400/ ran-(glcnac10/ glc90)-1-hh-03082013/ 1/ fid
2	Title	glc90)-1-hh-03082013.1.fid
3	Origin	Bruker BioSpin GmbH
4	Spectrometer	spect
5	Solvent	CDCl3
6	Temperature	298.0
7	Pulse Sequence	zg30
8	Experiment	1D
9	Probe	5 mm PABBO BB/ 19F-1H/ D Z-GRD Z116098/ 0058
10	Number of Scans	35
11	Receiver Gain	85
12	Relaxation Delay	1.0000
13	Pulse Width	10.1000
14	Modification Date	2013-03-08T17:14:58
15	Spectrometer Frequency	399.83
16	Spectral Width	8223.7
17	Lowest Frequency	-1650.2
18	Nucleus	1H
19	Acquired Size	32768
20	Spectral Size	65536

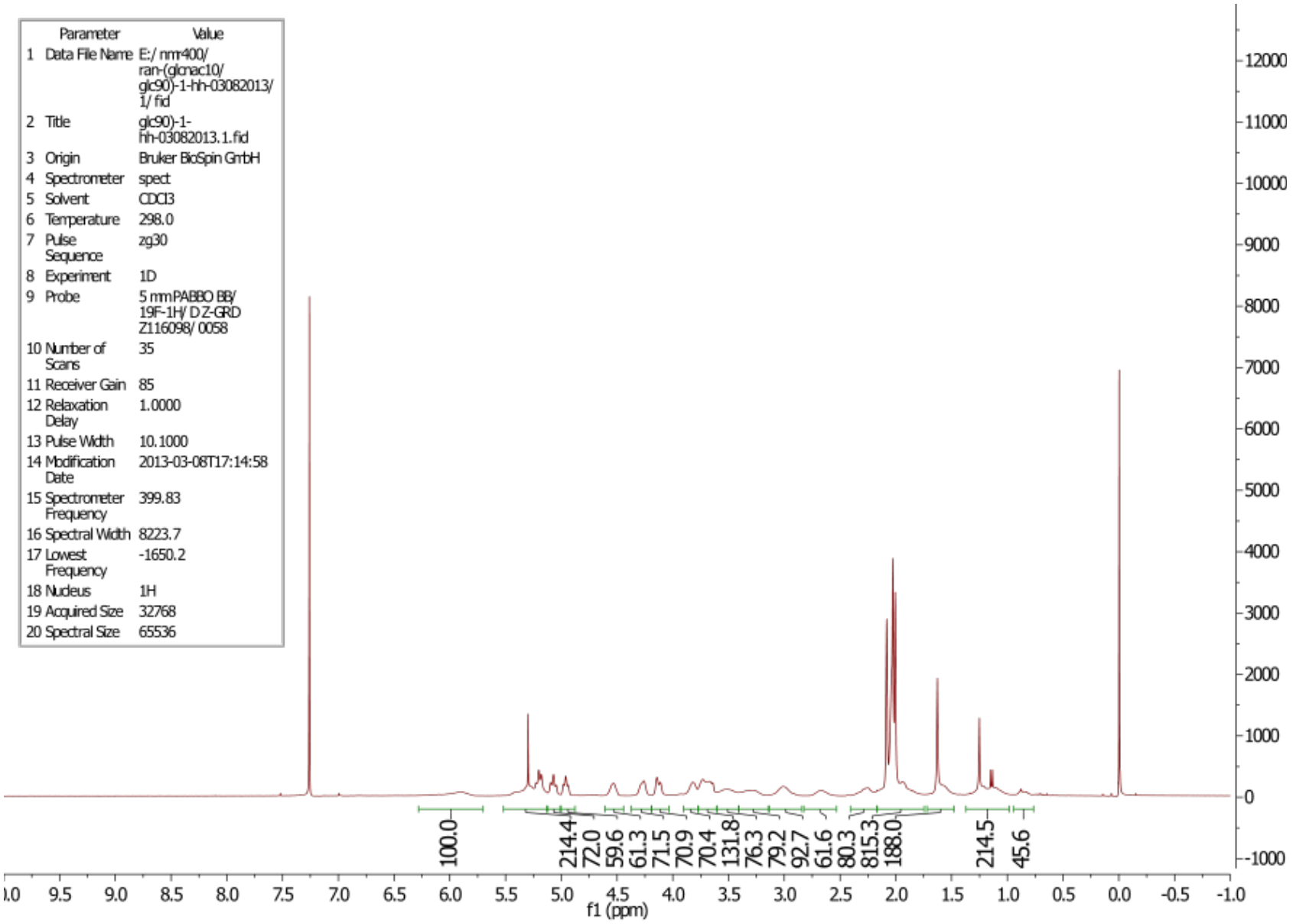

^{1}H NMR poly(**1c**'$_{10}$-*ran*-**1d**'$_{90}$)

	Parameter	Value
1	Data File Name	C:/ Documents and Settings/ User/ Desktop/ nmr400/ b-(m6f5)-mc-05052014-hh/ 1/ fid
2	Title	b-(m6f5)-mc-05052014-hh.1.fid
3	Origin	Bruker BioSpin GmbH
4	Spectrometer	spect
5	Solvent	CD2Cl2
6	Temperature	298.1
7	Pulse Sequence	zg30
8	Experiment	1D
9	Probe	5 mm PABBO BB/ 19F-1H/ D Z-GRD Z116098/ 0058
10	Number of Scans	16
11	Receiver Gain	59
12	Relaxation Delay	1.0000
13	Pulse Width	10.1000
14	Modification Date	2014-05-05T16:22:12
15	Spectrometer Frequency	399.83
16	Spectral Width	8223.7
17	Lowest Frequency	-1642.7
18	Nucleus	1H
19	Acquired Size	32768
20	Spectral Size	65536

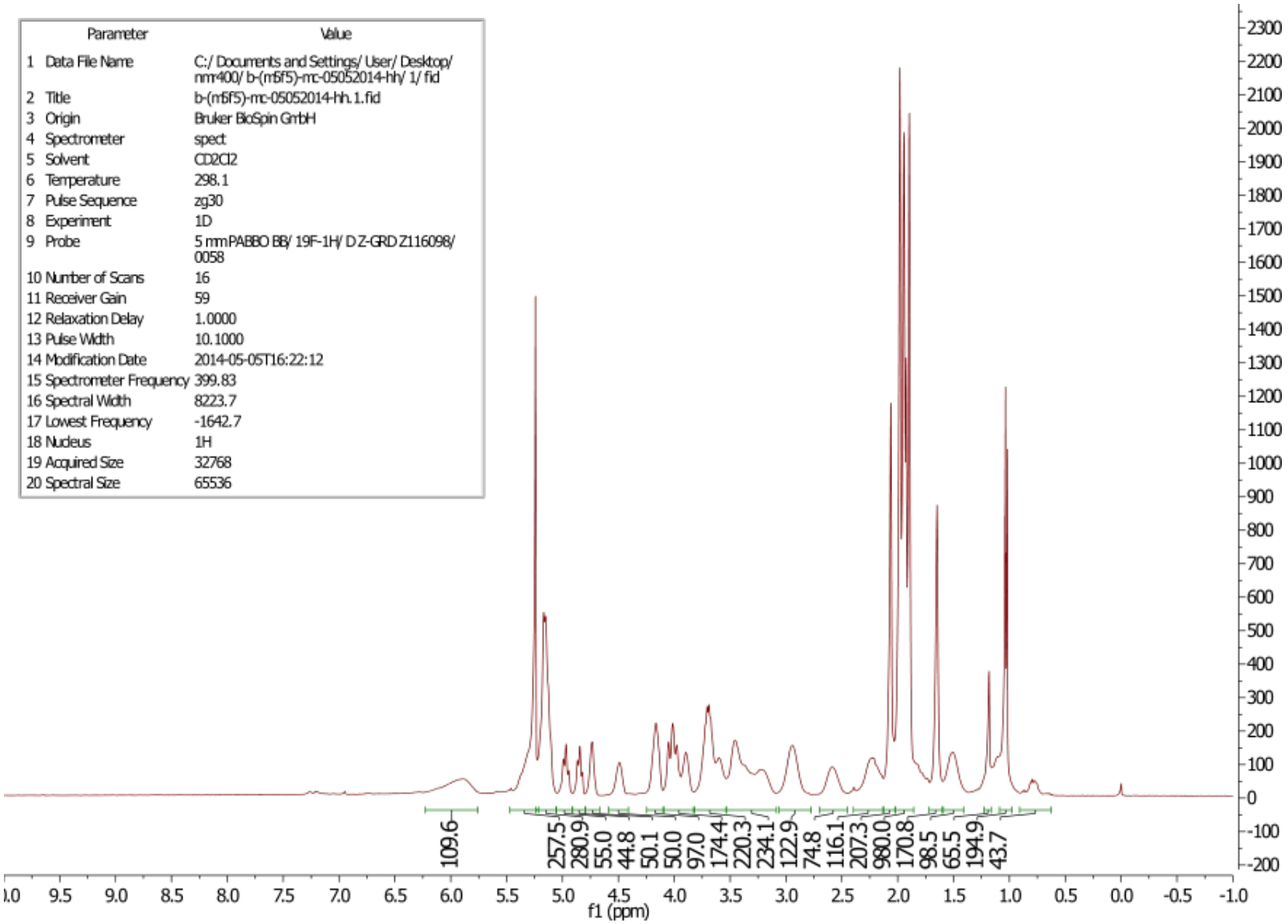

^{1}H NMR poly(**1b**'$_{50}$-*block*-**1a**'$_{50}$)

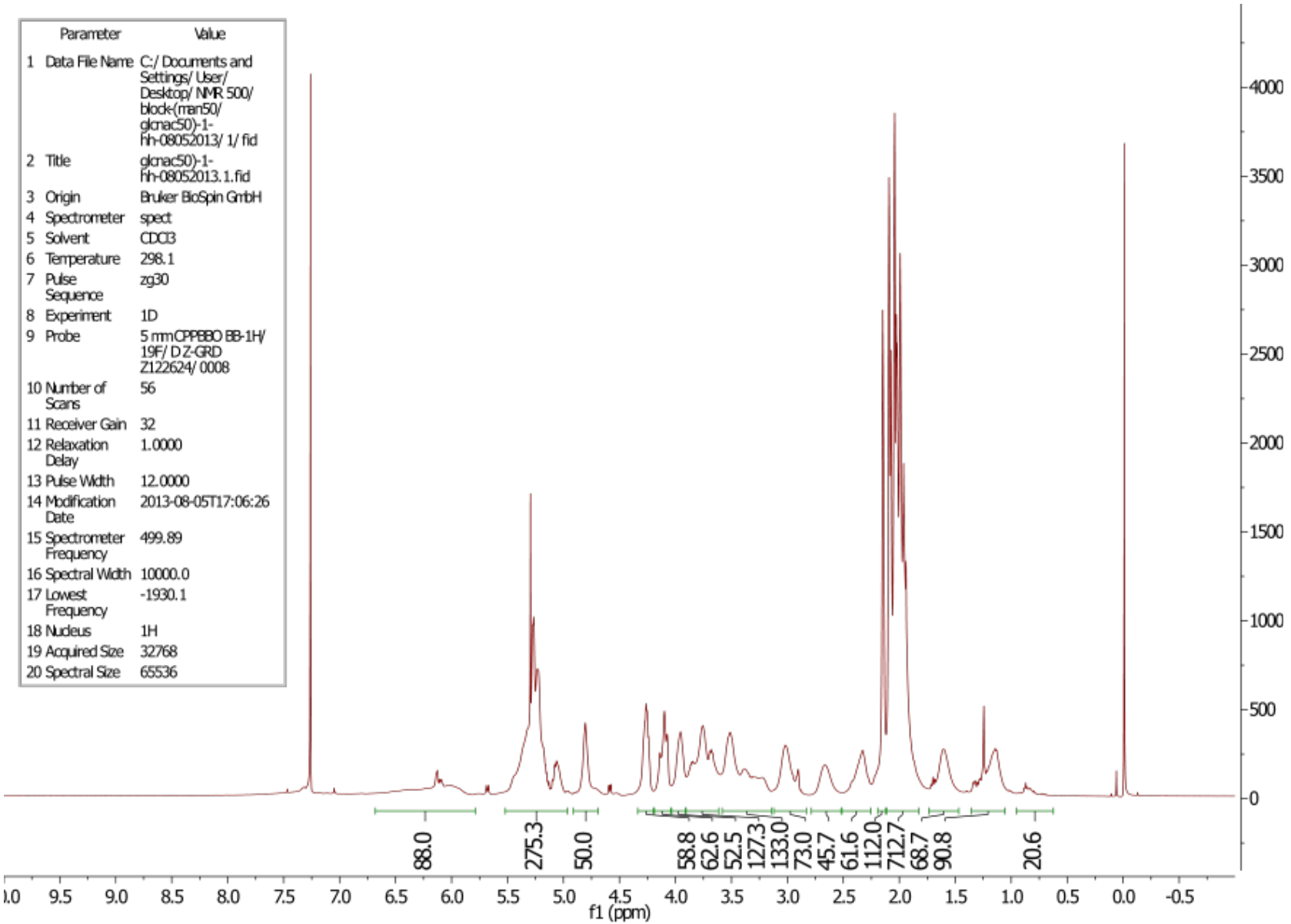

^{1}H NMR poly(**1b**'$_{50}$-*block*-**1c**'$_{50}$)

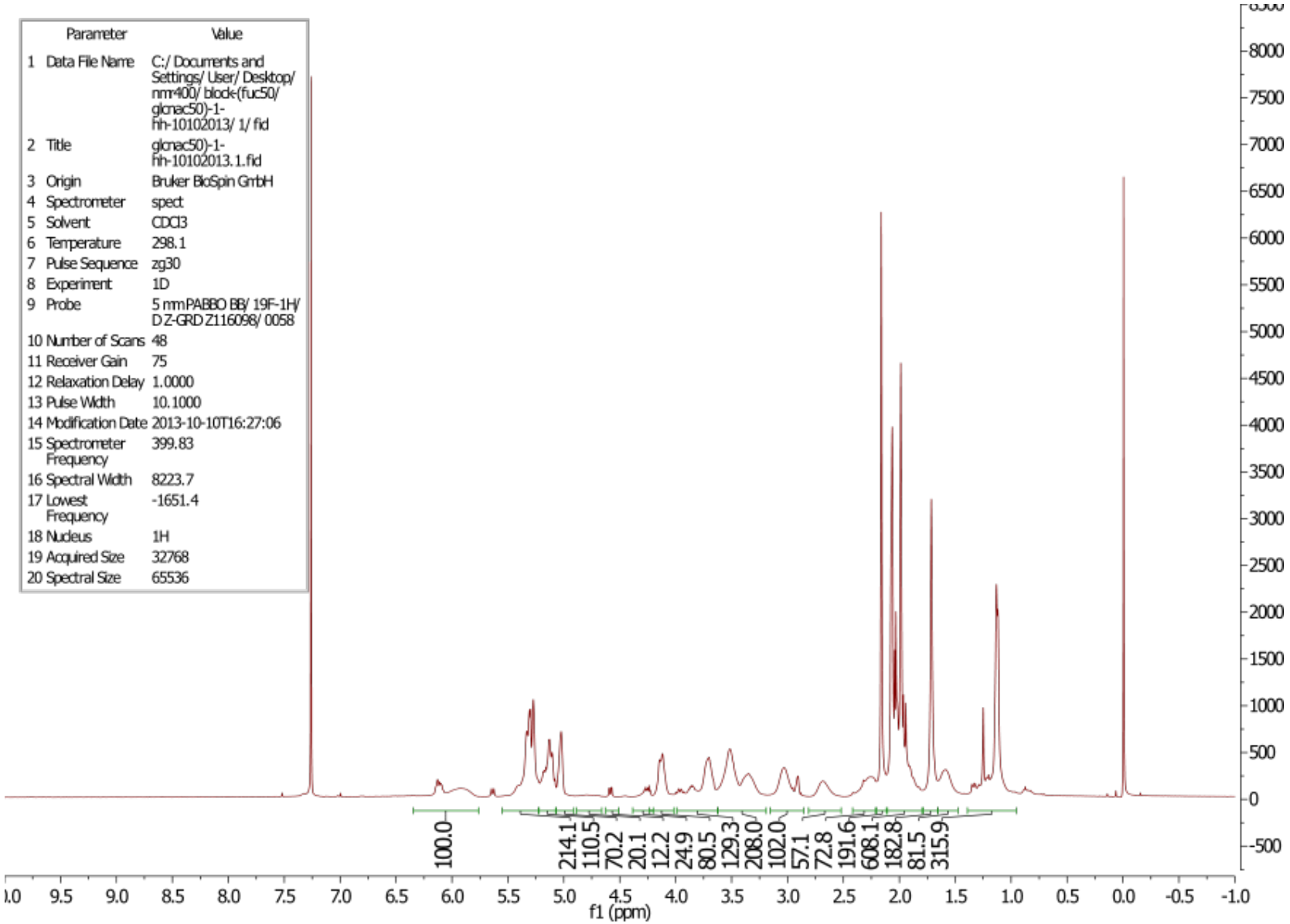

^{1}H NMR poly(**1a**'$_{50}$-*block*-**1c**'$_{50}$)

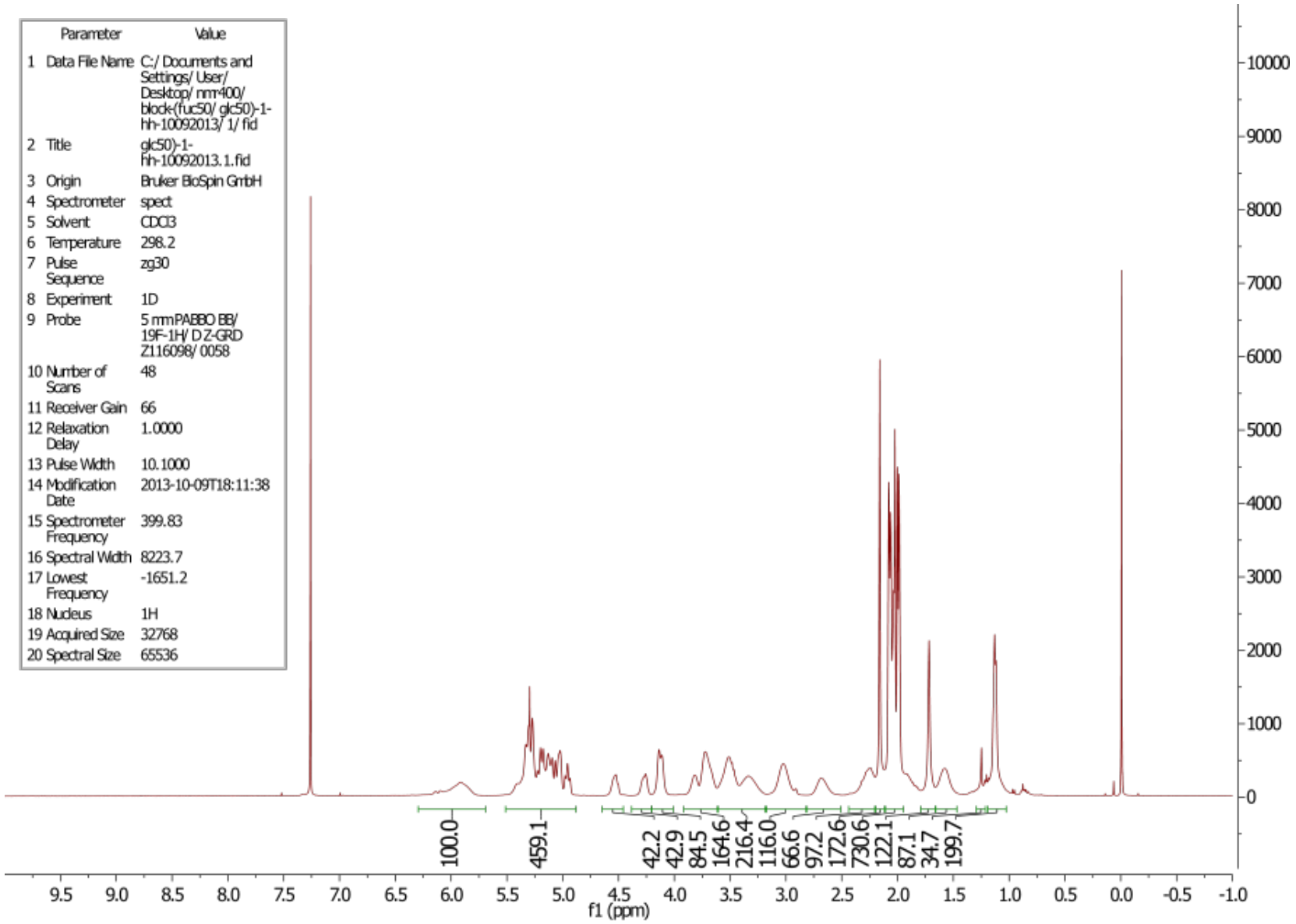

^{1}H NMR poly(**1a**'$_{50}$-*block*-**1d**'$_{50}$)

	Parameter	Value
1	Data File Name	C:/ Documents and Settings/ User/ Desktop/ NMR 500/ block-(man50/ glc50)-2-hh-03312014/ 1/ fid
2	Title	glc50)-2-hh-03312014.1.fid
3	Origin	Bruker BioSpin GmbH
4	Spectrometer	spect
5	Solvent	CDCl3
6	Temperature	298.0
7	Pulse Sequence	zg30
8	Experiment	1D
9	Probe	5 mm CPPBBO BB-1H/ 19F/ D Z-GRD Z122624/ 0008
10	Number of Scans	16
11	Receiver Gain	32
12	Relaxation Delay	1.0000
13	Pulse Width	12.0000
14	Modification Date	2014-03-31T16:06:48
15	Spectrometer Frequency	499.89
16	Spectral Width	10000.0
17	Lowest Frequency	-1960.4
18	Nucleus	1H
19	Acquired Size	32768
20	Spectral Size	65536

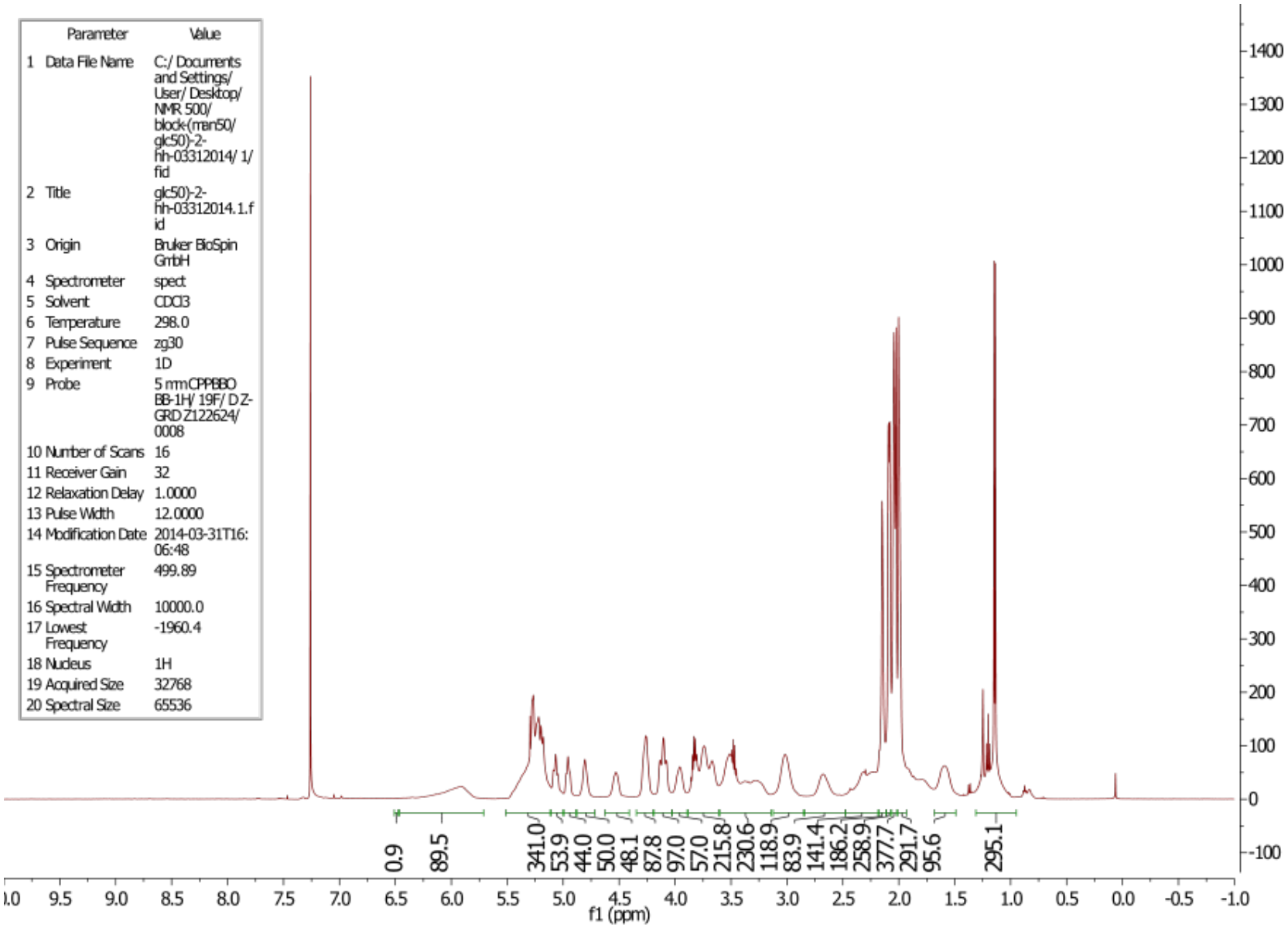

^{1}H NMR poly(**1b**'$_{50}$-*block*-**1d**'$_{50}$)

	Parameter	Value
1	Data File Name	C:/ Documents and Settings/ User/ Desktop/ nmr400/ block-(glcNAc50/ glc50)-1-hh-10102013/ 1/ fid
2	Title	glc50)-1-hh-10102013.1.fid
3	Origin	Bruker BioSpin GmbH
4	Spectrometer	spect
5	Solvent	CDCl3
6	Temperature	298.2
7	Pulse Sequence	zg30
8	Experiment	1D
9	Probe	5 mm PABBO BB/ 19F-1H/ D Z-GRD Z116098/ 0058
10	Number of Scans	64
11	Receiver Gain	85
12	Relaxation Delay	1.0000
13	Pulse Width	10.1000
14	Modification Date	2013-10-10T16:40:24
15	Spectrometer Frequency	399.83
16	Spectral Width	8223.7
17	Lowest Frequency	-1651.3
18	Nucleus	1H
19	Acquired Size	32768
20	Spectral Size	65536

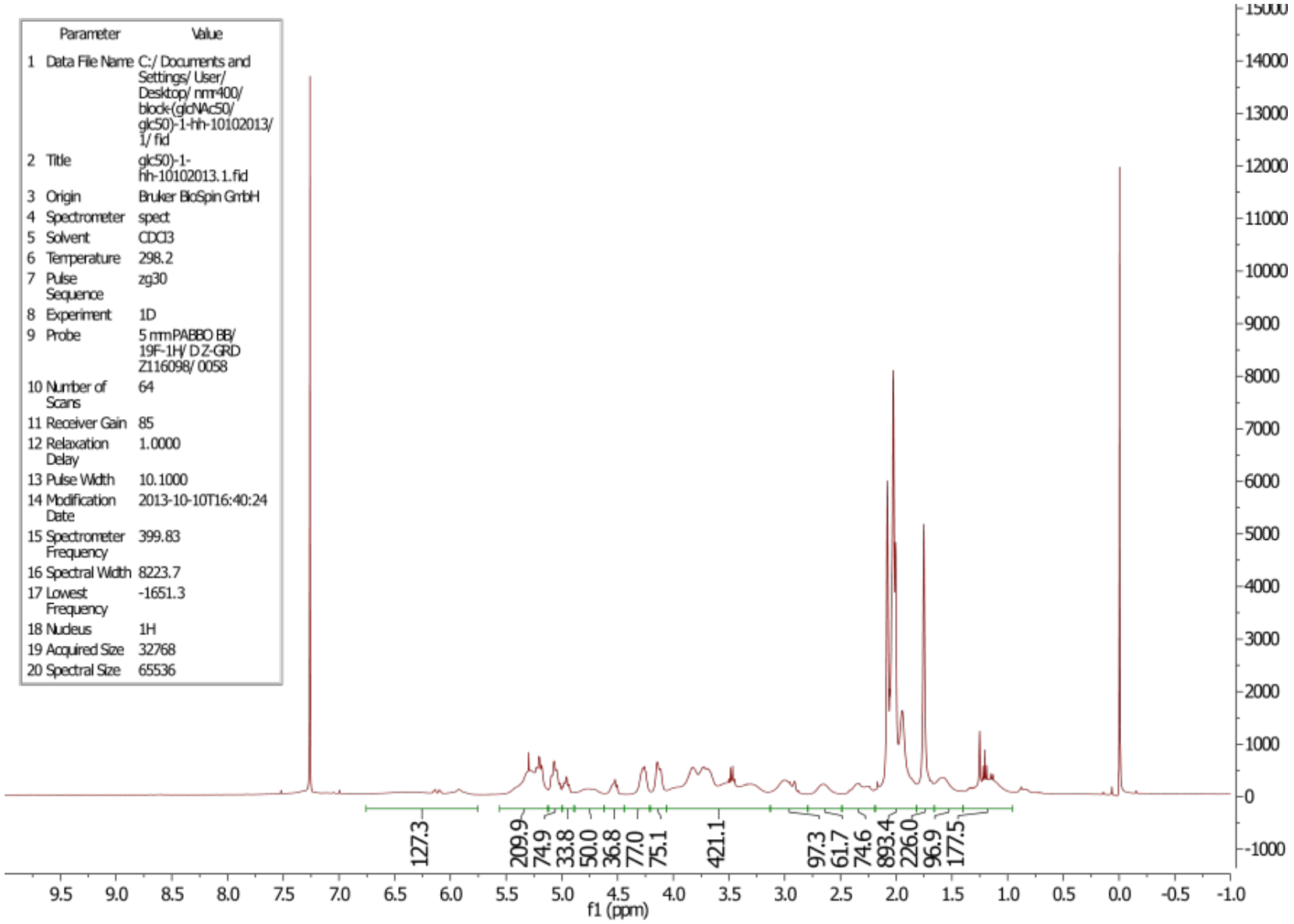

^{1}H NMR poly(**1c**'$_{50}$-*block*-**1d**'$_{50}$)

	Parameter	Value
1	Data File Name	C:/ Documents and Settings/ User/ Desktop/ NMR 500/ deprot-poly(fuc)100-1-hh-07262013/ 1/ fid
2	Title	deprot-poly(fuc)100-1-hh-07262013.1.fid
3	Origin	Bruker BioSpin GmbH
4	Spectrometer	spect
5	Solvent	D2O
6	Temperature	298.1
7	Pulse Sequence	zg30
8	Experiment	1D
9	Probe	5 mm CPPBBO BB-1H/ 19F/ D Z-GRD Z122624/ 0008
10	Number of Scans	40
11	Receiver Gain	56
12	Relaxation Delay	1.0000
13	Pulse Width	12.0000
14	Modification Date	2013-07-26T13:12:16
15	Spectrometer Frequency	499.89
16	Spectral Width	10000.0
17	Lowest Frequency	-1873.5
18	Nucleus	1H
19	Acquired Size	32768
20	Spectral Size	65536

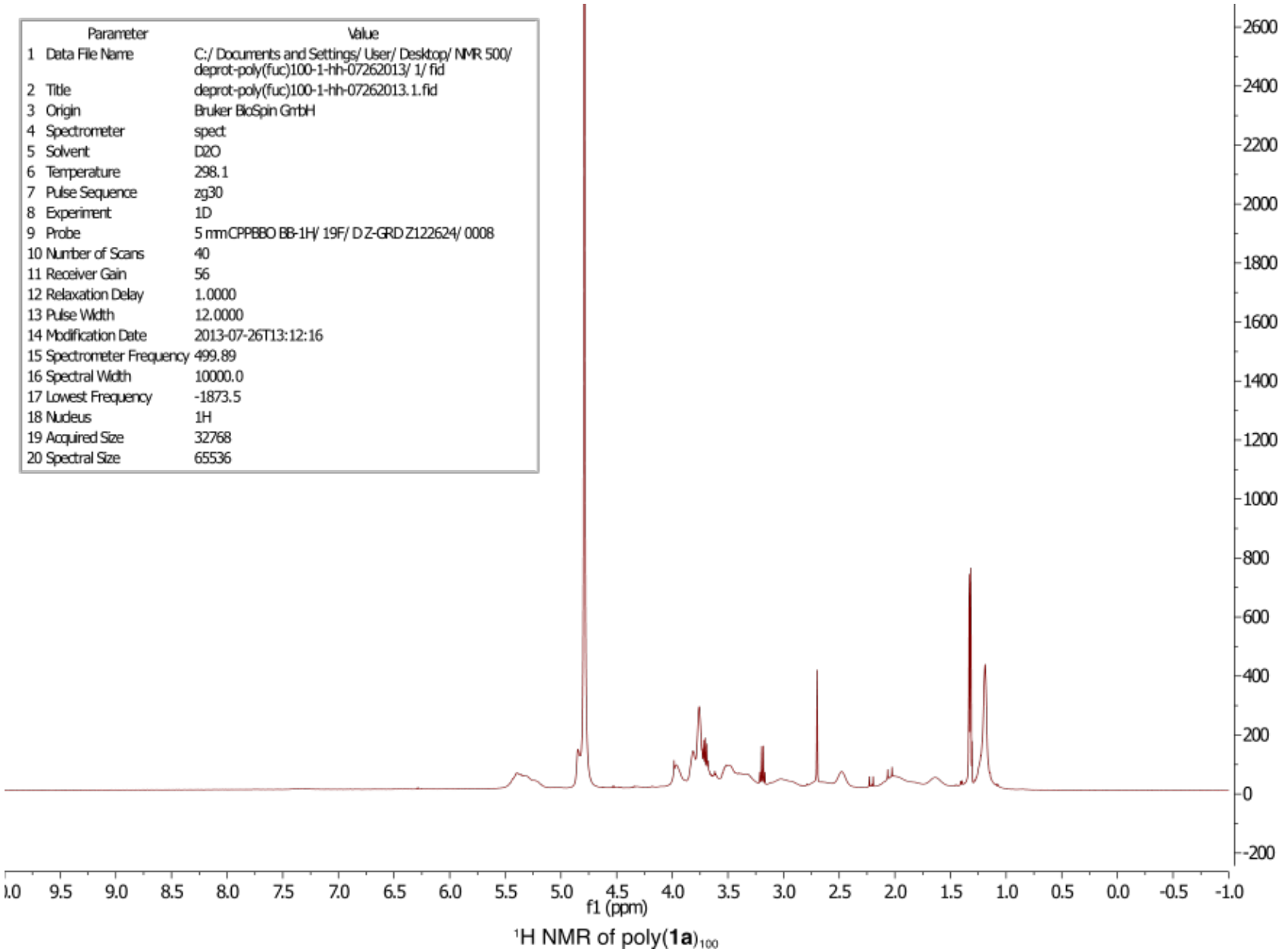

^{1}H NMR of poly(**1a**)$_{100}$

	Parameter	Value
1	Data File Name	C:/ Documents and Settings/ User/ Desktop/ NMR 500/ NB-mannose 100mer-1 Deprot. hh-10032012/ 1/ fid
2	Title	NB-mannose 100mer-1 Deprot. hh-10032012.1.fid
3	Origin	Bruker BioSpin GmbH
4	Spectrometer	spect
5	Solvent	D2O
6	Temperature	298.1
7	Pulse Sequence	zg30
8	Experiment	1D
9	Probe	5 mm CPPBBO BB-1H/ 19F/ D Z-GRD Z122624/ 0008
10	Number of Scans	16
11	Receiver Gain	32
12	Relaxation Delay	1.0000
13	Pulse Width	12.0000
14	Modification Date	2012-10-03T17:55:28
15	Spectrometer Frequency	499.89
16	Spectral Width	10000.0
17	Lowest Frequency	-1874.0
18	Nucleus	1H
19	Acquired Size	32768
20	Spectral Size	65536

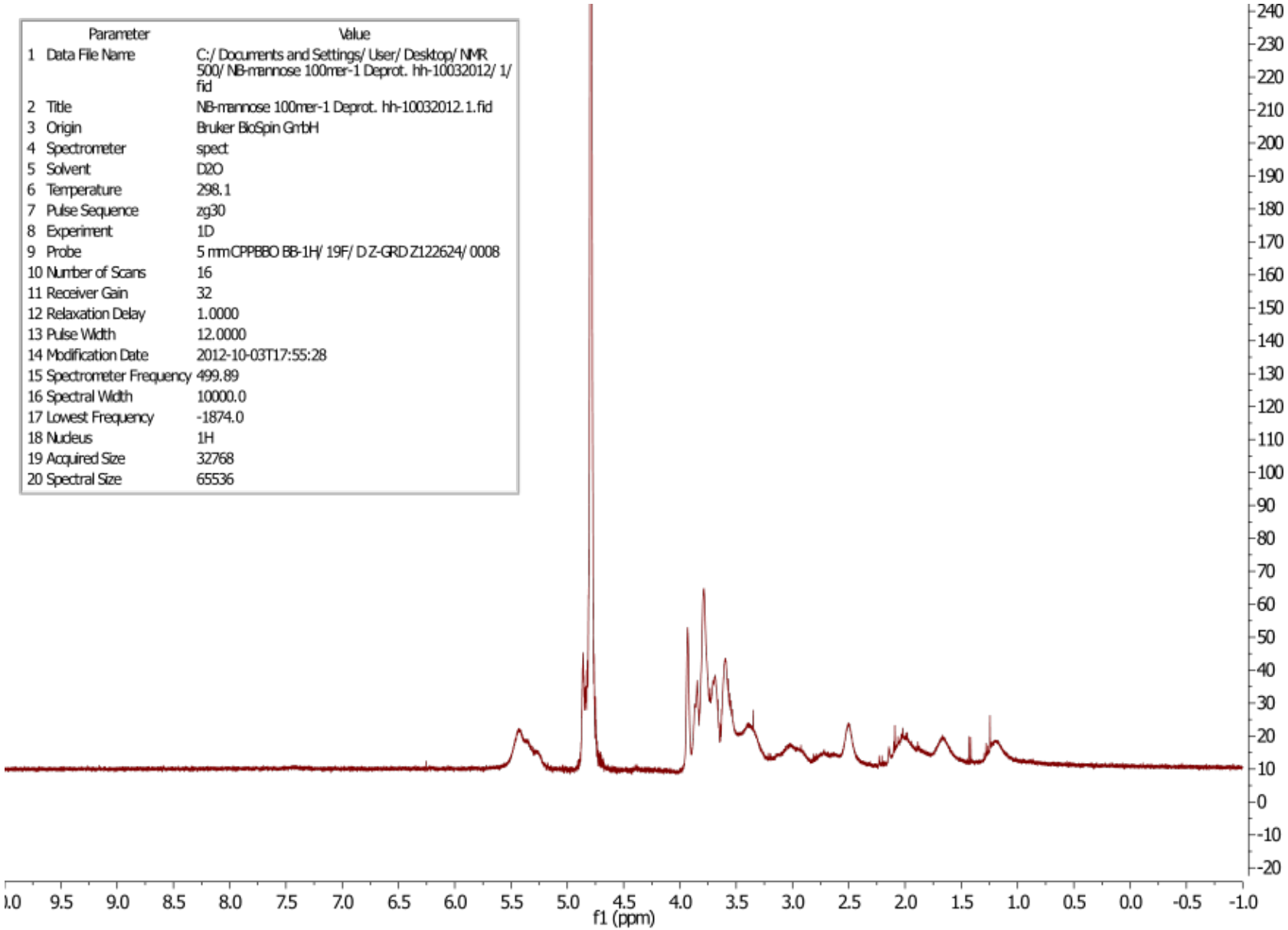

^{1}H NMR of poly(**1b**)$_{100}$

Parameter	Value
1 Data File Name	C:/ Documents and Settings/ User/ Desktop/ NMR 500/ deprot-poly(glcnac)100-1-hh-03152013/ 1/ fid
2 Title	deprot-poly(glcnac)100-1-hh-03152013.1.fid
3 Origin	Bruker BioSpin GmbH
4 Spectrometer	spect
5 Solvent	D2O
6 Temperature	298.2
7 Pulse Sequence	zg30
8 Experiment	1D
9 Probe	5 mm CPPBBO BB-1H/ 19F/ D Z-GRD Z122624/ 0008
10 Number of Scans	48
11 Receiver Gain	32
12 Relaxation Delay	1.0000
13 Pulse Width	12.0000
14 Modification Date	2013-03-15T13:15:12
15 Spectrometer Frequency	499.89
16 Spectral Width	10000.0
17 Lowest Frequency	-1873.4
18 Nucleus	1H
19 Acquired Size	32768
20 Spectral Size	65536

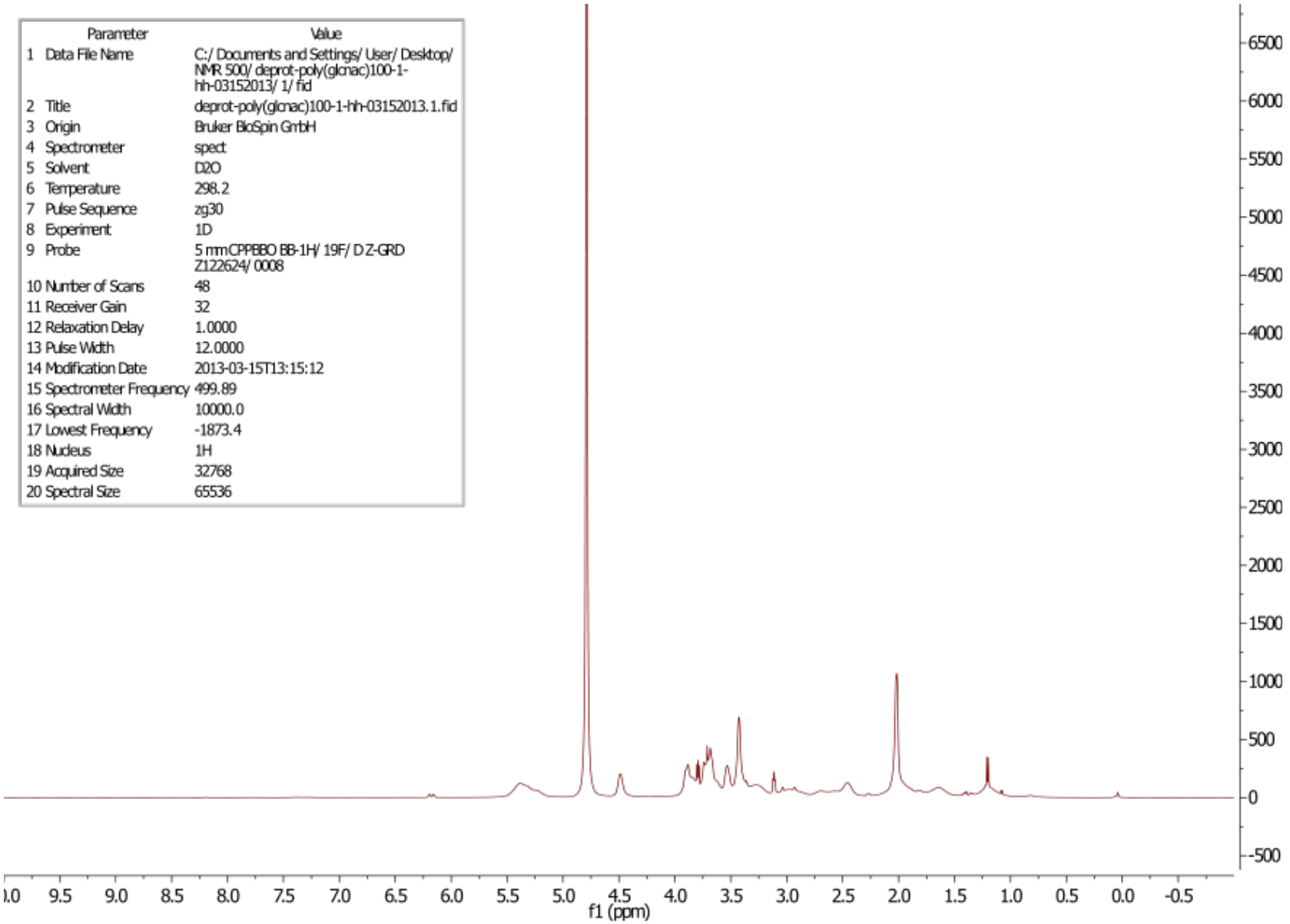

^{1}H NMR of poly(**1c**)$_{100}$

	Parameter	Value
1	Data File Name	C:/ Documents and Settings/ User/ Desktop/ nmr400/ poly-(glc)100-3 08312015/ 1/ fid
2	Title	poly-(glc)100-3 08312015.1.fid
3	Origin	Bruker BioSpin GmbH
4	Spectrometer	spect
5	Solvent	D2O
6	Temperature	298.1
7	Pulse Sequence	zg30
8	Experiment	1D
9	Probe	5 mm PABBO BB/ 19F-1H/ D Z-GRD Z116098/ 0058
10	Number of Scans	32
11	Receiver Gain	85
12	Relaxation Delay	1.0000
13	Pulse Width	10.1000
14	Modification Date	2015-08-31T11:45:00
15	Spectrometer Frequency	399.83
16	Spectral Width	8223.7
17	Lowest Frequency	-1605.9
18	Nucleus	1H
19	Acquired Size	32768
20	Spectral Size	65536

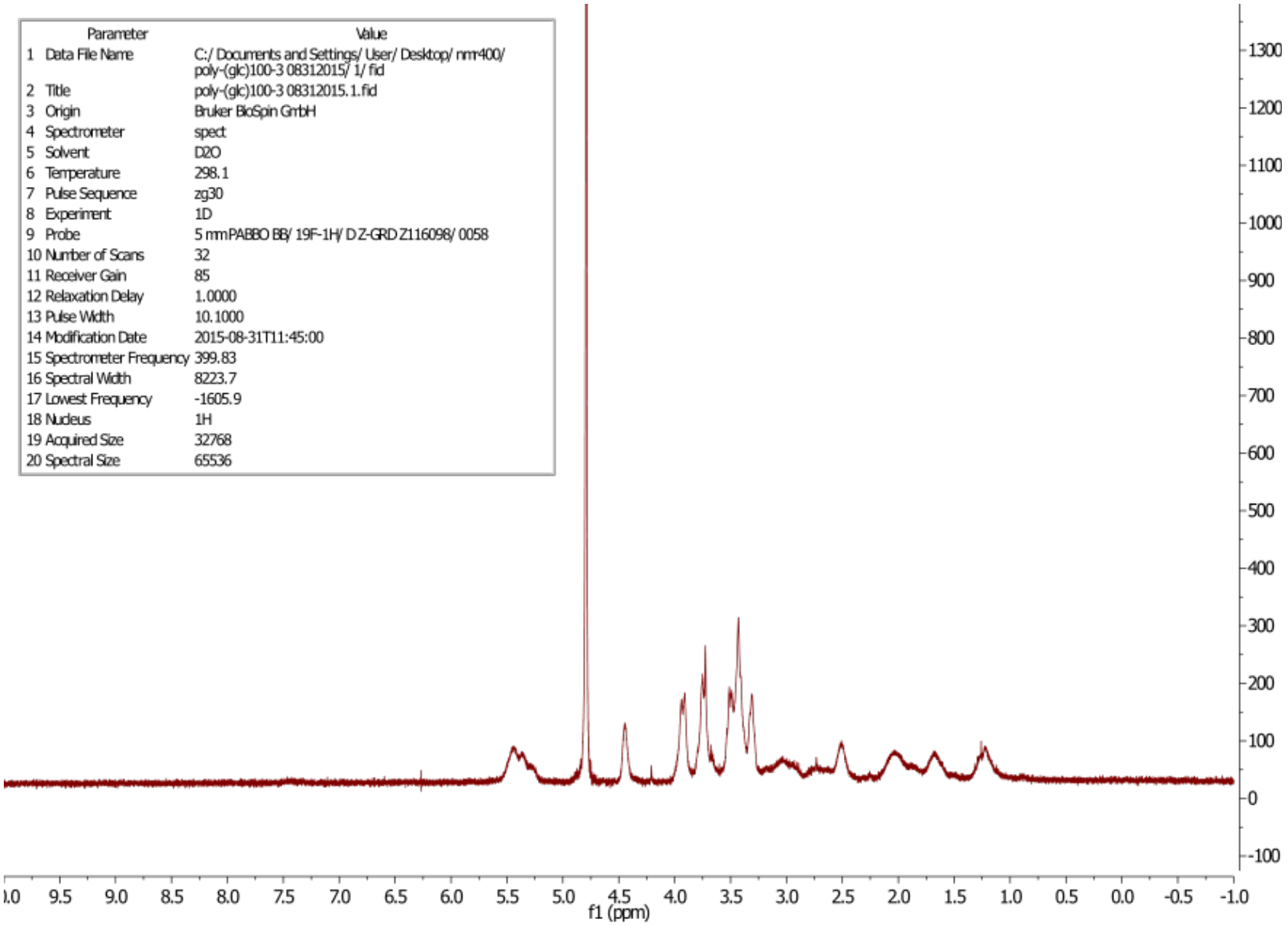

^{1}H NMR of poly(**1d**)$_{100}$

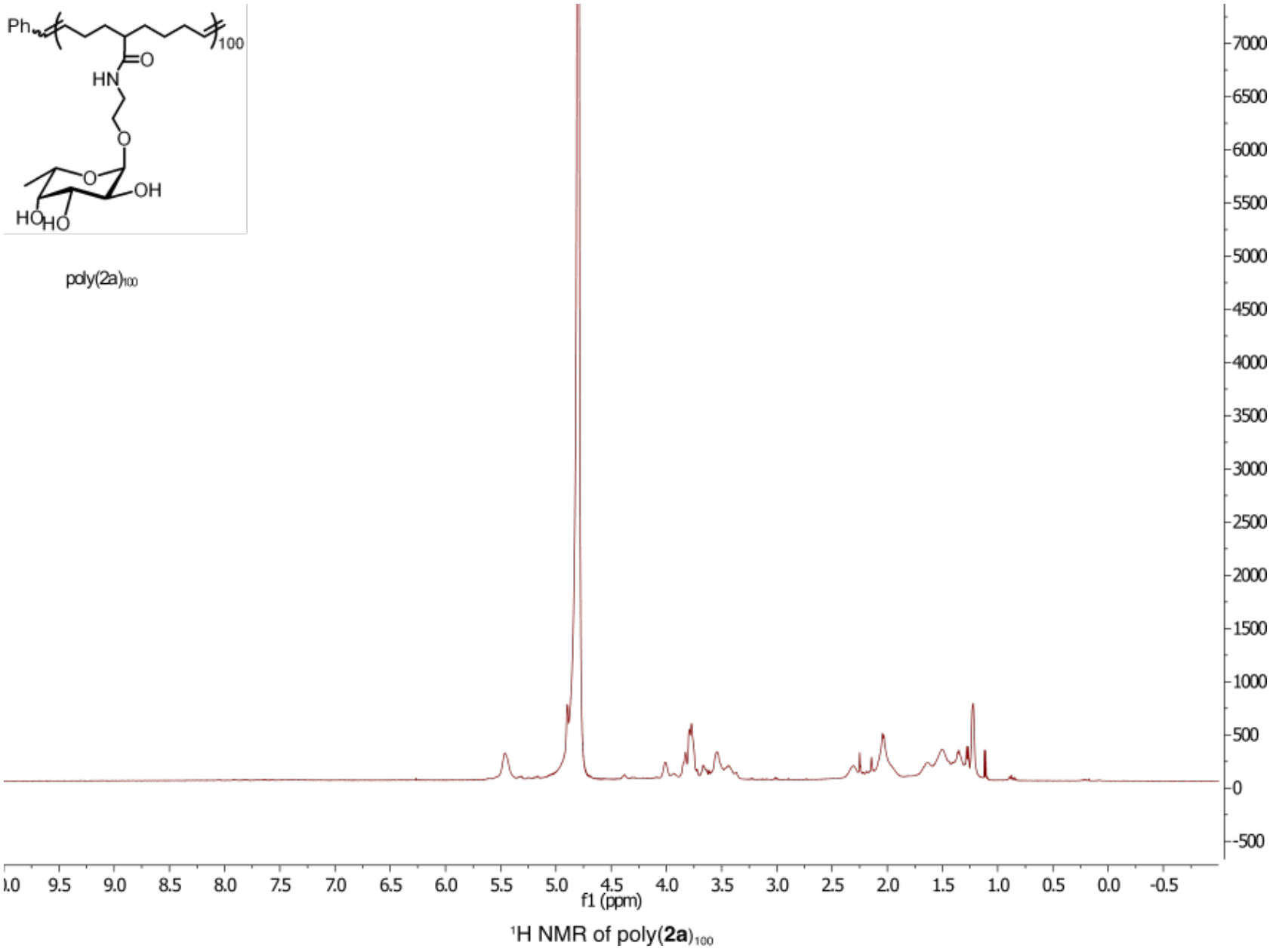

^{1}H NMR of poly(**2a**)$_{100}$

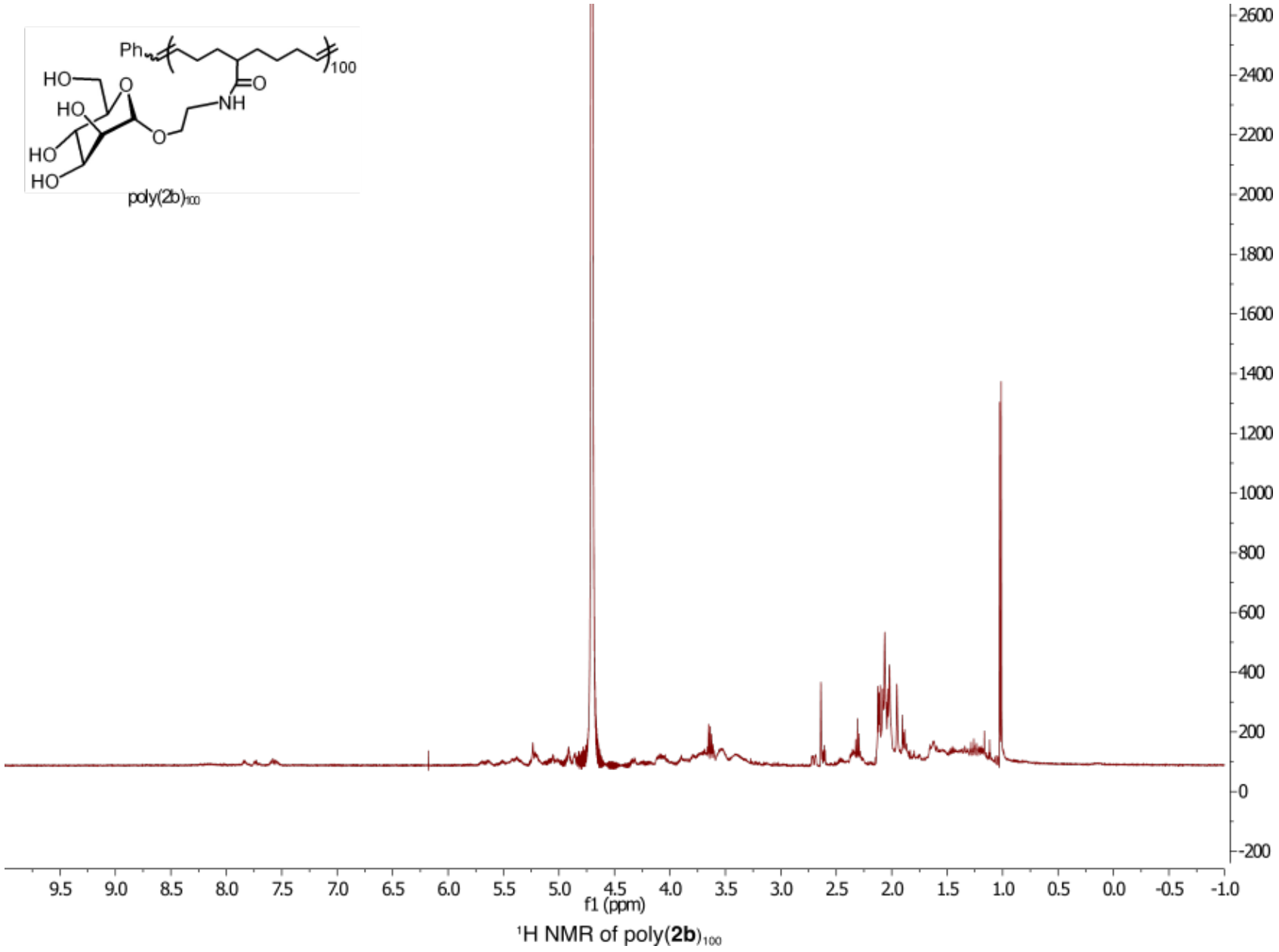

^{1}H NMR of poly(**2b**)$_{100}$

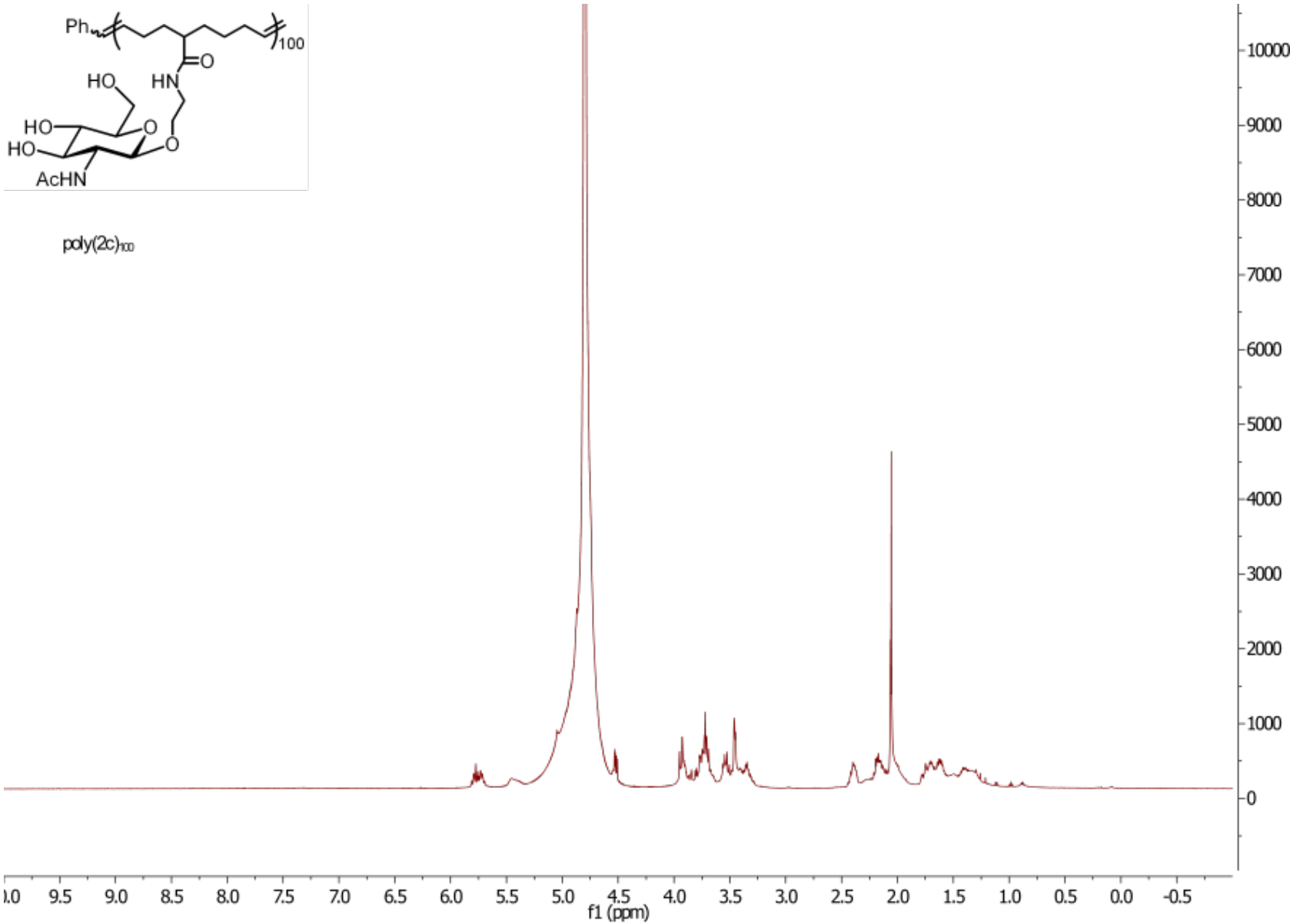

^{1}H NMR of poly(**2c**)$_{100}$

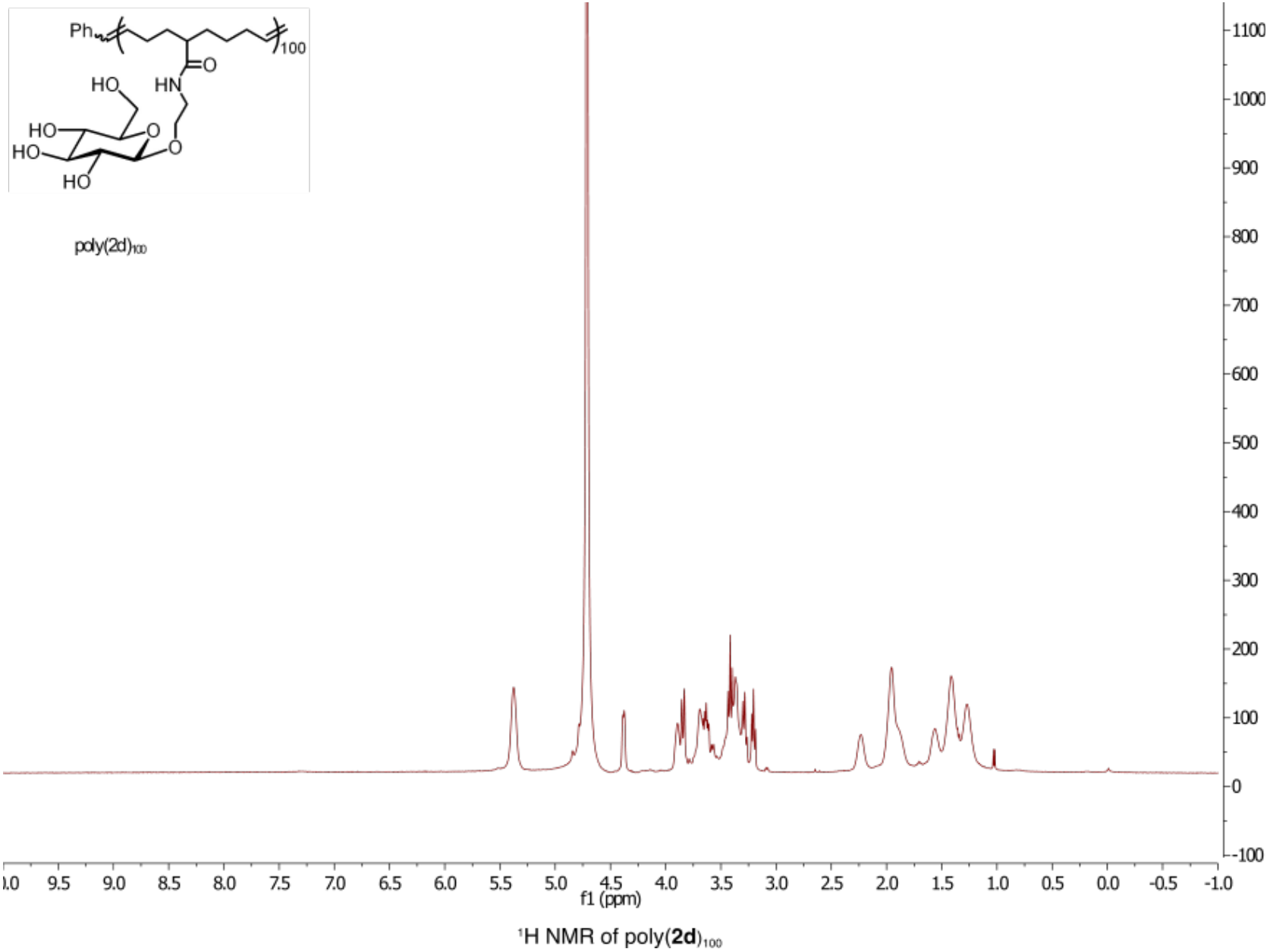

^{1}H NMR of poly(**2d**)$_{100}$

	Parameter	Value
1	Data File Name	C:/ Documents and Settings/ User/ Desktop/ NMR 500/ deprot-ran-(fuc50/ glc50)-1-hh-07262013/ 1/ fid
2	Title	glc50)-1-hh-07262013.1.fid
3	Origin	Bruker BioSpin GmbH
4	Spectrometer	spect
5	Solvent	D2O
6	Temperature	298.1
7	Pulse Sequence	zg30
8	Experiment	1D
9	Probe	5 mm CPPBBO BB-1H/ 19F/ D Z-GRD Z122624/ 0008
10	Number of Scans	64
11	Receiver Gain	32
12	Relaxation Delay	1.0000
13	Pulse Width	12.0000
14	Modification Date	2013-07-26T13:21:38
15	Spectrometer Frequency	499.89
16	Spectral Width	10000.0
17	Lowest Frequency	-1913.0
18	Nucleus	1H
19	Acquired Size	32768
20	Spectral Size	65536

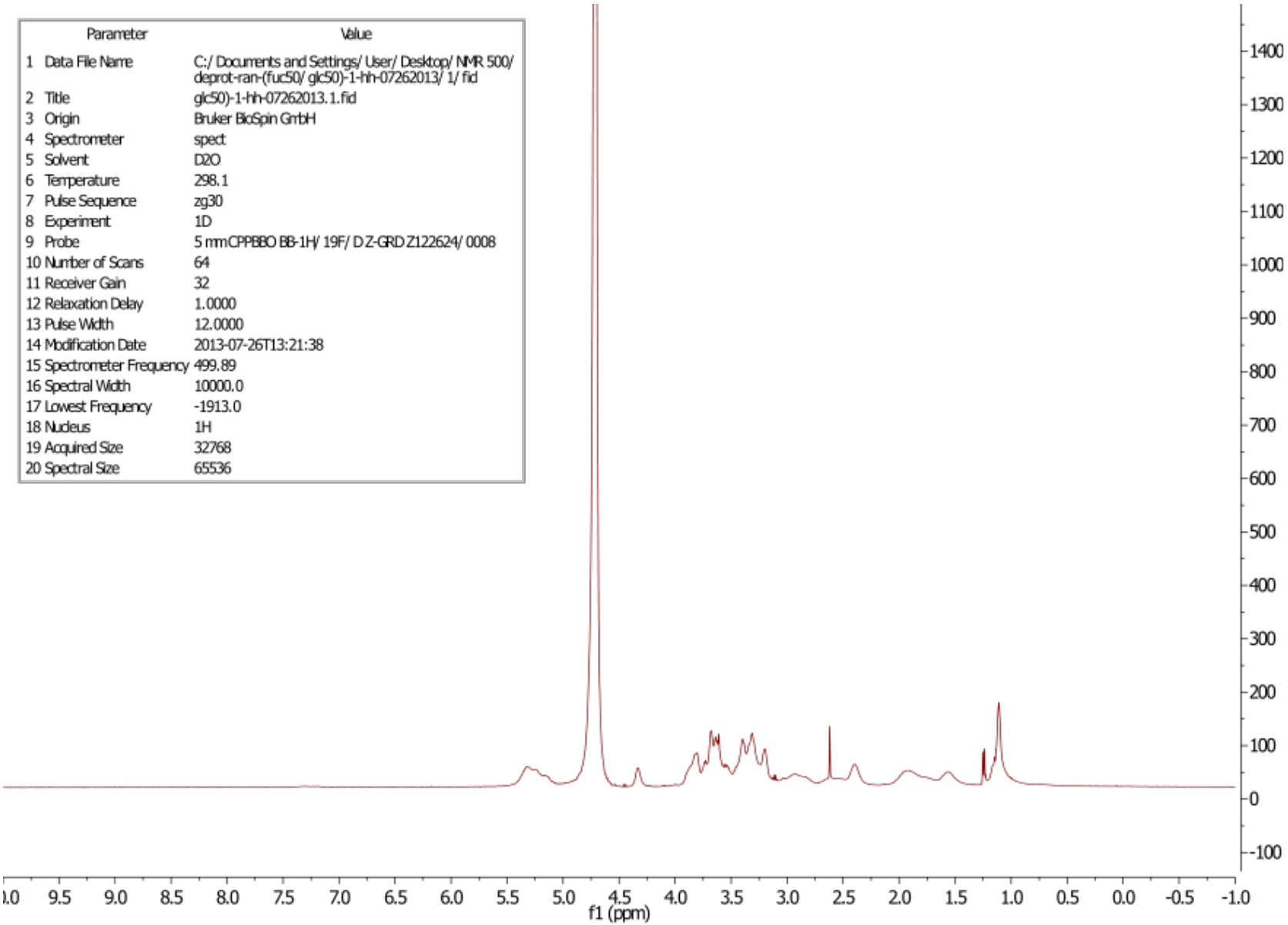

^{1}H NMR poly(**1a**$_{50}$-*ran*-**1d**$_{50}$)

	Parameter	Value
1	Data File Name	C:/ Documents and Settings/ User/ Desktop/ NMR 500/ deprotected-ran-(fuc10/ glc90)-1-hh-08122013/ 1/ fid
2	Title	glc90)-1-hh-08122013.1.fid
3	Origin	Bruker BioSpin GmbH
4	Spectrometer	spect
5	Solvent	D2O
6	Temperature	298.1
7	Pulse Sequence	zg30
8	Experiment	1D
9	Probe	5 mmCPPBBO BB-1H/ 19F/ D Z-GRD Z122624/ 0008
10	Number of Scans	32
11	Receiver Gain	49
12	Relaxation Delay	1.0000
13	Pulse Width	12.0000
14	Modification Date	2013-08-12T16:48:24
15	Spectrometer Frequency	499.89
16	Spectral Width	10000.0
17	Lowest Frequency	-1913.0
18	Nucleus	1H
19	Acquired Size	32768
20	Spectral Size	65536

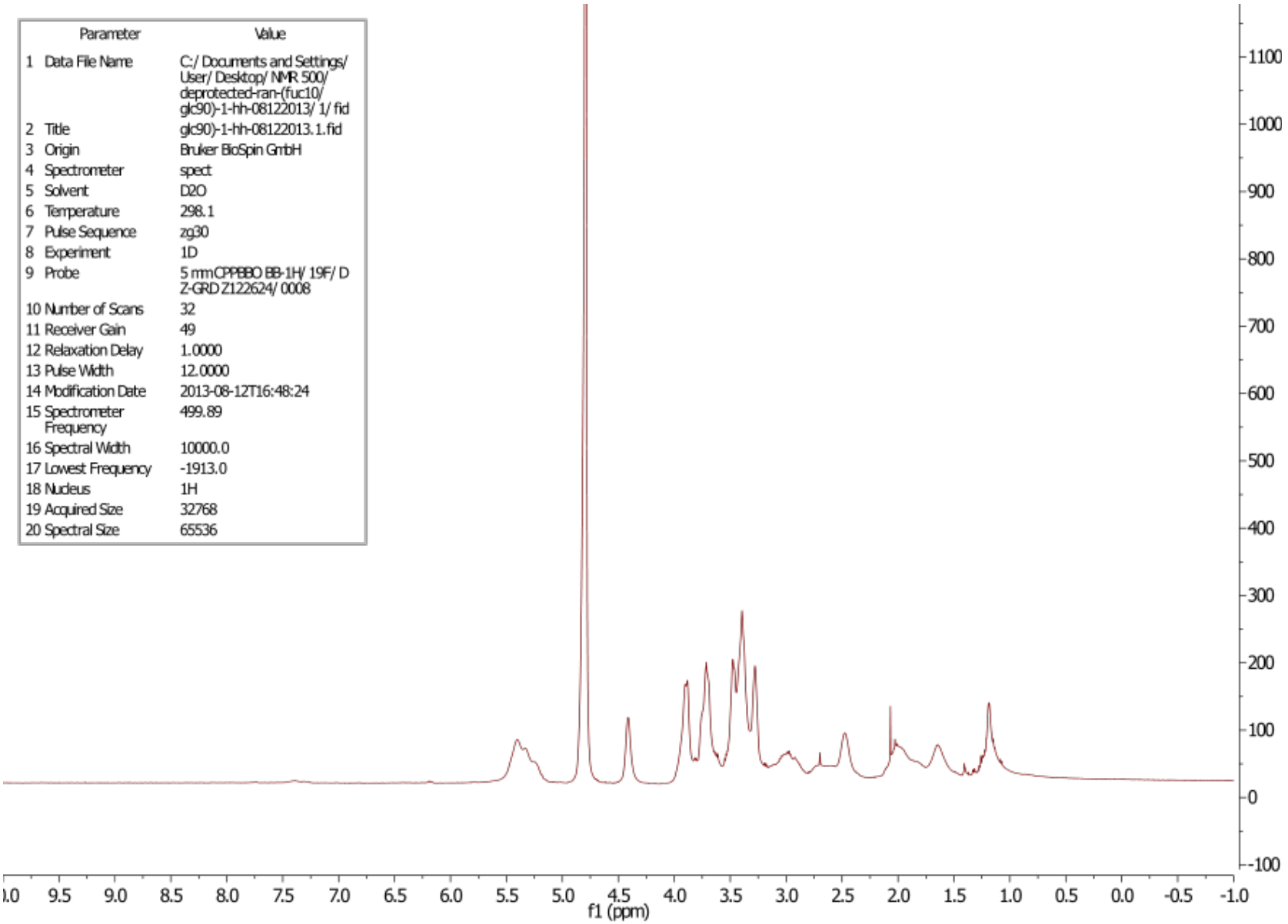

^{1}H NMR poly(**1a**$_{10}$-*ran*-**1d**$_{90}$)

Parameter		Value
1	Data File Name	G:/ 10122017/ deprot-ranman50glc50/ 1/ fid
2	Title	deprot-ranman50glc50.1.fid
3	Origin	Bruker BioSpin GmbH
4	Spectrometer	spect
5	Solvent	D2O
6	Temperature	298.1
7	Pulse Sequence	zg30
8	Experiment	1D
9	Probe	Z122624_0008 (CPP BBO 500S2 BB-H&F-D-05 Z)
10	Number of Scans	160
11	Receiver Gain	56
12	Relaxation Delay	1.0000
13	Pulse Width	12.0000
14	Modification Date	2016-12-21T12:31:40
15	Spectrometer Frequency	499.89
16	Spectral Width	10000.0
17	Lowest Frequency	-1913.2
18	Nucleus	1H
19	Acquired Size	32768
20	Spectral Size	65536

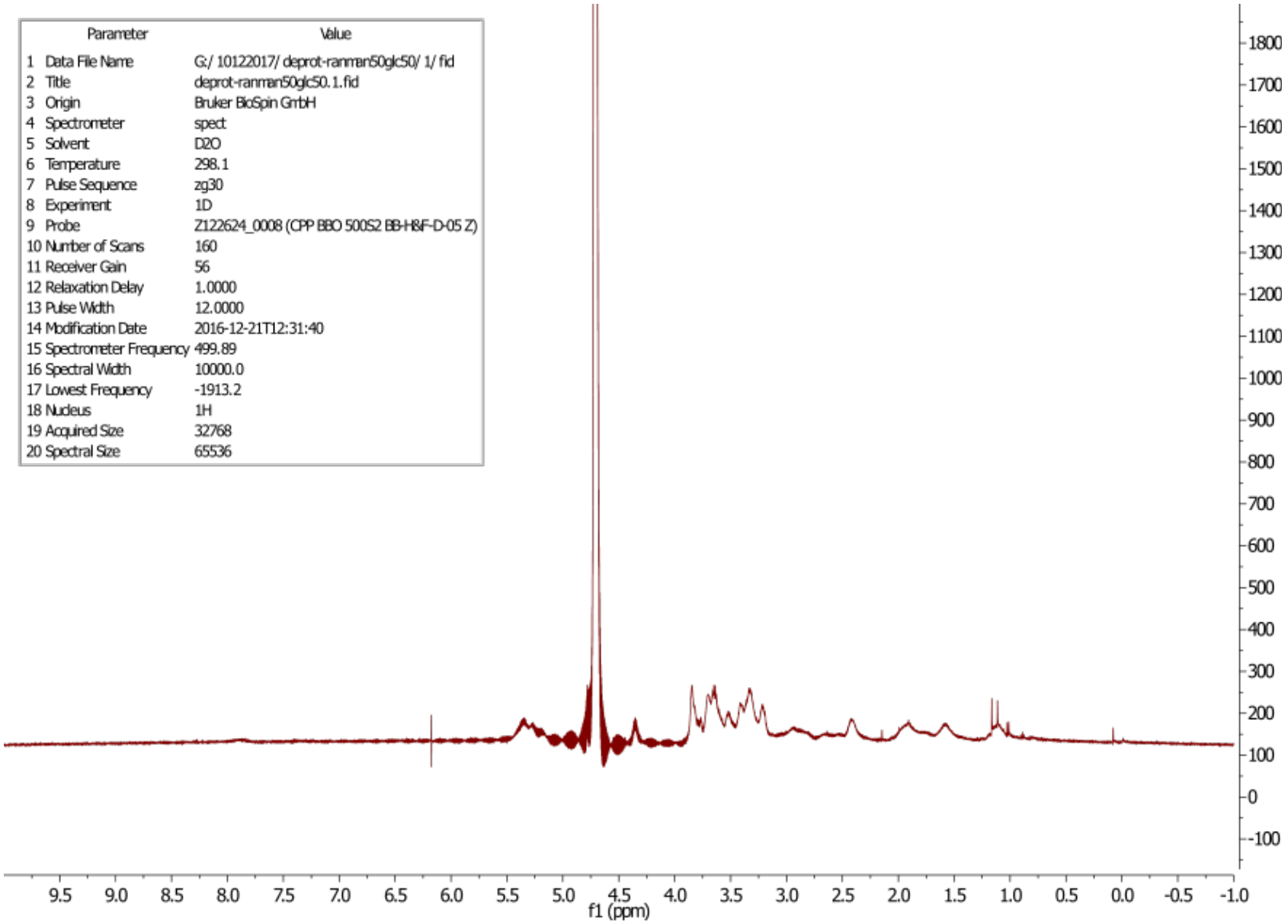

^{1}H NMR of poly(**1b**$_{50}$-*ran*-**1d**$_{50}$)

	Parameter	Value
1	Data File Name	C:/ Documents and Settings/ User/ Desktop/ NMR 500/ deprotect-ran(man10/ glc90)-3-hh-12112012/ 1/ fid
2	Title	glc90)-3-hh-12112012.1.fid
3	Origin	Bruker BioSpin GmbH
4	Spectrometer	spect
5	Solvent	D2O
6	Temperature	298.2
7	Pulse Sequence	zg30
8	Experiment	1D
9	Probe	5 mm CPPBBO BB-1H/ 19F/ D Z-GRD Z122624/ 0008
10	Number of Scans	100
11	Receiver Gain	32
12	Relaxation Delay	1.0000
13	Pulse Width	12.0000
14	Modification Date	2012-12-11T18:08:56
15	Spectrometer Frequency	499.89
16	Spectral Width	10000.0
17	Lowest Frequency	-1913.0
18	Nucleus	1H
19	Acquired Size	32768
20	Spectral Size	65536

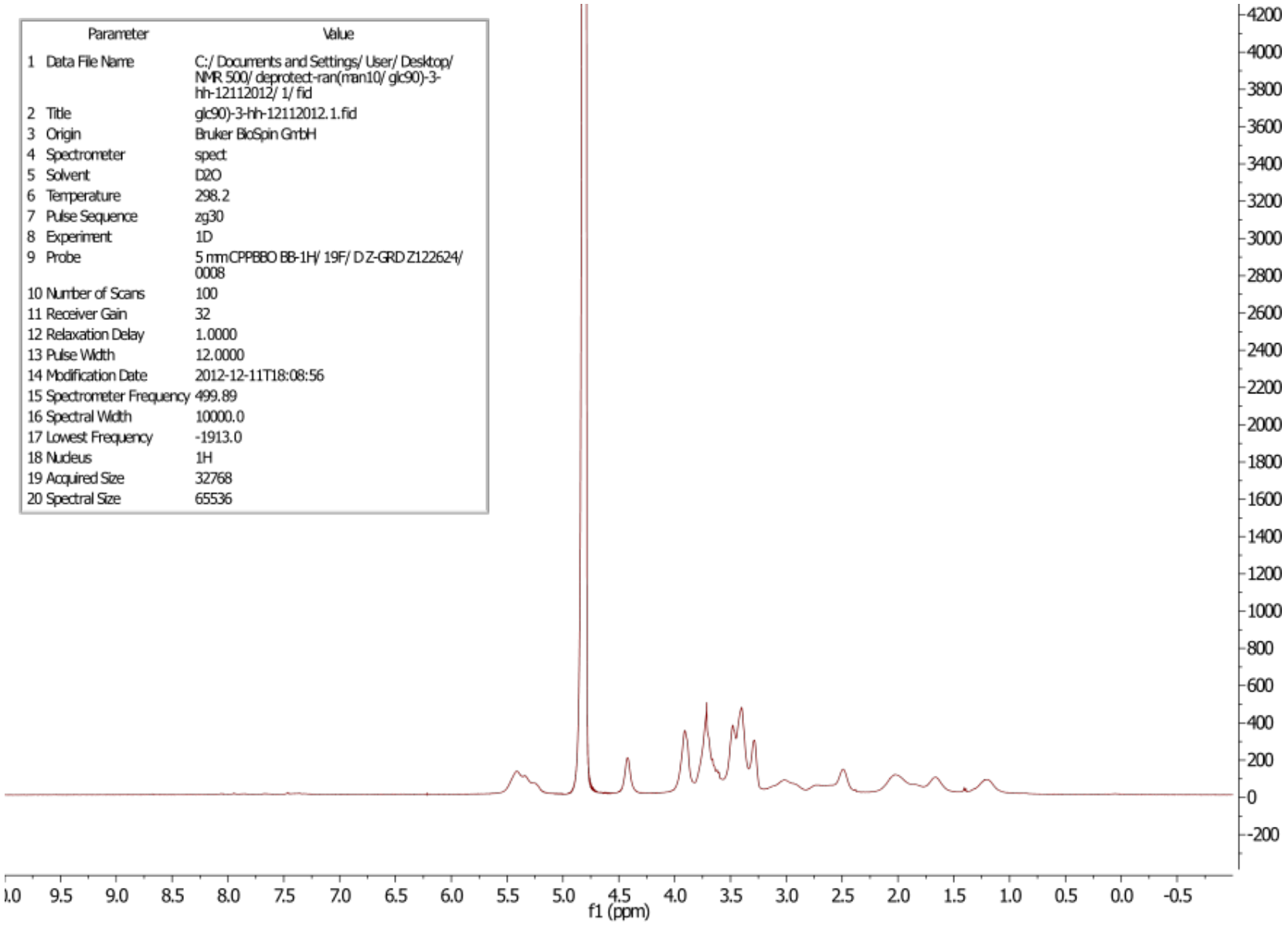

^{1}H NMR poly(**1d**$_{10}$-*ran*-**1d**$_{90}$)

	Parameter	Value
1	Data File Name	C:/ Documents and Settings/ User/ Desktop/ NMR 500/ deprot-ran-(glcnac50/ glc50)-1-hh-03152013/ 1/ fid
2	Title	glc50)-1-hh-03152013.1.fid
3	Origin	Bruker BioSpin GmbH
4	Spectrometer	spect
5	Solvent	D2O
6	Temperature	298.2
7	Pulse Sequence	zg30
8	Experiment	1D
9	Probe	5 mm CPPBBO BB-1H/ 19F/ D Z-GRD Z122624/ 0008
10	Number of Scans	36
11	Receiver Gain	32
12	Relaxation Delay	1.0000
13	Pulse Width	12.0000
14	Modification Date	2013-03-15T13:23:34
15	Spectrometer Frequency	499.89
16	Spectral Width	10000.0
17	Lowest Frequency	-1873.0
18	Nucleus	1H
19	Acquired Size	32768
20	Spectral Size	65536

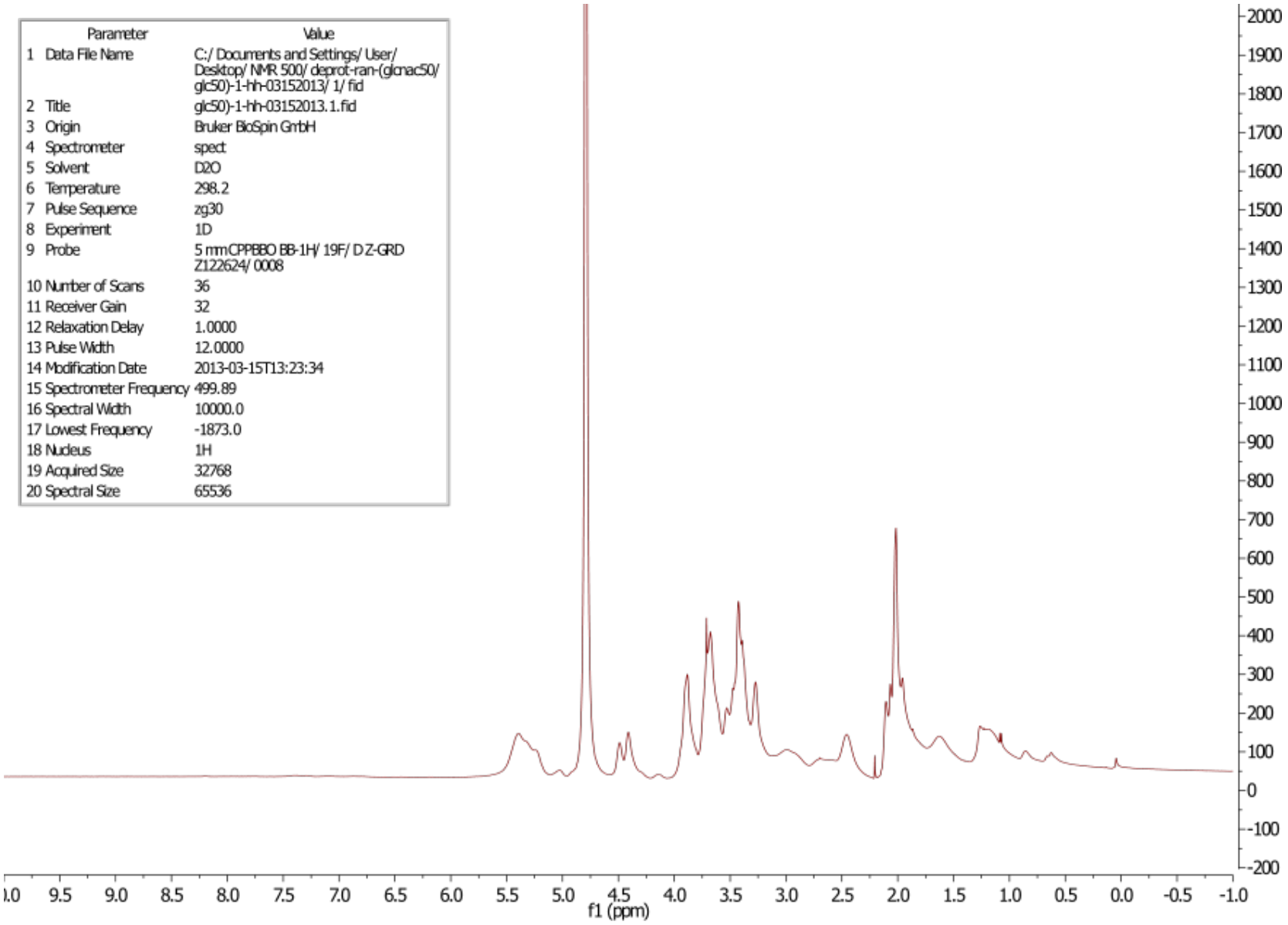

^{1}H NMR poly(**1c**$_{50}$-*ran*-**1d**$_{50}$)

	Parameter	Value
1	Data File Name	C:/ Documents and Settings/ User/ Desktop/ NMR 500/ deprotect-ran(man10/ glc90)-3-hh-12112012/ 1/ fid
2	Title	glc90)-3-hh-12112012.1.fid
3	Origin	Bruker BioSpin GmbH
4	Spectrometer	spect
5	Solvent	D2O
6	Temperature	298.2
7	Pulse Sequence	zg30
8	Experiment	1D
9	Probe	5 mm CPPBBO BB-1H/ 19F/ D Z-GRD Z122624/ 0008
10	Number of Scans	100
11	Receiver Gain	32
12	Relaxation Delay	1.0000
13	Pulse Width	12.0000
14	Modification Date	2012-12-11T18:08:56
15	Spectrometer Frequency	499.89
16	Spectral Width	10000.0
17	Lowest Frequency	-1913.0
18	Nucleus	1H
19	Acquired Size	32768
20	Spectral Size	65536

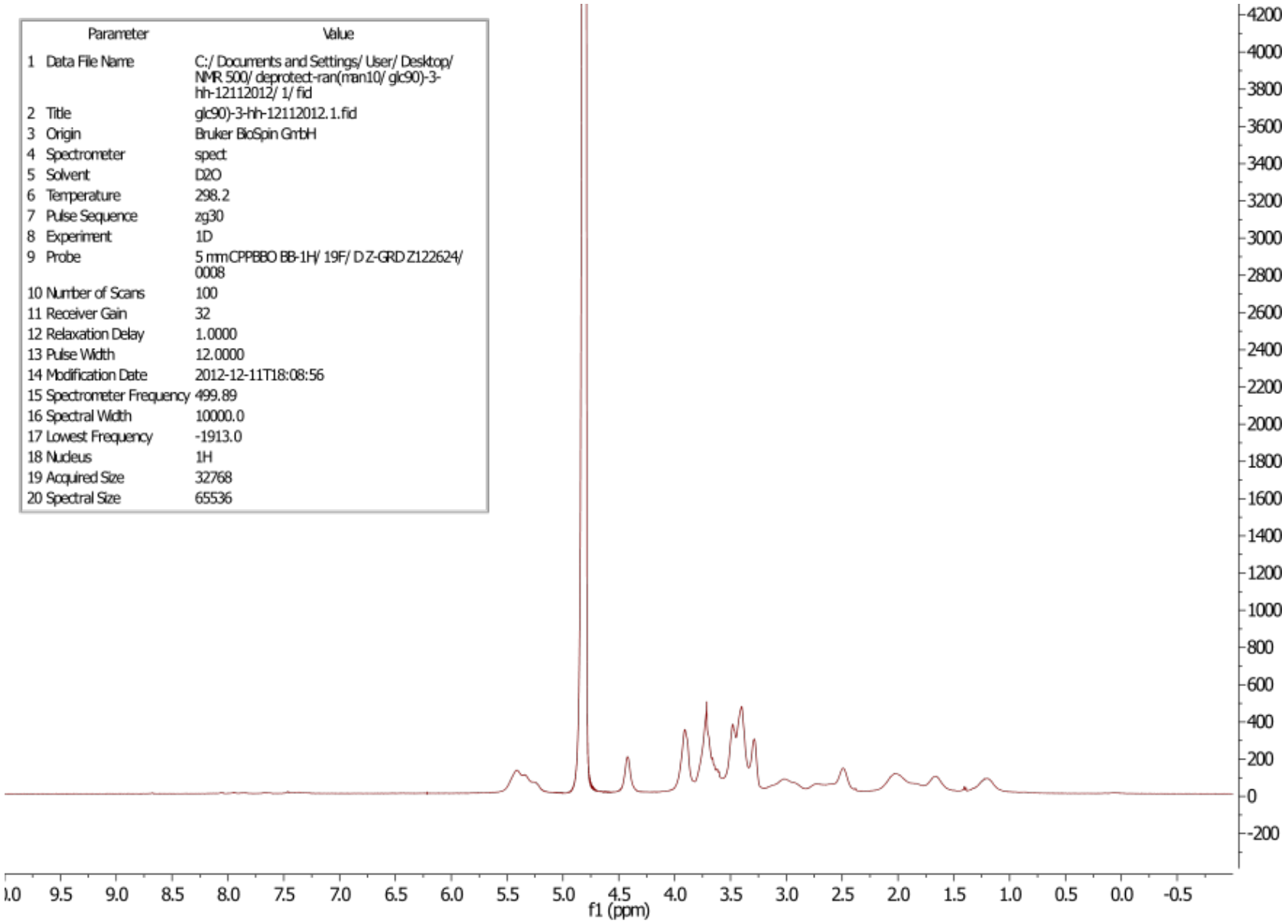

^{1}H NMR poly(**1c**$_{10}$-*ran*-**1d**$_{90}$)

	Parameter	Value
1	Data File Name	C:/ Documents and Settings/ User/ Desktop/ NMR 500/ deprot-block-(man50/ fuc50)-hh-1-10102013/ 1/ fid
2	Title	fuc50)-hh-1-10102013.1.fid
3	Origin	Bruker BioSpin GmbH
4	Spectrometer	spect
5	Solvent	D2O
6	Temperature	298.1
7	Pulse Sequence	zg30
8	Experiment	1D
9	Probe	5 mmCPPBBO BB-1H/ 19F/ D Z-GRD Z122624/ 0008
10	Number of Scans	100
11	Receiver Gain	56
12	Relaxation Delay	1.0000
13	Pulse Width	12.0000
14	Modification Date	2013-10-10T18:14:26
15	Spectrometer Frequency	499.89
16	Spectral Width	10000.0
17	Lowest Frequency	-1872.0
18	Nucleus	1H
19	Acquired Size	32768
20	Spectral Size	65536

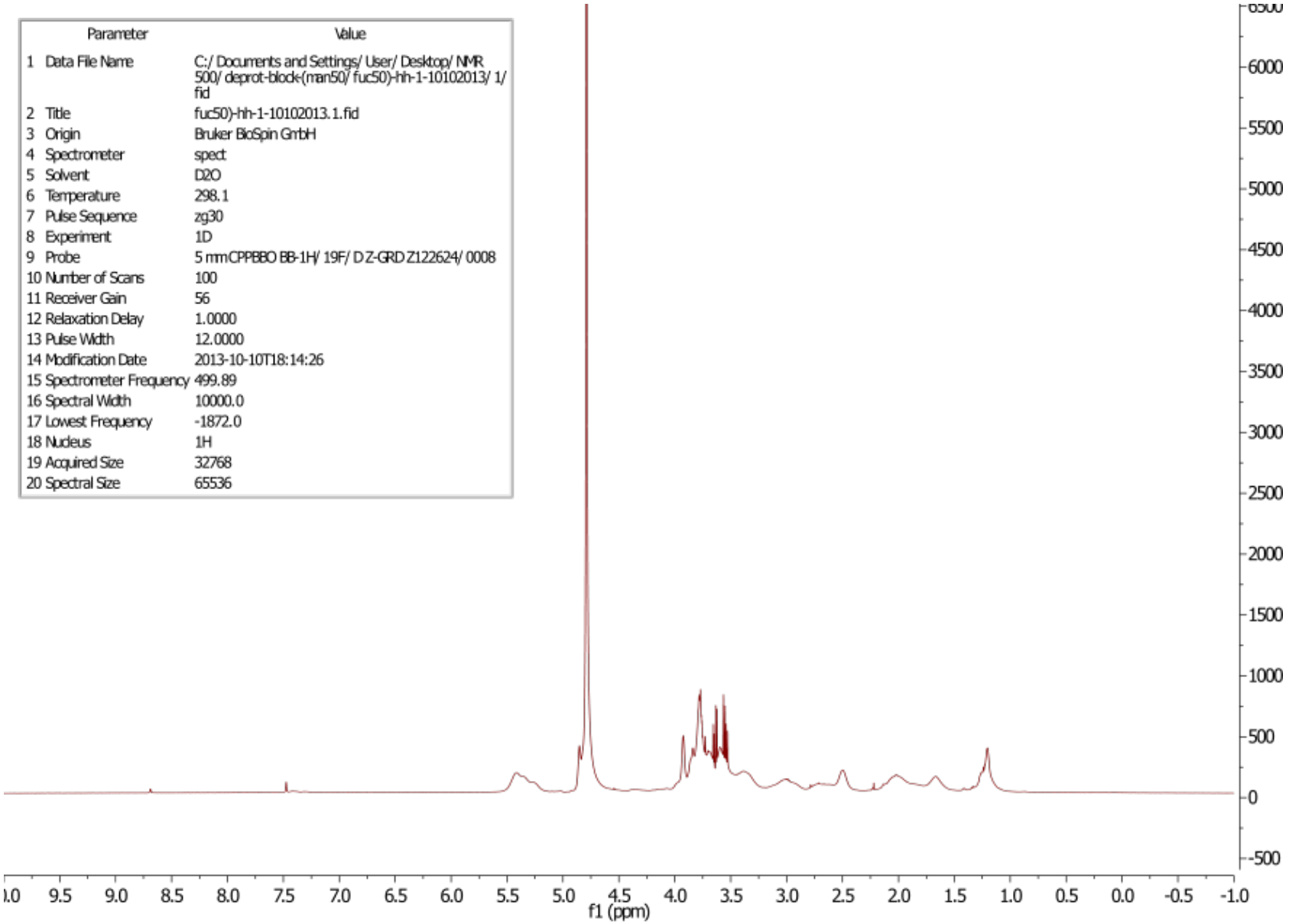

^{1}H NMR poly(**1b**$_{50}$-*block*-**1a**$_{50}$)

	Parameter	Value
1	Data File Name	C:/ Documents and Settings/ User/ Desktop/ NMR 500/ deprotected-blo-(man50/ glcnac50)-1-hh-08122013/ 1/ fid
2	Title	glcnac50)-1-hh-08122013.1.fid
3	Origin	Bruker BioSpin GmbH
4	Spectrometer	spect
5	Solvent	D2O
6	Temperature	298.1
7	Pulse Sequence	zg30
8	Experiment	1D
9	Probe	5 mm CPPBBO BB-1H/ 19F/ D Z-GRD Z122624/ 0008
10	Number of Scans	21
11	Receiver Gain	32
12	Relaxation Delay	1.0000
13	Pulse Width	12.0000
14	Modification Date	2013-08-12T16:55:06
15	Spectrometer Frequency	499.89
16	Spectral Width	10000.0
17	Lowest Frequency	-1874.5
18	Nucleus	1H
19	Acquired Size	32768
20	Spectral Size	65536

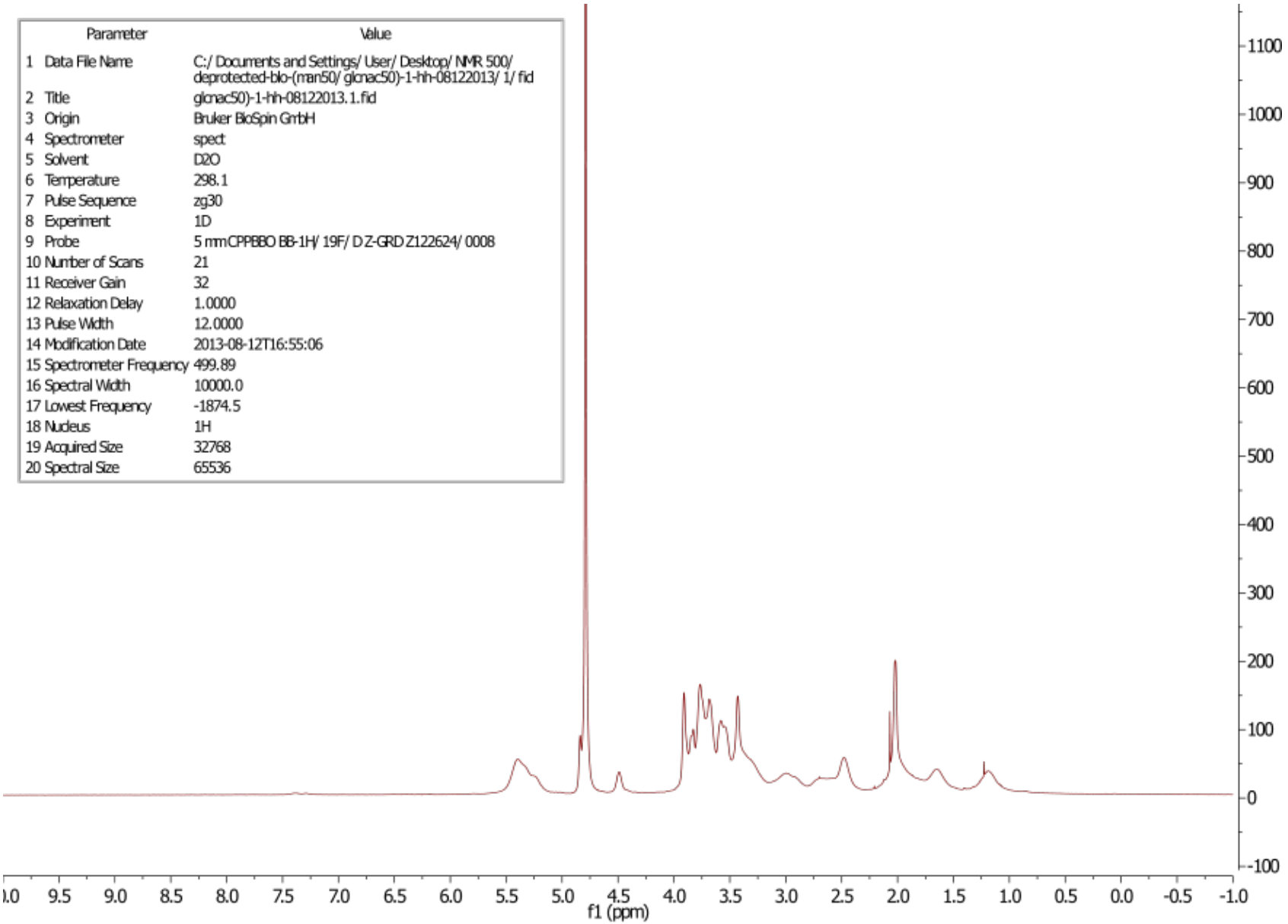

^{1}H NMR of poly(**1b**$_{50}$-*block*-**1c**$_{50}$)

Parameter		Value
1	Data File Name	G:/ 10122017/ deprot-blockfuc50glcnac50/ 1/ fid
2	Title	deprot-blockfuc50glcnac50.1.fid
3	Origin	Bruker BioSpin GmbH
4	Spectrometer	spect
5	Solvent	D2O
6	Temperature	298.1
7	Pulse Sequence	zg30
8	Experiment	1D
9	Probe	Z122624_0008 (CPP BBO 500S2 BB-H&F-D-05 Z)
10	Number of Scans	160
11	Receiver Gain	56
12	Relaxation Delay	1.0000
13	Pulse Width	12.0000
14	Modification Date	2016-12-21T12:49:54
15	Spectrometer Frequency	499.89
16	Spectral Width	10000.0
17	Lowest Frequency	-1913.2
18	Nucleus	1H
19	Acquired Size	32768
20	Spectral Size	65536

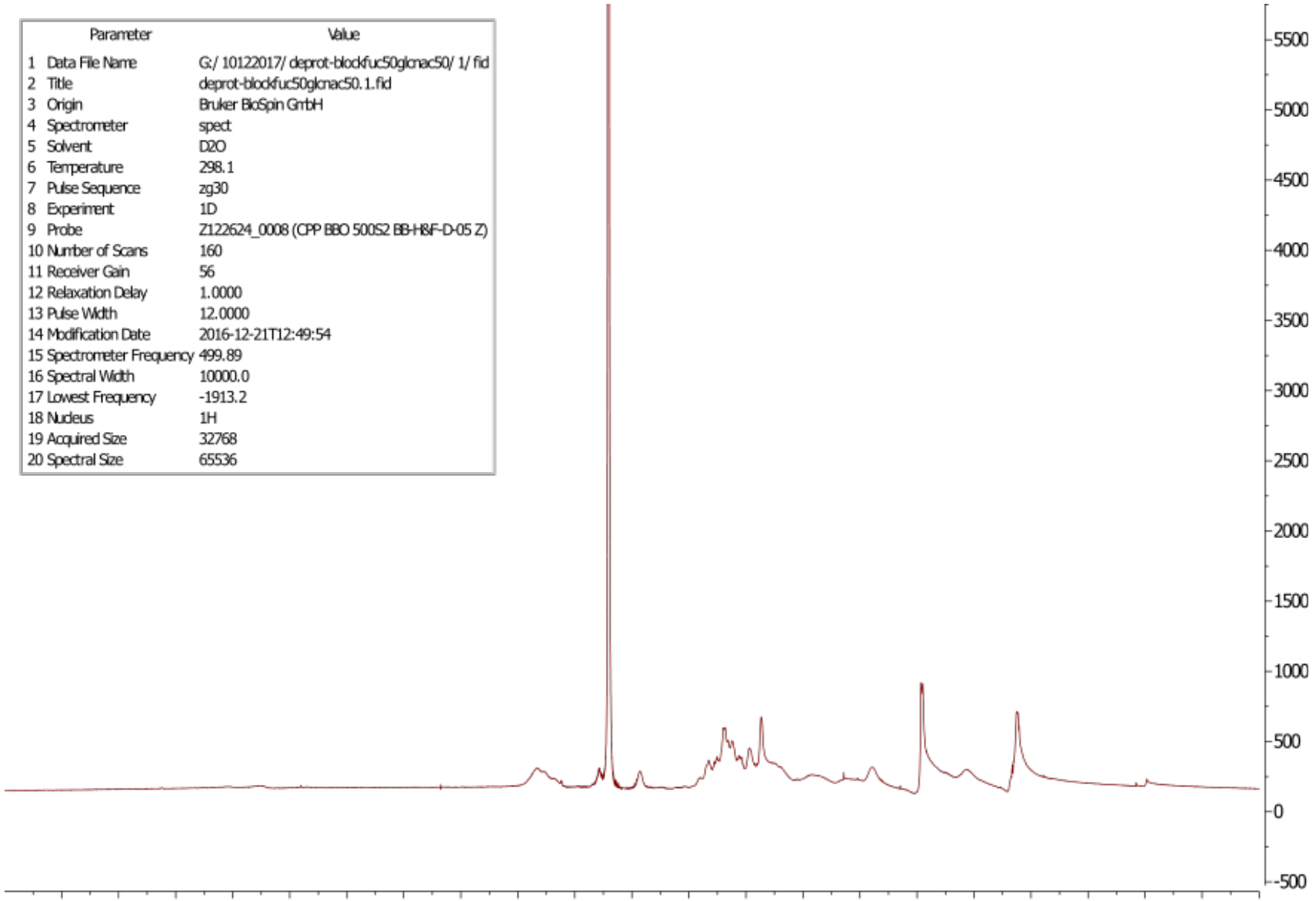

^{1}H NMR of poly(**1a**$_{50}$-*block*-**1c**$_{50}$)

Parameter		Value
1	Data File Name	C:/ Documents and Settings/ User/ Desktop/ NMR 500/ deprot-block-(fuc50/ glc50)-1-11062013/ 1/ fid
2	Title	glc50)-1-11062013.1.fid
3	Origin	Bruker BioSpin GmbH
4	Spectrometer	spect
5	Solvent	D2O
6	Temperature	298.2
7	Pulse Sequence	zg30
8	Experiment	1D
9	Probe	5 mm CPPBBO BB-1H/ 19F/ D Z-GRD Z122624/ 0008
10	Number of Scans	100
11	Receiver Gain	56
12	Relaxation Delay	1.0000
13	Pulse Width	12.0000
14	Modification Date	2013-11-06T16:59:50
15	Spectrometer Frequency	499.89
16	Spectral Width	10000.0
17	Lowest Frequency	-1873.5
18	Nucleus	1H
19	Acquired Size	32768
20	Spectral Size	65536

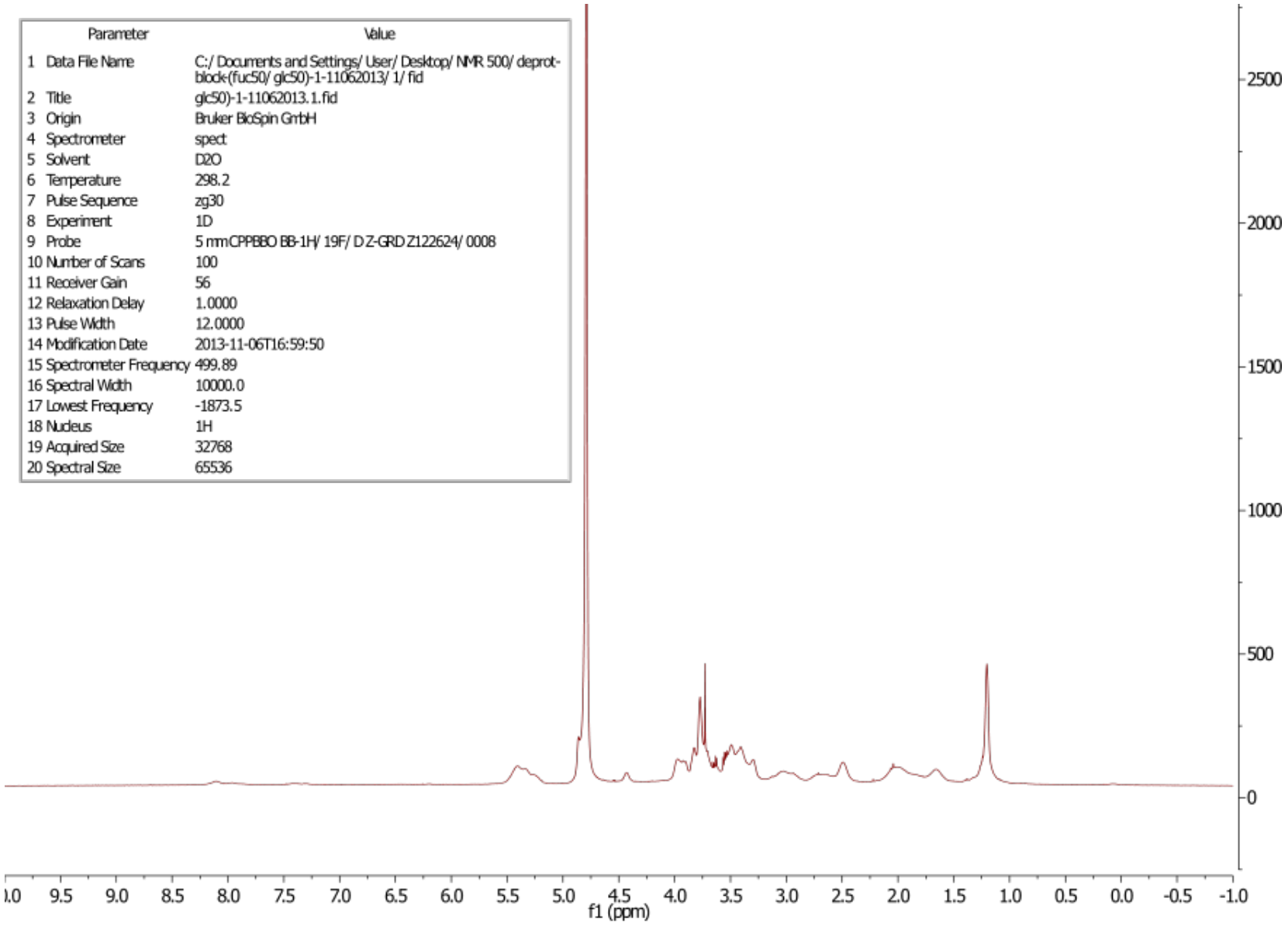

^{1}H NMR poly(**1a**$_{50}$-*block*-**1d**$_{50}$)

	Parameter	Value
1	Data File Name	C:/ Documents and Settings/ User/ Desktop/ nmr400/ deprotect-blcok-(man50/ glc50)-1-hh-10142013/ 1/ fid
2	Title	glc50)-1-hh-10142013.1.fid
3	Origin	Bruker BioSpin GmbH
4	Spectrometer	spect
5	Solvent	D2O
6	Temperature	298.1
7	Pulse Sequence	zg30
8	Experiment	1D
9	Probe	5 mm PABBO BB/ 19F-1H/ D Z-GRD Z116098/ 0058
10	Number of Scans	32
11	Receiver Gain	75
12	Relaxation Delay	1.0000
13	Pulse Width	10.1000
14	Modification Date	2013-10-14T18:44:10
15	Spectrometer Frequency	399.83
16	Spectral Width	8223.7
17	Lowest Frequency	-1605.9
18	Nucleus	1H
19	Acquired Size	32768
20	Spectral Size	65536

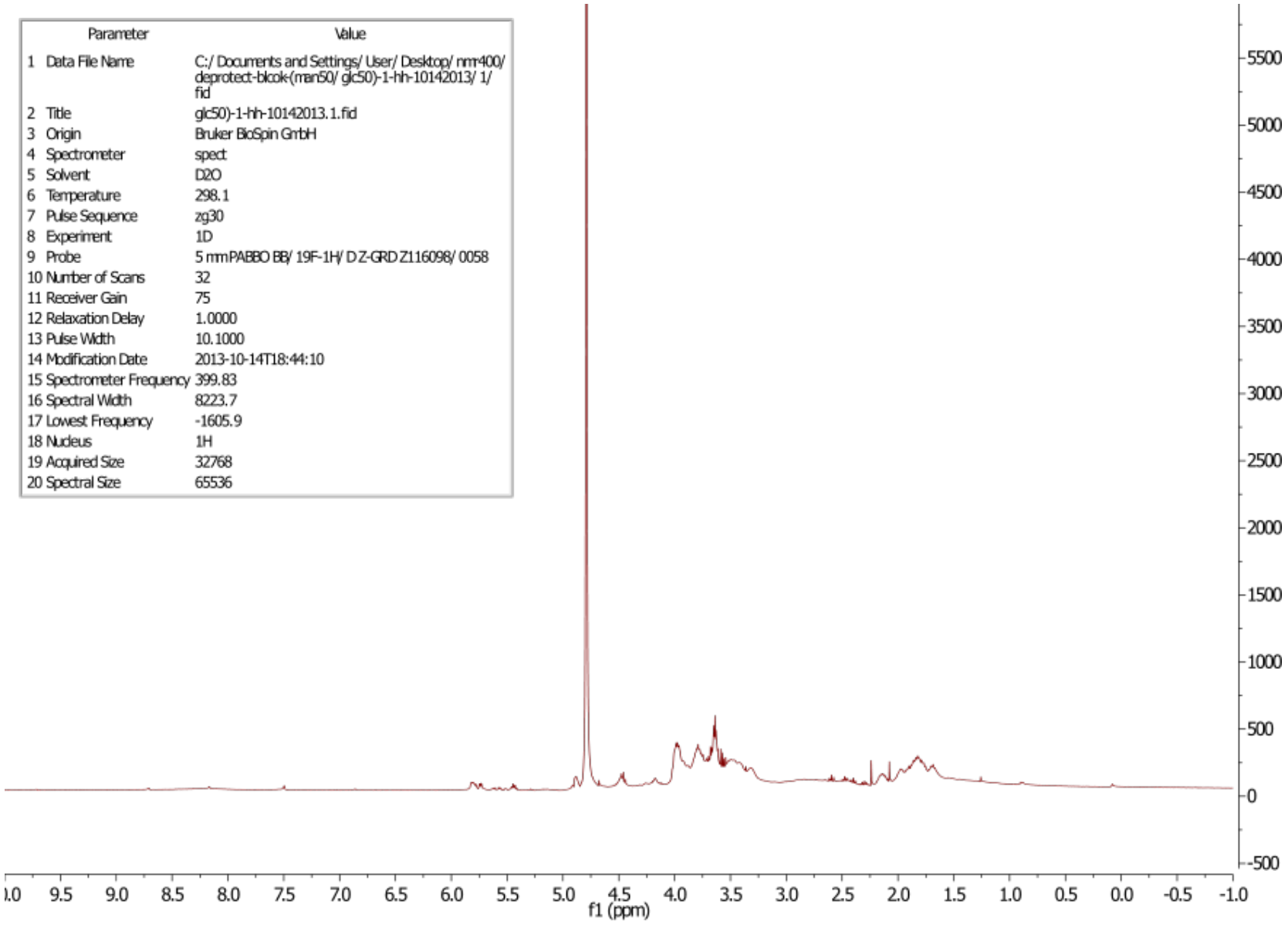

^{1}H NMR poly(**1b**$_{50}$-*block*-**1d**$_{50}$)

	Parameter	Value
1	Data File Name	C:/ Documents and Settings/ User/ Desktop/ NMR 500/ deprot-block-(glcnac50)-glc50)-1-hh-11062013/ 1/ fid
2	Title	glc50)-1-hh-11062013.1.fid
3	Origin	Bruker BioSpin GmbH
4	Spectrometer	spect
5	Solvent	D2O
6	Temperature	298.1
7	Pulse Sequence	zg30
8	Experiment	1D
9	Probe	5 mm CPPBBO BB-1H/ 19F/ D Z-GRD Z122624/ 0008
10	Number of Scans	100
11	Receiver Gain	49
12	Relaxation Delay	1.0000
13	Pulse Width	12.0000
14	Modification Date	2013-11-06T17:15:08
15	Spectrometer Frequency	499.89
16	Spectral Width	10000.0
17	Lowest Frequency	-1874.0
18	Nucleus	1H
19	Acquired Size	32768
20	Spectral Size	65536

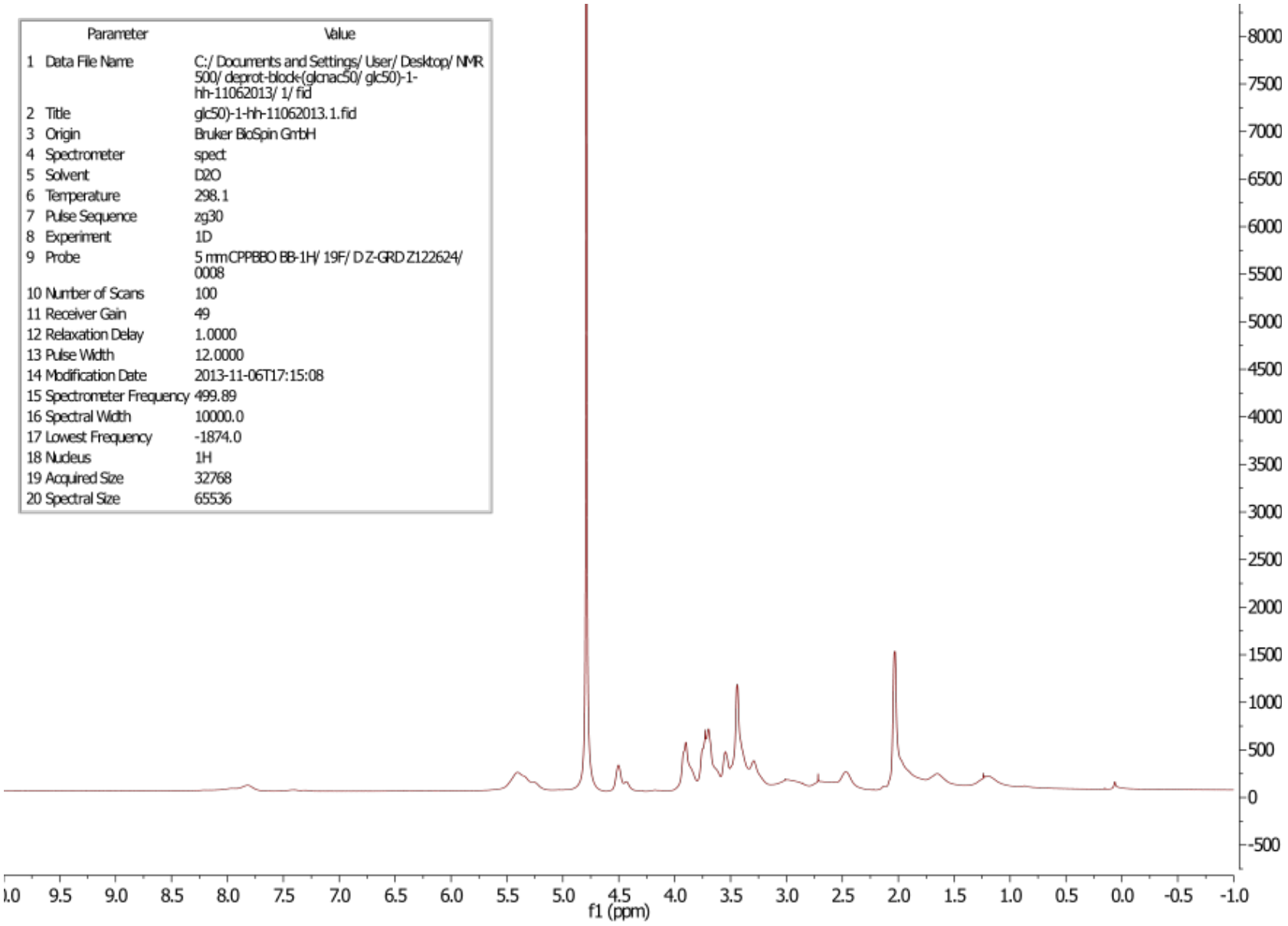

^{1}H NMR poly(**1c**$_{50}$-*block*-**1d**$_{50}$)